

European Office of Aerospace  
Research and Development

РОССИЙСКАЯ АКАДЕМИЯ НАУК  
RUSSIAN ACADEMY OF SCIENCES  
P.N. LEBEDEV PHYSICS INSTITUTE




Ф И А Н  
INSTITUTE OF QUANTUM RADIOPHYSICS

Approved by  
Representative of EOARD

Approved by  
Deputy Director of IQR

\_\_\_\_\_, 1996

 Dr. A. Starodub  
25 Sept, 1996

**Degenerate four-wave mixing and phase conjugation of  
molecular mid-IR lasers radiation in their inverted media**

Scientific report

Time period: September 1, 1995 - September 1, 1996.

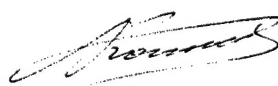
*The research work has been done in accordance with a special contract SPC-95-4043 between  
European Office of Aerospace Research and Development and P.N. Lebedev Physics Institute.*

Scientific leader:

Research workers:



Prof. A. Ionin



Dr. M. Galushkin



Mr. A. Kotkov



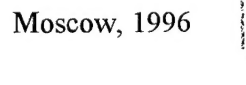
Mr. K. Mitin



Mr. L. Afanas'ev



Mr. L. Seleznev



Mr. D. Sinitsyn



Mrs. N. Ionina

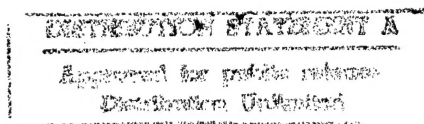


Mr. Yu. Klimachev

19970130 083

DTIC QUALITY INSPECTED 3

Moscow, 1996



REPORT DOCUMENTATION PAGE			Form Approved OMB No. 0704-0188	
Public reporting burden for this collection of information is estimated to average 1 hour per response, including the time for reviewing instructions, searching existing data sources, gathering and maintaining the data needed, and completing and reviewing the collection of information. Send comments regarding this burden estimate or any other aspect of this collection of information, including suggestions for reducing this burden to Washington Headquarters Services, Directorate for Information Operations and Reports, 1215 Jefferson Davis Highway, Suite 1204, Arlington, VA 22202-4302, and to the Office of Management and Budget, Paperwork Reduction Project (0704-0188), Washington, DC 20503.				
1. AGENCY USE ONLY (Leave blank)		2. REPORT DATE		3. REPORT TYPE AND DATES COVERED  Final Report
4. TITLE AND SUBTITLE  Degenerate four-wave mixing and phase conjugation of molecular mid- IR lasers radiation in their inverted data			5. FUNDING NUMBERS  F6170895W0411	
6. AUTHOR(S)  Dr. Andrei Ionen				
7. PERFORMING ORGANIZATION NAME(S) AND ADDRESS(ES)  P N Lebedev Physics Institute Quantum raiophysics Department Leninsky Prospect, 53 Moscow 117924 Russia			8. PERFORMING ORGANIZATION REPORT NUMBER  N/A	
9. SPONSORING/MONITORING AGENCY NAME(S) AND ADDRESS(ES)  EOARD PSC 802 BOX 14 FPO 09499-0200			10. SPONSORING/MONITORING AGENCY REPORT NUMBER  SPC 95-4043	
11. SUPPLEMENTARY NOTES				
12a. DISTRIBUTION/AVAILABILITY STATEMENT  Approved for public release; distribution is unlimited.			12b. DISTRIBUTION CODE  A	
13. ABSTRACT (Maximum 200 words)  This report results from a contract tasking P N Lebedev Physics Institute as follows: The contractor will perform in degenerate four-wave mixing and phase conjugation of molecular mid-IR laser radiation in their inverted media. He will investigate the phase conjugation process for IR pulses of duration between 10 mic c and 1 msec. Analytical and numerical solutions of wave equations coupled with corresponding equations of the laser active medium and the inverted media will be used.				
14. SUBJECT TERMS  Geophysics			15. NUMBER OF PAGES  145	
			16. PRICE CODE N/A	
17. SECURITY CLASSIFICATION OF REPORT  UNCLASSIFIED	18. SECURITY CLASSIFICATION OF THIS PAGE  UNCLASSIFIED	19. SECURITY CLASSIFICATION OF ABSTRACT  UNCLASSIFIED	20. LIMITATION OF ABSTRACT  UL	

## 1. Introduction

A large variety of physical factors are responsible for a deterioration of optical quality of laser radiation propagating through an active medium, optical elements, atmosphere etc. The laser optical quality can be substantially improved by using a nonlinear optical method of phase conjugation (PC) of laser radiation [1], which exhibits the inherent capability of correcting and preventing a laser beam from optical aberrations. The feasibility of PC process has been already demonstrated, practically, almost for every kind of a laser. The physical mechanisms of PC and nonlinear optical media, where PC takes place, are quite different for different lasers and wavelengths. There is no PC mirror which would effectively operate for each sort of a laser.

Until recently PC mirrors with good characteristics were only available for lasers operating in the visible and near IR. High power (HP) CO<sub>2</sub> and CO lasers, which are very prospective for different kinds of applications, however, operate in the mid IR:  $\lambda \sim 9-11 \mu\text{m}$  for CO<sub>2</sub> and  $\lambda \sim 5-6 \mu\text{m}$  for CO lasers.

The degenerate four wave mixing (DFWM) technique [2, 3] appears to be more suitable for PC of HP CO<sub>2</sub> and CO lasers radiation. For the first time PC at DFWM for short (submicrosecond) pulse CO<sub>2</sub> laser was experimentally observed in semiconductors and inverted medium [4, 5], and absorbing gas [6, 7]. Afterwards PC at DFWM for CO<sub>2</sub> laser was investigated both experimentally and theoretically very intensively [8, 9] for different nonlinear media.

However, the usage of semiconductors and liquids as PC mirrors for HP CO<sub>2</sub> and CO lasers is strongly restricted because of heating and feasibility of destroying a nonlinear medium itself. That is why the main attention for HP pulsed and repetitively pulsed CO<sub>2</sub> and CO lasers (especially for electron beam controlled discharge (EBCD) lasers), which operate in long pulse mode (10-50  $\mu\text{s}$  for CO<sub>2</sub> and 100 - 1000  $\mu\text{s}$  for CO laser) is paid to gas media which can be removed from an interaction zone very rapidly.

PC at DFWM for long ( $\tau_{\text{out}} \gg 10^{-6} \text{ s}$ ) CO<sub>2</sub> laser pulses in absorbing SF<sub>6</sub> gas was observed in [10] with efficiency up to 100%, though the pulse length of a reflected signal was half as much as that of a probe signal. The pulse length of a PC signal was increased in [11] up to 25  $\mu\text{s}$  at pulse length of a probe signal of 40  $\mu\text{s}$ . But PC efficiency (PC reflectivity (PCR)) dropped very strongly down to 5-10%. An application of PC techniques with absorbing gas for HP repetitively pulsed CO<sub>2</sub> laser was demonstrated in [12]. The main disadvantage of using absorbing gas like SF<sub>6</sub> as a PC mirror is a deterioration of optical homogeneity of the nonlinear medium, that decreases the efficiency and optical quality of a PC signal for long laser pulse. It should be noted that for CO lasers absorbing gas media as PC mirror were not investigated altogether.

The active or inverted medium of HP CO<sub>2</sub> and CO lasers appears to be a promising PC mirror at DFWM of laser radiation inside the medium. In case of the intracavity DFWM the pumping waves are counter-propagating intracavity ones ( $E_1$ ,  $E_2$  with intensities and wave vectors  $I_1$ ,  $I_2$  and  $k_1$ ,  $k_2$ , respectively) inside active medium of a laser, the probe beam ( $E_3$  with intensity  $I_3$  and wave vector  $k_3$ ) is the laser output weakened with attenuator. The interaction of the waves results in a spatial modulation of laser gain (resonant or amplitude mechanism) and that of refractive index (thermal or phase mechanism). This spatial modulation represents a volume hologram (grating) in the nonlinear medium (laser active medium in our case). If we consider the backward (counter-propagating) pumping wave as the read out beam in this holographic analogy, we see that fourth wave ( $E_4$  with intensity  $I_4$  and wave vector  $k_4$ ) is produced by the scattering of this backward wave on the interference pattern in the nonlinear medium. Any phase information in the incident probe wave is recorded in the gain grating and in the thermal one and it is transferred to the scattered signal which is reversed in time (or conjugated). Fig. 1.1a schematically shows this interference pattern formed between the forward (co-propagating) pumping wave and the probe one with spacing  $\Lambda_{13} = \lambda (2 \sin \theta/2)^{-1}$  ( $\Lambda_{13} \sim \lambda/\theta$  for small interaction angle  $\theta \ll 1$ ). A similar interference pattern is produced between the backward pumping wave and the probe one (Fig. 1.1b) that also gives rise to the phase conjugated (PC) signal. It should be noted that the spacing of the interference fringes is much smaller in the latter case ( $\Lambda_{23} = \lambda (2 \cos \theta/2)^{-1} \sim \lambda/2$  for small interaction angle  $\theta \ll 1$ ).

For the first time PC process under DFWM inside own active medium of CO<sub>2</sub> laser was experimentally observed in [4, 5] for short laser pulse ( $\tau_{out} \leq 0.2 \mu s$ , where  $\tau_{out}$  - pulse duration of laser output). To explain the observed results the authors of the paper used the theory of the PC process [13] which based on the theory of wave mixing [14]. The PC theory [13, 15] dealt with resonant (amplitude) mechanism of PC process for two-level medium under non-transient DFWM. Transient PC process should be described by the theory involved a system of kinetic equations of inverted medium [16]. Another mechanism of the PC process (thermal or phase mechanism or light induced medium perturbation (LIMP)) was analyzed theoretically and observed experimentally for long pulse CO<sub>2</sub> laser ( $\tau_{out} \geq \tau_{rel}$ , where  $\tau_{rel}$  - relaxation time of upper laser level) in [17-21]. There was demonstrated in [20, 21] that complicated temporal behaviour of the PC signal can be explained only by both mechanisms of PC process at DFWM inside own active medium of CO<sub>2</sub> laser.

The PC at DFWM for CO laser with feedback optical scheme may be observed in [22], the theory of PC at DFWM being developed now [23,24] and still far from its finishing.



It should be strongly emphasized, that experimental results published earlier contradict each other. For instance, reflectivity for CO<sub>2</sub> laser observed in [17, 18] reaches 30-50%, PCR was 0.15% in [19] and 2% in [20]; for CO laser - 11% in [22] and 0.2% in [20]. Some papers [17, 18, 22] did not demonstrate an experimental proof of a signal observed being a PC one. That is why a main objective of this paper is a thorough parametric study of a PC process at DFWM and the study of physical mechanisms of the PC process in active medium of CO<sub>2</sub> and CO lasers both theoretically and experimentally. The special attention was paid to experimental techniques which proves the signal detected to be a PC one.

The paper consists of four parts. First one (Introduction) introduces to the PC problem and terminology. The second part deals with theoretical model of the PC process and presents main theoretical results. The third part presents experimental results of the PC process inside active medium of CO<sub>2</sub> laser, comparison of the results with the theory and also the experimental results of the PC process inside active medium of CO laser. The comparison of the experimental results for CO and CO<sub>2</sub> lasers and main conclusions will be presented in the fourth part. The research on high-frequency temporal structure of probe and PC signals at DFWM of radiation of CO<sub>2</sub> and CO lasers in their inverted medium with nanosecond resolution is discussed in Part 4.

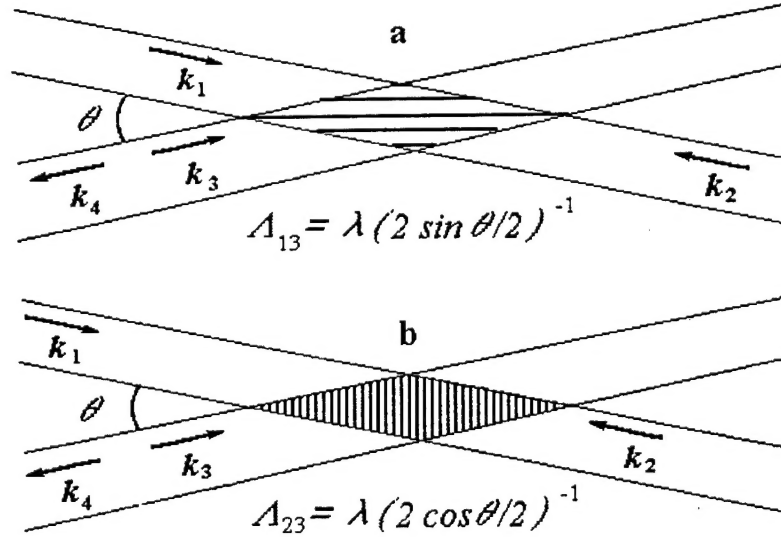


Fig. 1.1. Interference pattern demonstrating the large scale grating (a) between the probe wave  $k_3$  and the forward (co-propagating) pumping wave  $k_1$  and the small scale grating (b) between the probe wave  $k_3$  and the backward (counter-propagating) pumping wave  $k_2$  at degenerate four-wave mixing.  $k_4$  - the phase conjugated wave,  $\theta$  - an angle of interaction,  $\lambda$  - a laser wavelength.

## 2. Theoretical investigation of phase conjugation at DFWM of pulsed CO<sub>2</sub> laser radiation inside inverted medium

A calculation of a PC reflectivity (PCR or  $R$ ) for a signal wave is one of main problems of the PC theory. When obtaining a formula for PCR, the interacting waves are usually represented as plane ones for a cubic nonlinear medium. The obtained expressions remain true for a more common case of wide angular spectrum of a signal wave and conjugated pumping waves. It is also supposed that the light waves forming a transient gratings are coherent. In practice the condition of coherency is frequently realized by using the same radiation source for creating signal and pumping waves with an acceptable optical delay between them. A frequency selection with the purpose of a stabilization of rotational-vibrational transition during radiation pulse is required for CO<sub>2</sub> laser. When no frequency selection taking place (for example at pressure of laser mixture of  $\sim 1$  atm), the number of a rotational spectral line can be varied during the laser pulse [25]. As a result temporal behaviour of amplitude grating is changed and a strong decrease of phase thermal grating amplitude takes place.

In the DFWM theory presented longitudinal optical resonator modes are assumed to form amplitude and phase gratings. A total contribution of these longitudinal modes is the same one as for a single longitudinal mode with intensity equal to a sum of intensities of all these modes. In fact, this assumption is close to the model of a smooth laser pulse model.

DFWM problems in the media with cubic nonlinearity have been investigated intensively both experimentally and theoretically. The problems include selective and polarization properties of PC mirrors, creation of pumping waves etc. However, we do not touch these problems in this paper and give main attention to DFWM in the inverted medium of pulsed EBCD CO<sub>2</sub> laser. The properties of a nonlinear medium are very important for transient DFWM as compared to usual volumetric hologram and occupy an important place in the DFWM theory. The properties of a thermodynamically nonequilibrium nonlinear media, which include active laser media, are much more important for the DFWM process. These nonlinear media are characterized, as a rule, by high order of nonlinearity. The relaxation processes in them are reflected in temporal characteristics of a PC signal at DFWM. Besides there is a lot of thermodynamically nonequilibrium nonlinear medium parameters which influence on pulse temporal characteristics and power efficiency of PC process that complicates the problem of its optimization.

Also the presence of two mechanisms of nonlinearity (nonlinearity, connected with gain saturation and thermal nonlinearity) is the important feature of the CO<sub>2</sub> laser gain medium. The cooperative operation of these two types of nonlinearity strongly distinguished on response time

creates a complicated temporal behaviour of DFWM. An amplification of mixing waves strongly affects the characteristics of this process, as well.

Further we shall consider the theoretical problems in detail and analyze the features of temporal behaviour of DFWM in the active medium of EBCD CO<sub>2</sub> laser.

## **2.1. Transient theory of phase conjugation at degenerate four - wave mixing.**

### **2.1.1. Physical mechanisms of PC.**

The special situation takes place in CO<sub>2</sub> and CO lasers, the wavelengths of which lie in a mid-IR range. The situation is connected with a limited choice of the suitable media for PC mirrors which have sufficient transparency for a radiation of interacting waves. Stimulated Brillouin scattering (SBS) is not realized efficiently for this reason and also because of large duration of transient period in the mid-IR range. That is why the methods of PC for a CO<sub>2</sub> and CO laser radiation are based on DFWM. Absorbing gas SF<sub>6</sub>, some liquids (CS<sub>2</sub>, CCl<sub>4</sub>), semiconductors (InSb, GaAs, Ge) and own active medium can be used as the nonlinear media.

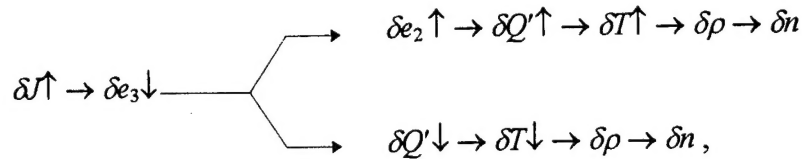
An optical homogeneity for absorbing substances is deteriorated during the PC process because of strong heating and for this reason PC reflectivity and PC optical quality are spoiled. Moreover there is a problem of chemical stability of resonance absorbing media under the influence of intensive laser radiation. Various physical mechanisms of nonlinearity for PC are used in semiconductors but in any case the DFWM process is accompanied by a rather high absorptivity which is a limitation in use of these materials for high power repetitively pulsed laser because of destroying a nonlinear medium.

An active medium of laser appears to be the most suitable nonlinear medium for PC of a powerful CO<sub>2</sub> laser radiation. The medium does have rather high nonlinearity, optical homogeneity and long interaction range. All these conditions can give rise to high PC efficiency at DFWM. Besides methods of self-PC at DFWM with a feed-back are realized in the gain media [26, 27], that can solve a problem of creating powerful conjugated waves.

### **2.1.2. Medium nonlinearity.**

A nonlinearity of a laser gain connected with its saturation in a strong radiation field takes place in inverted CO<sub>2</sub> as in any laser medium. The nonlinearity of a real part of a dielectric constant (refraction index) can arise at a radiation frequency detuning from a center of a laser

spectral line. However, in practice only a nonlinearity of a laser gain is realized, inasmuch as frequency detuning is usually small or there is the large number of longitudinal modes of lasing. The frequencies of these modes are equally spaced on both sides of the center of a laser line and consequently their contribution to a nonlinearity of a refraction index is mutually compensated. A thermal nonlinearity takes place together with a gain nonlinearity inside active medium of a long pulse ( $\tau_{\text{out}} > 1\mu\text{s}$ ) CO<sub>2</sub> laser. The physical mechanism can be expressed by the following scheme:



where  $\delta I$ ,  $\delta e_3$ ,  $\delta e_2$ ,  $\delta Q$ ,  $\delta T$ ,  $\delta \rho$ ,  $\delta n$  are variations of radiation intensity, average quantum number of antisymmetric and deformational vibrational mode of a CO<sub>2</sub> molecule, specific heat liberation, temperature, density and refraction index. Here the vertical arrows show an increase or a decrease of the appropriate values. The upper set of variations is connected with laser induced heating of the active medium and lower one concerns to its cooling by a laser radiation. Both ways of relaxation of vibrationally excited molecules are nonlinear ones with respect to intensity of a radiation but have a different response time. The first way as the most "fast" one takes place in the beginning of laser pulse, because V - T relaxation rate of the deformational mode is much higher as compared to nonradiative relaxation rate for antisymmetric mode.

The transient amplitude and phase gratings which are due to gain and thermal nonlinearity, respectively, are created at DFWM process in the own active CO<sub>2</sub> laser medium. As it will be theoretically shown below, the efficiency of the thermal mechanism of nonlinearity strongly depends on pressure of laser mixture. Its contribution to the DFWM process becomes predominant at pressure of  $\sim 1$  atm.

## 2.2 PC reflectivity calculation methods.

### 2.2.1 DFWM on gain nonlinearity in active medium of EBCD CO<sub>2</sub> laser.

In general case the gain nonlinearity of the laser media has a high order of nonlinearity. The cubic nonlinearity takes place at weak saturation when radiation intensity is less than value of saturation one.

The theory of DFWM in the laser media has been essentially developed in [13], where authors consider a case of PC for weak probe wave as compared to pump waves. This condition ensures a

cubic nonlinearity at DFWM. However, the model of the gain medium was very simple in [13]. It was two-level and nontransient model. The theory was developed in [28-30] to take into account more completely properties of the concrete inverted medium at DFWM, particularly, CO<sub>2</sub> laser active medium. This theory is founded on solution of the nontransient and transient kinetic equations together with the nonlinear Helmholtz equation.

*Wave mixing in a medium with a gain nonlinearity.*

An interference of a signal wave with two conjugate pumping waves lays in a basis of DFWM. As a result of this interaction, standing waves of intensity at degenerate interaction or running waves at nondegenerate one arise in the nonlinear medium. Further we shall deal with the case of degenerate DFWM.

When designating pump waves through  $E_1$  and  $E_2$ , it is possible to write expression for a total intensity

$$E^2 = (E_1 + E_2 + E_3 + E_4)^2 = \sum_{i=1}^4 E_i^2 + 2 \sum_{\substack{i,j \\ i \neq j}}^4 E_i E_j. \quad (2.1)$$

The theory of nonlinear optics is based on a parabolic approximation. Therefore slow complex amplitudes  $a_i$  are introduced:

$$E_j = \frac{1}{2} \left[ a_j \exp(i\omega t + i \vec{k}_j \vec{r}) + C.C. \right]. \quad (2.2)$$

We shall enter the denotations:  $E_0 = E_1 + E_2$  and  $\Delta E = E_3 + E_4$ . According to a condition  $|E_3|, |E_4| < |E_1|, |E_2|$  following relation for a gain per unit of length takes place

$$\alpha \cong \alpha \left( |\tilde{E}_0|^2 \right) + \delta\alpha, \quad (2.3)$$

where  $\delta\alpha$  is a spatial - temporal variation of a gain, caused by a variation of intensity

$$\delta \tilde{E}^2 = 2(\tilde{E}_0 \Delta \tilde{E}). \quad (2.4)$$

Here the tilde designates values without containing high-frequency temporal oscillations because a response time of the nonlinear medium is much more than a period of the oscillation.

The process of Bragg scattering on transient amplitude gratings arisen in laser medium is described by the nonlinear Helmholtz equation

$$\nabla^2 E + k^2 E + ik\alpha E = 0, \quad (2.5)$$

where  $k = 2\pi/\lambda$  is wave number. Let's assume that the plane signal wave is propagated along an axis  $z$  with a coordinate origin on a front edge of the nonlinear medium and the pumping waves

are propagated under small angle  $\theta$  to an axis  $z$ . Then  $\vec{k}_3\vec{r} = kz$ ;  $\vec{k}_4\vec{r} = -kz$  and for a variation of intensity  $\delta J = \mu|\delta E|^2$ , where  $\mu = c/4\pi$ ,  $c$  - speed of light, we obtain

$$\delta J = \frac{\mu}{2} \left\{ \sqrt{\varphi_0(t)} \left[ A_1 \exp(i\vec{k}_1\vec{r}) + A_2 \exp(-i\vec{k}_2\vec{r}) \right] \times \left[ a_3^* \exp(ikz) + a_4^* \exp(-ikz) \right] + C.C. \right\}, \quad (2.6)$$

where  $A_1, A_2$  are the maximum values of pumping wave amplitudes,  $\varphi_0(t)$  is a function defining the intensity profile of these waves. The space variation of intensity  $\delta J$  causes a variation of medium parameters upon which laser gain depends. For  $\text{CO}_2$  laser such parameters are average vibrational quantum numbers  $e_i$ .

### Equations for nonlinear medium.

Let's consider the kinetic equations describing the balance of  $e_i$  in each vibrational mode of a  $\text{CO}_2$  molecule

$$\frac{d}{dt} e_3 = P'_3 - \frac{e_3}{\tau_3} - \frac{\alpha J}{\gamma_1 N \hbar \omega_0}, \quad (2.7)$$

$$\frac{d}{dt} e_2 = (2P'_1 + P'_2) + 3 \frac{e_3}{\tau_3} - \frac{e_2 - e_{2T}}{\tau_2} + \frac{2\alpha J}{\gamma_1 N \hbar \omega_0}, \quad (2.8)$$

$$\frac{d}{dt} T = \frac{q_T W}{NC_V} + \gamma_1 N \left( \hbar \omega_2 \frac{e_2 - e_{2T}}{\tau_2} + \hbar \omega'_0 \frac{e_3}{\tau_3} \right), \quad (2.9)$$

$$\alpha = \frac{\gamma_1 N A}{4\pi^2 \Delta \nu} \frac{2hcB}{k_B T} \lambda_{0j}^2 Z \left[ \exp\left(-\frac{\theta_3}{T_3}\right) - \exp\left(-\frac{2\theta_2}{T_2}\right) \right] (2j+1) \exp\left(-\frac{j(j+1)hcB}{k_B T}\right), \quad (2.10)$$

where  $P'_i = \frac{\delta_i W}{\gamma_i N \hbar \omega_3}$  ( $i=1, 2, 3$ );  $W$  - specific input power;  $e_{2T} = 2[\exp(\hbar \omega_2/T) - 1]^{-1}$ ;

$$\hbar \omega'_0 = \theta_3 - 3\theta_2 = 500K; \hbar \omega_2 = 960K; \tau_3^{-1} = p \sum_{m=1}^3 \gamma_m K_{32m}; \tau_2^{-1} = p \sum_{m=1}^3 \gamma_m K_{20m},$$

$p, T, C_V$  are pressure, temperature and specific heat of gas mixture;  $\gamma_m$  is relative concentration of gas mixture components;  $K_{32m}, K_{20m}$  are relaxation rate of antisymmetric and deformation modes of a  $\text{CO}_2$  molecule;  $\delta_i, \delta_T$  are relative part of pumping power transmitted into various vibrational modes of molecules ( $\text{CO}_2, \text{N}_2$ ) and into translational and rotational degree of freedom;  $N$  is concentration of molecules;  $J$  is radiation intensity;  $\hbar \omega_0, \hbar \omega_3$  are quantum energy of laser transition and antisymmetric mode;  $A$  is Einstein coefficient;  $\Delta \nu$  is a spectral width of a laser line;  $Z$  is vibrational statistical sum;  $\lambda_{0j}$  is radiation wavelength;  $j$  is rotational quantum number;  $B$  is

rotational constant;  $h$  is Planck constant;  $k_B$  is Boltzman constant;  $c$  is speed of light. From (2.7) - (2.10) we obtain

$$\frac{d}{dt}\delta e_3 - D\nabla^2\delta e_3 = -\frac{\delta e_3}{\tau_3} - \frac{J}{\gamma_1 N\hbar\omega_0}\delta\alpha - \frac{\alpha}{\gamma_1 N\hbar\omega_0}\delta J, \quad (2.11)$$

$$\frac{d}{dt}\delta e_2 - D\nabla^2\delta e_2 = 3\frac{\delta e_3}{\tau_3} - \frac{\delta e_2}{\tau_2} + \frac{2J}{\gamma_1 N\hbar\omega_0}\delta\alpha + \frac{2\alpha}{\gamma_1 N\hbar\omega_0}\delta J, \quad (2.12)$$

here  $D$  is diffusion coefficient. It is shown in [30] that the diffusion influences on PC reflectivity at DFWM very strongly. Let's write down a gain (2.10) as follows

$$\alpha = \sigma\gamma_1 N(e_3 - e_2^2), \quad (2.13)$$

where  $\sigma$  is cross-section of laser transition. Then the variation of  $\alpha$  is equal to

$$\delta\alpha = \sigma\gamma_1 N(\delta e_3 - 2e_2\delta e_2). \quad (2.14)$$

Within the framework of the selected description of a EBCD CO<sub>2</sub> laser's active medium kinetics expressions (2.7) - (2.13) give the system of the equations for a nonlinear medium which are solved together with the nonlinear Helmholtz equation (2.5).

#### *Definition of intensity variation.*

At known intensity of pumping waves  $J(t) = J_1(t) + J_2(t)$  a solution of the kinetic equations allows us to determine coefficients (time-dependent in a general case) of the linear equations system (2.11), (2.12) and (2.14). The coefficients in the linear equations for variations  $\delta e_3$  and  $\delta e_2$  having been defined, it is required to find solution of the equations system. For this purpose let's select standing waves of intensity with identical value of wave numbers  $q_1$  and  $q_2$  in an intensity variation (2.6):

$$\delta J = (\delta J)_1 + (\delta J)_2, \quad (2.15)$$

$$(\delta J)_1 = \frac{\mu\sqrt{\varphi_0(t)}}{2} \left\{ A_1(z)\sqrt{\varphi_3(t)}A_3^*(z)\exp(-i\vec{q}_1\vec{r}) + A_2(z)\sqrt{\varphi_4(t)}A_4^*(z)\exp(i\vec{q}_2\vec{r}) + C.C. \right\},$$

$$(\delta J)_2 = \frac{\mu\sqrt{\varphi_0(t)}}{2} \left\{ A_1(z)\sqrt{\varphi_4(t)}A_4^*(z)\exp(-i\vec{q}_2\vec{r}) + A_2(z)\sqrt{\varphi_3(t)}A_3^*(z)\exp(i\vec{q}_1\vec{r}) + C.C. \right\},$$

$$\vec{q}_1 = \vec{k}_1 - \vec{k}_3, \quad \vec{q}_2 = \vec{k}_2 - \vec{k}_4, \quad \vec{k}_1 = -\vec{k}_2, \quad \vec{k}_3 = -\vec{k}_4,$$

$$\vec{q}_1 = 2k \sin\left(\frac{\theta}{2}\right), \quad \vec{q}_2 = 2k \sin\left(\frac{\pi - \theta}{2}\right),$$

$A_3$  and  $A_4$  are the maximum value of  $a_3(z, t)$  and  $a_4(z, t)$  with the temporal pulse profile of



$\sqrt{\varphi_3(t)}$  and  $\sqrt{\varphi_4(t)}$  respectively,  $\theta$  is the angle between directions of propagation for the signal and the first pumping waves. Normally, selected angle  $\theta$  is small one  $\theta \ll 1$ . Transient space gratings with large period (large-scale) and small-scale gratings with period which closes to the laser wavelength are created at the given scheme of interaction in the nonlinear medium.

*A coefficient of nonlinear coupling and equations for coupled waves.*

After a substitution (2.15) into (2.11) and (2.12) for low PC reflectivities  $R = J_4 / J_3 \ll 1$  we receive following system in parabolic approximation:

$$\delta \varepsilon_3 = (\delta \varepsilon_3)_1' (\delta J)_1 + (\delta \varepsilon_3)_2' (\delta J)_2, \quad (2.16)$$

$$\delta \varepsilon_2 = (\delta \varepsilon_2)_1' (\delta J)_1 + (\delta \varepsilon_2)_2' (\delta J)_2, \quad (2.17)$$

$$\frac{d}{dt} (\delta \varepsilon_3)_i' + Dq_i^2 (\delta \varepsilon_3)_i' = \frac{(\delta \varepsilon_3)_i'}{\tau_3} - \frac{J}{\gamma_1 N \hbar \omega_0} (\delta \alpha)_i' - \frac{\alpha \sqrt{\varphi_0(t)} \sqrt{\varphi_3(t)}}{\gamma_1 N \hbar \omega_0}, \quad (2.18)$$

$$\frac{d}{dt} (\delta \varepsilon_2)_i' + Dq_i^2 (\delta \varepsilon_2)_i' = \frac{3(\delta \varepsilon_3)_i'}{\tau_3} - \frac{(\delta \varepsilon_2)_i'}{\tau_{21}} + \frac{2J}{\gamma_1 N \hbar \omega_0} (\delta \alpha)_i' + \frac{2\alpha \sqrt{\varphi_0(t)} \sqrt{\varphi_3(t)}}{\gamma_1 N \hbar \omega_0}, \quad (2.19)$$

$$(\delta \alpha)_i' = \sigma \gamma_1 N \left[ (\delta \varepsilon_3)_i' - 2e_2 (\delta \varepsilon_2)_i' \right], \quad (2.20)$$

$i = 1, 2$ .

Here  $\varphi_m(t) = \varphi_m(t, z=0) \exp\{[\bar{\alpha}(t) - \bar{\alpha}(0)]z\}$ ,  $m = 0, 3$ .

In order to simplify the calculations we consider the gain as  $\alpha = \bar{\alpha}$ , intensity as  $J = J_1 + J_2$  and profile of a radiation pulse

$$\varphi_m(t) = \varphi_m(t, z=0) \frac{\exp\{[\bar{\alpha}(0) - \bar{\alpha}(t)]L_n\} - 1}{[\bar{\alpha}(0) - \bar{\alpha}(t)]L_n}, \quad (m = 0, 3)$$

as independent of coordinate  $z$  ( $L_n$  is interaction length).

Further using a relation  $\delta \alpha = (\delta \alpha)_1' (\delta J)_1 + (\delta \alpha)_2' (\delta J)_2$  and taking into consideration that the gain medium response time is much more than period of high-frequency oscillations of interaction waves we obtain a set of equations for slow changed amplitudes of coupled waves from the nonlinear Helmholtz equation (2.5) in Bragg approximation:

$$\begin{aligned} \frac{d}{dz}a_1 - \frac{1}{2}\alpha a_1 = \frac{1}{4} & \left[ (\delta\alpha)_1' (a_1 a_3^*) a_3 + (\delta\alpha)_2' (a_1 a_4^*) a_4 + \right. \\ & \left. + (\delta\alpha)_2' (a_2^* a_3) a_4 + (\delta\alpha)_1' (a_2^* a_4) a_3 \right], \end{aligned} \quad (2.21)$$

$$\begin{aligned} -\frac{d}{dz}a_2 - \frac{1}{2}\alpha a_2 = \frac{1}{4} & \left[ (\delta\alpha)_2' (a_2 a_3^*) a_3 + (\delta\alpha)_1' (a_2 a_4^*) a_4 + \right. \\ & \left. + (\delta\alpha)_1' (a_1^* a_3) a_4 + (\delta\alpha)_2' (a_1^* a_4) a_3 \right], \end{aligned} \quad (2.22)$$

$$\begin{aligned} \frac{d}{dz}a_3 - \frac{1}{2}\alpha a_3 = \frac{1}{4} & \left[ (\delta\alpha)_1' (a_1^* a_3) a_1 + (\delta\alpha)_2' (a_2^* a_3) a_2 + \right. \\ & \left. + (\delta\alpha)_1' (a_2 a_4^*) a_1 + (\delta\alpha)_2' (a_1 a_4^*) a_2 \right], \end{aligned} \quad (2.23)$$

$$\begin{aligned} -\frac{d}{dz}a_4 - \frac{1}{2}\alpha a_4 = \frac{1}{4} & \left[ (\delta\alpha)_2' (a_1^* a_4) a_1 + (\delta\alpha)_1' (a_2^* a_4) a_2 + \right. \\ & \left. + (\delta\alpha)_2' (a_2 a_3^*) a_1 + (\delta\alpha)_2' (a_1 a_3^*) a_2 \right], \end{aligned} \quad (2.24)$$

here the brackets select the amplitudes of waves writing down the gain gratings in the medium.

*Equations based on full kinetic model of a nonlinear medium.*

The usage of the more exact description of a laser kinetics (non-linearized four-temperature kinetic model) does not call any serious difficulties. For this purpose the equations (2.7) - (2.10) and (2.18) - (2.20) are substituted by following ones:

$$\frac{d}{dt}e_4 = F_4(e_3, e_4), \quad (2.25)$$

$$\frac{d}{dt}e_3 = F_3(e_2, e_3, e_4, J), \quad (2.26)$$

$$\frac{d}{dt}e_2 = F_2(e_2, e_3, J), \quad (2.27)$$

$$\frac{d}{dt}T = F_T(e_2, e_3), \quad (2.28)$$

$$\alpha = F_0(e_2, e_3), \quad (2.29)$$

$$\frac{d}{dt}(\delta e_4)_i' + Dq_i^2(\delta e_4)_i' = \frac{\partial F_4}{\partial e_3}(\delta e_3)_i' + \frac{\partial F_4}{\partial e_4}(\delta e_4)_i', \quad (2.30)$$

$$\begin{aligned} \frac{d}{dt}(\delta e_3)_i' + Dq_i^2(\delta e_3)_i' &= \frac{\partial F_3}{\partial e_2}(\delta e_2)_i' + \frac{\partial F_3}{\partial e_3}(\delta e_3)_i' + \\ &+ \frac{\partial F_3}{\partial e_4}(\delta e_4)_i' + \frac{\partial F_3}{\partial J} \sqrt{\varphi_0(t)} \sqrt{\varphi_3(t)}, \end{aligned} \quad (2.31)$$

$$\frac{d}{dt}(\delta e_2)_i' + Dq_i^2(\delta e_2)_i' = \frac{\partial F_2}{\partial e_2}(\delta e_2)_i' + \frac{\partial F_2}{\partial e_3}(\delta e_3)_i' + \frac{\partial F_2}{\partial J} \sqrt{\varphi_0(t)} \sqrt{\varphi_3(t)}, \quad (2.32)$$

$$(\delta \alpha)_i' = \frac{\partial F_0}{\partial e_2}(\delta e_2)_i' + \frac{\partial F_0}{\partial e_3}(\delta e_3)_i', \quad (2.33)$$

$$i = 1; 2,$$

$$\left. \begin{aligned} F_4(e_3, e_4) &= P_4' - \frac{\gamma_1 N}{\tau_4} (e_4 - e_3); \\ F_3(e_2, e_3, e_4, J) &= P_3' + \frac{\gamma_2 N}{\tau_4} (e_4 - e_3) - \frac{f_3}{\tau_3} - \frac{\alpha J}{\gamma_1 N \hbar \omega_0}; \\ F_2(e_2, e_3, J) &= f_2 \left( 2P_1' + P_2' + 3 \frac{f_3}{\tau_3} - \frac{e_2 - e_{2T}}{\tau_2} + 2 \frac{\alpha J}{\gamma_1 N \hbar \omega_0} \right); \\ F_T(e_2, e_3) &= \frac{\gamma_1}{C_V} \left[ \frac{\hbar \omega_0' f_3}{\tau_3} + \frac{\hbar \omega_2 (e_2 - e_{2T})}{\tau_2} \right] + 2.7 \frac{W(t) q_T}{NC_V}; \\ F_0(e_2, e_3) &= \sigma \gamma_1 N f_1; \end{aligned} \right\} \quad (2.34)$$

$$f_1 = \frac{1 + e_2}{(1 + 0.5e_2)^4 (1 + e_3)} \left[ \frac{e_3}{1 + e_3} - \left( \frac{0.5e_2}{1 + 0.5e_2} \right)^2 \right]; \quad f_2 = \frac{2(1 + e_2)^2}{2 + 6e_2 + 3e_2^2};$$

$$f_3 = e_3(1 + 0.5e_2)^3 - (1 + e_3)(0.5e_2)^3 \exp\left(-\frac{\hbar \omega_0'}{T}\right)$$

*A solution of equation set for coupled waves in approximation of constant pumping wave amplitude.*

Let's consider solutions of the equations for coupled waves (2.21) - (2.24). Within the framework of the approximation accepted for weak signal and PC waves as compared to pumping waves the equations (2.21) and (2.22) take a simple view

$$\frac{d}{dz} a_1 - \frac{1}{2} \alpha a_1 = 0, \quad (2.35)$$

$$-\frac{d}{dz} a_2 - \frac{1}{2} \alpha a_2 = 0. \quad (2.36)$$

Two other equations (2.23) and (2.24) because of complex conjugation of pumping waves are reduced to the following form

$$\begin{aligned} \frac{d}{dz} a_3 - \left[ \frac{1}{2} \alpha + \frac{\mu}{4} (\delta\alpha)_1' |a_1|^2 + \frac{\mu}{4} (\delta\alpha)_2' |a_2|^2 \right] a_3 = \\ = \mu \left[ (\delta\alpha)_1' + (\delta\alpha)_2' \right] |a_1| |a_2| a_4^*, \end{aligned} \quad (2.37)$$

$$\begin{aligned} -\frac{d}{dz} a_4 - \left[ \frac{1}{2} \alpha + \frac{\mu}{4} (\delta\alpha)_2' |a_1|^2 + \frac{\mu}{4} (\delta\alpha)_1' |a_2|^2 \right] a_4 = \\ = \mu \left[ (\delta\alpha)_1' + (\delta\alpha)_2' \right] |a_1| |a_2| a_3^*. \end{aligned} \quad (2.38)$$

Inasmuch as nonlinear coupling parameters (the nonlinearity parameters)  $(\delta\alpha)_1'$  and  $(\delta\alpha)_2'$  are negative ones on account of gain saturation, one can see from (2.37) and (2.38) that a gain for signal and PC waves is less than usual saturated coefficient  $\alpha$  (for one wave). The reason of such decrease of amplification for waves  $E_3$  and  $E_4$  is a well known two-wave interaction on own amplitude grating. As a result of the interaction the weak wave is weakened for the benefit of strong one (in our case for the benefit of pumping waves [25, 31, 32]). The degree of reduction of amplification for weak waves at DFWM depends on angle between the wave directions.

The expression in right parts of (2.37) and (2.38) describes DFWM process, the efficiency of which is proportional to a product of pumping wave intensities. A dependence on concrete conditions of creating pumping waves for various values of  $|a_1|$ ,  $|a_2|$  takes place. For example, for

intracavity DFWM  $J_1(z) \cdot J_2(z) \cong \left( \frac{R_{out}}{1 - R_{out}} \right)^2 \exp(2 \bar{\alpha} L_n) \cdot J_{out}^2$ , where  $R_{out}$  is

reflectivity of an output mirror of a laser resonator,  $J_{out}$  is radiation intensity on an output coupler of the resonator,  $\bar{\alpha}$  is average value of a laser gain on interaction length  $L_n$ . If the intensity of the first pumping wave is given at  $z = 0$  and second at  $z = L_n$  then

$$J_1(z) \cdot J_2(z) \cong J_1(0) \cdot J_2(L_n) \exp(\bar{\alpha} L_n).$$

To consider DFWM features in the inverted CO<sub>2</sub> qualitatively it is possible to use a two-level model of a nonlinear medium. When  $e_3 \gg e_2$ ,  $\alpha \cong \sigma \gamma_1 N e_3$  and instead of (2.7), (2.8) we have

$$\frac{d}{dt} \alpha = \frac{\alpha_0}{\tau_3} - \frac{1 + J/J_s}{\tau_3} \alpha, \quad (2.39)$$

where  $J_s$  is saturation intensity,  $\alpha_0$  is a gain for a weak signal wave.

Corresponding to (2.39) we obtain the following equation for a variation of a laser gain:

$$\frac{d}{dt} \delta\alpha - D\nabla^2 \delta\alpha = -\left(1 + \frac{J}{J_s}\right) \frac{1}{\tau_3} \delta\alpha - \frac{\alpha}{\tau_3 J_s} \delta J. \quad (2.40)$$

Further, using (2.15) we obtain

$$\frac{d}{dt} (\delta\alpha)_i' + Dq_i^2 (\delta\alpha)_i' = -\left(1 + \frac{J}{J_s}\right) \frac{1}{\tau_3} (\delta\alpha)_i' - \frac{\alpha}{\tau_3 J_s} \sqrt{\varphi_0(t)\varphi_3(t)}. \quad (2.41)$$

For  $J(t) = \text{const}$  the solution of (2.41) is as follows

$$(\delta\alpha)_i' = \frac{1}{\tau_3 J_s} \exp(-t/\tau_{ri}) \int_0^t \alpha(t') \exp(t'/\tau_{ri}) \sqrt{\varphi_0(t')\varphi_3(t')} dt', \quad (2.42)$$

$$\text{where } \tau_{ri}^{-1} = Dq_i^2 + \left(1 + \frac{J}{J_s}\right) \frac{1}{\tau_3}, \quad i = 1, 2.$$

It follows from the analysis of the expression (2.42), that the parameter of nonlinear coupling  $(\delta\alpha)_i'$ , which determines temporal characteristics of a reflected signal, strongly depends on initial value of  $\alpha(t)$ , that is a gain at the moment of a DFWM beginning. To confirm this conclusion it is enough to consider two special cases for radiation pulse of the rectangular form  $\varphi_0(t)$  and  $\varphi_3(t)$ : when  $\alpha(t=0) = 0$  and when  $\alpha(t=0) \neq 0$ . In the first case it is possible to suppose that  $\varphi_0(t) = 1$ ,  $\varphi_3(t) = 1$  and the time of nonlinear parameter increase is determined by the response

time of the nonlinear medium  $\tau_3' = \frac{\tau_3}{(1 + J/J_s)}$ . The second case represents a greater interest

from the point of view of DFWM temporal behaviour. Inasmuch as exponential parameters  $\exp(t/\tau_{ri})$  and  $\alpha(t)$  in the equation (2.42), as the very slow functions, can be taken out from the integral at the moment of fast exponential growth of  $\varphi_0(t)$  and  $\varphi_3(t)$ , the parameters of nonlinear

coupling  $(\delta\alpha)_i'$  in many respects repeat a sharp temporal growth of initial part of the laser pulse front.

It should be noted, that the temporal parameter  $\tau_3$  characterizes a response time of a gain  $\alpha$  when laser radiation having intensity  $J$  (2.39). Therefore the value of  $1/\tau_3$  together with a rate of diffusion  $\tau_D^{-1} = Dq_i^2$  characterizes a resulting rate of amplitude grating formation (2.41).

Let's note that the rate of amplitude grating decay at absence of laser radiation (which determined by diffusion and relaxation rate  $1/\tau_3$ ) appears to be less than the rate of their formation because of influence of light intensity on response time of nonlinear medium. Therefore, if a record of amplitude grating is stopped by a fast turn of polarization of one of two waves  $E_1$  or  $E_3$ , its decay takes place with the same rate as a record one  $\tau_{ri}^{-1}$  (because laser radiation is in the medium).

The numerical calculations, results of which are presented below, display more precisely temporal behaviour of a PC radiation and also reflect the features of a PC signal and parameter of nonlinear coupling discussed above.

For nontransient DFWM it follows from (2.41) that

$$(\delta\alpha)_i' = -\frac{\tau_{ri}}{\tau_3} \frac{1}{J_s} \alpha. \quad (2.43)$$

#### *An amplification of mixing waves in nonlinear medium.*

Let's suppose that the diffusion does not take place ( $D = 0$ ) and total intensity  $J = J_1(z) + J_2(z)$  does not depend on coordinate  $z$ . In this case the solution of the equations (2.23), (2.24) for slowly varying amplitudes of the signal and PC waves can be easily found. It precisely coincides with a well known result obtained in [13]. In this case idealized for gas lasers, the signal and PC waves would have a following gain

$$\alpha = \frac{\alpha_0}{1 + J/J_s} - \frac{\alpha_0}{(1 + J/J_s)^2} \frac{J}{J_s} = \frac{\alpha_0}{(1 + J/J_s)^2}. \quad (2.44)$$

Actually, the gain  $\alpha$  for  $E_3$  and  $E_4$  can be many times higher on account of diffusion. As a matter of fact, let's consider practically important case of a small interaction angle ( $\theta \ll 1$ ). Then the small-scale gratings appear to be strongly weakened by a diffusion of a vibrationally excited

CO<sub>2</sub> molecules and consequently  $(\delta\alpha)_2' \ll (\delta\alpha)_1'$ . As a result we have for  $E_3$

$$\bar{\alpha} = \frac{\alpha_0}{L_n} \int_0^{L_n} \left[ \frac{1}{1 + \frac{J_1 + J_2}{J_s}} - \frac{1}{2} \frac{J_1/J_s}{1 + \frac{(J_1 + J_2)^2}{J_s}} \right] dz, \quad (2.45)$$

and for  $E_4$

$$\bar{\alpha} = \frac{\alpha_0}{L_n} \int_0^{L_n} \left[ \frac{1}{1 + \frac{J_1 + J_2}{J_s}} - \frac{1}{2} \frac{J_2/J_s}{1 + \frac{(J_1 + J_2)^2}{J_s}} \right] dz. \quad (2.46)$$

Thus, the diffusion weakening the amplitude gratings reduces DFWM efficiency on the one hand. On the other hand it increases an amplification of the probe and PC waves by reducing the two-wave interaction of the waves.

For the  $\text{CO}_2$  laser gain medium typical DFWM reflectivity is low  $R \ll 1$ . Therefore approximation of a constant field of a signal wave  $|a_3| \gg |a_4|$  is applicable

$$\begin{aligned} a_3 &= a_3(0) \exp\left(\int_0^z \alpha_3 dz\right), \\ a_4(0) - a_4(z) &= \frac{1}{2} \sqrt{J_1 J_2} \cdot a_3^*(0) \exp\left(-\int_0^z \alpha_4 dz'\right) \times \\ &\times \int_0^z (\delta\alpha)_1' \exp\left(\int_0^z (\alpha_3 + \alpha_4) dz''\right) dz', \end{aligned} \quad (2.47)$$

$$\alpha_3 = \frac{1}{2} \alpha + \frac{1}{4} (\delta\alpha)_1' J_1,$$

$$\alpha_4 = \frac{1}{2} \alpha + \frac{1}{4} (\delta\alpha)_1' J_2,$$

$$\sqrt{J_1 J_2} = J_0 \exp(\alpha L_n), \quad J_0 = J_1(0), \quad J_1 = J_0 \exp(\alpha z), \quad J_2 = J_0 \exp(2\alpha L_n - \alpha z).$$

If we take  $\bar{\alpha}_3 \approx \frac{1}{L_n} \int_0^{L_n} \alpha_3 dz$ ,  $\bar{\alpha}_4 \approx \frac{1}{L_n} \int_0^{L_n} \alpha_4 dz$  we have from (2.47)

$$a_4(0) \approx \frac{1}{2} J_0 \exp[(\alpha - \bar{\alpha}_4) L_n] (\delta\alpha)_1' \frac{\exp[(\bar{\alpha}_3 + \bar{\alpha}_4) L_n] - 1}{\bar{\alpha}_3 + \bar{\alpha}_4} a_3^*(0). \quad (2.48)$$



The parameter of nonlinear coupling  $(\delta\alpha)_1'$ , which depends on time for transient and quasi-stationary modes of laser operation, is calculated from the solution of the equations obtained above and in general case can be found numerically. At a steady state mode, when the transient processes are finished, as already was mentioned above, analytical solution for  $(\delta\alpha)_1'$  is obtained. It looks absolutely simple for a two-level model of the medium:

$$\begin{aligned}\alpha &= \sigma\gamma_1 N e_3, \\ \alpha &= \frac{\alpha_0}{1 + J/J_s}, \\ (\delta\alpha)_1' &= -\frac{\alpha_0}{(1 + J/J_s)^2} \frac{1}{J_s}, \\ \alpha_3 &= \frac{1}{2} \left\{ \alpha - \frac{1}{2} \frac{\alpha_0}{(1 + J/J_s)^2} \frac{J_1(0)}{\alpha L_n} [\exp(\alpha L_n) - 1] \right\}, \\ \alpha_4 &= \frac{1}{2} \left\{ \alpha - \frac{1}{2} \frac{\alpha_0}{(1 + J/J_s)^2} \frac{J_1(0)}{\alpha L_n} [1 - \exp(-\alpha L_n)] \exp(2\alpha L_n) \right\}.\end{aligned}\quad (2.49)$$

For a more exact nontransient model of a kinetics of a CO<sub>2</sub> laser medium in the form of linearized equations (2.7), (2.8) the nonlinear parameter  $(\delta\alpha)_1'$  is also calculated analytically

$$\begin{aligned}(\delta\alpha)_1' &= -\frac{\alpha}{J_s'} \cdot \frac{\tau_3'/\tau_3 - 6(\tau_2'/\tau_3)e_2}{1 - J/J_s' + 6e_2\tau_2'J/(\tau_3J_s') - 4e_2\tau_2'J/(\tau_3J_s')}, \\ J_s' &= \frac{\hbar\omega_0}{\sigma\tau_3'}, \quad \frac{1}{\tau_i'} = Dq_i^2 + \frac{1}{\tau_i}, \quad i = 1, 2, \\ e_2 &= \left( \frac{1}{\tau_3} - \sqrt{\frac{1}{\tau_3^2} - 4x_1x_2} \right) (2x_1)^{-1}, \\ x_1 &= \frac{3\tau_3'}{\tau_3} \sigma I - 2(\sigma I)^2 \tau_3' + 2\sigma I, \\ x_2 &= 2P_1' + P_2' + \tau_3'P_3' \left( \frac{3}{\tau_3} - 2\sigma I \right), \\ I &= J/\hbar\omega_0.\end{aligned}\quad (2.50)$$

It is necessary to notice that the nontransient solution describes a quasi-stationary fairly slow change of the gain nonlinear medium parameters in time which connects with temperature growth of laser mixture during a radiation pulse

$$\tau_2 = \tau_2(T), \tau_3 = \tau_3(T), \sigma = \sigma(T), D = D(T).$$

*PC reflectivity at DFWM on gain nonlinearity.*

Thus, the PC reflectivity can be calculated by the formula

$$R = \frac{1}{4} J^2 \exp[2(\alpha - \bar{\alpha}_4)L_n] \left[ (\delta\alpha)_1' \right]^2 \frac{\left\{ \exp[(\bar{\alpha}_3 + \bar{\alpha}_4)L_n] - 1 \right\}^2}{(\bar{\alpha}_3 + \bar{\alpha}_4)^2},$$

$$\alpha = \sigma \gamma_1 N e_3,$$

$$\alpha = \frac{\alpha_0}{1 + J/J_s},$$

$$(\delta\alpha)_1' = -\frac{\alpha_0}{(1 + J/J_s)^2} \frac{1}{J_s},$$

$$\alpha_3 = \frac{1}{2} \left\{ \alpha - \frac{1}{2} \frac{\alpha_0}{(1 + J/J_s)^2} \frac{J_1(0)}{\alpha L_n} [\exp(\alpha L_n) - 1] \right\},$$

$$\alpha_4 = \frac{1}{2} \left\{ \alpha - \frac{1}{2} \frac{\alpha_0}{(1 + J/J_s)^2} \frac{J_1(0)}{\alpha L_n} [1 - \exp(-\alpha L_n)] \exp(2\alpha L_n) \right\}.$$

The parameter of nonlinear coupling, in a general case, is obtained from the numerical solution of (2.25) - (2.34).

For a nontransient DFWM on amplitude grating there is a possibility to approximate analytical calculation for  $(\delta\alpha)_1'$  with the simpler and less exact two-level model of the CO<sub>2</sub> laser medium (2.49) (the expression for  $R$  is demonstrated above) or with more exact model taking into consideration a population of a lower laser level (2.50). In both cases an average small signal gain  $\alpha_0$ , an intensity of saturation  $J_s$  and relaxation time  $\tau_3$ , intensity of a pumping wave at an input of interaction region and a length of this region  $L_n$  are used as original parameters.

### 2.2.2 DFWM on phase thermal gratings in the active medium of a EBCD CO<sub>2</sub> laser.

The dependence of heat liberation in CO<sub>2</sub> laser active medium on radiation intensity is due to two physical reasons: a laser induced heating of gas mixture owing to increase of heat liberation rate in a field of a laser radiation and a removal of energy by a laser radiation (laser induced cooling). In other words there are two nonlinear heat liberation channels. The first of them is connected with stimulated transitions of vibrationally excited CO<sub>2</sub> molecules from a upper laser level down to lower one with consequent fast V-T relaxation of deformational mode. The second heat liberation channel is connected with nonradiative V-T relaxation of a upper laser level, its population depending on radiation intensity.

#### *A specific power of heat liberation.*

Quasi-stationary approximation of a population for a lower laser level lies in a basis of the analytical theory of DFWM on thermal nonlinearity as well as in explanation of other effects of thermal laser self-action in CO<sub>2</sub> laser gain medium. The approximation takes into account high V-T relaxation rate of deformational mode. When using a condition  $\frac{d}{dt}e_2 \cong 0$  for the constant radiation intensity and parameters of the medium and input energy, the expression for specific heat liberation power can be found from the linearized kinetics equations (2.7) - (2.9)

$$Q'(J, t) = W \left( \frac{2\omega_2}{\omega_3} \delta_1 + \frac{\omega_2}{\omega_3} \delta_2 \right) + \frac{\omega_3 \tau_3}{\omega_0 \tau_3''} \alpha(0) J_s \exp \left( -\frac{t}{\tau_3'} \right) + \frac{\tau_3'}{\tau_3''} \delta_3 W \left[ 1 - \exp \left( -\frac{t}{\tau_3'} \right) \right], \quad (2.51)$$

$$\tau_3'' = \frac{\tau_3}{1 + \omega_1 J / (\omega_3 J_s)}, \quad \tau_3' = \frac{\tau_3}{1 + J / J_s}, \quad \frac{\omega_3 \tau_3}{\omega_0} \alpha(0) J_s \cong \gamma_1 \hbar \omega_3 N e_3(0),$$

$\alpha(0)$  is a laser gain at  $t = 0$ , which in case of lasing, is equal to threshold value  $\alpha_{th}$ ,  $\hbar\omega_1 \cong 2\hbar\omega_2$ ,  $\hbar\omega_2$ ,  $\hbar\omega_3$  are vibrational quantum energy of symmetric, deformational and antisymmetric modes of a CO<sub>2</sub> molecule.

#### *Two types of nonlinear heat liberation.*

Let's consider nonlinear heat liberation for two characteristic temporal intervals:

$$\tau_2 < t < \tau'_3,$$

$$Q'_n = \frac{\omega_1}{\omega_0} \alpha(0) J + \frac{\omega_1}{\omega_0} \alpha_0 J \frac{t}{\tau_3}; \quad (2.52)$$

$$t > \tau'_3,$$

$$Q'_n = \frac{1 + \omega_1 J / (\omega_3 J_s)}{1 + J / J_s} \frac{\omega_3}{\omega_0} \alpha_0 J_s, \quad (2.53)$$

where  $\frac{\omega_3}{\omega_0} \alpha_0 J_s \cong \delta_3 W$ . It follows from these equations, that in the beginning of pulse

( $t < \tau'_3$ ) laser induced heating of the active medium predominates, i.e. the specific heat liberation rate increases in a field of a laser radiation. When  $t > \tau'_3$  the heating goes on second channel (see chapter 2.1.2). Thus the duration of the process of laser induced heating depends on intensity of a laser radiation and is reduced with its growth.

It is necessary to notice, that in [19, 33] laser induced heating (2.52) only was taken into consideration. At duration of laser pulse ( $\tau_p > \frac{\tau_3}{1 + J/J_s}$ ) that fact leads to an essential error of calculations for thermal self-action, including DFWM. Therefore it is important to take into account two mechanisms of thermal nonlinearity, which are analytically described by the approximate formula (2.51). Nonlinearity  $Q'$  ( $J, t$ ), in a general case has the high order of nonlinearity.

#### *A thermal nonlinearity of CO<sub>2</sub> laser active medium.*

At the DFWM process, when  $J_1, J_2 \gg J_3, J_4$ , the space modulation of intensity (2.6) is small in comparison with intensity of pumping waves. Therefore it causes a space variation of specific heat liberation power which corresponds to a cubic nonlinearity

$$\delta Q' = \frac{\partial}{\partial J} Q' \delta J. \quad (2.54)$$

In turn, spatially modulated heat liberation causes the space modulation of temperature and, respectively, the density of the medium, upon which an index of refraction  $\delta n = k_g \delta \rho$  (where  $k_g$  is Gladstone - Dale coefficient) depends. The set of these physical processes is described by a set of hydrodynamics and heat conductivity equations :

$$\frac{\partial^2}{\partial t^2} \delta\rho - v_s^2 \nabla^2 \delta\rho - \Gamma \nabla^2 \frac{\partial}{\partial t} \delta\rho = v_s^2 \nabla^2 (\beta \rho \delta T), \quad (2.55)$$

$$\frac{\partial}{\partial t} \delta T - \chi \nabla^2 \delta T - \frac{\gamma - 1}{\beta \rho} \frac{\partial}{\partial t} \delta\rho = \frac{1}{\rho C_V} \delta Q', \quad (2.56)$$

where  $v_s$  is a sound speed,  $\Gamma = (\eta + 4\eta'/3)/\rho$ ,  $\eta$ ,  $\eta'$  are shift and volumetric coefficients of viscosity,  $\beta$  is a temperature coefficient of a volumetric extension,  $\gamma = C_p/C_V$ ,  $\chi$  is a temperature conductivity. The set of equations (2.55), (2.56) has characteristic times of transition of acoustic  $\tau_A$  and temperature  $\tau_T$  perturbations ( $\tau_A \ll \tau_T$ ) to a steady state. Therefore at  $t < \tau_A$  temperature conductivity in (2.56) can be ignored and then for a variation of density it is possible to write out the following equation

$$\frac{\partial^2}{\partial t^2} \delta\rho - \gamma v_T^2 \nabla^2 \delta\rho - \Gamma \nabla^2 \frac{\partial}{\partial t} \delta\rho = \frac{\beta}{C_V} v_T^2 \nabla^2 \left( \int \delta Q' dt \right). \quad (2.57)$$

For  $t \gg \tau_A$ , when acoustic perturbations reach a steady state, the equation (2.55) transforms to following one:

$$-\gamma \frac{\partial}{\partial t} \delta\rho + \chi \nabla^2 \delta\rho = \frac{\beta}{C_V} \delta Q'. \quad (2.58)$$

Let's pay attention to the fact, that in equation (2.54) the parameter  $\frac{\partial Q'}{\partial J}$  can be formally considered as a coefficient of an absorption, though with alternating signs and depending upon intensity of pumping waves and time. The calculation of  $\frac{\partial Q'}{\partial J}$  having been done, we obtain from (2.51):

$$\frac{\partial}{\partial J} Q' = \frac{\alpha_0}{1 + J/J_s} \left\{ \frac{\omega_1}{\omega_0} + \frac{\omega_3}{\omega_0} \frac{\tau'_3}{\tau_3} \left[ 1 + \frac{\omega_1}{\omega_3} \frac{J}{J_s} \right] \left[ \exp\left(-\frac{t}{\tau'_3}\right) - 1 \right] \right\}. \quad (2.59)$$

The PC reflectivity at DFWM on thermal nonlinearity of the CO<sub>2</sub> active medium is calculated as well as in the media with an usual linear absorption [16, 34, 35]. However, such possibility takes place only for a simplified model of a kinetics, within the framework of which equation (2.59) is obtained. Therefore, in a general case, it is necessary to apply numerical calculations.

*A definition of medium density variation (a coefficient of nonlinear coupling).*

At first, let's consider analytical approximate solution. One can see from (2.59), that in the beginning of laser pulse at  $t < \tau'_3$  laser induced heating of the medium, described by a positive coefficient of a "absorption" takes place

$$\frac{\partial}{\partial J} Q' = \frac{\omega_1}{\omega_0} \alpha. \quad (2.60)$$

Let's remark, that a thermal nonlinearity of the CO<sub>2</sub> active medium in such form was taken into account in [19, 33]. At duration of pulse  $t > \tau'_3$  the second mechanism of thermal nonlinearity appears, which reduces a heat liberation

$$\frac{\partial}{\partial J} Q' = -\frac{\alpha}{1 + J/J_s}. \quad (2.61)$$

A solution of the equation (2.57) allows us to find a time-history of a density variation growth, connected with a finite speed of an acoustic perturbation propagation, attenuation of  $\delta\rho$  being taken into account here, that can play an essential role.

As well as in case of amplitude gratings, we present a variation of intensity  $\delta J$  as (2.15). Then the variation of specific heat liberation power is written as

$$\delta Q' = \left( \frac{\partial Q'}{\partial J} \right)_1 (\delta J)_1 + \left( \frac{\partial Q'}{\partial J} \right)_2 (\delta J)_2. \quad (2.62)$$

After a substitution (2.62) to (2.58) and (2.59) taking into consideration a rather slow change of density variation amplitudes, temperature and  $\delta Q'$  in space we obtain

$$\begin{aligned} t < \tau_A, \\ \frac{\partial^2}{\partial t^2} (\delta\rho)_i' + \gamma v_T^2 q_i^2 (\delta\rho)_i' + \Gamma q_i^2 \frac{\partial}{\partial t} (\delta\rho)_i' = \\ = -\frac{\beta}{C_V} v_T^2 q_i^2 \int_0^t \left( \frac{\partial Q'}{\partial J} \right)_i' \sqrt{\varphi_0(t')} \sqrt{\varphi_3(t')} dt', \end{aligned} \quad (2.63)$$

$$t > \tau_A,$$

$$-\gamma \frac{\partial}{\partial t} (\delta \rho)_i' - \chi q_i^2 (\delta \rho)_i' = \frac{\beta}{C_V} \left( \frac{\partial Q'}{\partial J} \right)_i' \sqrt{\varphi_0(t')} \sqrt{\varphi_3(t')}. \quad (2.64)$$

$$\left( \frac{\partial Q'}{\partial J} \right)_i' = \frac{\alpha_0}{1 + J_0/J_s} \left\{ \frac{\omega_1}{\omega_0} + \frac{\omega_3}{\omega_0} \frac{\tau'_{3i}}{\tau_3} \left[ 1 + \frac{\omega_1}{\omega_3} \frac{J}{J_s} \right] \exp\left(-\frac{t}{\tau'_{3i}}\right) - 1 \right\}, \quad (2.65)$$

$$\tau'_{3i}{}^{-1} = \frac{1}{\tau_3} + Dq_i^2 = \frac{1 + J/J_s}{\tau_3} + Dq_i^2, \quad Dq_i^2 \tau_2 \ll 1.$$

Further let's assume  $\varphi_0(t) = 1$ ,  $\varphi_3(t) = 1$ . Then (2.63) has a solution of following sort

$$\begin{aligned} (\delta \rho)_i' &= C_1 \exp(a_1 t) + C_2 \exp(a_2 t) + \frac{b_0}{\omega_0^2} - \gamma_0 \frac{b_1}{\omega_0^2} + \\ &+ \frac{b_0}{\omega_0^2} t + b_3 \exp\left(-\frac{t}{\tau'_{3i}}\right), \end{aligned} \quad (2.66)$$

$$a_1 = -\frac{\gamma_0}{2} + \sqrt{\frac{\gamma_0^2}{4} - \omega_0^2}, \quad a_2 = -\frac{\gamma_0}{2} - \sqrt{\frac{\gamma_0^2}{4} - \omega_0^2},$$

$$\gamma_0 = \Gamma q_i^2, \quad \omega_0^2 = \gamma v_T^2 q_i^2,$$

$$b_0 = -\frac{\beta}{C_V} v_T^2 q_i^2 \alpha \frac{\omega_3}{\omega_0} \frac{(\tau'_{3i})^2}{\tau_3} \left( 1 + \frac{\omega_1}{\omega_3} \frac{J}{J_s} \right);$$

$$b_1 = -\frac{\beta}{C_V} v_T^2 q_i^2 \alpha \left[ \frac{\omega_1}{\omega_0} - \frac{\omega_3}{\omega_0} \frac{\tau'_{3i}}{\tau_3} \left( 1 + \frac{\omega_1}{\omega_3} \frac{J}{J_s} \right) \right],$$

$$b_2 = -b_0, \quad b_3 = \frac{b_2 (\tau'_{3i})^2}{1 + \omega_0^2 (\tau'_{3i})^2 - \gamma_0 \tau'_{3i}}.$$

A case of a quasistationary DFWM mode at  $t > (v_T q_i)^{-1}, (\Gamma q_i^2)^{-1}$  represents a practical interest. In this case the expression for  $(\delta \rho)_i'$  is obtained from (2.64)



$$(\delta\rho)_i' = \left[ \frac{d_0}{\chi q_i^2} + \frac{d_1(\tau_{3i}')^2}{1 + \chi q_i^2(\tau_{3i}')^2} \right] \exp(-\chi q_i^2 t) - \frac{d_0}{\chi q_i^2} - \frac{d_1(\tau_{3i}')^2}{1 + \chi q_i^2(\tau_{3i}')^2} \exp\left(-\frac{t}{\tau_{3i}'}\right), \quad (2.67)$$

$$d_0 = \left[ \frac{\omega_1}{\omega_0} - \frac{\omega_3}{\omega_0} \frac{\tau_{3i}'}{\tau_3} \left( 1 + \frac{\omega_1}{\omega_3} \frac{J}{J_s} \right) \right] \alpha,$$

$$d_1 = \frac{\omega_3}{\omega_0} \frac{\tau_{3i}'}{\tau_3} \left( 1 + \frac{\omega_1}{\omega_3} \frac{J}{J_s} \right) \alpha.$$

*Equations for coupled waves.*

For obtaining the equations, describing interaction of waves at DFWM on phase gratings, we use a nonlinear Helmholtz equation of the following sort

$$\nabla^2 E + k^2 \left( 1 + \frac{2\delta n}{n_0} \right) E + ik\alpha E = 0. \quad (2.68)$$

Taking into consideration (2.15) and (2.54), we receive from (2.67) the equations for slow amplitudes of interacting waves in approximation of given pumping condition.

$$\frac{d}{dz} a_1 - \frac{1}{2} \alpha a_1 = 0, \quad (2.69)$$

$$-\frac{d}{dz} a_2 - \frac{1}{2} \alpha a_2 = 0, \quad (2.70)$$

$$\begin{aligned} \frac{d}{dz} a_3 - \frac{1}{2} \alpha a_3 = \frac{ik}{2n_0} & \left[ (\delta n)_1' |a_1|^2 a_3 + (\delta n)_2' |a_2|^2 a_3 + \right. \\ & \left. + (\delta n)_1' a_1 a_2 a_4^* + (\delta n)_2' a_1 a_2 a_4^* \right], \end{aligned} \quad (2.71)$$

$$\begin{aligned} -\frac{d}{dz} a_4 - \frac{1}{2} \alpha a_4 = \frac{ik}{2n_0} & \left[ (\delta n)_2' |a_1|^2 a_4 + (\delta n)_1' |a_2|^2 a_4 + \right. \\ & \left. + (\delta n)_2' a_1 a_2 a_3^* + (\delta n)_1' a_1 a_2 a_3^* \right], \end{aligned} \quad (2.72)$$

$$(\delta n)_i' = k_g (\delta\rho)_i', \quad i = 1, 2.$$

*PC reflectivity at DFWM on thermal nonlinearity.*

Assuming PC reflectivity has a small value  $R \ll 1$  we have from (2.71)

$$R = \frac{k^2}{n_0^2} \left[ (\delta n)_1' + (\delta n)_2' \right]^2 J^2(0) \exp(2\alpha L_n) \left[ \frac{\exp(\alpha L_n) - 1}{\alpha} \right]^2. \quad (2.73)$$

For better understanding we duplicate the expression of  $(\delta n)_i'$  for the case of quasi-stationary DFWM:

$$\begin{aligned} (\delta n)_i' = & k_g \left[ \frac{d_0}{\chi q_i^2} + \frac{d_1 (\tau_{3i}')^2}{1 + \chi q_i^2 (\tau_{3i}')^2} \right] \exp(-\chi q_i^2 t) - \\ & - \frac{d_0}{\chi q_i^2} - \frac{d_1 (\tau_{3i}')^2}{1 + \chi q_i^2 (\tau_{3i}')^2} \exp\left(-\frac{t}{\tau_{3i}'}\right), \end{aligned}$$

$$d_0 = \left[ \frac{\omega_1}{\omega_0} - \frac{\omega_3}{\omega_0} \frac{\tau_{3i}'}{\tau_3} \left( 1 + \frac{\omega_1}{\omega_3} \frac{J}{J_s} \right) \right] \alpha,$$

$$d_1 = \frac{\omega_3}{\omega_0} \frac{\tau_{3i}'}{\tau_3} \left( 1 + \frac{\omega_1}{\omega_3} \frac{J}{J_s} \right) \alpha,$$

$$\tau_{3i}'^{-1} = \frac{1}{\tau_3} + Dq_i^2 = \frac{1 + J/J_s}{\tau_3} + Dq_i^2,$$

$$q_1 = 2k \sin\left(\frac{\theta}{2}\right), \quad q_2 = 2k \sin\left(\frac{\pi - \theta}{2}\right).$$

Approximate analytical solutions obtained for parameters of nonlinear coupling  $(\delta n)_i'$  allow to find not only PC reflectivity  $R$  and its temporal behavior, but also make it easy to analyze a dependence of  $R$  on main parameters of the laser medium. As well as in the case of gain nonlinearity, a degree of gain saturation  $J/J_s$  and thermal grating relaxation time  $(\chi q_i^2)^{-1}$  is very important parameters which influences on time-history and efficiency of DFWM. In comparison with a gain nonlinearity relative large response time and strong (quadratic) dependence on gas

mixture pressure are essential features of a thermal nonlinearity. It takes place because PC reflectivity  $R$  has a maximum at a defined value of  $J/J_s$ , and the intensity of saturation strongly depends on pressure. The decrease of  $J_s$  with lowering of pressure is not compensated by a growth of the parameter of nonlinearity, as it happens at DFWM on amplitude grating.

As the general DFWM feature in a gain gas medium it should be noted a positive influence of mixing wave amplification process on DFWM efficiency, rather long interaction length and high optical quality of the nonlinear medium.

*Equations based on a full kinetic model of a nonlinear medium.*

Let's pass now to a presentation of the numerical theory of DFWM on thermal nonlinearity in the  $\text{CO}_2$  active medium. For more exact account of the DFWM power characteristics on the basis of a full kinetic models we write down the equations (2.25) - (2.30) in the following form [36]

$$\frac{d}{dt}e_4 = F_4(e_3, e_4, T, \rho), \quad (2.74)$$

$$\frac{d}{dt}e_3 = F_3(e_2, e_3, e_4, T, \rho, J), \quad (2.75)$$

$$\frac{d}{dt}e_2 = F_2(e_2, e_3, T, \rho, J), \quad (2.76)$$

$$\frac{d}{dt}T = F_T(e_2, e_3), \quad (2.77)$$

$$\alpha = F_0(e_2, e_3, T, \rho), \quad (2.78)$$

$$Q' = Q'(e_2, e_3, T, \rho). \quad (2.79)$$

The appropriate equations for variations are as follows

$$\frac{d}{dt}(\delta e_4)_i' + Dq_i^2 = \frac{\partial F_4}{\partial e_3}(\delta e_3)_i' + \frac{\partial F_4}{\partial e_4}(\delta e_4)_i' + \frac{\partial F_4}{\partial T}(\delta T)_i', \quad (2.80)$$

$$\begin{aligned} \frac{d}{dt}(\delta e_3)_i' + Dq_i^2 &= \frac{\partial F_3}{\partial e_2}(\delta e_2)_i' + \frac{\partial F_3}{\partial e_3}(\delta e_3)_i' + \frac{\partial F_3}{\partial e_4}(\delta e_4)_i' + \\ &+ \frac{\partial F_3}{\partial T}(\delta T)_i' + \frac{\partial F_3}{\partial J}\sqrt{\varphi_0(t)}\sqrt{\varphi_3(t)}, \end{aligned} \quad (2.81)$$

$$\begin{aligned} \frac{d}{dt}(\delta e_2)_i' + Dq_i^2 = \frac{\partial F_2}{\partial e_2}(\delta e_2)_i' + \frac{\partial F_2}{\partial e_3}(\delta e_3)_i' + \\ + \frac{\partial F_2}{\partial T}(\delta T)_i' + \frac{\partial F_2}{\partial J} \sqrt{\varphi_0(t)} \sqrt{\varphi_3(t)}, \end{aligned} \quad (2.82)$$

$$\delta \alpha = \frac{\partial F_0}{\partial e_2}(\delta e_2)_i' + \frac{\partial F_0}{\partial e_3}(\delta e_3)_i' + \frac{\partial F_0}{\partial T}(\delta T)_i', \quad (2.83)$$

$$\delta Q' = \frac{\partial Q'}{\partial e_2}(\delta e_2)_i' + \frac{\partial Q'}{\partial e_3}(\delta e_3)_i' + \frac{\partial Q'}{\partial T}(\delta T)_i', \quad (2.84)$$

$$\frac{\partial^2}{\partial t^2}(\delta \rho)_i' - v_T^2 \nabla^2 (\delta \rho)_i' - \Gamma \nabla^2 \frac{\partial}{\partial t}(\delta \rho)_i' = v_T^2 \nabla^2 [\beta \rho (\delta T)_i'], \quad (2.85)$$

$$\frac{\partial}{\partial t}(\delta T)_i' - \chi \nabla^2 (\delta T)_i' - \frac{\gamma - 1}{\beta \rho} \frac{\partial}{\partial t}(\delta \rho)_i' = \frac{1}{\rho C_V} (\delta Q')_i'. \quad (2.86)$$

The variable in time coefficients of a nonlinear set of equations are obtained from the numerical solution of the kinetic equations (2.74) - (2.79). For a calculation of a temporal profile of the pumping wave inside a laser resonator the equation system is supplemented by the equation for a laser intensity.

### 2.3. An influence of medium parameters on PC reflectivity at DFWM of CO<sub>2</sub> laser radiation.

In order to get data for DFWM efficiency in the own active medium of EBCD CO<sub>2</sub> laser numerical calculations on the basis of the full mathematical model for amplitude and phase transient gratings (2.25) - (2.34), (2.48), (2.74) - (2.86), (2.73) were carried out. The main parameters of the pulsed EBCD CO<sub>2</sub> laser corresponded to laser setup described in Part 3.

In order to emphasize the main features of DFWM time-history we used a rectangular shape of laser radiation and input power pulses as a first step of the calculation.

A small signal gain calculated for rectangular pulse of specific input power is shown in Fig. 2.1. Time behaviour of PC signal intensity for DFWM at gain and thermal nonlinearity is represented in Fig. 2.2 for different intensities of probe and pump waves and also for different time delays  $\tau_{\text{shift}}$  between the beginning of input energy pulse and pulse of a radiation. Alongside with intensity of mixing waves time delay  $\tau_{\text{shift}}$  is also the important parameter strongly influencing

on DFWM features, because the time delay determines an initial value of a gain. It can be seen from dependencies of Fig. 2.2. At a sufficient intensity of mixing waves a PC signal has a strong spike in a transient part owing to gain nonlinearity. Its relative amplitude depends on intensity of waves and difference between nonsaturated (initial value) and saturated gain (see Fig. 2.3). At rather low intensities ( $J \ll J_s$ ) such feature of a PC signal profile does not take place because a saturation of an amplification is small and the relaxation processes have time to smooth PC intensity pulse in a transient part. The spike of a PC signal, which is characteristic of a gain nonlinearity, is not observed also at a zero time delay, because DFWM begins at the beginning of a laser input pulse. And the change of the gain  $\alpha$  during transient period is not significant. DFWM temporal behaviour in this case is determined by characteristic response time of a

nonlinear medium  $\tau'_3 = \frac{\tau_3}{1 + J/J_s}$  (for dependencies of Fig. 2.2 (a11-c13)  $\tau_3 \approx 45 \mu s$ ,

$J_s \approx 20 \text{ kW/cm}^2$ ). When pressure of laser mixture increasing, vibrational relaxation time of  $\text{CO}_2$  molecule decreases and, as a consequence, a duration of transient period is reduced proportionally to pressure.

All features of DFWM on gain nonlinearity mentioned above can be obtained from the analysis of the formula (2.42) for coefficient of nonlinear coupling (because  $J_4 \sim (\delta\alpha)'_i^2$ ). For short period of time it is possible to neglect an influence of exponential factors under an integral in formula (2.42) and, if consider the form of radiation pulse as being strictly rectangular, the coefficient of nonlinear coupling has values much more higher than for nontransient one. The value is proportional to the difference of  $\alpha(0) - \alpha(t)$ . Just this residual gain determines a character of time-history of PC signal on the initial stage of development of the DFWM process.

It should be noted, that for intracavity DFWM method  $\tau_{\text{shift}}$  is connected with the beginning of laser pulse and initial value of  $\alpha(0)$  is equal to a threshold value.

The dependencies shown in Fig. 2.2 demonstrate, that the transient stage of DFWM on amplitude grating is reduced, firstly, with increase of an initial gain, which is varied by increase of radiation pulse delay in relation to the beginning of input power pulse, and secondly, with a growth of an intensity of pumping waves. Such behaviour is observed at pressure of laser mixture  $p=0.28 \text{ atm}$  and  $p=1 \text{ atm}$ . At some values of an initial gain and intensity of pumping waves the profile of PC pulse front is almost the same, as for a pumping wave or signal wave pulse (it is supposed, that signal and pumping waves pulses have the identical profile).

In Tab. 2.2 the data for PC reflectivity (on intensity and on energy) and intensity of PC signal for different types of nonlinearity, corresponding to dependencies of Fig. 2.2 are represented.

From the analysis of the data one can see, that the PC reflectivity has a maximum on intensity, which corresponds to a value of  $J \approx J_s$ . The influence of time delay appears to be the most strong for gain nonlinearity, especially for peak values of  $J_4$  and  $R$ . It is necessary to notice, that at higher pressure of laser mixture the influence of thermal nonlinearity increases. This influence is reflected both in DFWM time behaviour and in the value of PC reflectivity, the latter reaching the value of  $\sim 1$ . The PC reflectivity on amplitude grating is changed poorly with a growth of pressure. It should be noted, that at values of  $R > 0.5$ , the numerical model described can lead to substantial errors.

All features of DFWM temporal behaviour, mentioned above, take place in case of PC for  $\text{CO}_2$  laser radiation pulses of a real (experimentally measured) temporal profile. The dependencies of PC signal intensity calculated for real experimental conditions (described in Part 3), for various types of nonlinearity are presented in Fig. 2.4 and Fig. 2.5. The influence of laser mixture pressure on DFWM parameters and its temporal behaviour is obtained from the analysis of dependencies in Fig. 2.6 and Fig. 2.7.

In general, the transient theory of DFWM on amplitude and phase gratings in the own  $\text{CO}_2$  active laser medium completely describes main features of this process and allows to receive quantitative data for estimation and optimization of PC reflectivity.

## 2.4. Conclusions.

1. Theoretical research of DFWM in own EBCD  $\text{CO}_2$  laser active medium has allowed to define temporal behaviour of PC wave intensity and PC reflectivity separately on transient gain (amplitude) and thermal (phase) gratings, that is very important for a study of properties of these complicated physical processes of light waves interaction.

2. The numerical calculations have confirmed the assumption that the gain nonlinearity response time can be very low, and it decreases with a growth of the interacted waves intensity and strongly depends on initial (at the moment of DFWM beginning) inversion, i.e. initial gain.

3. The thermal mechanism of nonlinearity caused by two channels of nonlinear heat liberation (by laser induced heating and by laser induced cooling), as more inertial one gives the largest contribution to DFWM for the rear part of a laser pulse.

4. Calculations have shown, that for DFWM process of relatively long pulses of radiation a diffusion of vibrationally excited  $\text{CO}_2$  is very important. On the one hand, it reduces PC reflectivity due to small-scale amplitude grating depressing, and on the other hand increases an amplification of probe and PC waves. It takes place, because due to diffusion, a two-wave interaction decreases,

causing decreasing weak waves for the benefit of strong pumping waves because of their diffraction on own amplitude gratings.

5. As a result of numerical calculations it is found, that the action time of operation of the first nonlinear heat liberation mechanism, connected with laser induced heating of the medium, is reduced with a growth of the pumping waves intensity, and duration of second one, stimulated by laser cooling, grows, on the contrary.

6. A usual amplification of all four interacting waves and a temporal change of saturated gain affected a value of PC reflectivity and its temporal behaviour substantially.

7. The amplitudes of phase and amplitude gratings, and, accordingly, PC reflectivity reach a maximum when saturated gain being,  $\alpha \approx 0.5\alpha_0$ .

8. The results of numerical computations are in a fairly good agreement with temporal profiles of PC wave intensity pulses (see Part 3).

9. Maximal discrepancy between theoretical and experimental data (see Part 3) was observed at high input energies or at high Q-factor, which was varied by changing output mirror reflectivity. Probably, in these cases the additional factors which are not taken into account by theoretical model take place in experiment. These factors depresses DFWM efficiency and for their study additional researches are required.



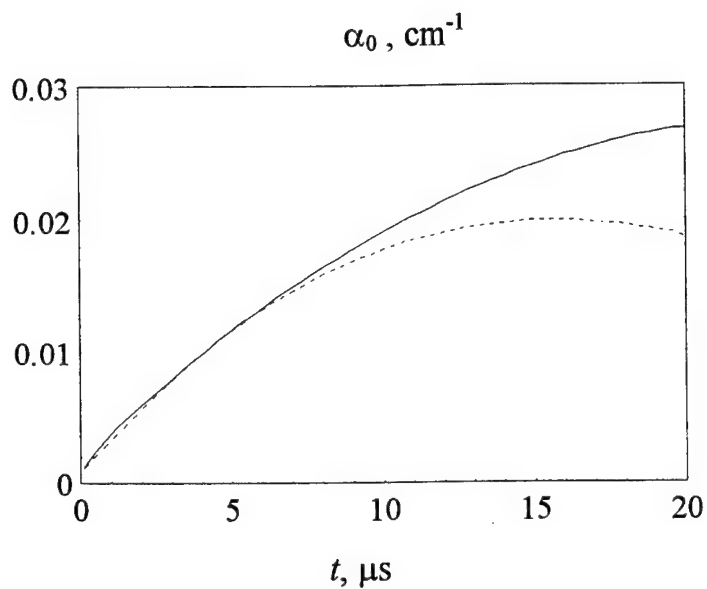


Fig. 2.1. Temporal profile of small signal gain calculated for rectangular profile of specific input power.

Active medium parameters:

Gas mixture  $\text{CO}_2 : \text{N}_2 : \text{He} = 1 : 2 : 4$ ;

Pressure - 0.28 atm ( ————— ),

- 1 atm ( ..... );

Initial temperature - 300 K;

Specific input energy - 120 J/l·atm;

Input power pulse duration - 20 μs.

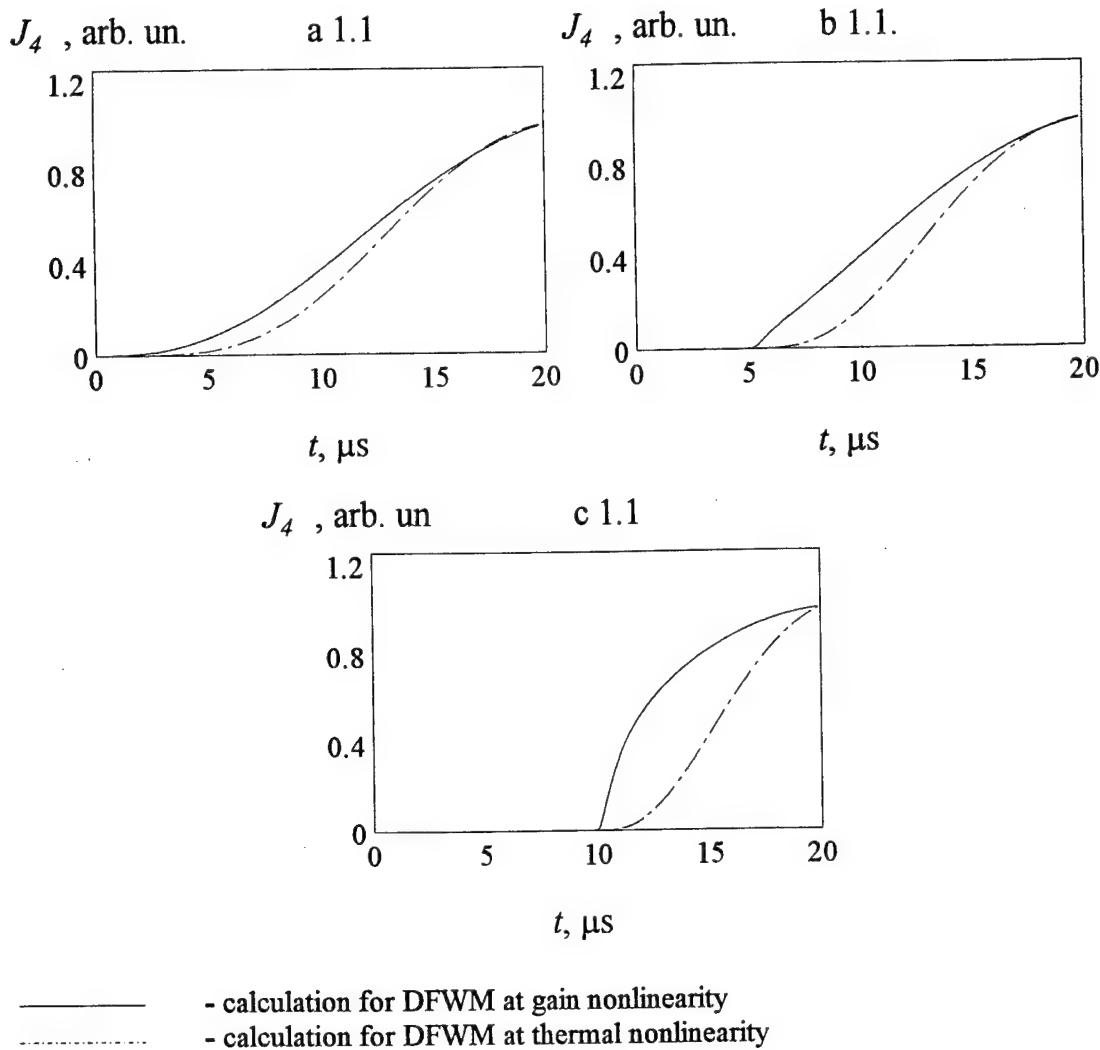


Fig. 2.2.

Theoretical dependencies of signal intensity on time for rectangular profile of the probe, pumping and input power pulses. Influence of different parameters (intensity of probe wave  $J_{30}$ , time delay of probe pulse relative to the beginning of the input power pulse  $\tau_{\text{shift}}$ , pressure  $p$ ) on time-behaviour of DFWM was taking into consideration. A numbering of the curves versus intensity of probe pulse  $J_{30}$  (kW/cm<sup>2</sup>) and time delay of probe pulse  $\tau_{\text{shift}}$  (μs) are presented in Tab. 2.1. The values of PC reflectivity and peak intensity of PC signal for different types of nonlinearity are presented in Tab. 2.2.

Tab. 2.1.

$p = 0.28 \text{ atm}$			
$J_{30} \backslash \tau_{\text{shift}}$	0	5	10
1	a 1.1	b 1.1	c 1.1
5	a 1.2	b 1.2	c 1.2
10	a 1.3	b 1.3	c 1.3

$p = 1 \text{ atm}$			
$J_{30} \backslash \tau_{\text{shift}}$	0	5	10
1	a 2.1	b 2.1	c 2.1
5	a 2.2	b 2.2	c 2.2
10	a 2.3	b 2.3	c 2.3

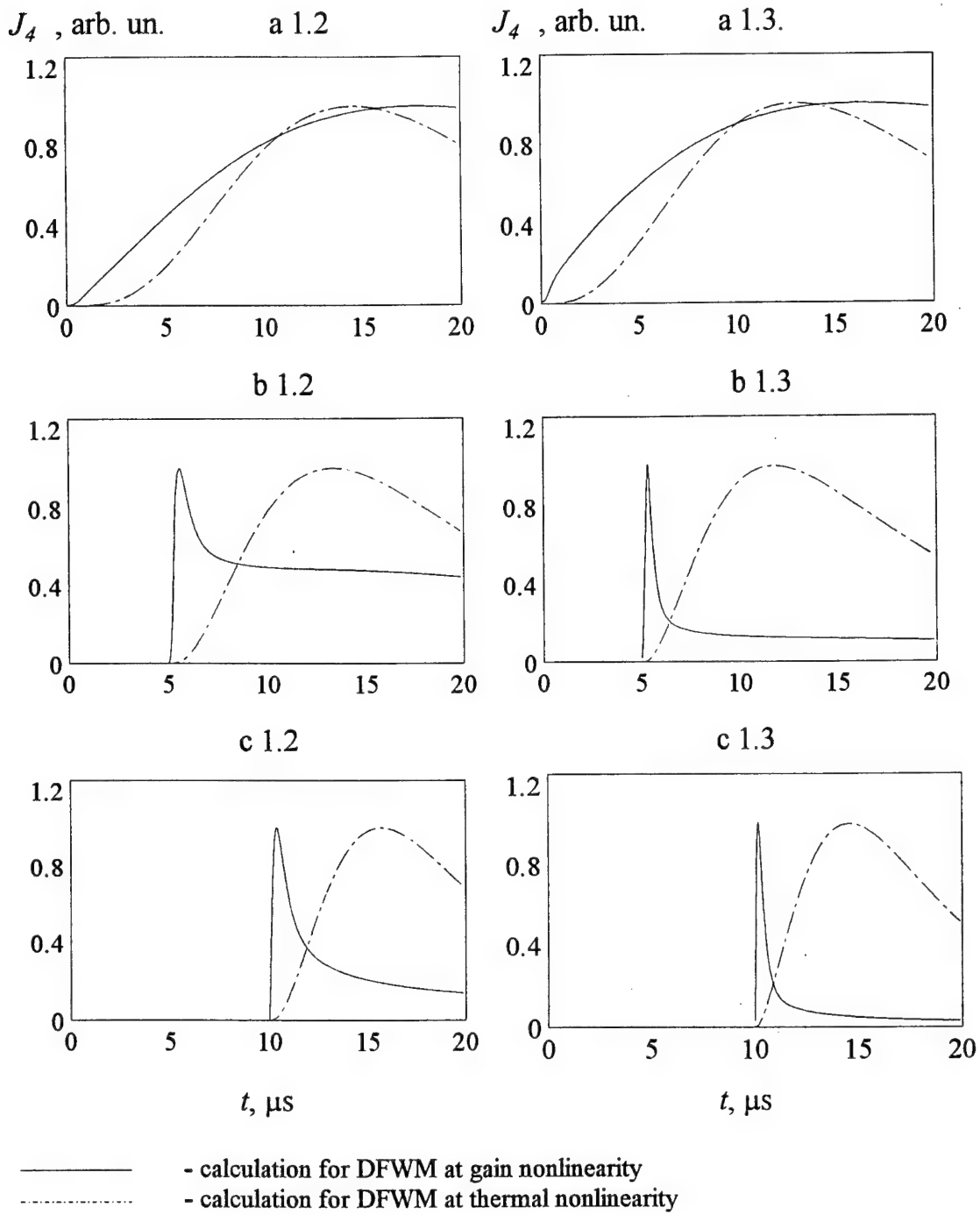


Fig. 2.2 (a 1.2 - c 1.2, a 1.3 - c 1.3).

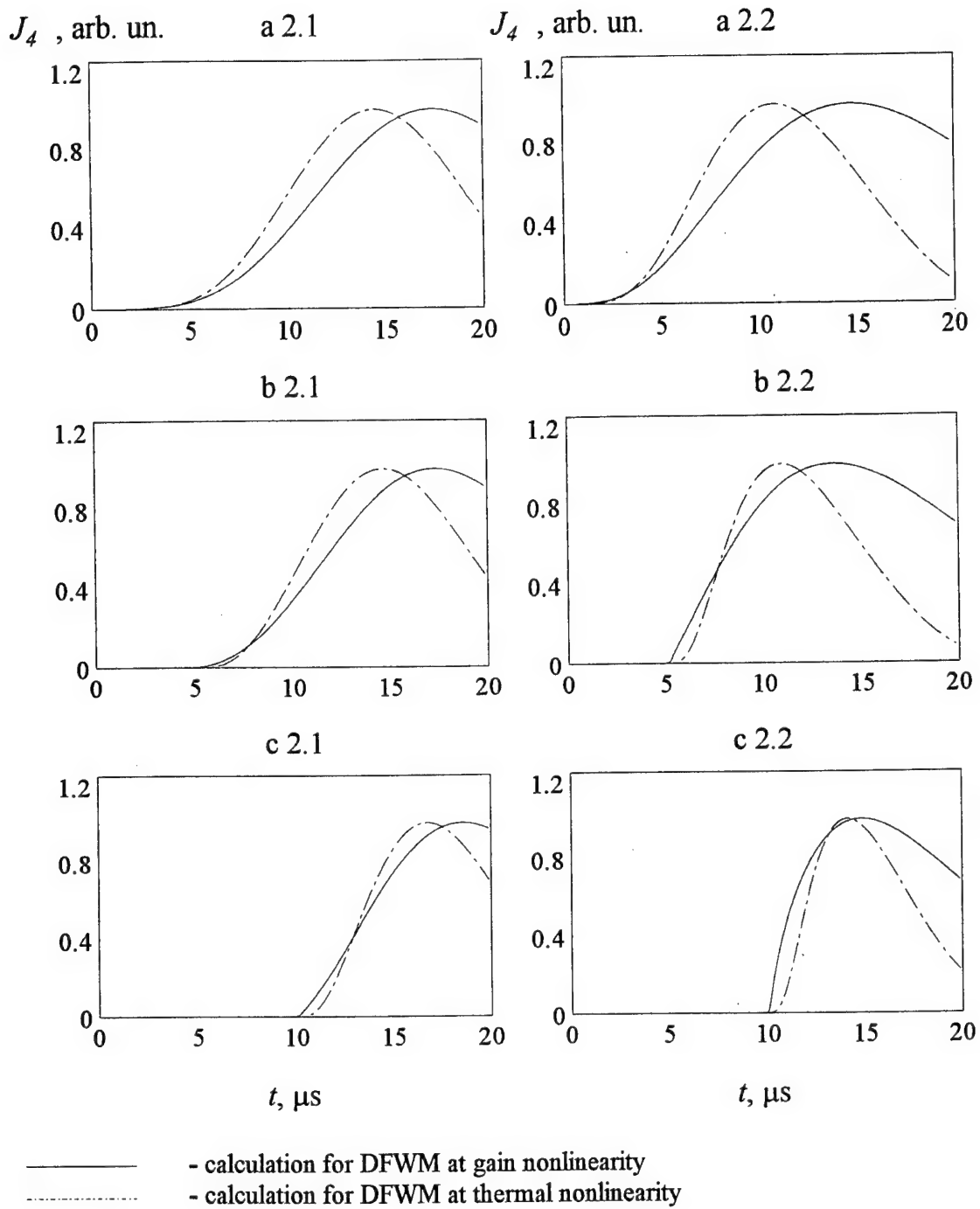


Fig. 2.2 (a 2.1 - c 2.1, a 2.2 - c 2.2).

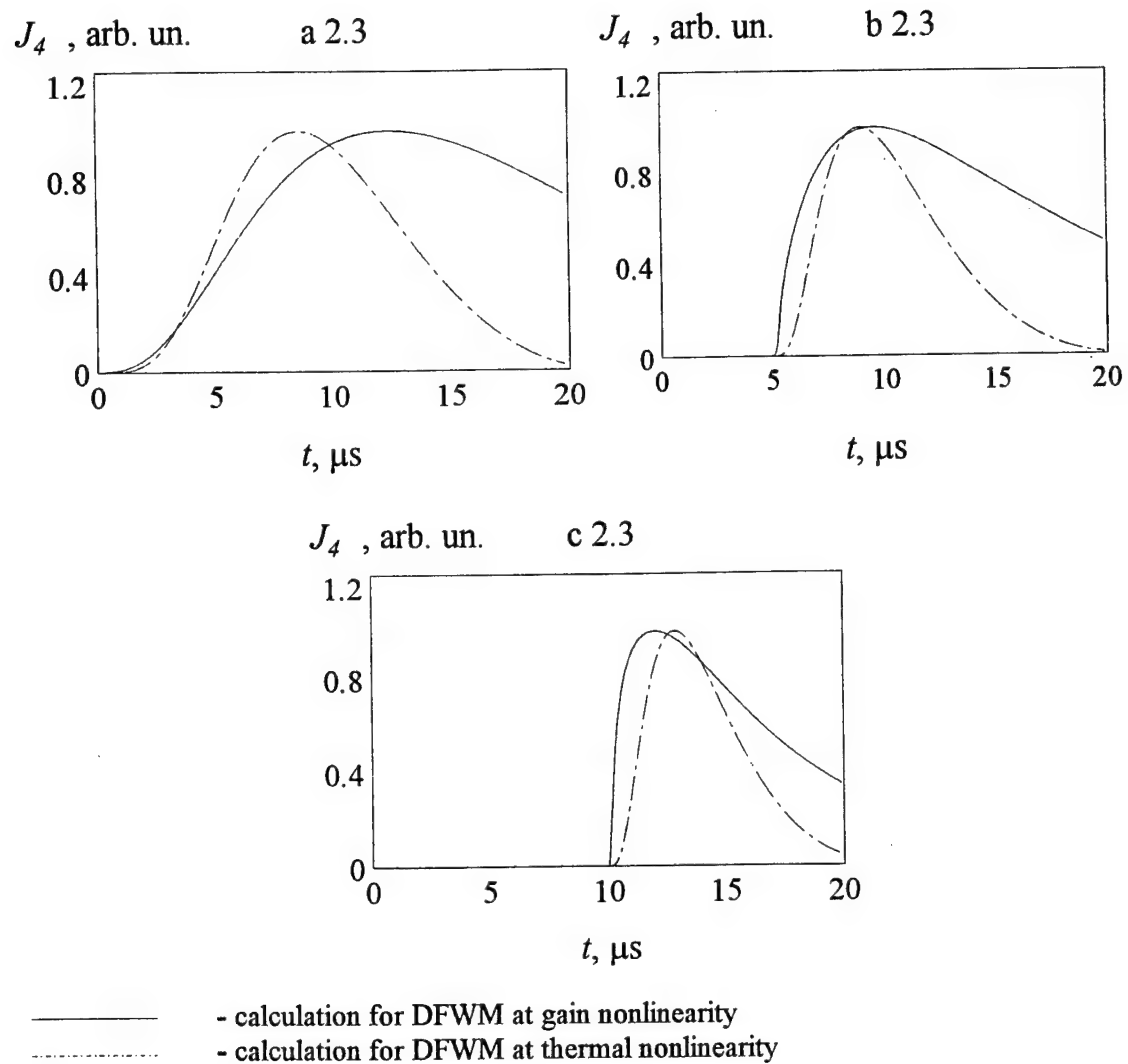


Fig. 2.2 (a 2.3 - c 2.3).

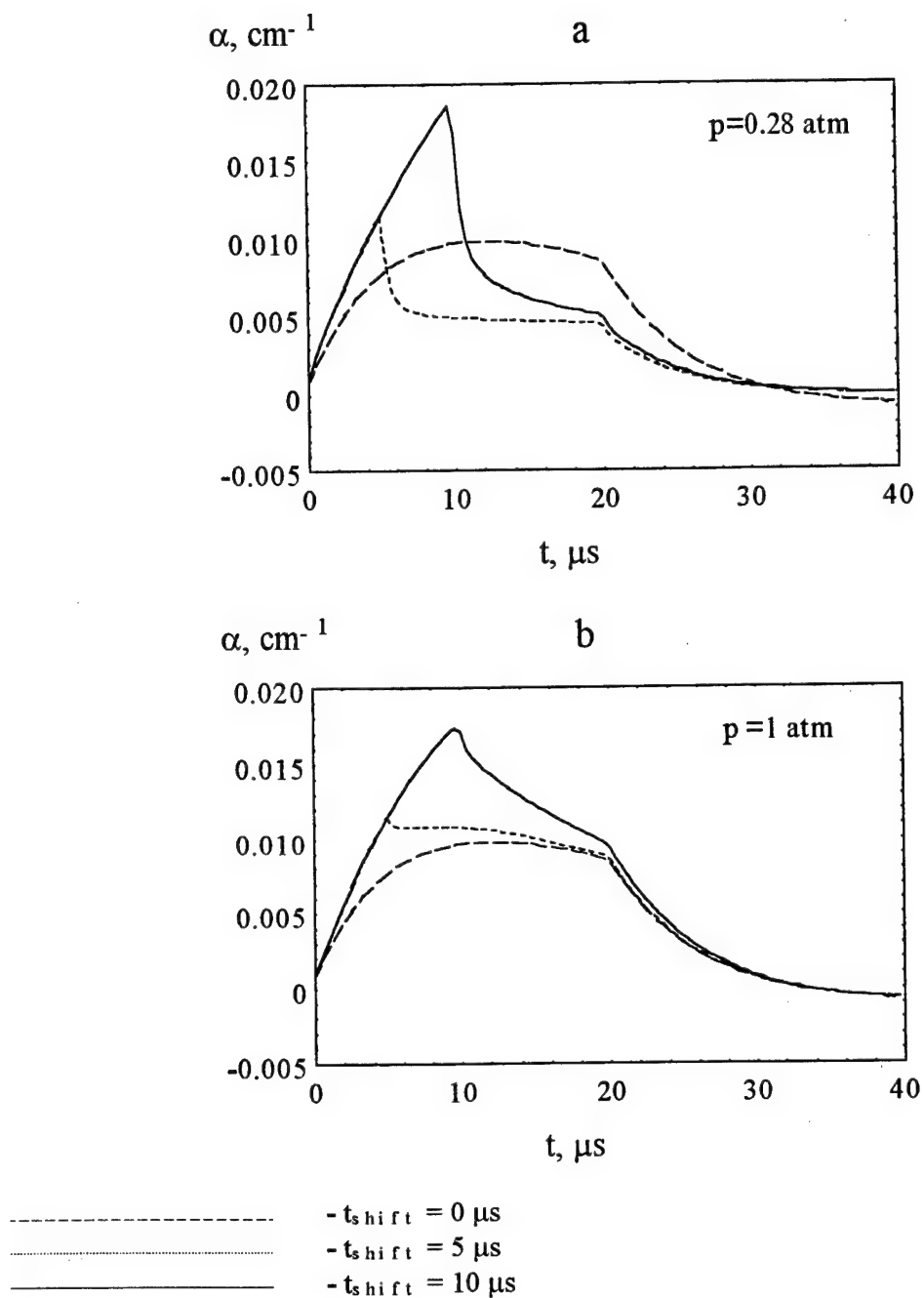


Fig. 2.3.

Time-history of the saturated gain for different values of laser mixture pressure (a - 0.28 atm, b - 1 atm). Calculation of the dependences is made for parameters and conditions used for building of curves in Fig. 2.2 (a 1.2 - c 1.2, a 2.2 - c 2.2).

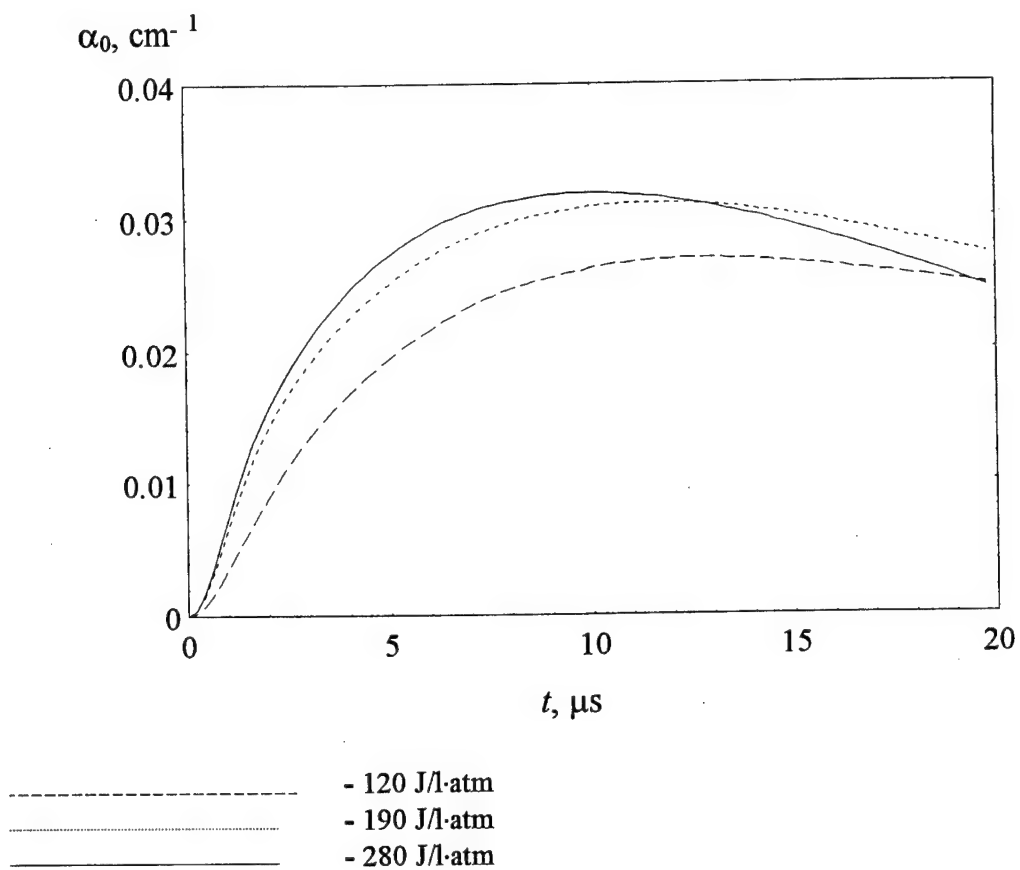


Fig. 2.4.

Temporal profile of small signal gain calculated for different values of specific input energy. A real experimentally measured time-history of specific input power was used in the calculations.

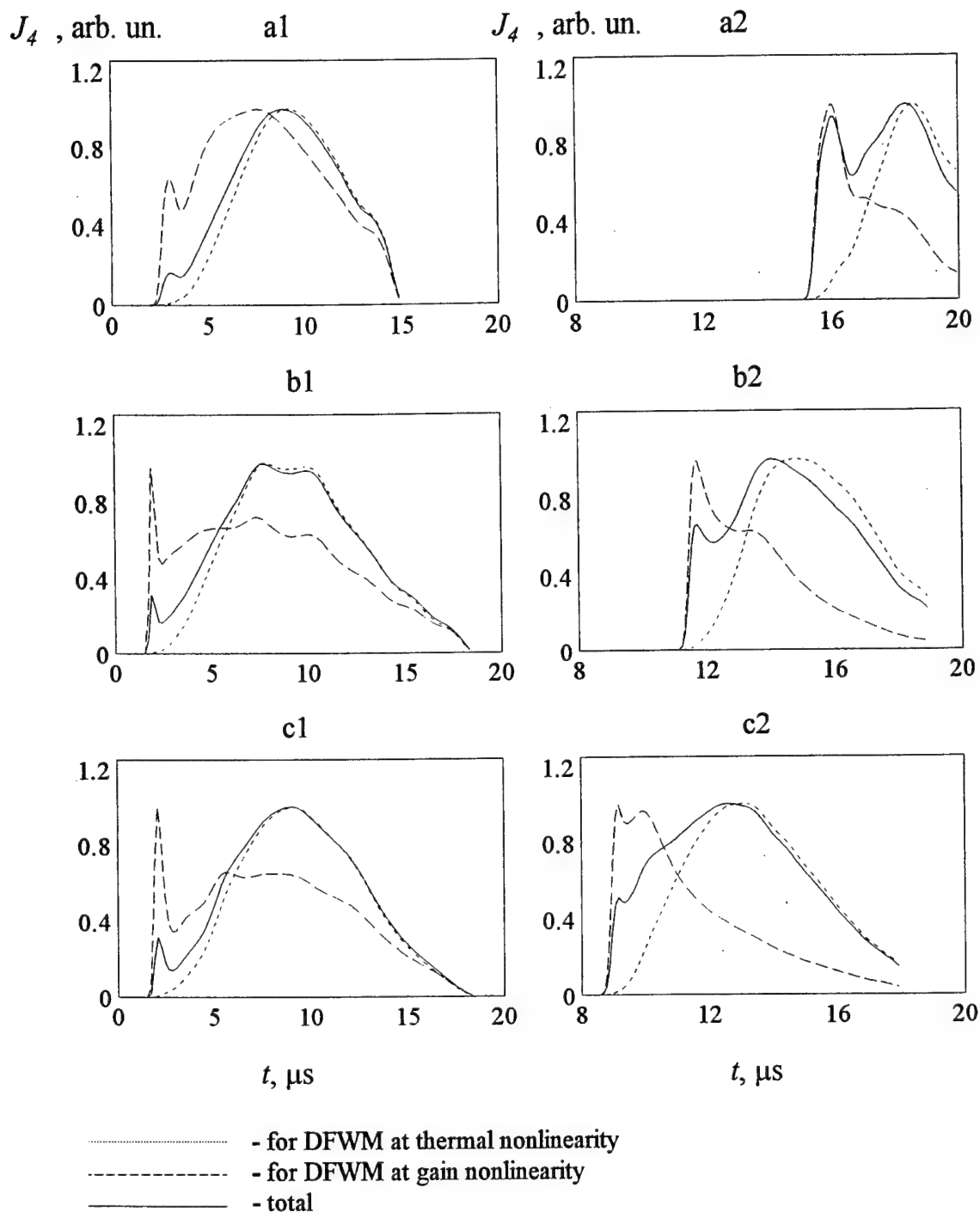


Fig. 2.5.

Temporal profiles of PC pulses calculated for two various laser output mirror (1 - 65%, 2 - 7.5%) and different values of specific input energy (a - 120 J/l·atm, b - 190 J/l·atm, c - 280 J/l·atm).

PC reflectivity and peak intensity of PC signal calculated for different types of nonlinearity are presented in Tab. 2.3. The values of main parameters used in calculations are listed in the same table.



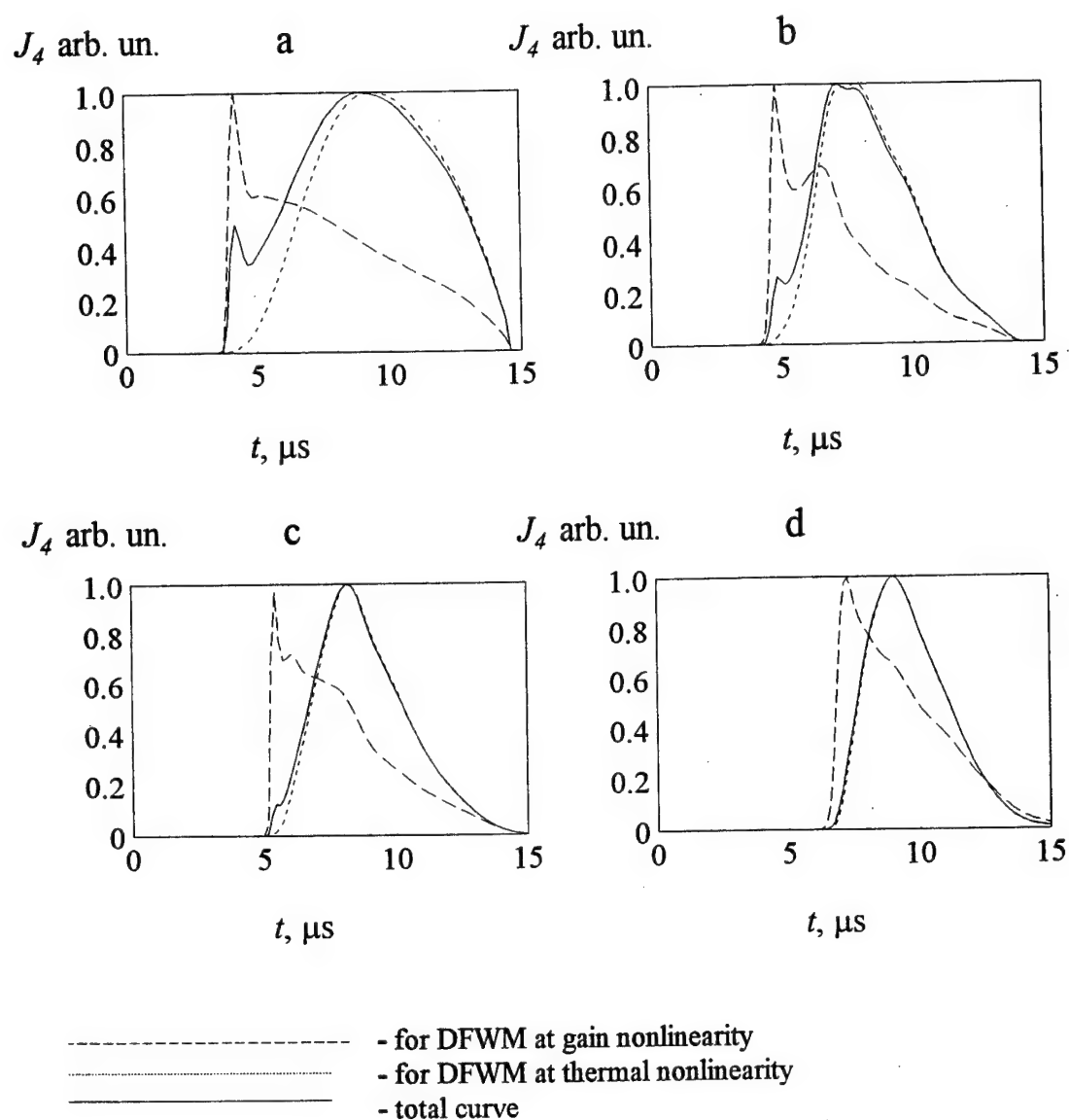


Fig. 2.6.

Temporal profile of intensity of PC signal calculated for different values of laser mixture pressure:

a - 0.28 atm,

b - 0.42 atm,

c - 0.56 atm,

d - 0.8 atm.

The real experimental conditions described in Part 3 are used for calculations. The values of intensity of PC signal and PC reflectivity are presented in Tab. 2.4, also main parameters used for calculation of dependencies in Fig. 2.6 are listed in it.

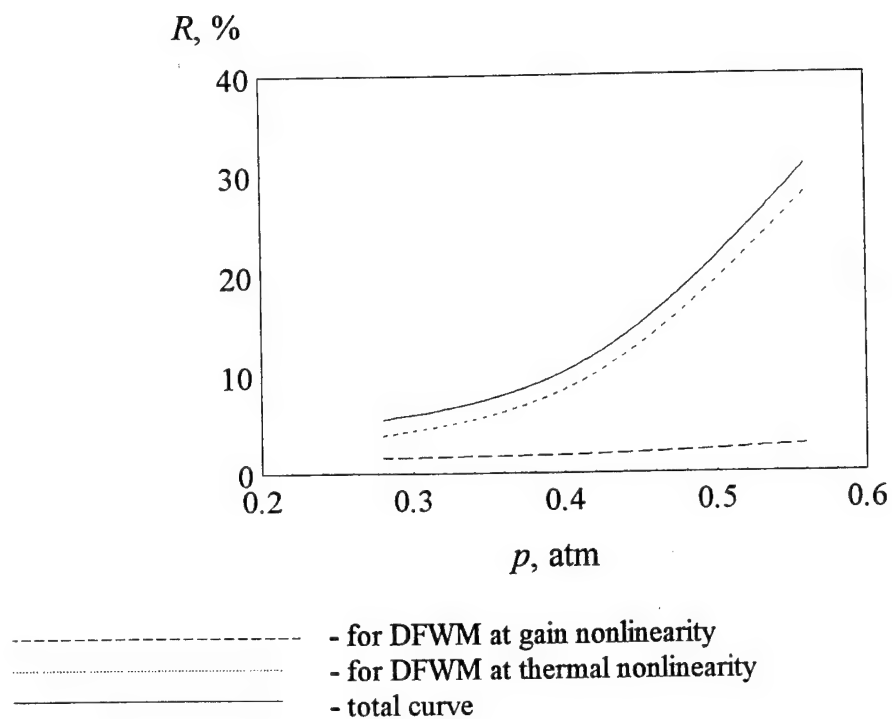


Fig. 2.7.

Calculated PC reflectivity (on energy) versus gas mixture pressure. The main parameters used for calculations are listed in Tab. 2.4.

Tab. 2.2. (with graphic illustrations)

**Active medium parameters and DFWM conditions:**

Gas mixture  $\text{CO}_2 : \text{N}_2 : \text{He} = 1 : 2 : 4$ . Initial temperature - 300 K.

Specific input energy - 120 J/l·atm. Input power pulse duration - 20  $\mu\text{s}$ .

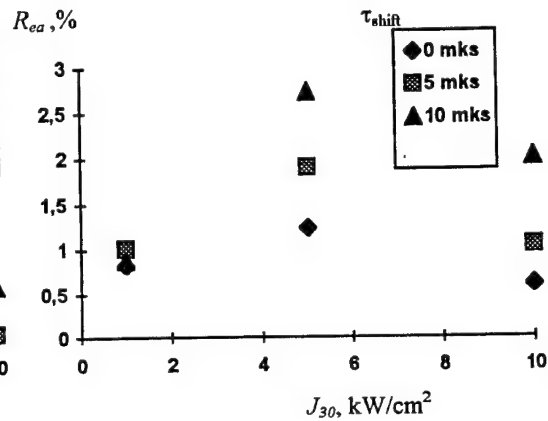
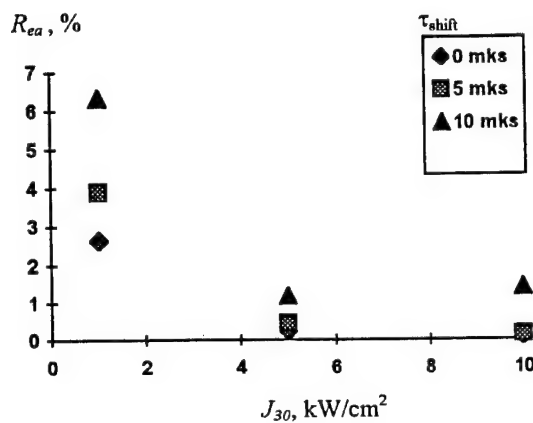
Interaction length - 70 cm. Relaxation time of thermal grating - 70  $\mu\text{s}$  ( $p = 0.28$  atm).

Intensity ratio for probe and pumping waves ( $J_{30}/J_{10}$ ) - 0.1.

**a). PC reflectivity (on energy)  $R_{ea} = E_{4\omega}/E_{3\omega}$  (%) for DFWM at gain nonlinearity**

$p = 0.28$ atm			
$J_{30} \backslash \tau_{\text{shift}}$	0	5	10
1	2.63	3.91	6.33
5	0.26	0.46	1.17
10	0.07	0.14	1.41

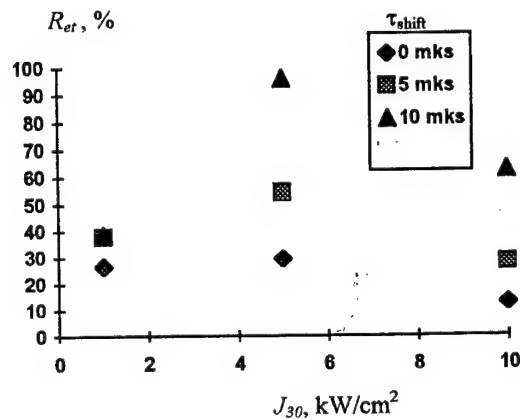
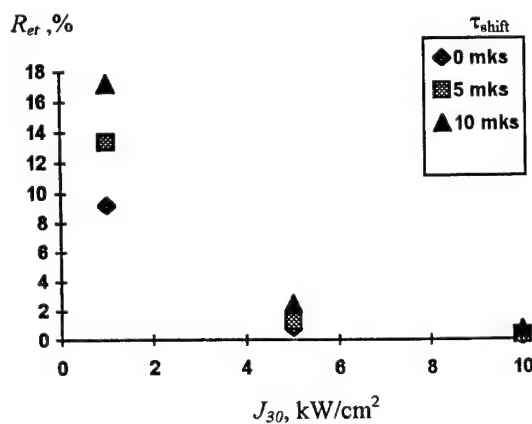
$p = 1$ atm			
$J_{30} \backslash \tau_{\text{shift}}$	0	5	10
1	0.83	1.01	0.88
5	1.23	1.89	2.73
10	0.60	1.04	2.00



**b). PC reflectivity (on energy)  $R_{et} = E_{4\omega}/E_{3\omega}$  (%) for DFWM at thermal nonlinearity**

$p = 0.28$ atm			
$J_{30} \backslash \tau_{\text{shift}}$	0	5	10
1	9.23	13.33	17.23
5	0.77	1.28	2.45
10	0.20	0.33	0.68

$p = 1$ atm			
$J_{30} \backslash \tau_{\text{shift}}$	0	5	10
1	26.85	37.66	38.85
5	29.41	54.38	96.20
10	12.92	27.86	62.81



Tab. 2.2. (continuation)

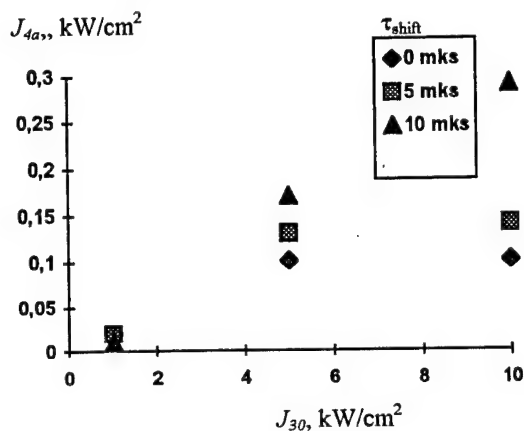
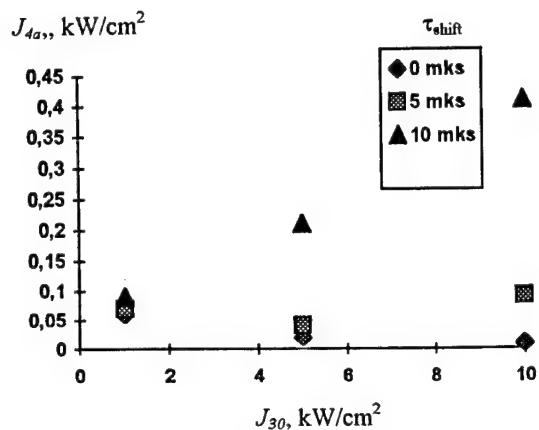
c). PC intensity  $J_{4a}$  (kW/cm<sup>2</sup>) for DFWM at gain nonlinearity

$p = 0.28 \text{ atm}$

$J_{30} \backslash \tau_{\text{shift}}$	0	5	10
1	0.06	0.07	0.09
5	0.02	0.04	0.21
10	0.01	0.09	0.41

$p = 1 \text{ atm}$

$J_{30} \backslash \tau_{\text{shift}}$	0	5	10
1	0.02	0.02	0.01
5	0.10	0.13	0.17
10	0.10	0.14	0.29



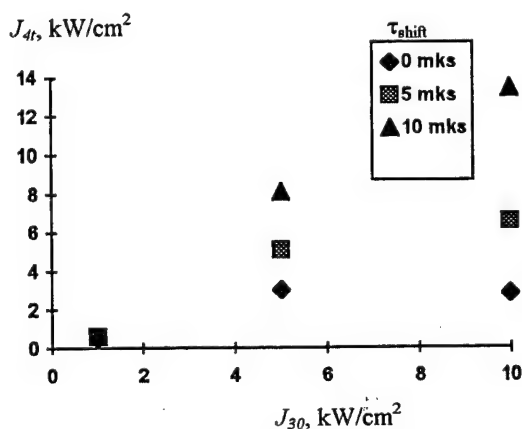
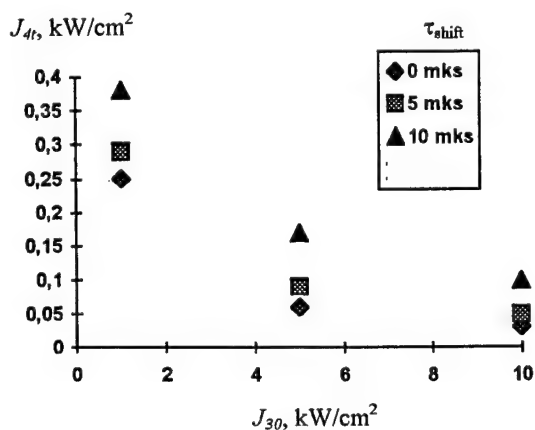
d). PC intensity  $J_{4t}$  (kW/cm<sup>2</sup>) for DFWM at thermal nonlinearity

$p = 0.28 \text{ atm}$

$J_{30} \backslash \tau_{\text{shift}}$	0	5	10
1	0.25	0.29	0.38
5	0.06	0.09	0.17
10	0.03	0.05	0.10

$p = 1 \text{ atm}$

$J_{30} \backslash \tau_{\text{shift}}$	0	5	10
1	0.57	0.65	0.62
5	3.02	5.06	8.14
10	2.85	6.60	13.43



Tab. 2.3.

Gas mixture  $\text{CO}_2:\text{N}_2:\text{He}=1:2:4$ .

Initial temperature - 300 K.

Pressure - 0.28 atm.

Specific input energy:

120 J/l·atm (a),

190 J/l·atm (b),

280 J/l·atm (c).

Interaction length - 70 cm.

Laser output mirror reflectivity:

65% (1),

7.5% (2).

Interaction angle -  $1^\circ$ .

Relaxation time of thermal grating - 70  $\mu\text{s}$ .

a). PC reflectivity (on energy)  $R_{ea}=E_{4a}/E_{30}$  (%), calculated for DFWM at gain nonlinearity (the numbers of curves for Fig. 2.5 is in brackets).

	120 J/l atm	190 J/l atm	280 J/l atm
$R_{out}=65\%$	(a1) 1.91	(b1) 1.50	(c1) 1.66
$R_{out}=7.5\%$	(a2) 1.50	(b2) 4.29	(c2) 3.50

b). PC reflectivity (on energy)  $R_{et}=E_{4t}/E_{30}$  (%), calculated for DFWM at thermal nonlinearity (the numbers of curves for Fig. 2.5 is in brackets).

	120 J/l atm	190 J/l atm	280 J/l atm
$R_{out}=65\%$	(a1) 5.04	(b1) 3.94	(c1) 4.70
$R_{out}=7.5\%$	(a2) 1.35	(b2) 7.29	(c2) 8.48

c). Peak PC intensity  $J_{4a}$  ( $\text{W}/\text{cm}^2$ ), calculated for DFWM at gain nonlinearity (the numbers of curves for Fig. 2.5 is in brackets).

	120 J/l atm	190 J/l atm	280 J/l atm
$R_{out}=65\%$	(a1) 14.7	(b1) 25.3	(c1) 38.5
$R_{out}=7.5\%$	(a2) 27.9	(b2) 263.0	(c2) 372.1

d). Peak PC intensity  $J_{4t}$  ( $\text{W}/\text{cm}^2$ ), calculated for DFWM at thermal nonlinearity (the numbers of curves for Fig. 2.5 is in brackets).

	120 J/l atm	190 J/l atm	280 J/l atm
$R_{out}=65\%$	(a1) 48.5	(b1) 61.6	(c1) 99.4
$R_{out}=7.5\%$	(a2) 21.1	(b2) 281.7	(c2) 618.8

e). Peak PC reflectivity (on intensity)  $R_a=J_{4a}/J_{30}$  (%), calculated for DFWM at gain nonlinearity (the numbers of curves for Fig. 2.5 is in brackets).

	120 J/l atm	190 J/l atm	280 J/l atm
$R_{out}=65\%$	(a1) 2.46	(b1) 2.21	(c1) 2.39
$R_{out}=7.5\%$	(a2) 2.02	(b2) 6.69	(c2) 7.57

Tab. 2.3. (continuation)

f). Peak PC reflectivity (on intensity)  $R_t = J_{4t}/J_{30}$  (%), calculated for DFWM at thermal nonlinearity (the numbers of curves for Fig. 2.5 is in brackets).

	120 J/l atm	190 J/l atm	280 J/l atm
$R_{out}=65\%$	(a1) 10.40	(b1) 8.33	(c1) 9.79
$R_{out}=7.5\%$	(a2) 5.44	(b2) 14.87	(c2) 13.09

g). Peak PC reflectivity (on intensity)  $R = J_4/J_{30}$  (%), calculated for DFWM at both types of nonlinearity (the numbers of curves for Fig. 2.5 is in brackets).

	120 J/l atm	190 J/l atm	280 J/l atm
$R_{out}=65\%$	(a1) 12.85	(b1) 10.54	(c1) 12.17
$R_{out}=7.5\%$	(a2) 6.83	(b2) 17.08	(c2) 15.64

Tab. 2.4.

Gas mixture  $\text{CO}_2:\text{N}_2:\text{He}=1:2:4$ .

Initial temperature - 300 K.

Pressure - 0.28 atm.

Specific input energy - 120 J/l·atm .

Interaction length - 70 cm.

Laser output mirror reflectivity 65% .

Interaction angle -  $1^\circ$ .

Relaxation time of thermal grating - 70  $\mu\text{s}$ .

The table presents dependences of following parameters on gas pressure:

- peak PC reflectivity (on intensity)  $R_a = J_{4a}/J_{30}$  (%), calculated for DFWM at gain nonlinearity;
- peak PC reflectivity (on intensity)  $R_t = J_{4t}/J_{30}$  (%), calculated for DFWM at thermal nonlinearity ;
- peak PC reflectivity (on intensity)  $R = J_4/J_{30}$  (%), calculated for DFWM at both types of nonlinearity;
- PC reflectivity (on energy)  $R_{ea} = E_{4a}/E_{30}$  (%), calculated for DFWM at gain nonlinearity;
- PC reflectivity (on energy)  $R_{et} = E_{4t}/E_{30}$  (%), calculated for DFWM at thermal nonlinearity;
- peak intensity of PC signal  $J_{4a}$  ( $\text{W}/\text{cm}^2$ ), calculated for DFWM at gain nonlinearity;
- peak intensity of PC signal  $J_{4t}$  ( $\text{W}/\text{cm}^2$ ), calculated for DFWM at thermal nonlinearity.

p, atm	$J_{4a}$	$J_{4t}$	$R_{ea}$	$R_{et}$	$R_a$	$R_t$	$R$
0.28	0.38	0.63	1.62	3.84	2.84	5.92	7.28
0.42	0.85	3.25	1.88	10.03	3.88	13.51	14.76
0.56	1.53	12.96	2.75	28.13	5.53	45.43	48.65
0.80	2.87	45.79	4.48	91.73	8.28	161.62	166.72

### 3. Experimental investigation of PC at DFWM of pulsed CO<sub>2</sub> /CO laser radiation inside its inverted medium

In this part we present results of parametric study of PC process under DFWM inside own active medium of the pulsed EBCD CO<sub>2</sub> and CO lasers. The main objective of this part is to investigate experimentally the phenomena associated with DFWM of CO<sub>2</sub> and CO lasers radiation in their active medium, to define the relative role of two physical mechanisms (amplitude and phase one) in PC process and investigate an influence of different parameters (gas mixture content, gas pressure, input energy, interaction angle etc.) upon energetic and temporal characteristics of PC signal. The main attention in this part we pay to CO<sub>2</sub> laser as a simpler laser system as compared to CO laser. The part of the report includes:

- description of the experimental laser setup, the test equipment and the experimental techniques;
- properties of the CO<sub>2</sub> active medium and that of the laser output;
- experimental results on PC for CO<sub>2</sub> laser;
- experimental results on PC for CO laser.

Most of the experimental results are shown in diagrams. Also some experimental data for several diagrams are presented in tables for a further theoretical analysis.

#### 3.1. Experimental laser setup

##### *EBCD laser chamber*

Our experiments were carried out with the pulsed electron-beam controlled discharge (EBCD) CO<sub>2</sub>/CO laser installation shown schematically in Fig. 3.1. This installation consisted of the vacuum electron gun chamber (1) containing the laser chamber (2) and the hot cathode (3) over it. The chambers were made from a stainless steel. The laser chamber was made in a shape of 1.35 m (length) x 0.35 m (in diameter; outward size) cylinder and was placed on the bottom of the electron gun chamber. The internal volume of the laser chamber was about 0.15 m<sup>3</sup> and the discharge volume was 1200 (length) x 140 (width) x 110 (height) mm<sup>3</sup> = 18.5 liters. The EBCD chamber had NaCl windows (4) that were oriented at the Brewster angle to the optical axis of the laser resonator in the most of the experiments (see chapter 3.2.6 of the report for other cases). The internal volume of the vacuum electron gun chamber was 1.5 (length) x 0.5 (width) x 0.7 (height) m<sup>3</sup>.

The EBCD took place between the mesh grounded cathode (5) and the copper anode (6). An electron beam penetrated into the laser chamber through the polyimide foil (7) of 40 μm thickness

pressed to this chamber by stainless steel flange with a lot of holes (e-beam transparency is about 40%). The e-beam current density in the laser chamber was  $10 \text{ mA/cm}^2$ . The EBCD electrical supply system is schematically presented in Fig. 3.2. The capacitor bank (1) was charged by the current rectifier (2) up to a high voltage of 50 kV. The capacity of the bank was usually  $21 \mu\text{F}$ . The gas pressure in the laser chamber did not exceed 0.8 atm on account of technical reason.

The laser chamber was designed for a CO laser as well. It had "jacket" surrounding the chamber and could be cooled down to 100 K by liquid nitrogen.

### *Electron-beam gun*

150 keV electron beam was formed by a hot cathode (3 in Fig. 3.1). The 1 m long cathode was fixed in the upper part of the e-beam gun chamber through a current supply channel with a high voltage isolation (8 in Fig. 3.1). It consisted of 0.5 mm diameter tungsten wires. We used three wires with the 3 cm gap between each other and parallel connected to the power source. The edges of the cathode as well as the sharp parts inside the vacuum chamber were protected by electrostatic screens. The gap between the thermoionic cathode and the laser chamber was 12 cm.

The e-beam gun supply system are schematically presented in Fig. 3.3. The e-beam gun was supplied by high voltage four-stage Marks generator (7) with the capacity of  $0.1 \mu\text{F}$ . The  $65 \Omega$  ballast resistor R (5) protected the foil in the case of a breakdown in the vacuum chamber. The hot cathode (2) of the e-beam gun was powered through a 13 kW current transformer (6) with a high voltage air isolation between the windings. The e-beam accelerating voltage had approximately a triangular form with the amplitude of 150 kV. The pulse duration of e-beam current was limited by a foil cut-off for electrons with energy less than 90 keV. The e-beam pulse duration was controlled by the heating power of the hot cathode in the range from 10 up to 1000  $\mu\text{s}$ .

### *Test equipment and experimental techniques*

The test equipment included calorimeters, photodetectors,  $\text{CO}_2/\text{CO}$  laser spectrometer, storage oscilloscopes and infra-red (IR) video system.

The laser output energy was measured by the calorimeter with sensitivity of 2 mJ and relative accuracy of 6%. The PC signal energy was measured by the calorimeter with sensitivity down to 0.1 mJ. The calorimeters were connected to a digital voltmeter.



The temporal characteristics were measured with a liquid-nitrogen cooled Ge-Au photodetector with a response time of 0.1-1  $\mu$ s. The high frequency component of a laser pulse was displayed by a photon-drag detector (response time  $\sim$ 1 ns).

To display all the lasing transitions of the laser the grating CO<sub>2</sub>/CO spectroscopy "CO Laser Spectrum Analyzer (Model 16-C)" was used. It was calibrated both in wavelength and rotational line designation to permit identification of laser transitions both between 5.0 and 5.7 microns and between 9.1 and 11.3 microns.

A degree of a linear polarization of a laser beam  $\gamma_p$  was analyzed with a plane plate (ZnSe, Si or Ge) oriented at Brewster's angle to the optical axis of the beam. To analyze an orientation of the polarization plane it was possible to rotate the plane plate (analyzer) around the axis of the laser beam. The plane of polarization was found when the energy of the signal reflected from the analyzer had a minimal value  $Q_{\perp}$ . Then the degree of linear polarization was estimated as the following ratio:

$$\gamma_p = \frac{|Q_{\parallel} - Q_{\perp}|}{Q_{\parallel} + Q_{\perp}} \quad (3.1),$$

where  $Q_{\perp}$  - the energy of reflected from the analyzer when its incident plane was oriented perpendicular to the polarization plane.

To record an IR distribution of laser output an IR video system was used. This system consisted of :

- IR video camera "THERMOCAM" which transforms an IR distribution to a video signal;
- TV monitor to display the video signal;
- VCR to record the video signal;
- digitizer of the video signal for a computer analysis;
- computer with a software to analyze the digital signal.

IR video camera is a sensitive photodetector of a thermal radiation. It was used to transform a slow altered thermal signal of an extended object into a video signal. The advantages of the system were the high sensitivity in IR range and the linear transformation of IR signal into video signal. The disadvantages were as follows:

- absence of synchronization between recording and beginning of the laser output pulse that gave us different "blurring" of a distribution image;
- high sensitivity of IR video camera required us to use a diffusely scattering screen, but a coherent radiation of a laser acquires a spot structure during diffuse reflection which distorts the distribution image.

The IR distribution of the laser output was measured by directing the laser beam to a diffusely scattering screen. The IR video was located near the screen ( $\sim 0.3$  m). The scattered radiation image was transformed by IR video camera into a video signal. Then the video signal was digitized for subsequent computer processing. To compare the distributions of the different laser beams they were recorded simultaneously with equalizing their intensities with calibrated attenuators. Thus we registered both probe and backscattered signals simultaneously. To decrease a "blurring" error and to compare IR distributions of the signals their position on the screen was chosen by such a way that both images were displayed at the same lines of video scanning.

The digitized image of IR distribution allows other techniques to determine PC reflectivity on energy. One of them uses ratio between peak values of both signals and it will be called in this paper as "peak reflectivity". Another technique takes into account a shape of the signals, i.e. PC reflectivity may be calculated as ratio of signals which was integrated on surface of image. The technique will be called in this paper as "integrated reflectivity". The integrated reflectivity can be calculated more simpler if the surface integration is changed with multiplication of peak value by squared full width of half maximum (FWHM).

The digitized image of IR distribution in far-field zone allows us to compare an angular divergency of the PC signal and that of the probe one. In fact an angular divergency of a laser beam is proportional to FWHM of the digitized image. A ratio between a FWHM of the probe signal and that of the PC signal was used to estimate an optical quality of the PC mirror.

### **3.2. PC at DFWM inside inverted medium of EBCD CO<sub>2</sub> laser**

#### **3.2.1. Characteristics of active medium of CO<sub>2</sub> laser**

An active medium of a molecular gas CO<sub>2</sub> laser is a gas mixture with an inverted population of energy levels. A CO<sub>2</sub> laser gas mixture includes carbon dioxide, nitrogen and helium. The laser gas mixture CO<sub>2</sub> : N<sub>2</sub> : He = 1 : 2 : 4 was usually used in our experiments. The pressure of the laser gas mixture was 0.28 atm in the most of the experiments. The initial gas temperature was about 300 K. Hereinafter these gas parameters will be considered as so-called "default" parameters (we use a computer slang word here, which means that if it is not specially pointed, those parameters characterize experiment being discussed). In some experiments (see chapter 3.2.6 of the report) the gas mixture and the gas pressure were varied.

To create an inversion population of energy levels in our CO<sub>2</sub> laser gas mixture we used an electron beam controlled discharge (see chapter 3.1 of the report). An active medium of an EBCD laser is characterized by a specific input energy and a small signal gain.

### *Input energy*

A specific input energy (SIE) is a gas discharge parameter that is determined as an input energy divided per one unit of a discharge volume (1 liter) and per one unit of a gas pressure (1 atm = 0.1013 MPa). The specific input energy was varied from 50 to 400 J/l atm in our experiments. The input energy pulse duration was about 30  $\mu$ s. The time-history of the EBCD input energy shown in Fig. 3.4 includes the time-history of the e-beam accelerating voltage (a), that of the e-beam current (b), that of the EBCD current (c) and that of the EBCD voltage (d). The maximal value of the e-beam accelerating voltage was of 150 kV. The maximal value of the e-beam current was of 2 A and that of e-beam current density was of 12 mA/cm<sup>2</sup>. The maximal value of the EBCD current depended on the EBCD high voltage and varied from 3 to 10 kA.

The EBCD high voltage was varied from 6 up to 25 kV. The dependence of the EBCD specific input energy on the specific field strength  $E/p$  (where  $E$  - field strength,  $p$  - gas pressure) is presented in Fig. 3.5 (data in Table 3.1).

### *Small signal gain*

A small signal gain is an important parameter of an active medium. It determines a laser output and nonlinear properties of the medium. To register a temporal behaviour of the small signal gain in the active medium the optical scheme of the experiment shown in Fig. 3.6a was used. The 10.6  $\mu$ m laser beam of the low pressure continuous wave (cw) CO<sub>2</sub> laser (1) passed through the inverted medium inside the pulsed EBCD CO<sub>2</sub> laser chamber (2). The temporal characteristics of the probe cw laser beam and the amplified one were monitored with the Ge: Au photodetectors (3). A mirror with reflectivity of 30% was used as a beam splitter (M). The gas pressure of the cw CO<sub>2</sub> laser was 6 - 12 Torr. The current of the self-sustained discharge was of 20 - 40 mA. The laser output was 0.3 - 0.7 W and the laser intensity was of 0.4 - 1 W/cm<sup>2</sup>. This intensity was much less than the saturation intensity in the inverted active medium. Thus the temporal behaviour of the amplified laser beam corresponded to the time-history of the small signal gain.

The time-history of the amplified laser signal (normalized on a maximal value of a signal) for different EBCD specific input energy (120, 190 and 280 J/l atm) is shown in Fig. 3.7.

To measure an average value of the small signal gain, the optical scheme of the experiment schematically shown in Fig. 3.6b was used. The output laser beam of the EBCD CO<sub>2</sub> laser (2) was introduced in the same laser chamber (1), but without crossing the laser resonator. We measured the energy of the probe laser beam and the energy of the amplified signal simultaneously. The energy of the probe laser beam was measured due to 8% reflection from the EBCD chamber NaCl window which was oriented at the 5° angle to the optical axis. The energy density of the amplified signal versus that of the probe one is presented in Fig. 3.8 (data in Table 3.2) for different EBCD specific input energy. The energy density was determined as the laser pulse energy per the area of 30 mm aperture diaphragm (D in Fig. 3.6b) before the calorimeters (3 in Fig. 3.6b). The small signal gain  $\alpha_0$  was determined as the limit when energy of the probe laser beam aspiring to zero in the expression:

$$\alpha_0 = \lim_{q_{pr} \rightarrow 0} \alpha; \quad \alpha = \frac{1}{L} \ln \left( \frac{q_{amp}}{q_{pr}} \right) \quad (3.2)$$

where  $L$  is the active medium length,  $q_{pr}$  and  $q_{amp}$  are the energy density of the probe laser beam and that of the amplified signal respectively,  $\alpha$  - average gain on energy. The dependence of the average gain on the energy density of the probe laser beam is shown in Fig. 3.9 for different EBCD specific input energy. The values of the small signal gain  $\alpha_0$  for different EBCD specific input energy are given in Table 3.3 and in Fig. 3.10. The value of the small signal gain was increased with increasing of the EBCD specific input energy. This dependence was approximated by logarithmic function shown in Fig. 3.10 (solid line). Maximum value of the small signal gain was of 1.7 m<sup>-1</sup>.

Fig. 3.9 enables us to estimate a saturation energy and intensity inside the EBCD CO<sub>2</sub> laser active medium. The value of the saturation energy was estimated as FWHM of the gain dependence upon the laser energy density. The saturation energy was equaled about 0.2 J/cm<sup>2</sup>. The saturation intensity corresponding to the energy was equaled about 10-20 kW/cm<sup>2</sup> being in a good agreement with the value of saturation intensity theoretically calculated from the system of kinetics equations (see part 2).

### 3.2.2. Characteristics of the EBCD CO<sub>2</sub> laser.

The EBCD laser chamber had aperture 120 mm in diameter and maximal volume of the laser active medium for this aperture was of 15 liters. Maximal CO<sub>2</sub> laser output energy was 400 J per one pulse. The specific output energy exceeded 70 J/l atm, the laser efficiency was of 24 %.

In our experiments the PC process under DFWM inside own active medium of the CO<sub>2</sub> laser was investigated. Thus the active medium of the CO<sub>2</sub> laser was used both as the nonlinear medium for the PC process under DFWM and as the laser source of the probe wave. To achieve maximum value of PC signal an interaction length of DFWM should be increased. But DFWM length was changed together with changing the interaction angle in our experimental setup. The interaction angle  $\theta$  was varied from 40 mrad down to 10-15 mrad in the experiments. The length of DFWM was up to 1 meter. To provide maximum value of PC reflectivity and analyze theoretically experimental results TEM<sub>00</sub> mode of the laser output was required. To satisfy these conditions the aperture of the laser beam was 10-30 mm in diameter at 12 m length optical resonator (Fresnel number  $\sim 1$ ). Characteristics of such EBCD CO<sub>2</sub> laser were not measured earlier before our experiments. Therefore we measured energetic, temporal, spatial and spectral characteristics of the CO<sub>2</sub> laser with small Fresnel number.

### *Laser output*

In our experiments we used a non-selective optical resonator, 12 m long, formed by one plane multicoating mirror and one concave rear mirror. The concave rear mirror had 24 m radius of curvature. To restrict oscillation to the TEM<sub>00</sub> mode intracavity apertures were used. A flat interference mirrors with reflectivity of 30%, 46% or 65% (wavelength  $\lambda \sim 10.6 \mu\text{m}$ ) were used as an output mirrors in these experiments. Multicoating mirrors mentioned above were also used as calibrated laser beam attenuators.

A specific output energy is energetic parameter which characterizes an active laser medium inside laser optical resonator. The parameter was determined as the output energy per one unit of a volume of the active medium inside laser resonator and per one unit of a gas pressure. The specific output energy of the laser had approximately linear dependence on the specific EBCD input energy (Fig. 3.11 and Table 3.4) for different output mirrors. The laser efficiency which was determined as a ratio of a specific output energy per a specific input energy depended on the output mirror (Fig. 3.12 and Table 3.5). The maximal value of the laser efficiency corresponded to 20% reflectivity of the output mirror.

Fig. 3.13 (data in Table 3.6) demonstrates that the laser output linear depends on the gas pressure for different specific energy input. Fig. 3.14 (data in Table 3.7) demonstrates that the gas laser mixture content (CO<sub>2</sub>: N<sub>2</sub>: He = 1 : 2 : 4, 3 : 3 : 8, 2 : 1 : 4 and 3 : 0 : 4) had small influence on the laser output under the experimental conditions. It should be noted that the low value of the

specific output energy and the laser efficiency as compared to normal wide aperture EBCD CO<sub>2</sub> laser was due to the large diffraction losses for laser resonator described.

### *Temporal behaviour of the laser output*

The EBCD CO<sub>2</sub> laser with the output pulse duration of 10-20  $\mu$ s was used in our experiments. The pulse length of the laser output and the shape of the laser pulse depended on the specific input energy, Q factor of laser resonator and gas parameters. However the laser output had complicated temporal behaviour. The behaviour reflected a formation process of a laser radiation inside the optical resonator. The pump waves of DFWM had the same time-history. Therefore to study the PC process under DFWM it is required to register the time-history of the waves. The basic properties of the temporal behaviour of the laser output will be discussed below.

The typical pulse shape of the laser output is shown in Fig. 3.15. The shape had a maximum near the beginning of the pulse. The pulse duration was 10-25  $\mu$ s in the experiments. The pulse shape depended on parameters of the active medium and the laser resonator. The end of the CO<sub>2</sub> laser pulse coincided with the end of the EBCD input energy pulse. The observable delay of the laser pulse beginning was due to growing of an inversion population of the active medium and amplifying of the laser radiation in the optical resonator. Thus the delay depended on the value of the specific input energy and Q factor of the optical resonator. The value of the delay varied from 4 to 10  $\mu$ s for a high Q resonator ( $R_{out} = 65\%$ ) and from 8 to 16  $\mu$ s for a low Q resonator ( $R_{out} \sim 8\%$ ). The laser output had a pre-pulse (first peak;  $\sim 1$   $\mu$ s pulse duration) at the beginning of the laser pulse. The pre-pulse was separated from the main pulse when the small signal gain was decreased or when the optical losses in the resonator was increased.

To display whole pulse duration of the laser output in our experiments the temporal behaviour was registered with Ge: Au photodetector with the resolution time of 0.1  $\mu$ s. The time-history of the laser pulse duration was used for the analysis of the PC mechanism and that of the temporary behaviour of PC reflectivity at the parametric study. The time-history of the waves will be shown at the description of those experiments. However the laser output time-history was smoothed by the photodetector resolution time (0.1  $\mu$ s).

It should be noted that the laser output had more complicated time-history. To analyze the time resolved structure of the laser pulse the amplified photon drag detectors with resolution time of  $\sim 1$  ns was used. In this experiment the resonator length was 3.6 m. The laser chamber optical windows was oriented at 5° angle to the optical axis of the resonator. The laser beam had output aperture of 19 mm in diameter.

The time resolved laser outputs are shown in Fig. 3.16. The Fig. 3.16a corresponds to default<sup>1</sup> gas parameters (see Table 3.8) and the SIE was 200 J/l atm. The number "1" after the letter indicates the pre-pulse of the laser output, the following part of the pulse is indicated by the number "2". Our analysis of the laser output showed that the output pulse had a periodic structure and the period was about 24 ns. The value of the period was equaled to a round-trip period  $T=2L/c$ , where  $L=3.6$  m - the length of the laser resonator,  $c$  - the speed of light. One can see that the laser output had the high frequency (HF) component which takes place because of longitudinal mode beating. In fact the Ge: Au photodetector displayed an envelope of the component. It should be noted that a number of longitudinal mode is very low. For instance, Fig. 3.16a demonstrates that, perhaps, two of them with different amplitudes takes part in lasing.

In additional inherent structure of the HF component had a complicated temporal behaviour as well. The diagrams in Fig. 3.16a-c are arranged in order of decreasing of a small signal gain inside the active medium. The decreasing was due to a decrease of a specific input energy down to 100 J/l atm (b) or due to using the gas mixture without nitrogen  $\text{CO}_2 : \text{He} = 3 : 4$  (c). Our analysis of the time resolved inherent HF structure showed that the small signal gain influenced on the structure of the laser output. The structure had more complicated (irregular to some extent) temporal behaviour when the small signal gain comes nearer to a threshold of lasing (Fig. 3.16 c1). From our point of view it was due to a competition between modes of the optical resonator. It should be also noted that the pre-pulse had more complicated structure in comparison with second part (a tail) of the pulse (Fig. 3.16 b2).

Thus the  $\text{CO}_2$  laser output had the complicated temporal behaviour. The structure should be taken into account in a further theoretical analysis. But the HF structure of a PC signal was not resolved in this experiment<sup>2</sup> because of a small value of the intensity of the signal preventing from using photon amplified drag detector.

### *Spatial and spectral characteristics*

A laser radiation is characterized by a set of parameters. The set includes an angular divergency, a spectral content, a degree of polarization and a degree of temporal coherency.

An *angular divergency* of radiation depended on parameters of the optical resonator and was 2 mrad in our experiments. The distribution of the laser output in a far-field zone will be presented below in chapter 3.2.4.

<sup>1</sup> See a definition of the term "default" at the beginning of the chapter 3.2

<sup>2</sup> HF structure of the laser output and PC signal for  $\text{CO}_2$  and CO lasers was observed in our joint experiments at P.N. Lebedev Institute having been done together with C. Beairisto, R. Penny, S. Squires (Dep. of Appl. Technology, White Sands, USA) and R. Walter (J. Schafer Ass., USA) in May 1996 (see Part 4).

A *degree of linear polarization* was measured with a Ge plate oriented at the Brewster's angle (analyzer). The degree of polarization of the CO<sub>2</sub> laser radiation exceeded 99.5% in the most of our experiments. In some experiments the degree of polarization was decreased down to 10% (see chapter 3.2.6).

A *spectral content* of the laser output was registered with a grating CO/CO<sub>2</sub> spectroscope. In our experiments the spectral band depended on a material of the optical window of the EBCD laser chamber.

#### NaCl windows:

Practically all the energy of the laser output was concentrated at single line 10.6  $\mu\text{m}$  P(20) without spectral selection. In additional, a weak lasing transition P(22) was observed when the laser output increasing.

#### BaF<sub>2</sub> windows:

The lasing transitions corresponded to 9.6  $\mu\text{m}$  band. A spectral content of the laser output had two strong lines P(24) and P(26). Also it was observed a weak line P(30).

A *degree of temporal coherency* is an important parameter for a DFWM process. In fact the degree determines a maximal contrast of the interference pattern under DFWM and then a maximal contrast of grating formed inside the non-linear medium. Because the output pulse had a complicated HF structure (see previous chapter) the degree of coherency itself was not measured in our experiments. However, an interference contrast was measured for different optical delay between two laser beams.

The schematic of the experiment is shown in Fig. 3.17. The laser beam was divided into two beams with a beam splitter. Then these beams were summarized on a screen at a small angle ( $\sim 10$  mrad). The interference pattern was registered by a carbon paper. The contrast was defined as a degree of a visibility of the pattern. In fact the measurement was the estimation of the visibility and had a small accuracy. But the estimation had enough accuracy to compare the interference patterns for the different optical delay. An optical delay between two laser beams was varied by means of moving one of folding mirrors. The optical delay was varied from a zero up to the double length of the laser resonator (in these experiment the resonator length was 3.6 m, the specific EBCD input energy being 200 J/l atm). The maximal contrast of the interference pattern was observed at zero delay. To compare a contrast at other optical delay with the maximal one the latter was taken as 1.0.

When the optical delay increasing from zero to half of the resonator length the contrast decreased slowly. When the optical delay being 2 m the contrast was 0.5-0.7 of the maximal value. When the optical delay increasing up to one length of the resonator the contrast decreased



more sharp. When the delay being one length of the resonator the interference pattern was weak but it was really observed. The contrast was about 0.1. When the optical delay increasing up to the double resonator length the contrast increased. The contrast was about 0.7 - 0.9 for the optical delay equaled to the double resonator length (the optical delay was equaled 7.2 m). Thus the contrast of the interference pattern was almost periodic function with an optical delay (with a period of double resonator length) and a maximal contrast corresponded to zero delay.

Therefore in the most of our experiments the optical delay between probe and pump waves was equaled to zero with an accuracy of  $\pm 0.1$  m. In some experiments the optical delay was varied (for example, see chapter 3.2.6).

The experiments demonstrated that the intensity grating did exist inside active medium in PC experiments and, also, that coherency length  $l_c$  of our CO<sub>2</sub> laser was longer, at least, than 2 meters. This result is confirmed by HF structure of the laser output observed. In fact, the CO<sub>2</sub> lasers spectral width  $\Delta\nu_L \sim l_c^{-1} \sim 0.005 \text{ cm}^{-1}$ , mode spectral spacing  $\Delta\nu_m = (2 L_{res})^{-1} \sim 0.0014 \text{ cm}^{-1}$ . Therefore  $\Delta\nu_L \approx 3.5 \Delta\nu_m$  and 2-5 longitudinal modes could take place in lasing.

### 3.2.3. Experimental scheme of DFWM of CO<sub>2</sub> laser radiation inside its active medium

The optical scheme of our experiments on DFWM of laser radiation inside its active medium is shown in Fig. 3.18. Default<sup>3</sup> parameters of the DFWM scheme are shown in Table 3.7. The pumping waves were formed by 12 m long optical resonator (2). The laser output was used as a source of the probe wave. The probe wave was directed to the EBCD active medium (1) of the laser at small angle ( $\sim 15$  mrad) to the optical axis of the laser resonator. The cross point was located at the center of the active medium. Then the amplified probe wave was directed to an absorber (3). The probe wave and a backscattered signal was measured due to a reflection from a beam splitter (BS). To provide maximal contrast of the interference pattern in the active medium the optical delay between the probe wave and the forward (co-propagating) pumping wave was equaled zero with an accuracy  $\pm 10$  cm (see previous chapter). Therefore, the accuracy enabled the optical delay to be not only within coherence length, but also to synchronize temporal structure of co-propagating pumping wave and probe waves. To vary an intensity ratio between the forward pumping and the probe wave ( $I_1/I_3$ ) a set of calibrated attenuators for the probe beam was used.

<sup>3</sup> See a definition of the term "default" at the beginning of the chapter 3.2

At DFWM the probe beam propagates through the active medium of the laser and can affect the process of lasing itself. In fact, the influence of the probe signal on laser output was observed when intensity of the probe signal was as much as a half of intensity of the co-propagating pumping wave.

In this case the process of DFWM was accompanied by an output energy decrease, by transformation of a profile of the laser pulse and intensity distribution in far- and near-field zones. The output energy of the EBCD CO<sub>2</sub> laser decreased by 30 - 40% while DFWM being used ( $I_1/I_3 \sim 1$ ).

The transformation of the laser pulse profile is shown in Fig. 3.19. The maximal transformation is observed in the middle of the laser pulse. When an intensity of the probe wave decreases, the profile of the laser pulse at DFWM is nearer to one without DFWM ( $I_1/I_3 \sim 2$ , Fig. 3.19b). For lower intensity of the probe beam both profiles were, practically, the same ones. Fig. 3.20 demonstrates the transformation of near-field intensity distribution upon the influence of DFWM. One can see in Fig. 3.20a the near-field pattern if DFWM does not take place. In this case the intensity distribution is fairly homogeneous. On the contrary, when DFWM being turned on ( $I_1/I_3 \sim 1$ ), the near-field pattern for the laser beam has a ring profile (Fig. 3.20b). The transformation of the near-field intensity distribution takes place because of a gain saturation in the active medium. For DFWM of gaussian beams the maximal total intensity corresponds to the point of intersection of axes of interacting beams. The region of maximal gain saturation is situated symmetrically to that point and stretched along the axes of intersecting beams. The cross-section of the region of interaction of the cylindrical beams (observed in direction of any beam) has an elliptical profile, stretched in direction perpendicular to the plane of interaction. The elliptical profile of laser intensity reduced in the center of intensity distribution was observed both for laser (probe) beam and for amplified signal propagated through the inverted medium (Fig. 3.20c).

Therefore we demonstrated, that DFWM leads to the change of energetic, temporal and spatial characteristics of CO<sub>2</sub> laser, if intensity of probe signal is more than a half of intensity of the forward pumping wave, i.e. intensity ratio  $I_1/I_3 < 2$ . When the intensity ratio  $I_1/I_3 > 2$ , no influence DFWM upon laser characteristics was observed within experimental error.

### 3.2.4. Experimental proofs for PC process.

To study a PC process under DFWM inside the laser active medium first of all an experimental proof is required that an observable backscattered signal is a PC signal. In chapters 3.2.5 and 3.2.6 it will be shown that the time-history of the backscattered radiation differed from that of the probe wave. Thus, the backscattered radiation was not any patch of light from a reflecting surface. However, a difference between temporal behaviour of the pulses is not any proof that an observable backscattered radiation is a PC signal. For example, a parasitic oscillation could also have the time-history differed from that of the laser output.

Therefore the additional set of the canonical tests for the PC process was carried out:

- reconstruction of an optical image and an aberrated laser beam in a near-field zone;
- reconstruction of angular divergence in a far-field zone;
- coherency (polarization) test.

#### *Reconstruction of an optical image in near-field zone*

The existence of the phase conjugation process in own active medium of the CO<sub>2</sub> laser was confirmed by experiments (see schematic in Fig. 3.18) in which the image of an object was reconstructed by the reflected signal in the near-field zone. We used different (I-, O-, L- and X-shaped) optical masks with slits of 2 mm width as an optical object and as an aberrator too. The image of L-shaped mask formed by thermal radiation is shown in Fig. 3.21a. The IR distribution of the laser radiation which crossed the optical mask is shown in Fig. 3.21b (at a distance of 4.5 m from the mask). The IR distribution was the complicated diffraction pattern obtained due to a diffraction at the edges of the mask. The IR distribution of the backscattered signal in the plane of the mask is shown in Fig. 3.21c. It was obtained by a location of the beam-splitter (1 in Fig. 3.18) which was equidistant from the mask and the scattering screen. The IR distribution shown in Fig. 3.21c had approximately the same shape as the probe signal passed through the mask. Thus the reflected signal reconstructed the image of the object when the four-wave interaction took place in the active medium of the EBCD laser. The imperfection of the reconstruction was connected with the optical quality of the phase conjugating mirror. It should be noted that the distance from the mask to the DFWM region was about 5 m. So some information about the object was lost because some part of the probe beam was out of zone of wave interaction on account of diffraction (Fig. 3.21b).

The case of O-shaped mask is shown in Fig. 3.21f (laser signal on the mask) and Fig. 3.21g (backscattered signal). The case of X-shaped mask is shown in Fig. 3.21i (backscattered signal). In latter case the X-shape of the backscattered signal had more imperfection which was due to more complicated shape of the mask. The IR distribution of an optical noise from the laser resonator is demonstrated in Fig. 3.21h. The distribution was consisted of a set of speckles randomly distributed within the aperture of the folding mirrors. To display the IR noise the video signal was multiplied by 100. Thus the signal/noise ratio exceeded one hundred in our experiments.

These experiments demonstrated that the backscattered signal under DFWM did reconstruct the image of the optical masks.

### *Reconstruction of angular divergency in far-field zone*

The angular distribution of the reflected radiation in a far-field zone was studied by recording the distribution of the radiation energy in the focal plane of a spherical mirror with a radius of curvature of 18 m. An angular divergency of a laser beam was determined in our experiments as FWHM of IR distribution in far-field zone. A comparison of the IR distribution of the probe beam (Fig. 3.22a) and that of the signal backscattered at the four-wave interaction in the active medium (Fig. 3.22b) demonstrated that the latter signal had the angular divergency differed by less than a factor of 1.5 from the divergency of the probe beam. It should be noted that in some cases the angular divergency of the reflected radiation was less than the divergency of the probe beam (see Fig. 3.22).

The comparison enables us to estimate an optical quality of the PC mirror. In fact an optical quality of a PC mirror is characterized by decreasing the angular divergency of aberrated beam down to that of the laser probe beam. Thus the ratio of FWHM of probe beam to that of PC signal could be a measure of optical quality of the PC mirror (see chapter 3.2.6).

To deteriorate an optical quality of the probe wave we used a set of aberrators (NaCl-plates with etched surface, crumpled polyester films). These aberrators provided a different degree of a phase aberration of the probe wave. These experiments demonstrated that the backscattered signal did reconstruct angular divergency of the laser beam when passing backward through the same aberrator. Thus the backscattered signal under DFWM of laser radiation inside its active medium had the property of PC signal, i.e. a reconstruction of angular divergency of the aberrated laser beam.

### *Coherent nature of backscattered signal*

PC by DFWM is a coherent nonlinear phenomenon taking place due to diffraction gratings created inside active medium. Hence, the PC reflectivity should depend on the degree of coherency of the interacting waves. To change the coherency at DFWM, a rotation of the polarization plane of the probe wave with respect to that of the pump waves proves to be most convenient. The influence of the mutual orientation of polarization planes of the interacting waves on the energy of the backscattered radiation has been studied by such polarization experiments. The polarization of the CO<sub>2</sub> laser radiation exceeded 99.5% in the experiments (see chapter 3.2.2). The rotation of the polarization of the probe wave was provided by a system of folding mirrors (Fig. 3.23). The insertion of the system did not change the optical delay between the probe and following pumping wave. By this procedure a minimum deviation from the condition of temporal synchronism between the probe and pump wave was reached. Two cases of mutual orientation of polarization planes of signal and pumping waves were considered: parallel and perpendicular ones. The energy of the backscattered radiation in the case of mutually perpendicular orientation strongly decreased in comparison with parallel orientation. The obtained value of the energy was comparable with the radiation background. By statistical processing of the experimental data it has been shown that in the case of the mutually perpendicular orientation the backscattered signal at DFWM is practically absent. The polarization experiment demonstrated that in fact in case of perpendicular orientation of polarization, there were no diffraction gratings in active medium on the contrary to the case of parallel orientation. The experiment also gives a basis to an imagined experiment on estimation of relaxation time  $\tau'_3$  of diffraction gratings (see Part 2). If one has DFWM scheme with parallel orientation of polarization and switches the polarization of a probe signal to the perpendicular one with time  $t \ll \tau'_3$ , the PC signal will disappear for a while of  $\tau'_3$ . Hence, in the case of parallel orientation the backscattered radiation was a result of the coherent interaction of the waves in nonlinear medium (diffraction on gratings).

Thus, on the basis of these studies of the backscattered radiation it was experimentally proven that the reflected radiation was a PC signal and that the signal/noise ratio exceeded 100 under the experimental conditions.

### 3.2.5. Two mechanisms of phase conjugation of CO<sub>2</sub> laser radiation at DFWM inside inverted medium

The time-history of the PC process (a formation of diffraction gratings, their transformation in time etc.) influences on time-behaviour of the PC signal. Fig. 3.24 demonstrates the profiles of the probe (laser) pulse (curve 1) and PC signal (curve 2) obtained in our experiments on PC at DFWM in inverted medium of CO<sub>2</sub> laser for different experimental parameters. One can see from the figure that the profile for the PC signal differs strongly from that of the probe signal. This difference between the profiles influences on time-history of the PC reflectivity (PCR or  $R$ , curve 3), defined as an intensity ratio for PC and probe signals ( $R=I_4/I_3$ ). In [20] they suggested the complicated structure of PCR pulse to involve two mechanisms of formation for diffraction gratings inside an active medium of CO<sub>2</sub> laser. It is shown in this chapter, that under the condition of our experiment these two mechanisms do determine the time-behaviour for PC signal and PCR pulse.

To study the temporal behaviour of the PC process at DFWM inside the CO<sub>2</sub> laser active medium the experiments were carried out for two cases of cavity Q factor and for three values of specific input energy. The intensity ratio  $\xi = I_1/I_3$  for the probe and co-propagating pumping wave in our experiments was held constant for a given Q factor. The origin of the time axis corresponds to the beginning of the input energy pulse. The normalized intensity of the radiation pulse and PC signal are marked on the vertical axis. To compare the time properties of the pulses the unit of the vertical axis corresponds to the maximal characteristic of each signal. The case of high Q factor ( $R_{\text{out}} = 65\%$ ,  $\xi = 50$ ) is shown at the right and low Q ( $R_{\text{out}} = 7.5\%$ ,  $\xi = 5,7$ ) - at the left side of the figure. Top graphs (Fig. 3.24a,d) correspond to the specific input energy of 120 J/l atm. The graphs for input energies 190 and 280 J/l atm (Fig. 3.24b,e and Fig. 3.24c,f, respectively) are located below. It should be noted that transient pulse profiles shown in Fig. 3.24 represent an envelope of high frequency intermode beating (see chapter 3.2.2).

The front parts of the probe wave and of the PC signal (curves 1,2, respectively,  $R_{\text{out}} = 65\%$ , 280 J/l atm,  $\xi = 50$ ) are presented in Fig. 3.25 with higher time resolution. It is clear that the front of the PC signal nearly repeats the front of the probe pulse with some delay. The time-history of PC reflectivity (Fig. 3.25, curve 3) has the same profile at the beginning of the pulse. This fact indicates the prevailing role of non-inertial mechanism at the front of the pulse. It is possible to suggest that the resonance (practically non-inertial) mechanism of PC does play the determining role at the beginning of the laser pulse. However, on the basis of the experimental data only

without supporting them by theoretical analysis, it is difficult to analyze the contribution of various mechanisms into the transient PC process.

All the diagrams for PC intensity (Fig. 3.24, curve 2) were characterized by a second maximum (a "hump"). The maximum was located at an interval of 3-5  $\mu\text{s}$  behind the front of the pulse. This approximately corresponds to the formation time of the thermal nonlinearity on a large-scale grating. Analyzing the transient PC behaviour it is clear that the relative role of the inertial mechanism increases with decreasing specific input energy and/or with decreasing Q factor of the optical resonator (see next chapter).

Thus, the time-history of the PC signal does not repeat that of the probe wave. The first peak of the PC signal has approximately the same sharpness as the probe wave. The delay of the PC pulse with respect to the probe wave was less than 0.2  $\mu\text{s}$ . The time-history of the PC signal can be explained by the participation of two main mechanisms of nonlinearity (resonance and thermal) in the PC process, the resonance mechanism (with the formation time less than  $\sim 10^{-7}$  s) being responsible for the first peak, and the inertial (with a response time of  $\sim 5$   $\mu\text{s}$ ) thermal mechanism affecting the second part of the pulse. To study the influence of these mechanisms on the PC process at DFWM inside the active medium of  $\text{CO}_2$  laser a comparison of the experimental and theoretical data was undertaken.

To analyze the PC process the time behaviour of PC reflectivity (R) is normally considered. However, the experimental determination of R as the relationship between the intensities of PC signal and probe wave caused a significant error, especially at the first peak of the probe wave. Therefore to compare experimental and theoretical data the intensity of the PC signal was considered (Fig. 3.26) in this research. The experimental data (Fig. 3.26, curve 1) were compared with the data obtained by numerical calculations for two considered mechanisms of nonlinearity (Fig. 3.26, curves 2,3). The case of high Q factor ( $R_{\text{out}} = 65\%$ ,  $\xi = 50$ ) is shown at the right and low Q ( $R_{\text{out}} = 7.5\%$ ,  $\xi = 5,7$ ) - at the left. Top graphs Fig. 3.26a,d correspond to specific input energy 120 J/l atm. The graphs for input energies 190 and 280 J/l atm (Fig. 3.26b,e and Fig. 3.26c,f, respectively) are located below. The start point of the time axis corresponds to the beginning of the input energy pulse. The normalized intensity of the radiation pulse is marked at the vertical axis. To compare the time properties of radiation pulses the unit of the vertical axis corresponded to the maximum intensity of each pulse.

The comparison of the experimentally obtained profile of the PC signal pulse and of the value calculated for each mechanism of nonlinearity shows that one of them not capable to describe temporal properties of PC process. However, it is possible to allocate the prevailing role to one mechanism in certain temporal interval of the pulse. In particular, the first peak of the PC signal



can be described only with the resonance mechanism of nonlinearity. It should be noted that the sharpness of the first peak of the theoretical PC signal depends on initial value of gain for the resonance mechanism (Fig. 3.26 curve 2). Thus, the growth of the front part of the first peak of the experimental PC signal at increasing specific input energy and/or with Q factor (Fig. 3.26 curve 1) indicates a resonance mechanism of nonlinearity.

After the first peak of the PC signal the contribution of the resonance mechanism is reduced due to a decrease of the gain in active medium. On the other hand the contribution of much more inertial mechanism (thermal one) to the PCR increases during the probe pulse as a result of an accumulation of thermal effects and an increase of spatial modulation of the thermal grating. All these factors lead to the increase of importance of thermal nonlinearity on the further stage of the PC process. A comparison of experimental and theoretical data (Fig. 3.26 curves 1,3) has shown that the thermal mechanism of nonlinearity can describe the observable time-history in the tail of the PC pulse.

Therefore two different physical mechanisms of creating diffraction gratings inside CO<sub>2</sub> inverted medium should be involved for physical description of the PC process. An influence of these mechanisms upon the PC process is displayed on time-behaviour of the PCR. The accurate definition of a degree of participation of each of these mechanisms involves the comparison of the experimental and theoretical data. We attempted such comparison for a number of experimental condition. The comparison has demonstrated the coincidence of profiles for PC signal obtained experimentally and theoretically (both for resonance and thermal nonlinearity) for the most of the cases. The front of the PC signal pulse can be described by resonance mechanism. For a description of the following parts of the PC pulse the thermal mechanism should be involved. The influence of this physical mechanism, as the most inertial one, prevails at the tail of the PC signal. Besides, the theoretical calculations (see Part 2) offer the value of an amplitude for the PCR due to thermal mechanism as being much higher than that observed in the experiment. The cause of the discrepancy for the amplitudes appears to be connected with the self-influence of laser radiation inside the active volume and different physical factors which were not included into the theoretical model. These factors could be the high-frequency structure of laser and PC signal (see Part 4), optical non-homogeneity of active medium, nonconjugation of two laser intracavity waves etc. When Q factor of the resonator and/or specific input energy increasing, the optical disturbances of the active medium rise also and distort the most inertial thermal grating.

As for profile of PC signal, the coincidence of theoretical and experimental results enabled us to investigate the influence of a number of different parameters on PC mechanisms. The inertial properties of the thermal and resonance mechanisms strongly differs from each other (formation



time and life time for amplitude and phase grating differ of the order of magnitude). We used this discrepancy for estimation of share of each of these mechanisms during parametric study of PC at DFWM in active medium of pulsed CO<sub>2</sub> laser. The resonance mechanism being less inertial strongly influences upon the front part of the PC signal. At the same period of time the thermal mechanism being more inertial practically does not influence upon the characteristics of the PC signal. Studying the time-behaviour of the PCR at the tail of the PC signal, one can estimate a contribution of the thermal mechanism, because the share of the resonance mechanism is reduced strongly, when intensity of interacting waves markedly decreases at the end of the laser pulse.

### 3.2.6. Parametric study of the PC process.

PC of laser radiation at DFWM inside own inverted medium is a complicated multy-parameter process, characteristics of which are mutually depended. The parametric study itself is supposed to deal with an investigation of influence of various parameters on properties of this process. The principal energetic characteristic of PC process is a PC reflectivity (PCR on energy), defined as an energy ratio for PC signal and probe one. The time-behaviour of PCR reflects the features of PC process, in particular, the role of the two principal mechanisms of PC at DFWM, existence of which was proved in the previous chapter.

In our experiments we investigated a dependence of the PC process on following DFWM's parameters: specific input energy, Q factor of the laser resonator, gas pressure, gas mixture, interaction angle, optical delay, intensity ratio, a degree of linear polarization and spectrum of the laser output. The object of this research was a study of the influence of these parameters on the relative contribution of those two PC mechanisms and on the PC reflectivity.

#### *Specific input energy*

The effect of specific input energy (SIE) on PC process at DFWM in active medium of CO<sub>2</sub> laser is discussed in this chapter. The experimental techniques for measurement of energetic and temporal characteristics are described above (chapter 3.1).

The dependence of PCR on SIE is presented in Fig. 3.27 (suitable data are in Table 3.9) and Fig. 3.28. The SIE varied from 100 up to 450 J/l atm. The experimental data were obtained for various gas pressure 0.1-0.4 atm, the reflectivity of output coupler being 46% and intensity ratio  $I_1/I_3$  for co-propagating and probe waves being  $\sim 1.5$ . The other parameters are in Table 3.8. Fig. 3.28 shows also the experimental data for PC reflectivity (on energy) obtained for other laser

mixture  $\text{CO}_2 : \text{N}_2 : \text{He} = 1:5:3$  ( $p = 0.28 \text{ atm}$ ) with high nitrogen content and different geometry of the laser resonator. The geometry enabled us to select flexibly the laser wavelengths. All data refer to a PC reflectivity rise with an increase of SIE. The dependence of PCR averaged over all data is linear one with the rate of  $\sim 3\% (\text{kJ/l atm})^{-1}$ . For data of Fig. 3.28 the suitable rate is  $\sim 8\% (\text{kJ/l atm})^{-1}$ . The maximal value of PCR (on energy) for condition of Fig. 3.27 (laser mixture  $\text{CO}_2 : \text{N}_2 : \text{He} = 1:2:4$ ,  $p = 0.4 \text{ atm}$ ) is higher than 1.5% and reaches  $\sim 2.8\%$  for Fig. 3.28 (laser mixture  $\text{CO}_2 : \text{N}_2 : \text{He} = 1:5:3$ ,  $p = 0.28 \text{ atm}$ ), the SIE being  $\sim 400 \text{ J/l atm}$ . Thus, our experimental data demonstrate the PCR to rise with an increase of SIE.

The analysis of PC process in active medium of  $\text{CO}_2$  laser and analysis of a relative role of two principal PC mechanisms when SIE is changed, is complicated because SIE determines a lot of characteristics (particularly, temporal ones) of active medium such as SSG time-history and its maximal amplitude (see chapter 3.2.1) and of laser itself (see time behaviour of the laser pulse, its profile and length, intensity of the laser pulse and intracavity waves in chapter 3.2.2). Thus the temporal behaviour of probe and PC signals should be useful for the analysis. Here we use these data, which were discussed at the previous chapter 3.2.5 for understanding how the two mechanisms depend on SIE.

To simplify the analysis of the two mechanisms the experimental data of Fig. 3.24 for PC reflectivity are presented separately in Fig. 3.29. The maximal value of PCR due to resonance mechanism, as follows from the theoretical description (Part 2, Fig. 2.2), takes place at the vicinity of front part of the laser pulse ( $t_1 < 1 \mu\text{s}$ ). The process of thermal grating formation is characterized by time of propagation of acoustic waves between the maximums of interference pattern  $\lambda/\theta v_{\text{ac}}$ , where  $v_{\text{ac}}$  - is a speed of acoustic wave. This time is, approximately,  $2 \mu\text{s}$  for gas mixture  $\text{CO}_2:\text{N}_2:\text{He} = 1:2:4$  and exceeds  $t_1$ . Besides the process includes the relaxation of thermal grating with time much longer than  $t_1$  and laser pulse length itself (see Part 2). Therefore, the share of thermal mechanism at  $t_1$  is very low and PCR measured at  $t_1 = 0.5 \mu\text{s}$  corresponds to a value close to maximal amplitude PCR. Inasmuch as relaxation time of the thermal grating is much longer as compared to laser pulse length the PCR on this grating might expected to increase as far as the laser pulse tail and its maximal value takes place near the end of laser pulse (see Fig. 2.2; we use the level of 0.1 of peak intensity for definition of time  $t_2$ ). The theoretical calculations (Part 2) and PCR growth normally observed at the tail of the laser pulse demonstrate, that PCR at time  $t_2$  ( $R_2$ ) is due to the most inertial thermal mechanism. The ratio of suitable PCR ( $R_1/R_2$  or  $R_2/R_1$ ) characterizes a relative role (or a relative share) of each mechanism in PC process. We will use the ratio for the analysis of influence of different parameters on PC mechanisms in experimental multi-parameter studying the PC process in active medium of  $\text{CO}_2$  laser.

The analysis of the effect of SIE on relative role of PC mechanism shows (Fig. 3.29), that with growth of SIE the share of thermal mechanism does not increase, at least (Fig. 3.29d-f; a set of  $R_2/R_1 = 4.0; 2.1; 3.6$ ), and for high Q-resonator (Fig. 3.29a-c; a set of  $R_2/R_1 = 8.0; 3.2; 1.1$ ) even decreases. On the contrary, the share of resonance mechanism  $R_1/R_2$  increases with growth of SIE. At the same time, taking into consideration the growth of an absolute value of PCR (on energy), the relative share of resonance mechanism increases together with its absolute contribution to the PC process.

The reason for the growth of resonance mechanism is exceeding of SSG over the threshold gain on the laser pulse front. This exceeding arises as a result of increase of SSG rate (see chapter 3.2.1) with increase of input power (input power pulse length was not altered during the experiment) and results in an increase of rate of laser intensity growing on the laser pulse front and a decrease of response time of the inverted medium (see Part 2). As a result of the phenomenon, the contribution of the resonance mechanism to the PCR increases on the front of laser pulse with a growth of SIE, that we did observe it in our experiments. A comparison of experimental and theoretical profiles of PC signal front for different output couplers confirms this conclusion (compare Fig. 3.26a-c and Fig. 3.26d-f).

An analysis of PCR pulse profile (Fig. 3.29) demonstrates, that alteration of growth of PCR in the middle part and on the tail of the pulse takes place with an alteration of SIE. The growth of the PCR towards the tail of PCR pulse refers to the predominating role of the most inertial (thermal) mechanism. The alteration of rate of the PCR pulse growth refers to the fact, that the temporal properties of this mechanism and first of all the relaxation time of thermal grating are being changed during the laser pulse. Therefore the decrease of rate of PCR at the second half of the pulse with SIE rise (Fig. 3.29) testifies the decrease of relaxation time of thermal grating. In case of high Q resonator the alteration of PCR pulse rate is very strong (Fig. 3.29a-c). One can observe even a decrease of PCR on the pulse tail for maximal SIE of 280 J/l atm (Fig. 3.29c) unlike in different cases presented in Fig. 3.29. Even an oscillatory regime of PCR takes place under condition of Fig. 3.29b. These two cases (Fig. 3.29b,c) are very interesting because enable us to estimate an effective (for both mechanisms) response time of PC process, which corresponds to an approach to the steady-state PCR and is comparable with or even less (for these cases) than laser pulse length (10-15  $\mu$ s). It should be noted that just for these cases the PCR profile in the middle part and on the tail of the pulse is different from the theoretical results (see Fig. 3.26b,c, curve 3) and approaches to the calculated profile for the resonance mechanism (with lower relaxation time; see Fig. 3.26b,c, curve 2).

With SIE growth the intensity of intracavity waves increases. When intensity ratio for co-propagating and probe waves is kept constant, an amplitude of a spatial modulation of intensity in active medium also increases. As a result the alteration of laser induced heat-liberation in active medium takes place. The heat-liberation is both a source of thermal grating formation and optical disturbances inside the active medium (self-influence of laser radiation, shock waves etc.) and can involve the thermal grating decay, especially, in high Q resonator. As a result, the effective relaxation time for thermal grating can be reduced and prevent from accumulation of thermal grating amplitude and higher contribution of the mechanism to the PC process. These disturbing factors have been already discussed in the previous chapter and theoretical Part 2, as ones possibly being the reason for discrepancy between experimental and theoretical results both for PCR pulse profile in case of high Q resonator (Fig. 3.26b,c) and a value of PCR (on energy) itself for thermal mechanism of PC.

The comparison between experimental and theoretical results for PCR (on energy) at gas pressure of 0.28 atm is presented in Fig. 3.28 (theoretical data are taken from Table 2.3 calculated for experimental conditions of Fig. 3.24). One can easily see that experimental results one eighth - one twentieth times as much as theoretical ones. This discrepancy appears to take place due to an alteration of thermal grating relaxation time, i.e. inertial accumulating property of the grating under the influence of disturbances in active medium.

Thus we discussed the dependence of PCR at DFWM in active medium of CO<sub>2</sub> laser on SIE in the range of 100 - 450 J/l atm. The PCR increases with a growth of SIE, the relative contribution of resonance or amplitude mechanism into PC process rising also. The consideration of extra factors such as disturbance of active medium etc. is needed for adequate description of thermal PC mechanism.

### *Q factor of optical resonator*

The Q factor of optical resonator affects the intensity of intracavity waves, gain and profile of laser pulse (see chapter 3.2.2). Nonlinear properties of the active medium, which are reflected in nonlinear effects such as PC, involves the intensity of the electromagnetic waves propagated through the medium. The interrelation between Q factor and intracavity intensity is a nonlinear one, inasmuch as the same nonlinear effects (gain saturation, laser induced heat liberation etc.), which result in producing PC signal at DFWM in laser active medium, take part in producing laser pulse itself. Therefore, as a matter of fact, the study of the effect of Q factor on PC reflectivity in our experiments is the research of influence of intracavity waves intensity on properties of PC

process at DFWM of CO<sub>2</sub> laser radiation. In the experiments the main attention was paid to the study of influence of Q factor on temporal behavior of PC process.

The Q factor of the resonator was changed by altering a reflectivity of the output coupler, which amounted to 7.5%; 45% and 65% in the set of experiments. The experimental results are presented in Fig. 3.24 and have been already used for comparison with the theoretical results (Fig. 3.26) with a purpose of understanding of the main mechanisms (chapter 3.2.5). Here we will use these results concerning a relative role of the two main mechanisms for studying the Q factor affect on these mechanisms. The profiles of probe and PC signals and PC reflectivity for the three values of Q factor ( $R_{out} = 7.5\%$ ; 45% and 65%) at the SIE of 280 J/l atm (see other parameters at Table 3.8) are presented in Fig. 3.30 in addition to data of Fig. 3.24.

A change of reflectivity of the output coupler and, hence, the change of useful optical losses leads to the change of the threshold gain, which amounts to 1.1, 0.33 and 0.18 m<sup>-1</sup> for  $R_{out} = 7.5\%$ ; 45% and 65%, respectively. It should be noted, that averaged SSG for SIE of 280 J/l atm is 1.7 m<sup>-1</sup> (see chapter 3.2.1). At the same SIE the change of  $R_{out}$  results in changing time delay of laser pulse and also its length, profile and intensity (Fig. 3.30). The alteration of the laser pulse length influences upon maximal PCR of the most inertial (thermal) mechanism of PC. The alteration of intensity ratio  $I/I_s$  (where  $I$  is an intracavity intensity), so called the degree of gain saturation (DGS), taking place when Q factor is changed, affects the two PC mechanisms. Theoretical calculations demonstrated (Part 2) that the maximal PCR takes place at DGS close to 1.0. The DGS for active medium involves a Q factor and SSG. The DGS approaches to 1.0 when decreasing Q factor and/or difference between SSG and threshold gain.

The analysis of influence of Q factor on profile of PCR pulse demonstrates, that maximal peak PCR shifts to the pulse tail (Fig. 3.30) when Q factor decreases. However, the relative share of the thermal mechanism (see the definition in previous chapter) decreases. The decrease of the share of the thermal mechanism is connected with an increase of PCR (on intensity) for resonance mechanism at  $DGS \rightarrow 1$ , on the one hand, and with a decrease of the peak value of PCR for thermal mechanism, on the other hand, as a result of shortening laser pulse length, that prevents from phase grating amplitude accumulating.

In case of high Q factor (Fig. 3.30a) the temporal behaviour of PCR is characterized by oscillation taking place after maximal value of PCR. In previous chapter we came to the conclusion, that such PCR behaviour is connected with influence of active medium disturbances upon the thermal grating (see Fig. 3.24). Thus the analysis of the experimental data has shown that a decrease of Q factor results in a decrease of influence of disturbing factors in active medium on thermal mechanism of PC because of decreasing intracavity waves intensity. Together with this

effect the shortening of the pulse length at low Q factor prevents from rise or accumulation of thermal grating. As a result the PCR (on energy) is only 1.2 -1.5 times as much as that of high Q cavity with reflectivity of output coupler of 65%. The difference between PCR for output mirrors with 45% and 65% reflectivity lies within the error of PCR measurements. The difference in PCR for various Q factors enables us to compare the contribution of resonance mechanism to PCR with that of thermal one. Actually, the PCR on energy is a PCR on intensity integrated over the pulse length. The rise of relative share of resonance mechanism and PCR on energy at low Q factor refers to an increase of the maximal value of PCR on resonance grating. Such increase is due to decreasing intracavity waves intensity and its approach to the saturation intensity ( $DGS \rightarrow 1$ ).

It should be noted that a change of Q factor in our experiments results in a change of optical quality of PC signal defined as an angular divergency ratio for probe and PC signals (see chapter 3.1). The best optical quality of PC reflection was observed for high Q factor resonator with reflectivity of the output coupler of 80%. When decreasing Q factor (45% and 8% output coupler reflectivity), the optical quality decreases 1.4 times and is half as much as that of high Q resonator. The optical quality rise, when Q factor increasing, is connected with a change of inertial property of PC process as a result of a decay of thermal grating and hence, the decrease of its response time under the influence of disturbing factors in the active medium described in the previous chapter.

Thus we demonstrated that Q factor decreasing leads to the PCR (on energy) rise on 20-50% as a result of intracavity intensity weakening and its approaching to the saturation intensity. Together with this we observed an increase of relative role of the resonance mechanism of PC. The best optical quality of PC signal was observed for CO<sub>2</sub> laser with high Q resonator due to a decrease of thermal grating response time because of decay of the grating.

### *Gas pressure*

The results of the experiments on effect of gas pressure on PC process at DFWM of CO<sub>2</sub> laser in active medium are discussed in this chapter. As gas pressure ( $p$ ) rises the alteration of a number of properties of laser active medium takes place because of a growth of inter-molecular collision rate and a decrease of free-running length:

- there is a decrease of relaxation time of laser levels,  $\tau_{rel} \sim p^{-1}$ ;
- there is an increase of spectral width of laser gain,  $\Delta\nu \sim p$ ;
- there is an increase of saturation intensity  $I_s \sim p^2$  due to both factors mentioned above;

- there is a decrease of coefficients of diffusion  $D \sim 1/p$  and temperature conductivity  $\chi \sim 1/p$ , that leads to an increase of relaxation time of temperature and density fluctuations in gas medium, and, in case of DFWM, to an increase of a proper relaxation time for amplitude and phase diffraction gratings.

Thus gas pressure influences upon nonlinear and relaxation properties of laser active medium, which the PC process depends upon.

Gas pressure varied from 0.1 atm up to 0.8 atm in our experiments. The alteration of PCR (on energy) with gas pressure was studied for laser mixture  $\text{CO}_2:\text{N}_2:\text{He}=1:2:4$  (SIE  $\sim 250$  J/l atm; output coupler reflectivity 46%). The PCR values were averaged on a number of experiments. The results are presented in Table 3.10 and Fig. 3.31. The analysis of the experimental data shows the PCR rise. The maximal rate of PCR growing is observed for low gas pressure less than 0.2 atm and gas pressure higher than 0.4 atm. The maximal PCR for this set of the experiments amounted 1.8% for gas pressure 0.56 atm. There is a "plateau" in Fig. 3.31 for gas pressure in the range of 0.2 - 0.4 atm, i.e. the PCR is not changed within the errors of the measurement.

The output energy of  $\text{CO}_2$  laser increases with gas pressure rise because of the growth of the number of active molecules, hence, the intracavity intensity also increases. The intensity growth results in disturbances of laser active medium. These disturbances lead to an alteration of temporal properties of PC process in active medium and, first of all, of the most inertial thermal PC process. Therefore the cause of dependence observed should be looked for by analyzing the temporal behaviour of PC process.

The temporal profiles for probe, PC and PCR signals are presented in Fig. 3.32 and Fig. 3.33 (gas pressure 0.8; 0.56; 0.42 and 0.28 atm) for two Q factors corresponding to output coupler reflectivities of 65% (Fig. 3.32) and 8% (Fig. 3.33). Gas pressure rise leads to laser pulse shortening (5-8  $\mu\text{s}$ ), to an increase of time-delay (1-3  $\mu\text{s}$ ) and "smoothing" its front part. The laser pulse shortening is due to a growth of induced radiation transition rate. It should be noted that for keeping the same SIE of  $\sim 250$  J/l atm with pressure rise the specific field strength  $E/p$  was diminished that led to a growth of direct gas heating and, hence, to lowering SSG and an increase of time delay. Besides, for this set of experiments, we altered such parameters as input power and its duration ( $\tau_{in} \sim 40$   $\mu\text{s}$ ) in order to lower the shock loading (for gas pressures higher than 0.5 atm, in particular) on the foil separating e-gun from the laser chamber.

The typical feature nearly for all of the PCR pulses is PCR rise in the end of laser pulse, where PCR reaches its maximal value (the end of laser pulse proved to be cut off in Fig. 3.32b). One can observe the interrelation between the rate of PCR growth in the end of laser pulse and laser intensity such as an increase of the rate with an intensity decrease. By analysis of temporal



diagrams of Fig. 3.32 and Fig. 3.33 one can see that the temporal behaviour of PCR pulse in its middle part is also determined by intensity. In particular, one can see from Fig. 3.32b, where the part of the pulse analyzed is circled, that a fast growth of the intensity of the probe signal is accompanied by profile changing and diminishing PC signal intensity with time delay of 1-2  $\mu$ s.

All the features of PC and PCR pulses described display themselves more distinctly on the temporal diagrams in Fig. 3.33 ( $R_{out} \sim 8\%$ ) and in particular in Fig. 3.33d, where an alteration in middle part of PC signal with intensity changing is rather stronger, than in Fig. 3.32b. However, one should take into account the fact, that in this set of the experiments the intensity of the probe signal was twice as much as that of co-propagating wave ( $I_1/I_3 \sim 0.5$ ), though was less, of course, than total intracavity intensity. In this case the probe wave strongly affects the process of formation of laser radiation (see chapter 3.2.4).

The temporal behaviour of PC signal reflects the effect of disturbances on laser radiation. One can see from Fig. 3.33 and Fig. 3.32, that with gas pressure rise the effect of disturbance in active medium on PC process increases and takes an oscillatory feature with a period of  $\sim 2 \mu$ s at gas pressure higher than 0.4 atm. It should be noted that the same oscillatory temporal behaviour is observed when rising SIE at lower pressure (see, for example Part 4, Fig. 4.2 for SIE of 300 J/l atm). The period corresponds to acoustic wave period determined by space between interference maximums of grating inside active medium. The source of the disturbances seems to be laser beam itself spatially restricted in laser cavity and existence of spatial profile of laser beam. While weakening the intracavity intensity in the end of laser pulse, the source of disturbances is weakened also and PCR rises on account of relaxation time rise and accumulation of the thermal grating.

The PC signal rise towards the end of the laser pulse testifies the prevailing role of the most inertial thermal mechanism of PC process. The  $R_2/R_1$  ratio, which characterizes the role of the thermal mechanism (see previous chapters) was maximal one for PC pulse of Fig. 3.32a (0.8 atm). The comparison of the ratio for all other profiles indicates, that the higher pressure is, the higher role of the thermal mechanism of PC. However, the PCR rise in the middle part of the laser pulse is restricted by effect of disturbances induced by laser radiation on life time of thermal grating.

It should be noted that in PC process theory (Part 2), they considered the case of plane waves, i.e. the influence of laser induced disturbances in active medium on diffraction grating and on alteration of behaviour of it for spatially restricted laser beam was not taken into account. Therefore, the experimental dependence of PCR (on energy) on gas pressure (Fig. 3.28) strongly differs from theoretical one (Fig. 2.7) both on amplitude and profile. The main disagreement is in the rate of PCR growth with gas pressure rise. The theoretical calculations provide nearly square



dependence of PCR on gas pressure that could be explained by square rise of saturation intensity. The experimental data indicates the "plateau" for dependence of PCR on gas pressure at the pressure range of 0.2-0.4 atm. The existence of the plateau" seems to take place because of a balance between PCR rise with a decrease of active medium saturation (see Part 2) and a growth of laser induced disturbances in active medium, that decreases the relaxation time of thermal grating and diminishes PCR with gas pressure rise. The influence of these disturbances is displayed, in the most extent, in the middle part of the PC pulse with maximal laser intensity. When rising gas pressure higher than 0.4 atm a growth of nonlinearity coefficient for the medium prevails over the influence of these disturbances and PCR keeps on its rising. Thus it follows from the analysis of time history of PC and PCR signals, that the contribution and the role of the thermal PC mechanism increases with gas pressure rise, however, relaxation properties of diffraction grating are changed during pulse length (relaxation time is diminished in the middle part of the laser pulse) under the disturbances in active medium of CO<sub>2</sub> laser. These factors leads to a decrease of PCR (on energy) and an alteration of character of dependence of PCR on gas pressure compared to the results of the theoretical calculations.

#### *Laser gas mixture*

The influence of CO<sub>2</sub> laser gas mixture content on the properties of PC process at DFWM is discussed in this chapter. Apart from CO<sub>2</sub> the main components of the gas mixture are as follows: nitrogen as a reservoir of vibrational energy and helium as a buffer gas. Thus the main attention was paid to the effect of these components on the PC process.

In our experiments we used three gas mixtures CO<sub>2</sub>:N<sub>2</sub>:He = 1:2:4 (standard one); 1:5:3 (with high nitrogen content) and 1:2:7 (with high helium content) at gas pressure of 0.28 atm.

The maximal PCR (on energy) of 2.8% was observed for gas mixture 1:5:3, the PCR for gas mixture 1:2:4 being 1.8% and for 1:2:7 being 1.4%. Thus an increase of partial pressure for nitrogen leads to PCR rise. The reason of the PCR rise seems to be a decrease of relaxation rate for vibrational energy and a decrease of heat-liberation power in active medium, because a main part of vibrational energy is stored on long-life levels of nitrogen molecules and a content of helium, which depopulates a low laser level, is low. The decrease of relaxation rate proves to lead to a growth of laser induced nonlinear process of relaxation and PCR rise.

The temporal behaviour of PC process for laser mixture 1:5:3 is presented on Fig. 3.34. Due to the decrease of vibrational relaxation rate one can see much more clearly both two PC mechanisms separately (compare Fig. 3.34 and Fig. 3.30b): amplitude mechanism at the front part

of laser pulse and thermal one at the rear part. The same situation seems to take place when lower input power at the same SIE is used for laser pumping (see Fig. 4.2). It should be pointed out that the maximal PCR for resonance mechanism is approximately the same like for thermal one, i.e. the ratio  $R_2/R_1 \approx 1$ . Again the role of resonance mechanism is comparable with thermal one.

### *A degree of linear polarization of laser beam*

In the previous chapters we have discussed the experimental data concerning strong PCR dependencies on different parameters. But parametric study should also indicate the parameters, which render little if any influence upon PC process. One of such parameters seems to be a degree of linear polarization (DLP) of the CO<sub>2</sub> laser beam.

Every time in our experiments the CO<sub>2</sub> laser radiation had a particular plane of polarization. The DLP exceeded 99.5% with a use of laser chamber output windows situated under the Brewster angle to the optical axis. But even in the case, when the output windows were perpendicular to the optical axis and then were tilted at the angle of  $\sim 5^\circ$  in mutually perpendicular planes, the DLP exceeded 95%. The existence of a few intracavity folding mirrors seems to be a cause for the phenomenon. By using an extra plane plate situated inside the laser resonator under the variable angle to the optical axis, we could decrease the DLP down to 10%, the output energy decreasing of 10%.

The theory (Part 2) considered DLP as being 100%. To study the influence of the DLP on the PC process we carried out the experiment on DFWM with two different DLP of 95% and 10%, SIE being 200 J/l atm. For the two DLP we obtained PCR of 1.30% and 1.25% averaged over the results of series of the experiment, i.e. there was no difference between PCR within the accuracy of the measurements. Thus the DLP does not influence upon PC process.

### *Spectral range of CO<sub>2</sub> laser radiation*

In this chapter we compare the results on PC experiments for two spectral ranges (9.6  $\mu\text{m}$  and 10.6  $\mu\text{m}$ ) of CO<sub>2</sub> laser. Experimentally the particular range was chosen by using particular optical windows for the laser chamber: NaCl or BaF<sub>2</sub>. In case of BaF<sub>2</sub> we had lasing in 9.6  $\mu\text{m}$  range (two strong lines; see chapter 3.2.2), and in case of NaCl in 10.6  $\mu\text{m}$  range (one strong line P(20)). The output energy of 9.6  $\mu\text{m}$  laser was 0.85 times as much as that of 10.6  $\mu\text{m}$  laser for the same parameters of the laser. The temporal behaviour of gain and laser pulse was proved to be the same one for different spectral bands.

The PCR (on energy) averaged over a set of experiments demonstrated that PCR for 9.6  $\mu\text{m}$  band was 0.7-0.8 times as much as that obtained for 10.6  $\mu\text{m}$  spectral band. A comparison of the temporal behaviour of PCR for the two spectral bands showed, that the effect of disturbances inside active medium on PC process (the phenomenon is described in previous chapters) is stronger to some extent for 9.6  $\mu\text{m}$  band over 10.6  $\mu\text{m}$  one.

### *Interaction angle of DFWM*

The results of experiments on effect of an angle between the directions of propagation of interacting waves at DFWM on PC process for  $\text{CO}_2$  laser are discussed in this chapter.

The experiments were carried out for gas mixture  $\text{CO}_2:\text{N}_2:\text{He} = 1:2:7$  at gas pressure of 0.25 atm, the laser aperture being 20 mm. Fig. 3.35 demonstrates the experimental dependence of PCR on the interaction angle within the range of 15-40 mrad (data in Table 3.11). The PCR (on energy) can be seen from the figure to drop very rapidly with interaction angle growth.

The period of large scale interference pattern in active medium of intracavity DFWM is inversely proportional to the interaction angle ( $\Lambda_{13} \approx \lambda/\theta$ ). However, together with that fact, the number of those periods increases, though the cross-section of the interaction region is almost the same one. Thus the decrease of the period can not explain such strong decrease of PCR.

Moreover, the interaction angle affects the length of wave interaction range at DFWM of spatially restricted laser beams if the length of nonlinear medium is long enough. To explain this we will use the term "effective"(or averaged) length of interaction at DFWM. We will define the effective interaction length as a pure geometrical parameter or as a length of intersection of a probe beam with intracavity laser beam, the length being averaged on cross-section of the probe beam. In our case of cylindrical laser beam, the interaction angle rise leads to inversely proportional decrease of effective interaction length. The length strongly affects the PCR value. Actually, the theory [1] predicts the square dependence of PCR on the length ( $\text{PCR} \sim L^2 \sim \theta^2$ ). In our experiments the active medium length of 1.2 m exceeded the effective length of DFWM ( $< 1.0$  m). Therefore the decrease of PCR with interaction angle rise is connected with the decrease of the effective length of interaction region. The PCR rise with interaction decrease is accompanied by an energy rise of background radiation from the laser resonator. Thus, as a result of this experiment, the interaction angle for all experiments was 10-15 mrad, that resulted in optimal ratio between the maximal PCR and minimal energy of background radiation.

### *Optical delay between probe and co-propagating waves*

In this chapter we discuss the experiment on influence of an optical delay between probe and co-propagating waves upon PCR (on energy). The experimentally measured values of PCR (on energy) were averaged over a number of experiments. The optical delay was introduced into the optical scheme of DFWM by changing the optical way for the probe beam. For analyzing the effect of the optical delay it was compared with the resonator length (12.0 m), the value of PCR being compared with PCR at zero delay.

When changing optical delay within the range of 0-1.5 m (1/8 of the resonator length), the PCR was not affected within 10% accuracy of the measurement. While increasing it up to half a resonator length, PCR decreased 1.2-1.5 times in average. If increasing optical delay up to the length corresponding the laser resonator length, PCR was one fifth -one tenth as much as that obtained for zero delay. The energy of the PC signal was very low, but yet it could be separated from background radiation.

Previously, when describing properties of the CO<sub>2</sub> laser (chapter 3.2.2), we demonstrated that an alteration of optical delay between two laser beams results in an alteration of a contrast of interference pattern with a spatial period equaled to a double resonator length. The periodical behaviour of the contrast involves the high frequency temporal structure of laser radiation with a round-trip period of  $2 L_{res}/c$  (see Part 4). Therefore the optical delay of probe wave relative to co-propagating pumping wave alters the contrast of large scale interference pattern being produced in active medium at DFWM. As a result, characteristics of diffraction gratings, being produced under the intensity variations in interference pattern, are affected, PCR (on energy) being changed also. The complicated temporal behaviour of laser radiation on round-trip period leads to the fact, that the dependence of PCR on optical delay length, should have a complicated character depending on a number of parameters influencing upon temporal behaviour of laser pulse.

### *Pumping and probe intensity ratio*

Here we discussed the experiments on effect of pumping and probe wave intensity ratio  $I_1/I_3$  on PC process at DFWM for CO<sub>2</sub> laser. In our experiments we studied the influence of the ratio  $I_1/I_3$  lying within the interval of 0.2-50 on PC process. With IR camera we studied the PCR (on intensity and energy) and optical quality of PC process (the procedure was discussed in chapter 3.1). The results are presented in Fig. 3.36, 3.37 and Table. 3.12. It should be noted, that PCR (on intensity) was being found as a ratio for angular divergency of probe wave  $\theta_{probe}$  and PC

signal  $\theta_{PC}$ :  $\theta_{probe}/\theta_{PC}$ . The intensity of probe signal was altered by a set of optical attenuators. The results of the measurements were averaged over a set of experiments, experimental errors being presented on the diagrams. For better impression experimental dots were connected by curves (cubic spline).

One can see from Fig. 3.36 that in the whole range of the ratio  $I_1/I_3$  the PCR (on intensity) lies within the interval of 0.6-1.2% and reaches its maximal value at  $I_1/I_3 \sim 15$ . The optical quality is changed from 0.8 up to 1.3 and has its minimum at the same ratio. It should be pointed out, that the dependence of optical quality on intensity ratio  $I_1/I_3$  was altogether an inversion of dependence for PCR (on intensity), i.e. an increase of optical quality corresponded to a decrease of PCR. As a result, the averaged PCR (on energy) being an integral characteristic taking into account a spatial distribution of energy for probe and PC signal in far-field zone, i.e. being proportional to  $(\theta_{probe}/\theta_{PC})^2$ , emphasizes the features of above dependence much more clearly (Fig. 3.36). Thus the maximum of PCR (on energy) corresponded the same intensity ratio of 15 and reached 1.7% with optical quality of PC mirror 0.83. The most of experimental values of PCR (on energy) for other intensity ratio lay within the interval of 0.5-0.75%, the optical quality being higher than 1.0. We do not know yet the reason for such singularity at intensity ratio near 15. However, the more important fact here, that optical quality rise correlates with PCR drop. It should be noted that for the most of other experimental data the optical quality and PCR were almost independent of intensity ratio, but they also correlated with each other (compare Fig. 3.36 and 3.37). The correlation put a serious question, should we struggle for maximal PCR if, potentially, it can lead to a decrease of optical quality of PCR. Of course, the problem involves the further experimental and theoretical research.

The effect of intensity ratio on PC process for the case of strong probe wave ( $I_1/I_3 = 2; 0.6; 0.2$ ) was studied also by analysis of temporal behaviour of PC signal. The plane BaF<sub>2</sub> plate was used as output coupler with reflectivity of  $\sim 8\%$ . Fig. 3.38 demonstrates profiles of probe, PC and PCR pulses. The analysis of the profiles shows, that all features of PCR previously discussed take place also for high intensity probe wave:

- a restriction of PCR rise in the middle part of the laser pulse due to a decrease of relaxation time for thermal grating under the disturbances of active medium and oscillatory temporal behaviour of PCR pulse in this part of the pulse;
- an increase of PCR rate in the end of laser pulse due to a decrease of intracavity laser intensity towards the end of the pulse;
- comparable values of PCR for front and rear part of laser pulse, i.e. comparable contribution of the two mechanisms of PC process, resonance and thermal ones.

There are some features of pulses presented in Fig. 3.38, which display themselves with intensity ratio rise:

- little decrease (of  $\sim 5 \mu\text{s}$ ) laser pulse length and little increase of amplitude for the first peak, that might be connected with diminishing negative feed back for the laser;
- an increase of averaged PCR rate in the middle part of the laser pulse;
- a shift of PC signal maximum intensity towards the laser pulse end.

The PCR for these intensity ratio practically did not differ from each other and reached  $\sim 1\%$ . Thus, probe wave intensity exceeding over the intensity of co-propagating pumping wave render a low effect on PC process at intracavity DFWM.

### **3.3. PC at DFWM in active medium of CO laser.**

The results of the experiments on PC at DFWM of EBCD CO laser radiation in its active medium are discussed in this chapter. The optical scheme and procedure of measurement were, in generally, the same as for  $\text{CO}_2$  laser (see chapters 3.1 and 3.2). The only differences were in usage of different optical materials being transparent in spectral region of  $5.0\text{--}6.0 \mu\text{m}$ , different laser mixture  $\text{CO}:\text{N}_2:\text{He}=1:4:5$  and cooling laser chamber down to  $\sim 120 \text{ K}$ . The output windows of laser chamber were made of  $\text{CaF}_2$ . Diffraction grating (100 lines/mm, blazing angle of  $30^\circ$ ) was used for frequency selection of CO laser radiation. Gas density varied between  $0.1\text{--}0.5$  Amagat. The interaction angle was  $10 \text{ mrad}$ . The length of laser resonator was  $17.7 \text{ m}$ , laser aperture being  $15 \text{ mm}$  in diameter. Thus laser operated at  $\text{TEM}_{00}$  mode. The reflectivity of the output coupler was  $43\%$ .

The processes of inversion formation and lasing for CO laser differ strongly from those of  $\text{CO}_2$  laser, the principal difference being in vibrational-vibrational (V-V) mechanism of creation of inversion population in CO laser and cascade lasing. As a result, temporal and spectral characteristics of the two lasers differ from each other strongly. The CO laser pulse length was  $100\text{--}500 \mu\text{s}$  at the same SIE ( $\text{CO}_2$  laser  $\sim 10\text{--}20 \mu\text{s}$ ), laser spectrum consisting of  $\sim 30$  spectral lines for frequency nonselected CO laser (single line for  $\text{CO}_2$  laser). The delay time with respect to the beginning of pumping pulse for CO laser pulse was  $15\text{--}50 \mu\text{s}$  and depended either on SIE or selected wavelength (in case of frequency selected mode). The structure of CO laser pulse in detail will be described in Part 4 with much better temporal resolution.

The strongest CO laser lines lay within the spectral region of  $5.2\text{--}5.6 \mu\text{m}$  and corresponded to vibrational-rotational transitions with vibrational numbers from  $8 \rightarrow 7$  up to  $12 \rightarrow 11$  and with

rotational numbers of 13-15 (gas temperature 120 K). Notwithstanding the difference between temporal and spectral characteristics of the two lasers, output energy and SSG were approximately the same ones at the same SIE being up to 3 J and  $1.8 \text{ m}^{-1}$  at SIE of 300 J/l Amagat for nonselected mode of operation (full spectrum). For frequency selection mode the output energy was one half - one third as much as that obtained for nonselected CO laser pulse. It was valid for "strong" lines such as  $P_{10 \rightarrow 9}(15)$   $5.40 \text{ }\mu\text{m}$ , for example.

#### *An evidence of PC for CO laser*

The set of the experiments on reconstruction of IR image in near field and recovering an angular divergency in far field has been carried out like in case of  $\text{CO}_2$  laser (chapter 3.2.4) to obtain an evidence for signal observed to be the real PC signal (see Fig. 3.21d,e). The experimental results did confirm the backscattered signal to be PC signal, signal/noise ratio being of 10-50. A comparison of images recovered for  $\text{CO}_2$  and multiline CO lasers (Fig. 3.21) demonstrated for the optical quality of PC mirror to be higher for CO laser as compared to  $\text{CO}_2$  laser, notwithstanding of the grater number of lines in CO laser spectrum. It should be noted that we did not observe the influence of DFWM upon the spatial characteristics of CO laser (unlike in case of  $\text{CO}_2$  laser, chapter 3.2.3) even if probe wave intensity exceeded the intensity of intracavity co-propagating wave. The maximal value of PCR (on intensity) did not exceed 1%, PCR (on energy) being of 0.1-0.5%, i.e. being much less than for  $\text{CO}_2$  laser.

#### *Temporal characteristics of PC process for CO laser*

The cause of the singularities of PC process for CO laser compared to  $\text{CO}_2$  laser lies in singularity of CO laser physics and PC mechanisms for CO laser. Fig. 3.39 demonstrates the typical temporal behaviour for probe (a), PC (b) and PCR (c) pulses (SIE 300 J/l Amagat, frequency selected resonator,  $5.39 \text{ }\mu\text{m}$  spectral range). The analysis of the time behaviour for PCR shows, that maximal peak value of PCR (on intensity) is at the front of laser pulse. The maximal value is twice as much as that of averaged value or PCR (on energy). The PCR rise towards the pulse tail, that is characteristic of PCR signal for  $\text{CO}_2$  laser, was not observed practically for CO laser pulse. Moreover, an analysis of pulses in Fig. 3.39 shows that PCR decreases nearly proportionally to the intensity of probe wave falling to the end of CO laser pulse. This temporal behaviour of PCR is characteristic of noninertial (or low inertial) PC mechanism. Just the resonance (amplitude) mechanism is the low inertial one. In accordance with resonance



(low inertial) mechanism transient theory (chapter 2.2), the maximal value of PCR at laser pulse front is connected with exceeding SSG over the threshold gain inside laser resonator. After the first peak, the decrease of PCR is due to a decrease of SSG to threshold value and a decrease of intracavity intensity (Fig. 3.39a). A contribution of the thermal mechanism to the PC process in active medium of CO laser is weakened as a result of CO laser physics. The process of laser induced heat liberation is much lower and much slower as compared to CO<sub>2</sub> laser. The laser transition is not accompanied by strong heat liberation like in case of CO<sub>2</sub> laser. Small laser induced heating can take place due to V-V exchange during laser pulse and transformation of quantum defect (~1% of vibrational quantum) to heat, and also due to very slow V-T (vibrational-translational transitions) relaxation,  $\tau_{rel} > 1$  ms. Of course, a theoretical analysis is needed for reliable estimation of these effects. Thus, the temporal behaviour of PCR signal demonstrates that resonance mechanism seems to be the most important one for CO laser.

For comparison the pulses of probe, PC and PCR signals are presented in Fig. 3.40 for three different spectral bands with center lines 5.23  $\mu\text{m}$  (a), 5.39  $\mu\text{m}$  (b) and 5.52  $\mu\text{m}$  (c) and spectral width of 15  $\text{cm}^{-1}$ . Lasing within these spectral bands took place generally on a few vibrational rotational transitions (on one-two ones for 5.23  $\mu\text{m}$  and 5.52  $\mu\text{m}$  bands and up to three-four transitions for 5.39  $\mu\text{m}$  band) of CO molecule. The strongest lines were selected with a decrease of SIE. One can see below the energy of laser pulses (at SIE of 290 J/l Amagat and reflectivity of output coupler of 43%) and the strongest transitions for spectral bands mentioned above:

- 5.23  $\mu\text{m}$  - 0.42 J,  $P_{8 \rightarrow 7}(14)$ , 1906  $\text{cm}^{-1}$ , 5.247  $\mu\text{m}$ ;
- 5.39  $\mu\text{m}$  - 1.0 J,  $P_{10 \rightarrow 9}(14)$ , 1855  $\text{cm}^{-1}$ , 5.391  $\mu\text{m}$ ;
- 5.52  $\mu\text{m}$  - 0.72 J,  $P_{12 \rightarrow 11}(13)$ , 1808  $\text{cm}^{-1}$ , 5.530  $\mu\text{m}$ .

It should be noted, that laser pulse length increased with wavelength rise (from ~70  $\mu\text{s}$  for 5.23  $\mu\text{m}$  band up to ~250  $\mu\text{s}$  for 5.52  $\mu\text{m}$  band in the experiment), i.e. with an increase of the quantum number of V-V transition. In all diagrams of Fig. 3.40 the PCR pulse (thin line) has a maximum of laser pulse front, that is displayed in PC signal (thick line) front sharpening. The further research of PC and PCR signals time behaviour of laser pulse front claims a use of photodetectors with nanosecond response time. The result of such research are presented in Part 4. The further time behaviour of PCR pulse after the first peak at the front is characterized by a low decrease towards the end of the laser pulse following approximately the decrease of laser intensity, though the decrease of PCR is not so fast for 5.23  $\mu\text{m}$  band as compared to 5.39  $\mu\text{m}$  band. Some PCR rise at the rear of laser pulse, that can be seen in Fig. 3.40a,b, is very weak. Moreover, the error of PCR calculation increases with a decrease of intensity of the probe wave. Thus we can not claim for the PCR increase observed to be due to



thermal mechanism of PC process. Therefore the time behaviour of PC and PCR pulses for CO laser are quite different as compared to CO<sub>2</sub> laser and refers to prevailing role of the resonance mechanism of nonlinearity. There seems to be some singularities for various spectral bands depended on relaxation properties of vibrational transitions of CO molecule. A theory of PC process in active medium of CO laser should be developed in more detail for explaining some effects observed.

#### *The influence of SIE on PC process.*

The experimental results on influence of SIE upon PCR (on intensity) are presented in Fig. 3.41 for various output couplers with reflectivities of 25%, 43% and 74% (threshold gain estimated is  $\alpha_{thr} = 0.6 \text{ m}^{-1}$ ,  $0.35 \text{ m}^{-1}$  and  $0.13 \text{ m}^{-1}$ ; spectral band is  $5.40 \text{ }\mu\text{m}$  with strong transition  $P_{10 \rightarrow 9}(15)$ ;  $\nu = 1851 \text{ cm}^{-1}$ ;  $\lambda = 5.403 \text{ }\mu\text{m}$ , the intensity ratio  $I_1/I_3$  is indicated in the figure). The experimental error was 10%. Within the accuracy there was no dependence of PCR upon SIE (the lines on the diagram are given only for convenience). The output energy increased with SIE rise (for instance, from 0.5 J up to 1.3 J for the case of output coupler with reflectivity 43%). It should be noted that CO laser pulse length depends on a number of parameters: gas parameters (mixture, pressure, temperature), SIE and laser parameters (Q factor, spectral transitions). In the experiment for the same output coupler the laser pulse length decreased from  $350 \text{ }\mu\text{s}$  down to  $150 \text{ }\mu\text{s}$  with SIE rise. Thus the averaged laser intensity in the experiment increased of 6-fold. So, on the one hand the time behaviour of PCR approximately followed that of probe wave, on the other hand did not depend on the value of laser intensity averaged over the pulse length. Comparison of the results with the non-transient theory of resonance mechanism developed for two-level quantum system (Part 2) has shown that the PC process in CO laser should be described by more complicated theoretical model.

#### *Various output couplers.*

A comparison of PCR for various reflectivities of the output coupler demonstrates that the maximal PCR is observed for the laser cavity with the low Q factor (see Fig. 3.41  $R_{out}=25\%$ ). There is the approximately the same value of PCR for high Q resonators ( $R_{out}=43\%$  and  $74\%$ ), which is half as much as that of low Q cavity. This phenomenon can be connected with an intensity drop for low Q cavity and its approaching to the intensity of saturation (see Part 2). The intracavity intensity in high Q resonator is much higher than saturation intensity, i.e. the degree of

saturation is much higher than 1.0. Hence, the nonlinearity is lower in accordance with steady-state theory, but because of intensity rise the PCR keeps being constant. By comparing the experimental results for different output couplers one can conclude also that resonance mechanism might seem to describe the PC process in active medium of CO laser.

*Intensity ratio for intracavity co-propagating wave and probe signal.*

The experimental results are presented in Fig. 3.42 for three values of SIE. When intensity ratio  $I_1/I_3$  is changed between 0.4 and 8.0, i.e. with intensity decrease of probe wave and decrease of modulation depth for interference pattern taking place in active medium at DFWM, the linear (within the experimental error) rise of PCR is observed. However, with further decrease of probe wave intensity (or with intensity ratio rise from 8 up to 18) the PCR is almost not changed, or decreases. The reason of the PCR behaviour should be looking for in temporal behaviour of probe and PC signals. But time behaviour of the two signals in these experiments with response time of 0.1-1  $\mu$ s practically did not depend upon intensity ratio. Besides, the ratio did not affect the spatial characteristics of CO laser. Only the research of temporal behaviour of probe and PC signals with much better response time allowed us to find the change taking place in high frequency structure under various intensity ratios (see Part 4). Going ahead a little, we use a result of the Part 4, that with probe wave intensity rise, i.e. with a drop of intensity ratio, the high frequency structure becomes more complicated or more irregular within a round-trip period. As a result of the influence of probe wave intensity on temporal structure of laser pulse, the process of writing down and reading out the diffraction grating is deteriorated with intensity ratio decrease (for  $I_1/I_3$  less than 10 in our experiments). With higher intensity ratio ( $I_1/I_3 > 10$ ) the intensity of the probe wave does not affect the laser pulse structure and PCR approaches to a constant value.

*Gas density influence upon PC process.*

The experimental results are in Fig. 3.43 for two spectral bands of 5.39  $\mu$ m and 5.23  $\mu$ m. The permanent rise of the PCR is observed with gas density rise from 0.1 up to 0.5 Amagat for 5.39  $\mu$ m band. For 5.23  $\mu$ m spectral band, however, the rise of PCR takes place only between 0.1 and 0.2 Amagat, being more sharp compared to 5.39  $\mu$ m band. The further density rise leads to a decrease of PCR. Thus, the behaviour of PCR versus gas density for frequency selected CO laser depends upon spectral line (or band) itself. It should be noted that for a number of spectral bands we observed much more complicated behaviour. Such PCR behaviour seems to be due to kinetic

processes taking place in active medium of CO laser itself. The gas density rise changes the vibrational population function for CO laser, changes the gain spectrum distribution, laser intensity on selected wavelength, saturation intensity etc. Both lasing itself and PC process depends on vibrational-rotational transition selected. For relatively low vibrational transition 8-7 of 5.23  $\mu\text{m}$  band gas density rise leads to a decrease of SSG and intracavity intensity, that together with saturation intensity rise can result in PCR decrease with gas density rise from 0.2 up to 0.4 Amagat.

#### *Gas temperature.*

It should be noted that a decrease of PCR was observed with an increase of an initial gas temperature rise. For instance, with gas temperature rise from 120 K up to 140 K the PCR drops nearly two times ( $N = 0.3$  Amagat,  $\text{SIE} = 300 \text{ J/l Amagat}$ , 5.39  $\mu\text{m}$  band). The PCR fall seems to be connected also with kinetic processes in CO laser active medium, namely a change of vibrational population function, spectral distribution shift to higher laser levels, a SSG drop etc.

### **3.4 Conclusions**

1. The experimental research of PC process at DFWM of  $\text{CO}_2$  laser radiation selected the laser parameters which affected the PCR (on energy) very strongly. These parameters are as follows: specific input energy, Q factor of laser resonator, gas pressure, laser mixture content, interaction angle, optical delay between probe and co-propagating pumping wave. The other laser parameters such as a degree of linear polarization, spectral band, intensity ratio do not strongly influence upon PCR (though additional study is needed to understand the role of the intensity ratio).

The comparison of theoretical and experimental data demonstrated that experimentally obtained PCR was 1/8-1/20 as much as that obtained in theory. Besides, the analysis of the experimental data shows, that PCR increases with gas pressure rise, but there is a "plateau" in the pressure range of 0.2-0.4 atm. Theoretical calculation predicted for PCR rise to be square proportional to gas pressure. The disagreement between theoretical and experimental data might be due to process taking place in active medium of  $\text{CO}_2$  laser and being connected with self-influence of laser radiation. These processes were not taking into account in theory, but were observed when studying experimentally a temporal behaviour of PC and PCR signals.

The study demonstrated that there were two principal mechanisms which were responsible for PC process at intracavity DFWM of  $\text{CO}_2$  laser radiation: resonance (amplitude) and thermal

(phase) ones. When increasing nitrogen content in laser mixture or decreasing input power the two mechanisms display themselves very distinctly. The maximum value of PCR of resonance mechanism was observed for the front part of the laser pulse in accordance with the theory of the mechanism. The PCR rise in the end of the laser pulse refers to more inertial thermal mechanism. It should be noted that the amplitudes of PCR for both mechanisms are comparable, i.e. the contribution of the two processes (resonance and thermal one) are comparable also.

The complicated temporal behaviour of PCR is due to alteration of laser intensity in time and also due to effect of disturbances in active medium upon the processes of formation of laser radiation itself and of PC signal. In particular, PCR rise is restricted in the middle part of the CO<sub>2</sub> laser pulse on account of decrease of relaxation time of thermal grating. When analyzing the PC process, it follows that relaxation properties of thermal grating are changed during laser pulse under the influence of disturbances in active medium. That fact leads to a decrease of experimental PCR compared to theoretical one. Thus the self-influence of laser radiation should be taken into account when analyzing the thermal mechanism in theory. The correlation between higher optical quality and lower PCR involves also and additional experimental theoretical research.

2. The parametric study of PCR at DFWM in active medium of EBCD CO laser enables us to make following conclusions:

- the PC process does take place for CO laser at DFWM of its radiation in its active medium;
- the PCR (on intensity) reaches 1.0%, the PCR (on energy) amounting 0.5%;
- the functional dependencies of PCR and temporal behaviour of PC and PCR signals differ strongly from those obtained for EBCD CO<sub>2</sub> laser;
- the parametric study refers to the resonance mechanism to be responsible for PC process in CO laser active medium;
- a theory taking into account the real laser parameters should be developed for describing the PC process in active medium of CO laser.

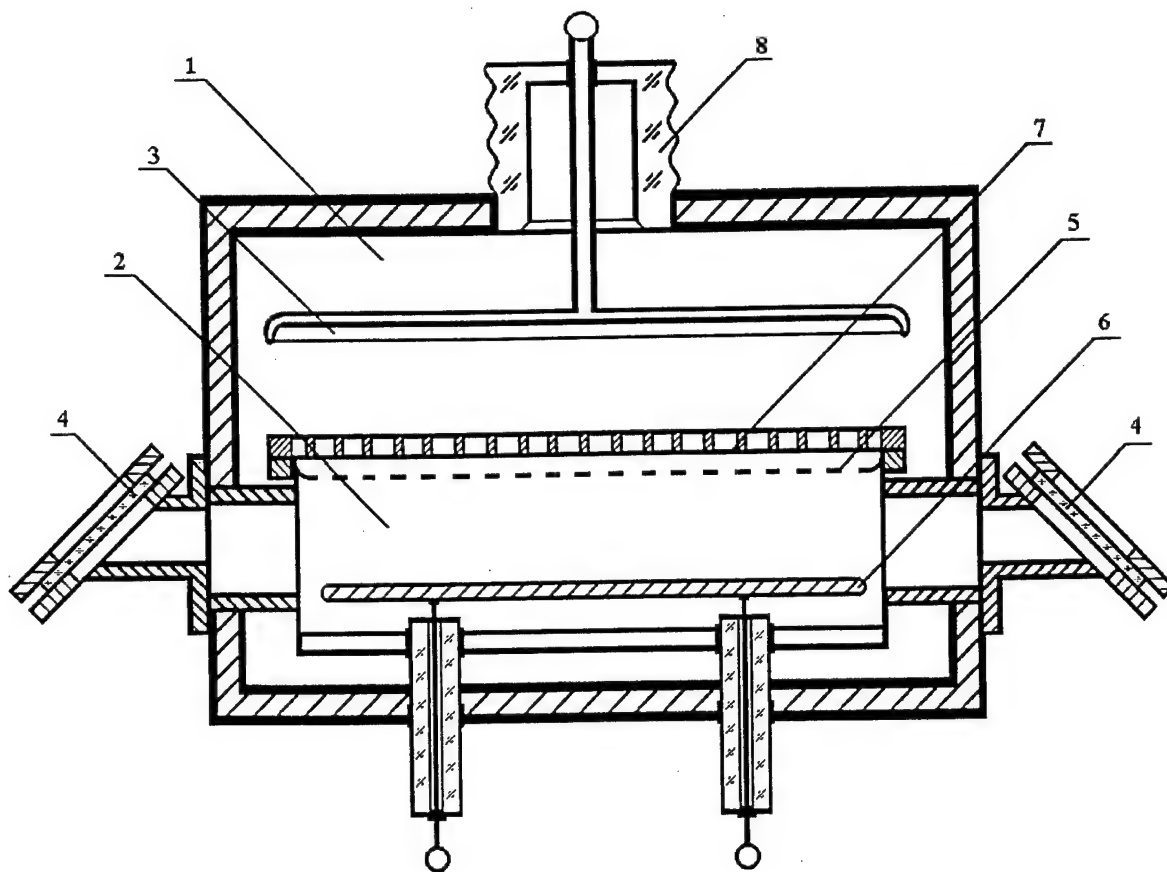


Fig. 3.1. Electron-beam controlled discharge (EBCD) CO<sub>2</sub> / CO laser installation

- 1 - vacuum e-beam gun chamber  
internal volume: 1.5 (length) x 0.5 (width) x 0.7 (height) m<sup>3</sup>;
- 2 - EBCD laser chamber  
internal volume: 0.150 m<sup>3</sup>;  
discharge volume: 120 (length) x 14 (width) x 11 (height) cm<sup>3</sup> = 18.5 litres;
- 3 - hot cathode;
- 4 - EBCD laser chamber windows  
(at the Brewster angle to the optic axis of the resonator);
- 5 - mesh grounded cathode;
- 6 - copper anode;
- 7 - 40 µm polyimide foil and stainless steel flange  
(e-beam transparency about 40%);
- 8 - high voltage isolator.

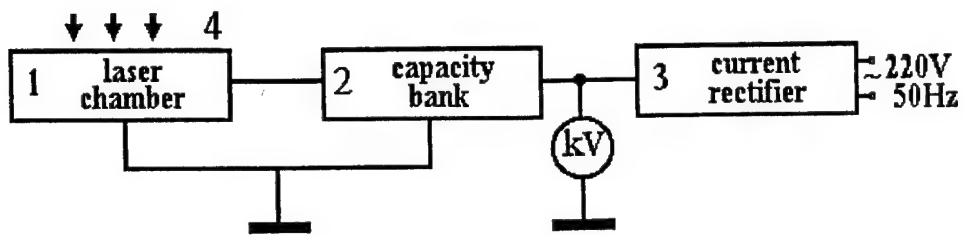


Fig. 3.2. EBCD high voltage supply system

- 1 - EBCD laser chamber;
- 2 - 21  $\mu\text{F}$  capacitor bank;
- 3 - 25 kW current rectifier (high voltage up to 50 kV);
- 4 - 150 keV e-beam.

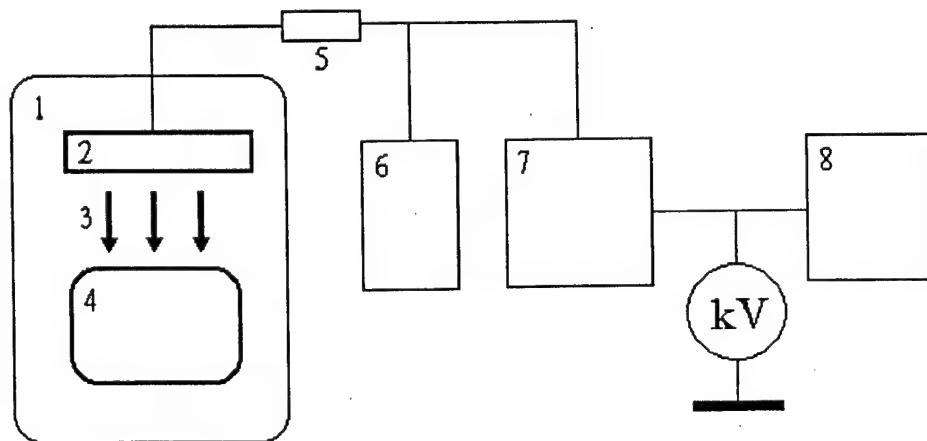


Fig. 3.3. E-beam gun supply system

- 1 - vacuum electron-beam gun chamber;
- 2 - hot cathode;
- 3 - 150 keV electron-beam;
- 4 - EBCD laser chamber;
- 5 - 65  $\Omega$  ballast resistor;
- 6 - 13 kW current transformer;
- 7 - 150 kV four-stage Marks generator (0.1  $\mu\text{F}$ );
- 8 - 25 kW current rectifier (high voltage up to 50 kV).

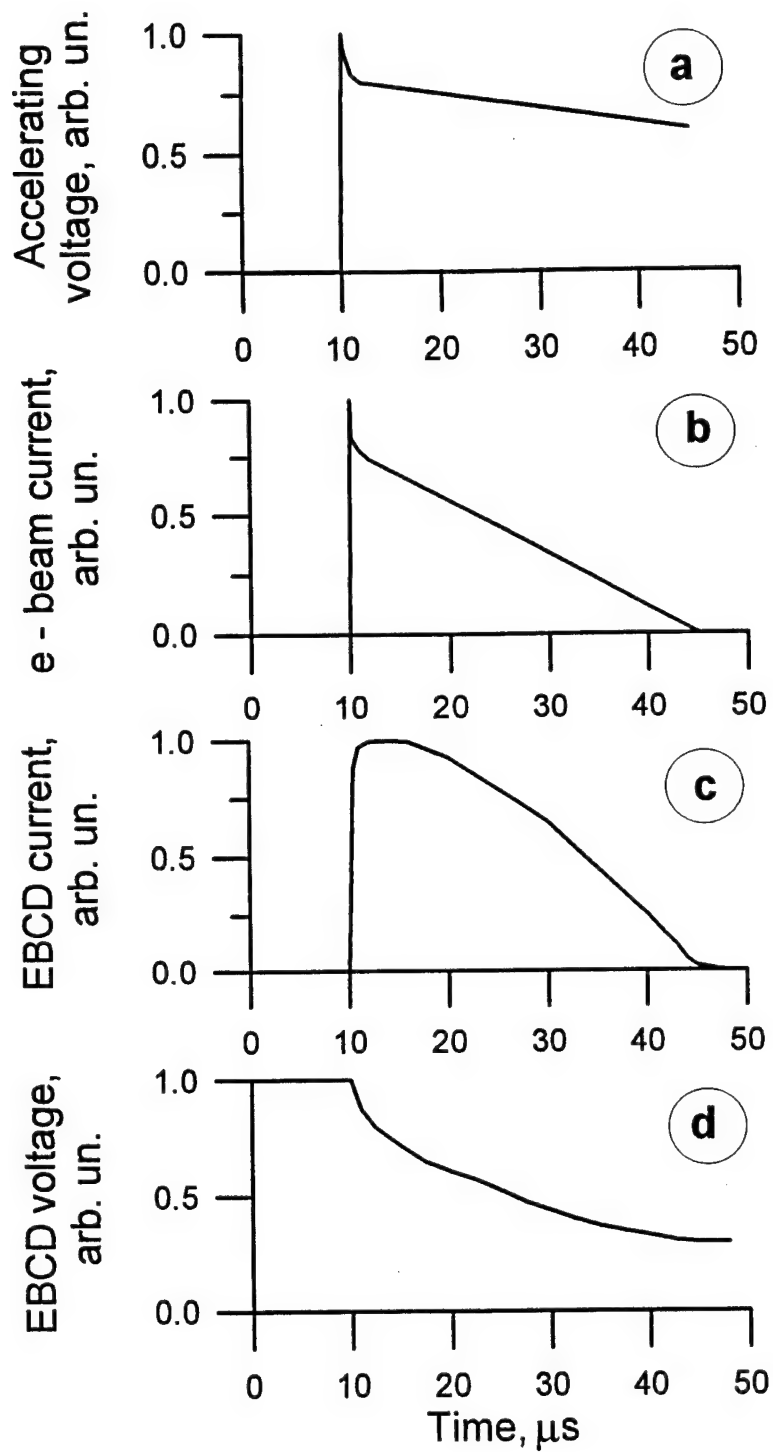


Fig. 3.4. Time-history of EBCD input energy  
 a - e-beam accelerating voltage;  
 b - e-beam current;  
 c - EBCD current;  
 d - EBCD voltage.

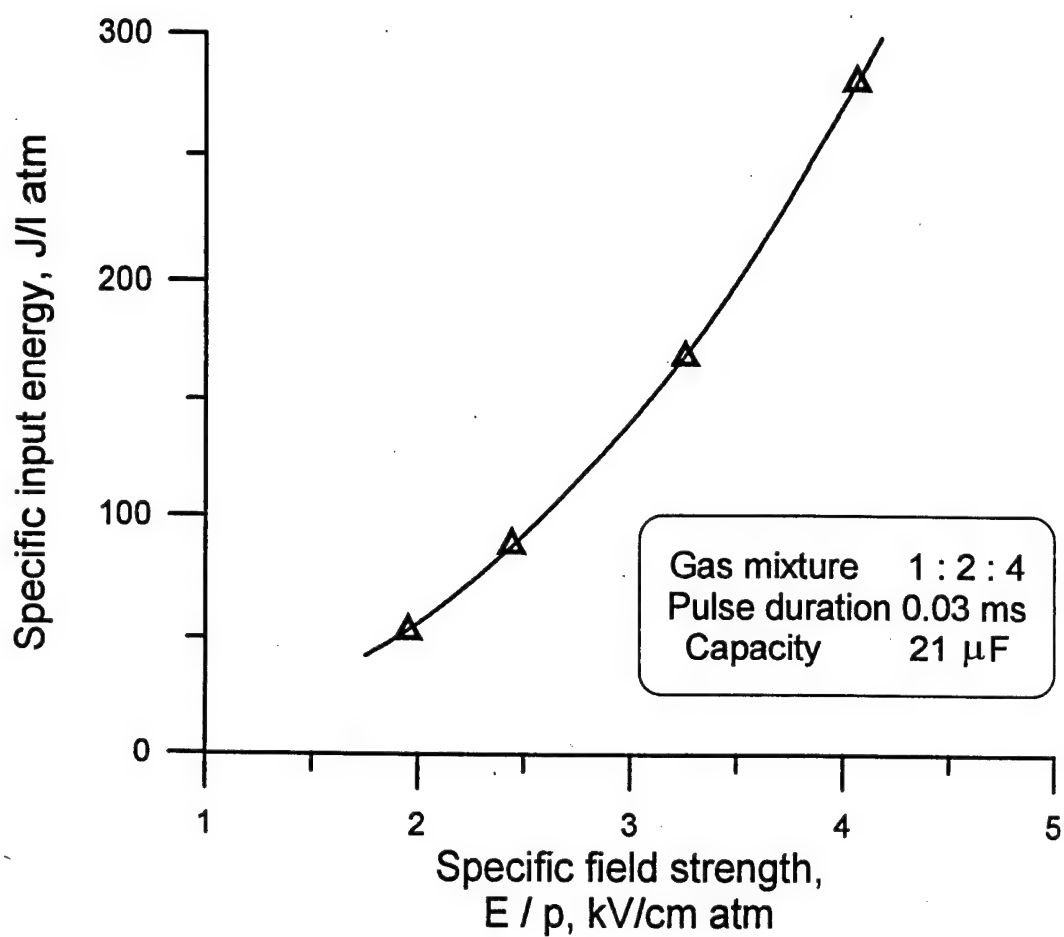


Fig. 3.5. EBCD specific input energy vs specific field strength,  $E / p$   
( $\text{CO}_2 : \text{N}_2 : \text{He} = 1 : 2 : 4$ , 0.28 atm).

Table 3.1. EBCD specific input energy vs specific field strength,  $E / p$   
( $\text{CO}_2 : \text{N}_2 : \text{He} = 1 : 2 : 4$ , 0.28 atm) (data for Fig. 3.5).

$E / p$ , kV/cm atm	1.95	2.44	3.25	4.06
Specific input energy, J/l atm	53	89	169	281



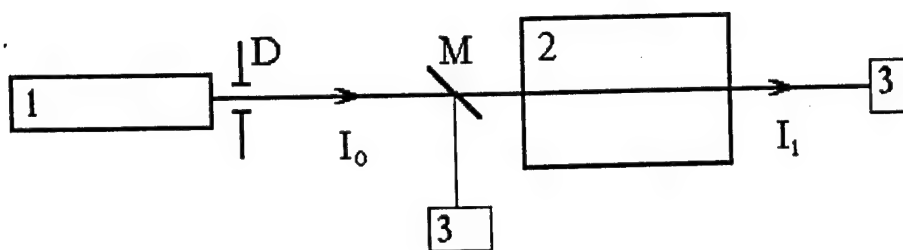


Fig. 3.6a. Optical scheme for the experiments on temporal behavior of small signal gain in the CO<sub>2</sub> inverted medium.

- 1 - CW 10.6 μm low pressure CO<sub>2</sub> laser;
- 2 - EBCD laser chamber with inverted gas mixture  
(CO<sub>2</sub> : N<sub>2</sub> : He = 1 : 2 : 4);
- 3 - photodetectors;
- $I_0$  - 10.6 μm laser probe beam intensity;

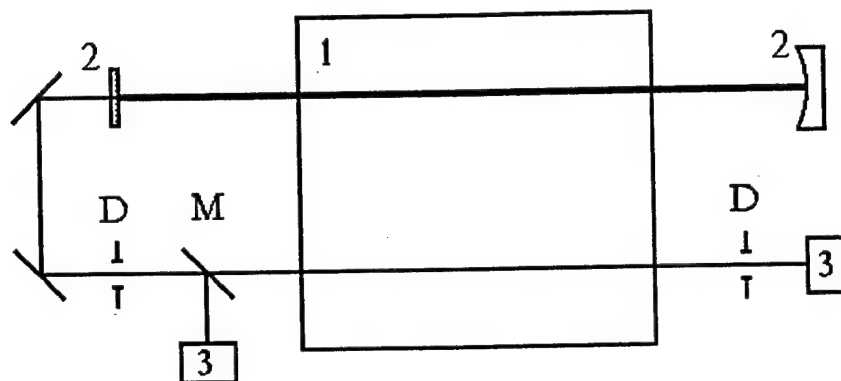


Fig. 3.6b. Optical scheme for measurement of laser gain.

- 1 - EBCD laser chamber with inverted gas medium;
- 2 - mirrors of the optical resonator;
- 3 - calorimeters or photodetectors;
- M - laser beam splitter;
- D - diaphragm.

Intensity  
of amplified  
signal, arb. un.

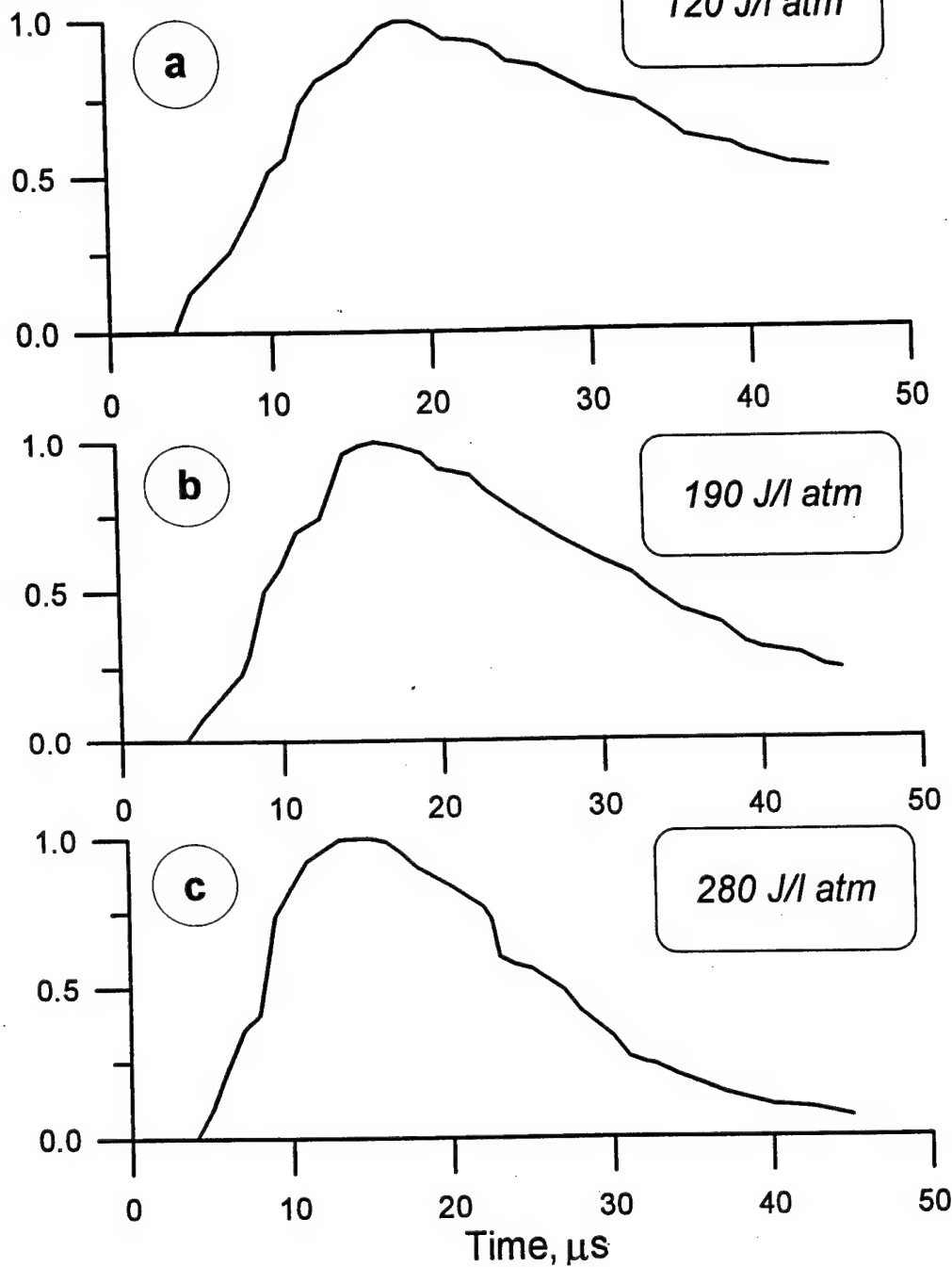


Fig. 3.7. Time-history of the amplified small  $10.6 \mu\text{m}$  laser signal in the inverted medium for different specific input energy:

a - 120 J/l atm;

b - 190 J/l atm;

c - 280 J/l atm.

Gas mixture

$\text{CO}_2 : \text{N}_2 : \text{He} = 1 : 2 : 4.$

Gas pressure

0.28 atm.

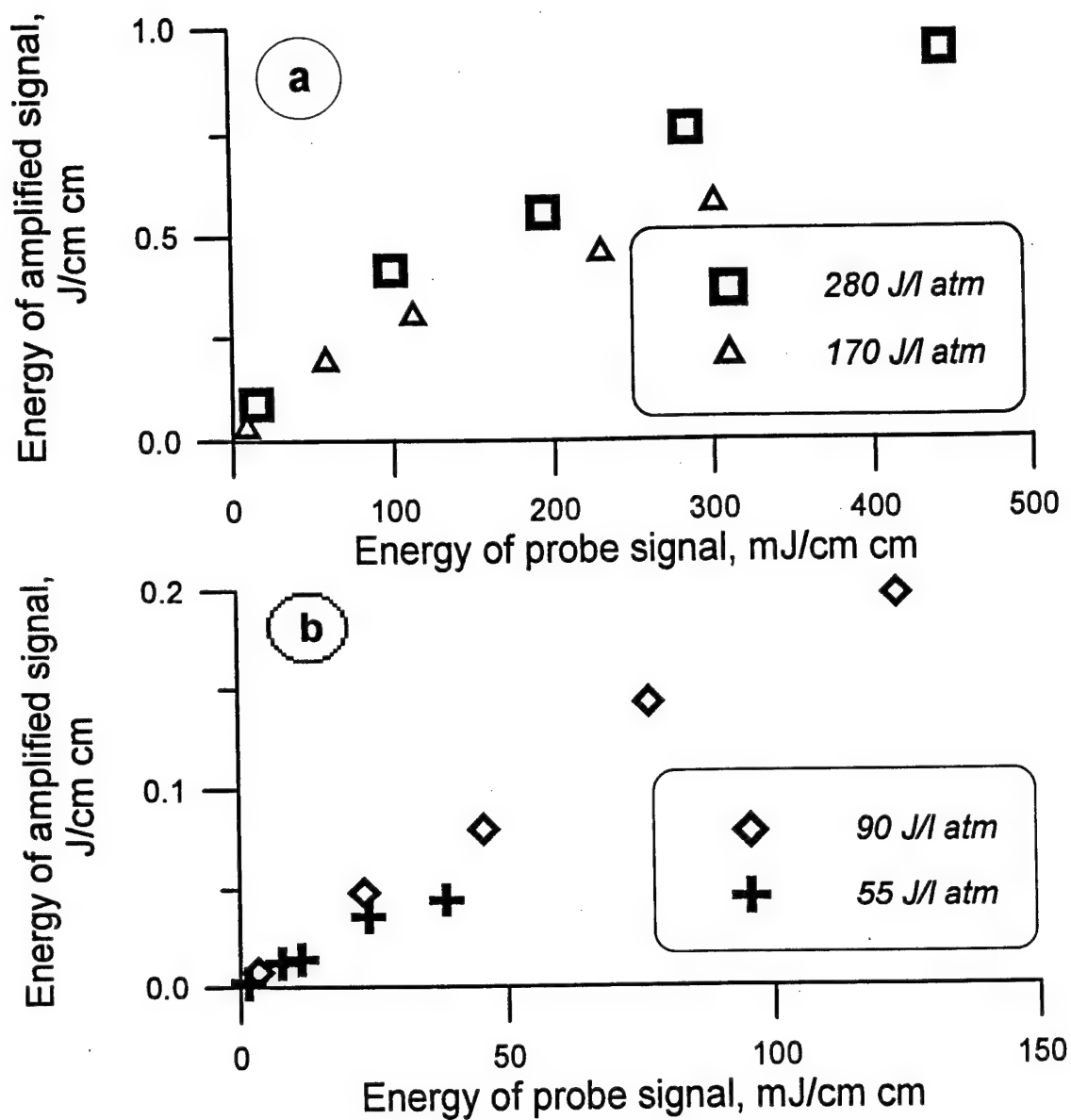


Fig. 3.8. Energy density of amplified signal versus that of probe one for different specific input energy:

a - 280 J/l atm and 170 J/l atm;

b - 90 J/l atm and 55 J/l atm.

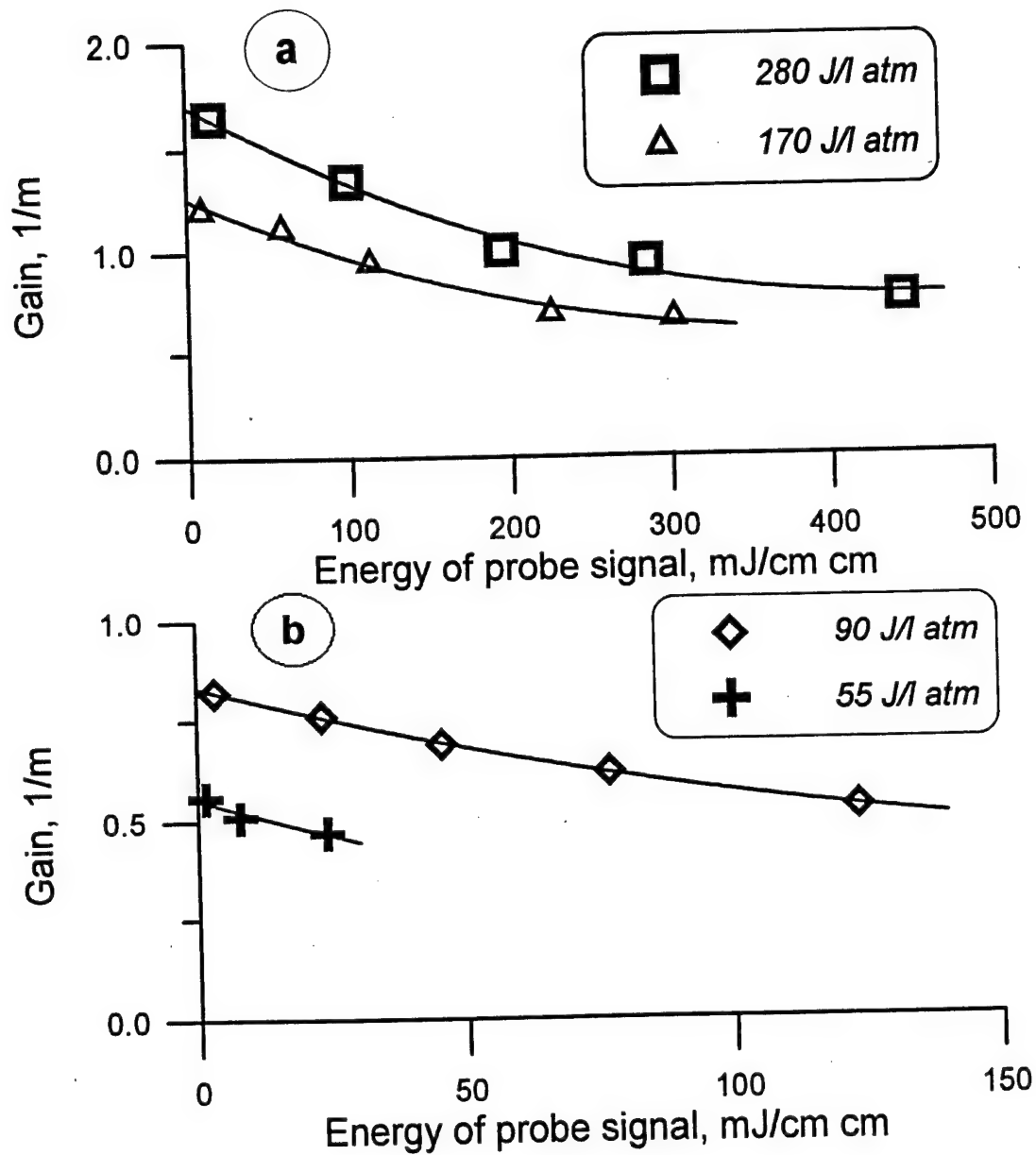


Fig. 3.9. Gain vs energy density of probe signal for different EBCD specific input energy:

- a - 280 J/l atm and 170 J/l atm;
- b - 90 J/l atm and 55 J/l atm.

Table 3.2. Energy density of amplified signal ( $q_{amp}$ ) and gain ( $\alpha$ ) versus energy density of probe one ( $q_{pr}$ ) for different specific energy ( $Q_{in}^{sp}$ ) (data for Fig. 3.8 and Fig. 3.9).

Gas mixture 1 : 2 : 4.  
Gas pressure 0.28 atm.  
Reflectivity of laser output mirror 50%.

$Q_{in}^{sp}$	280 J/l atm		170 J/l atm			90 J/l atm			55 J/l atm		
$q_{pr}, \frac{mJ}{cm^2}$	$q_{amp}, \frac{mJ}{cm^2}$	$\alpha, 1/m$	$q_{pr}, \frac{mJ}{cm^2}$	$q_{amp}, \frac{mJ}{cm^2}$	$\alpha, 1/m$	$q_{pr}, \frac{mJ}{cm^2}$	$q_{amp}, \frac{mJ}{cm^2}$	$\alpha, 1/m$	$q_{pr}, \frac{mJ}{cm^2}$	$q_{amp}, \frac{mJ}{cm^2}$	$\alpha, 1/m$
14	89	1.65	8	30	1.21	3	7	0.82	1	2	0.56
98	416	1.35	57	191	1.12	23	48	0.76	7	12	0.51
194	554	1.01	112	301	0.95	45	80	0.69	23	36	0.47
284	758	0.95	224	437	0.69	76	143	0.62			
443	942	0.76	301	574	0.66	123	198	0.53			

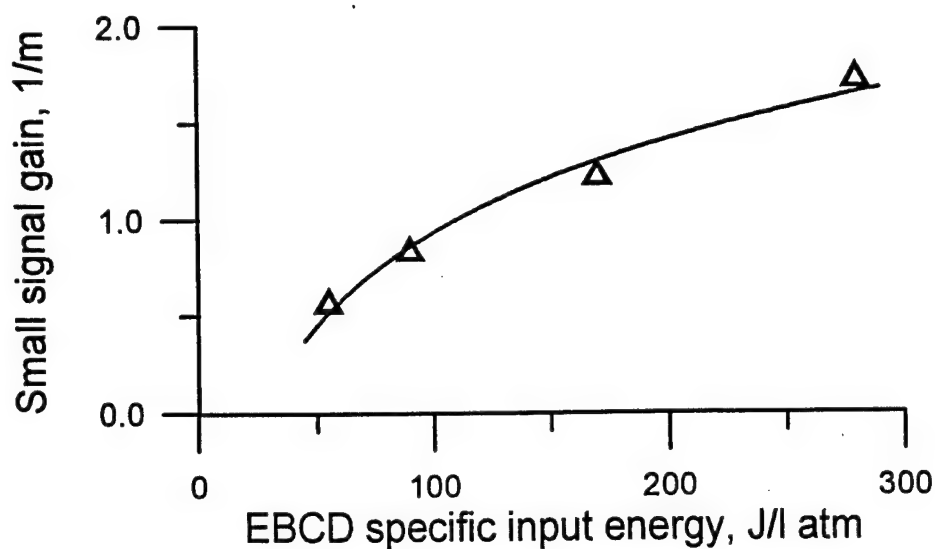


Fig. 3.10. Small signal gain versus EBCD specific input energy .

Table 3.3. Small signal gain ( $\alpha_0$ ) versus EBCD specific input energy ( $Q_{in}^{sp}$ ) (data for Fig. 3.10).

Gas mixture 1 : 2 : 4.  
Gas pressure 0.28 atm.

$Q_{in}^{sp}, J/l atm$	280	170	90	55
$\alpha_0, 1/m$	1.72	1.22	0.83	0.56

Table 3.4. Specific output energy ( $Q_{out}^{sp}$ ) versus EBCD specific input energy ( $Q_{in}^{sp}$ ) for different reflectivity of laser output mirror ( $R_{out}$ ) (data for Fig. 3.11).

Gas mixture 1 : 2 : 4.  
Gas pressure 0.28 atm

$R_{out} = 45\%$		$R_{out} = 65\%$	
$Q_{in}^{sp},$ J/l atm.	$Q_{out}^{sp},$ J/l atm.	$Q_{in}^{sp},$ J/l atm.	$Q_{out}^{sp},$ J/l atm.
158	4.8	116	3.7
245	10.6	187	6.6
348	15.6	277	8.7

Table 3.5. Laser efficiency ( $\eta$ ) versus reflectivity of laser output mirror ( $R_{out}$ ) for the same EBCD specific input energy: 280 J/l atm (data for Fig. 3.12).

Gas mixture 1 : 2 : 4.  
Gas pressure 0.28 atm

$R_{out}, \%$	8	30	45	65
$\eta, \%$	5.2	6.0	4.3	3.1

Table 3.6. Energy density of laser output signal versus gas pressure for two EBCD specific input energy: 300 and 200 J/l atm (data for Fig. 3.13).

Gas mixture 1 : 2 : 4.  
 $R_{out}$  50%.

p, atm	$q_{las}, J/cm^2$	
	$Q_{in}^{sp}, = 200 J/l atm$	$Q_{in}^{sp}, = 300 J/l atm$
0.1	0.20	0.29
0.14	0.29	0.43
0.20	0.44	0.65
0.28	0.64	0.97
0.40	0.89	1.41

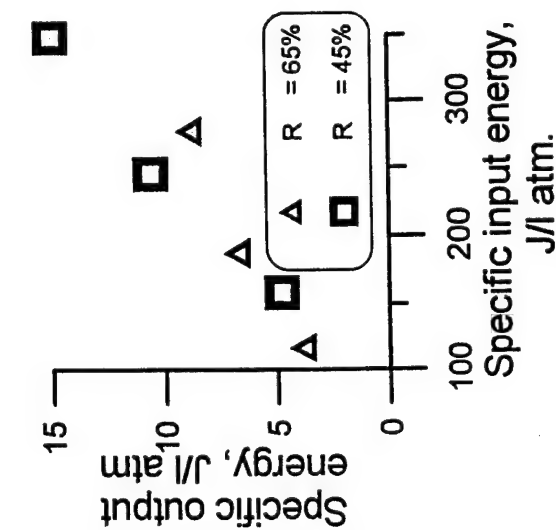


Fig. 3.11. Specific output energy versus EBCD specific input energy for different reflectivity of laser output mirror (R).  
 Gas mixture 1 : 2 : 4.  
 Gas pressure 0.28 atm

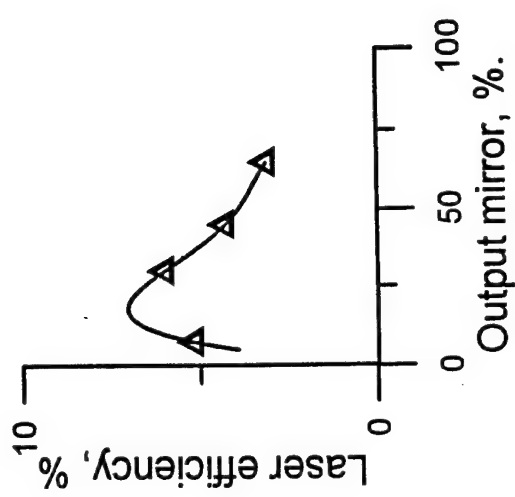


Fig. 3.12. Laser efficiency versus reflectivity of laser output mirror for the same EBCD specific input energy: 280 J/l atm.  
 Gas mixture 1 : 2 : 4.  
 Gas pressure 0.28 atm

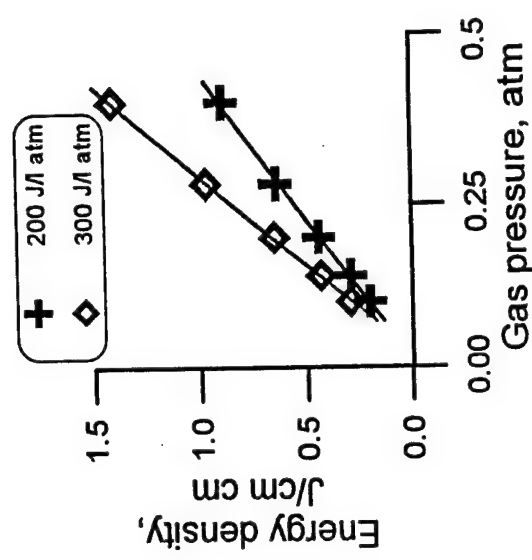


Fig. 3.13. Energy density of laser output signal versus gas pressure for two EBCD specific input energy: 300 and 200 J/l atm.  
 Gas mixture 1 : 2 : 4.  
 $R_{out}$  50%.

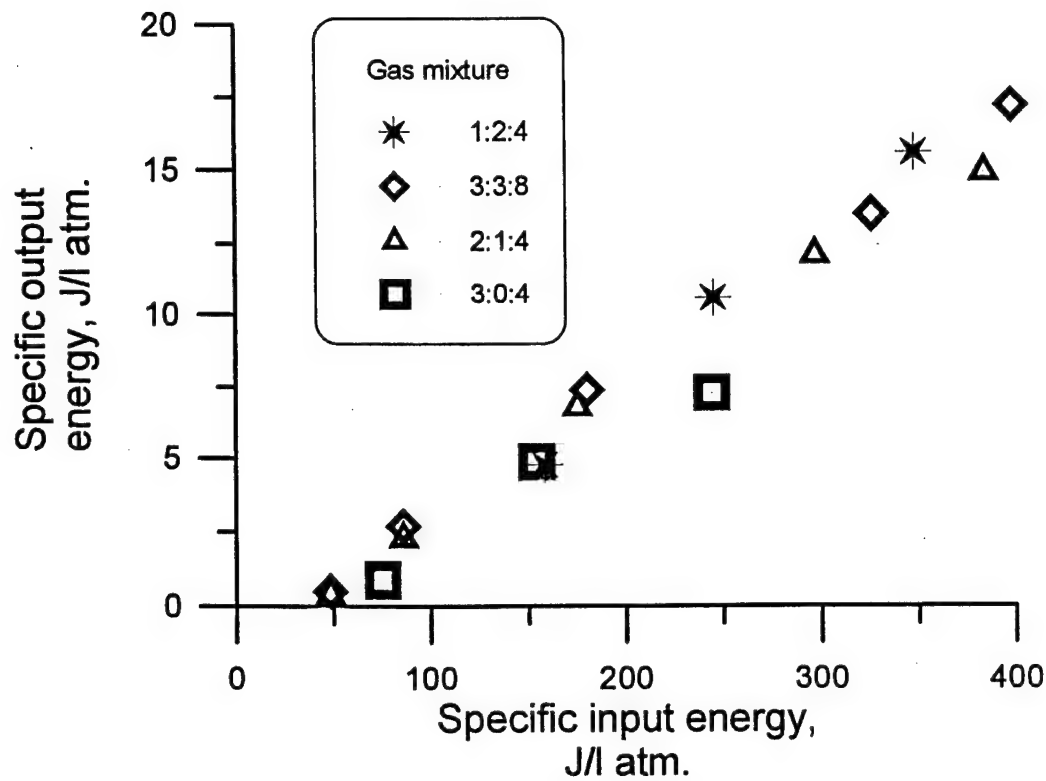


Fig. 3.14. Specific laser output energy versus specific input energy for different gas mixture ( $\text{CO}_2 : \text{N}_2 : \text{He} = x : y : z$ ).

Table 3.7. Specific laser output energy ( $Q_{\text{out}}^{\text{sp}}$ ) versus specific input energy ( $Q_{\text{in}}^{\text{sp}}$ ) for different gas mixture ( $\text{CO}_2 : \text{N}_2 : \text{He} = x : y : z$ ) (data for Fig. 3.14).

Gas pressure 0.28 atm.

Reflectivity of output mirror 46%

1 : 2 : 4			3 : 3 : 8			2 : 1 : 4			3 : 0 : 4		
$Q_{\text{in}}^{\text{sp}},$ J l atm.	$Q_{\text{out}}^{\text{sp}},$ J l atm.	$\eta, \%$	$Q_{\text{in}}^{\text{sp}},$ J l atm.	$Q_{\text{out}}^{\text{sp}},$ J l atm.	$\eta, \%$	$Q_{\text{in}}^{\text{sp}},$ J l atm.	$Q_{\text{out}}^{\text{sp}},$ J l atm.	$\eta, \%$	$Q_{\text{in}}^{\text{sp}},$ J l atm.	$Q_{\text{out}}^{\text{sp}},$ J l atm.	$\eta, \%$
158	4.8	3.0	48	0.5	1.0	48	0.4	0.8	75	0.9	1.2
245	10.6	4.3	86	2.7	3.1	86	2.3	2.7	154	4.9	3.2
348	15.6	4.5	180	7.4	4.1	175	6.8	3.9	244	7.3	3.0
---	---	---	326	13.5	4.1	297	12.1	4.1	---	---	---
---	---	---	398	17.2	4.3	384	14.9	3.9	---	---	---



Table 3.8 Default\* parameters of the parametric study of the PC process

gas mixture CO <sub>2</sub> : N <sub>2</sub> : He	1 : 2 : 4
gas pressure	0.28 atm
gas temperature	300 K
length of the laser resonator	12 m
spectral content of the laser output	10.6 $\mu$ m single line P(20) without spectral selection
degree of linear polarization	more than 99.5%
length of the active medium	1.2 m
location of the cross point	the center of the active medium
interaction angle of DFWM	15 mrad
optical delay between the probe wave and the forward pump	$\pm 10$ cm

\* See a definition of the term "default" at the beginning of the chapter 3.2

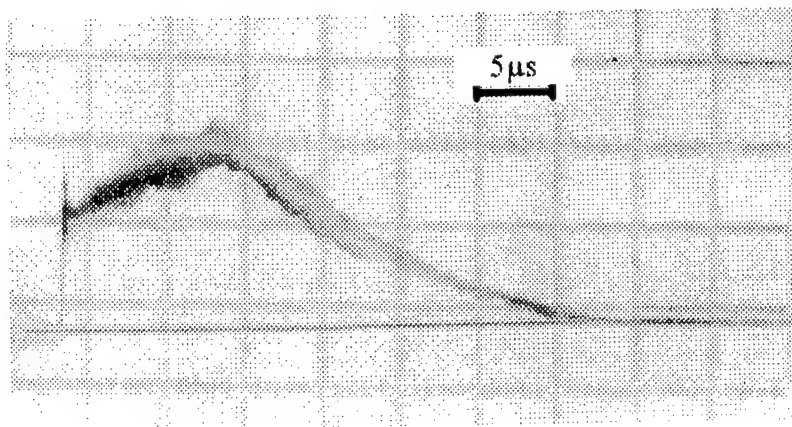


Fig. 3.15. Typical EBCD CO<sub>2</sub> laser pulse profile measured with Ge: Au photodetector.

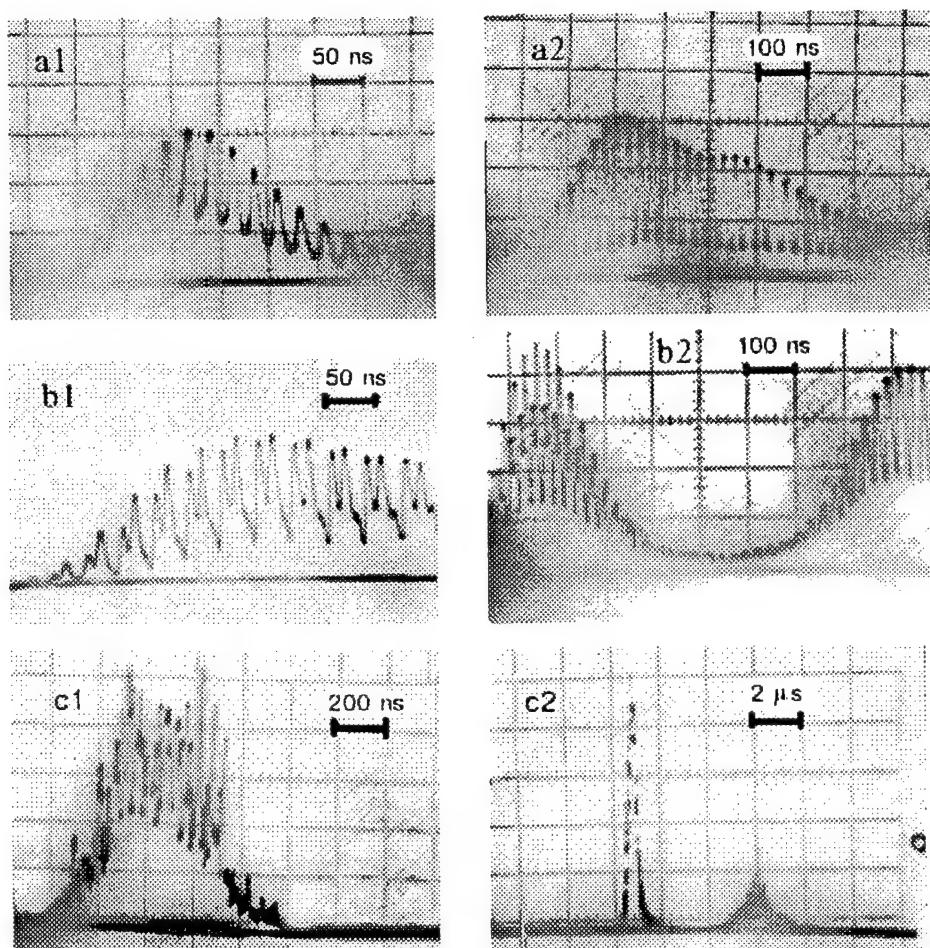


Fig. 3.16. First peak (1) and following part (2) of the EBCD CO<sub>2</sub> laser pulse time resolved with photon- drag detector for different experimental conditions:

- a - CO<sub>2</sub>:N<sub>2</sub>:He = 1:2:4, SIE 200 J/l atm;
- b - CO<sub>2</sub>:N<sub>2</sub>:He = 1:2:4, SIE 100 J/l atm;
- c - CO<sub>2</sub>:N<sub>2</sub>:He = 3:0:4, SIE 200 J/l atm.

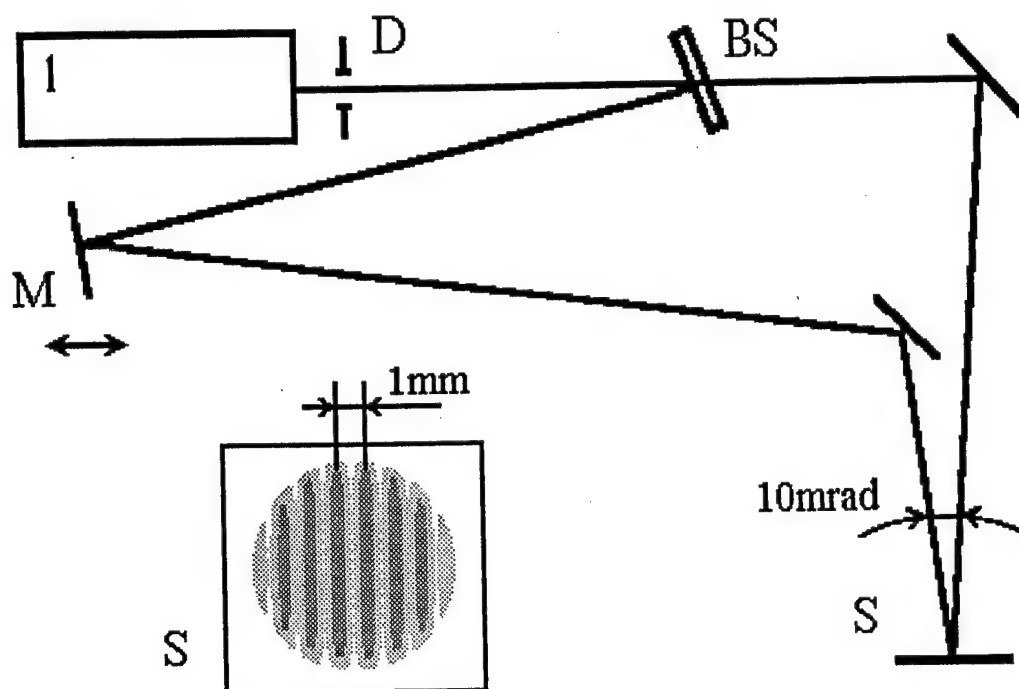


Fig. 3.17. Optical scheme of measurement of coherent length of laser output.

- 1 - EBCD laser;
- BS - laser beam splitter ( $R = 50\%$ );
- M - a folding mirror changing an optical delay;
- S - a screen with an interference pattern;
- D - 15 mm diaphragm.

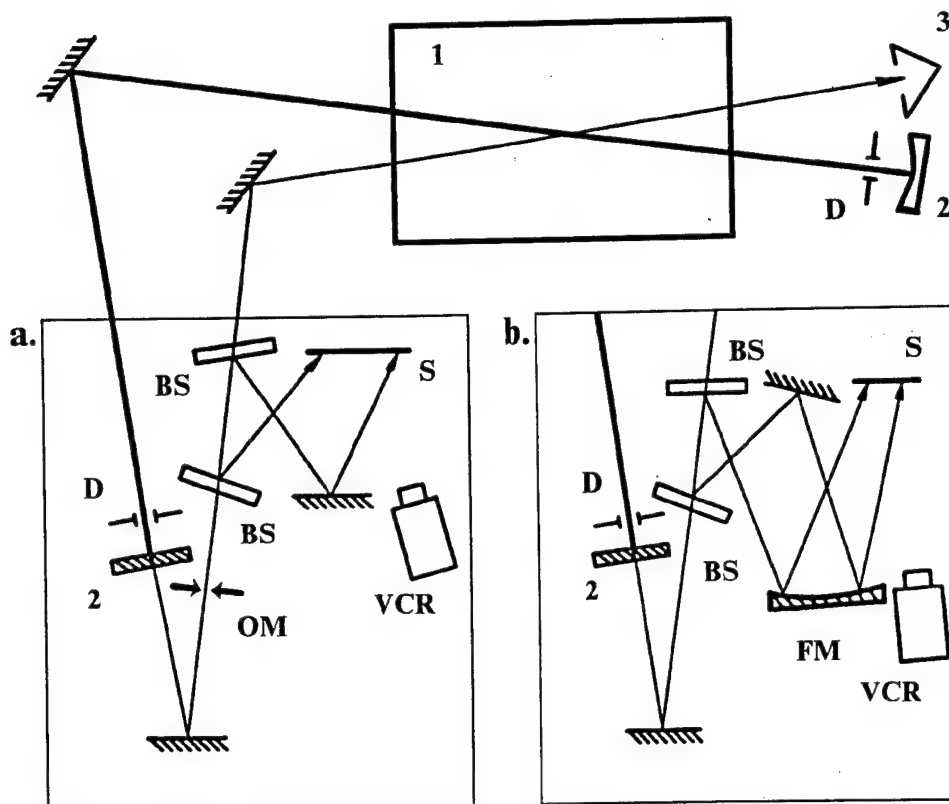


Fig. 3.18. Schematic of near-field zone (a) and far-field zone (b) experiments.

- 1 - EBCD laser chamber with inverted gas medium;
- 2 - mirrors of the optical resonator;
- 3 - absorber;
- BS - laser beam splitter;
- S - diffusely scattering screen;
- OM - optical mask;
- FM - focusing mirror;
- VCR - IR video system;
- D - diaphragm.

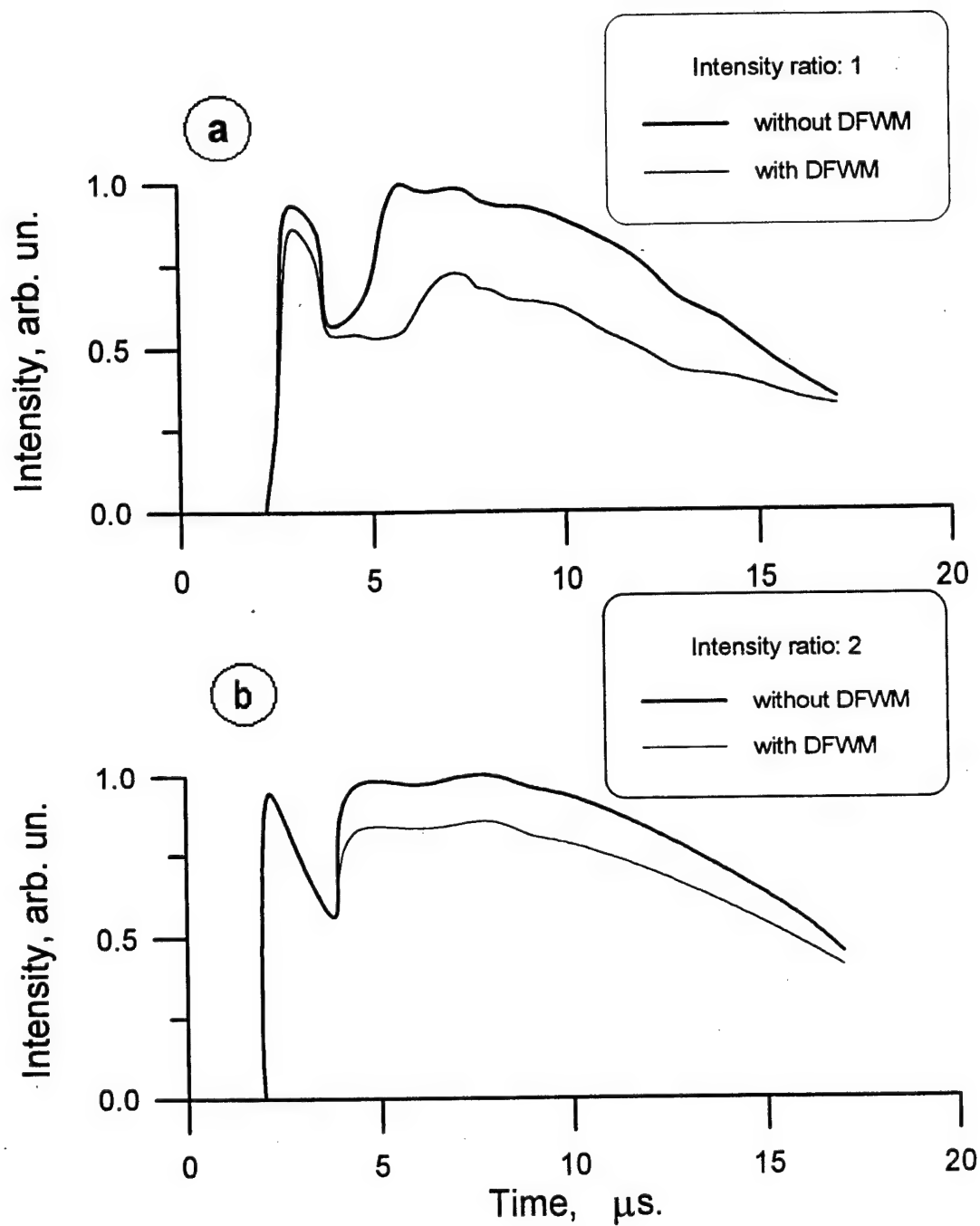


Fig. 3.19. Influence of DFWM on the time-history of laser pulse.

Intensity ratio of a pumping signal to a probe one:

a  $I_1 / I_3 = 1$ ;

b  $I_1 / I_3 = 2$ .

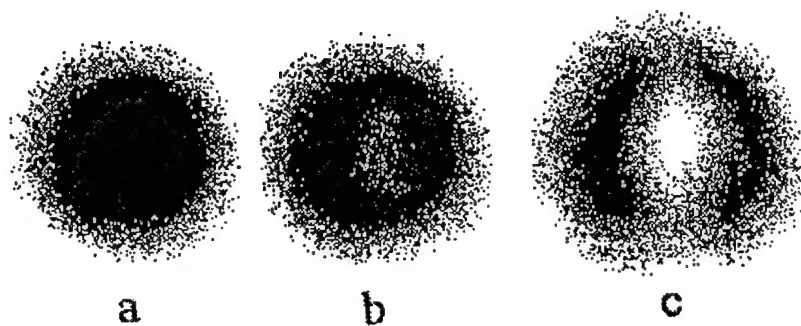


Fig. 3.20. The transformation of near-field intensity distribution of  $\text{CO}_2$  laser pulse ( $I_1$ ) under the influence of DFWM:

a - DFWM turned off;

b - DFWM turned on ( $I_1/I_3 \sim 1$ );

c - the amplified signal propagated through the inverted medium at DFWM.

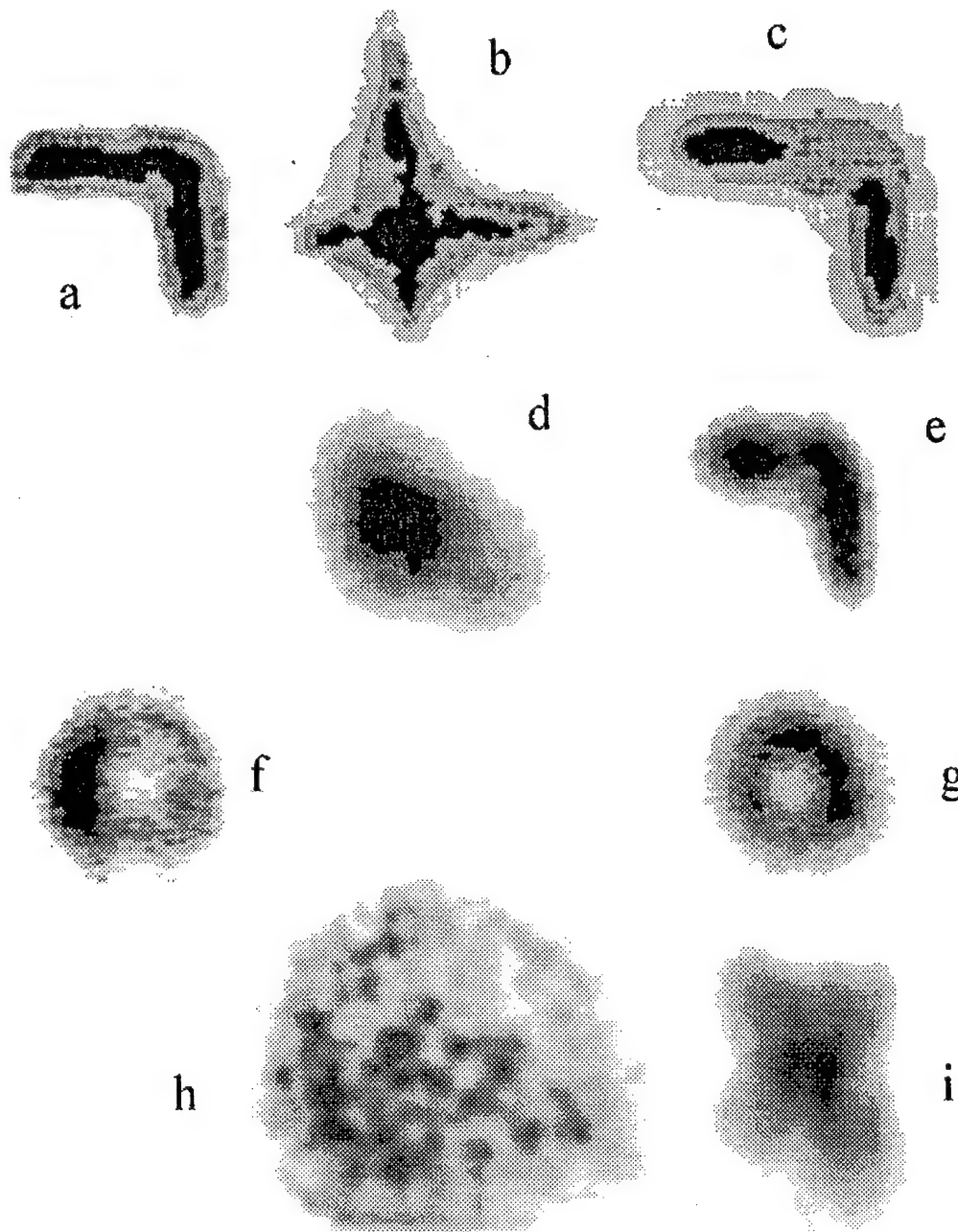


Fig. 3.21. IR distribution of laser (probe) beam and backscattered (at DFWM) one:

- a - CO<sub>2</sub> laser radiation crossed L-shaped optical mask;
- b - the laser radiation at a distance of 4.5 m from the mask;
- c - the backscattered (at DFWM in active medium of the CO<sub>2</sub> laser) signal in the plane of the mask;
- d - CO laser radiation crossed L-shaped optical mask and measured at a distance of 3 m from the mask;
- e - the backscattered (at DFWM in active medium of the CO laser) signal in the plane of the mask;
- f - CO<sub>2</sub> laser radiation crossed O-shaped optical mask;
- g - the backscattered (at DFWM in active medium of the CO<sub>2</sub> laser) signal in the plane of the mask;
- h - an optical noise from the CO<sub>2</sub> laser resonator without DFWM (multiplied by 100);
- i - the backscattered (at DFWM in active medium of the CO<sub>2</sub> laser) signal in the plane of the X-shaped optical mask.

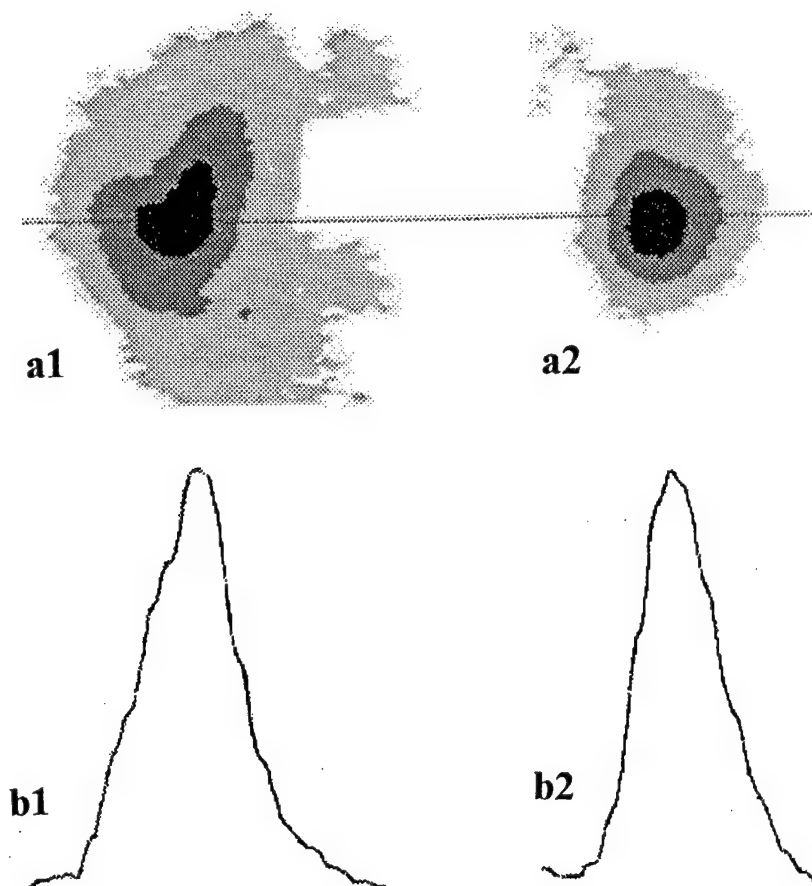


Fig. 3.22. IR distribution (a) and its intensity profile (b) for  
1- CO<sub>2</sub> laser (probe) beam;  
2 - backscattered at DFWM radiation.



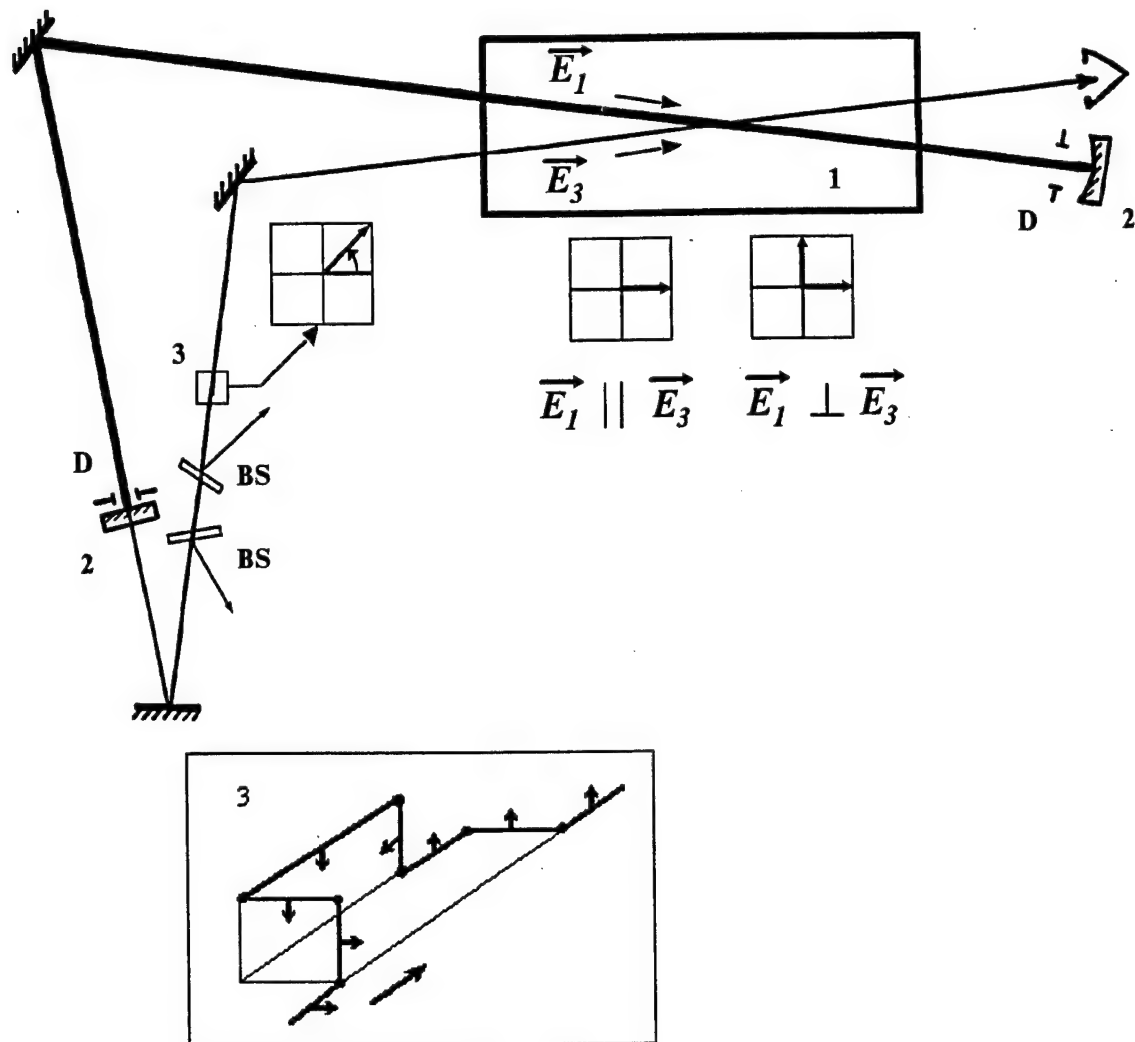


Fig. 3.23. Optical scheme of polarization tests.

- 1 - EBCD laser chamber with inverted gas mixture;
- 2 - mirrors of the optical resonator;
- 3 - system of the flat mirrors for rotation of polarization plane;
- BS - laser beam splitter;
- D - diaphragm.

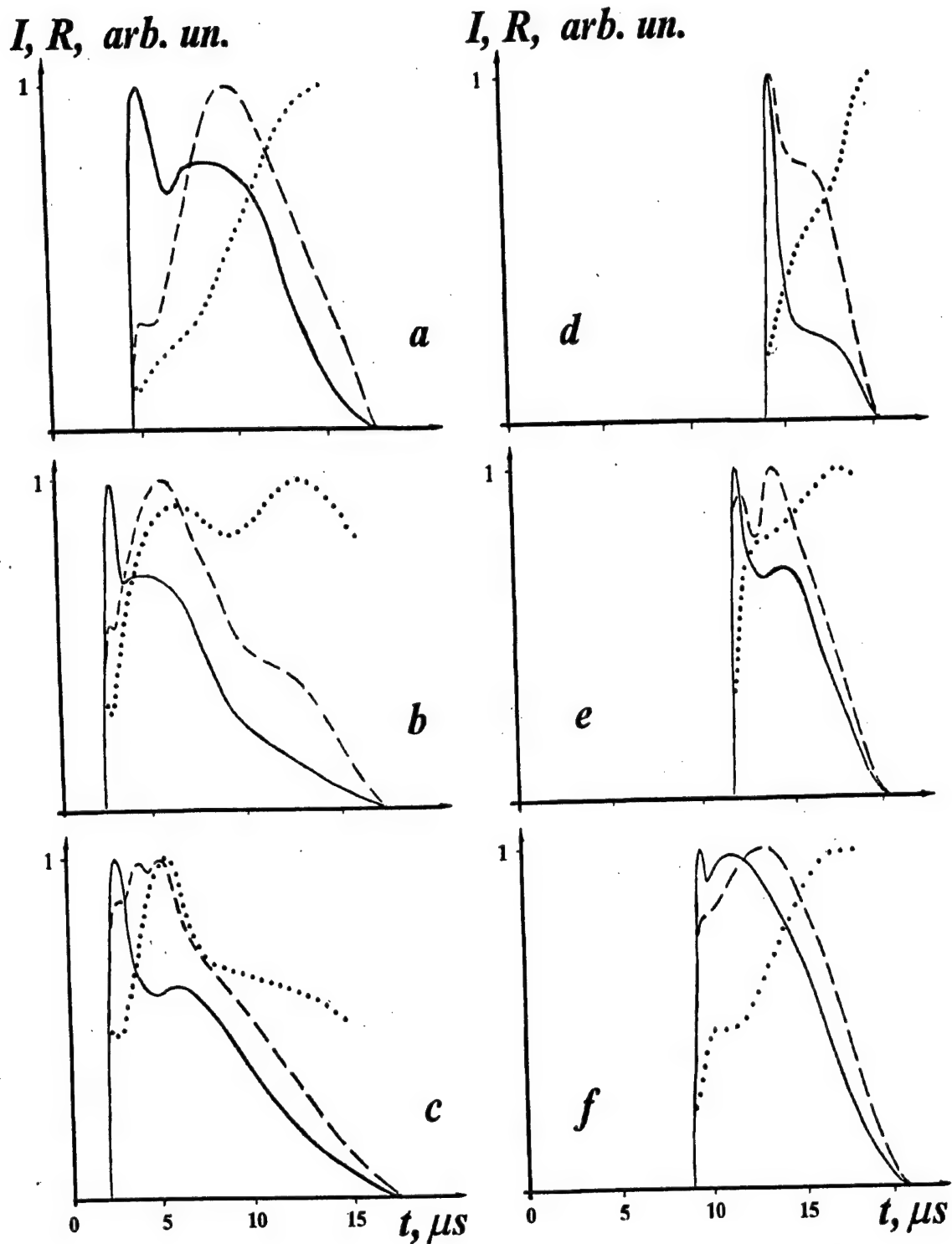


Fig. 3.24. Probe (curve 1 - solid line), PC (curve 2 - dashed line) and PCR (curve 3 - dotted line) pulses under different experimental conditions:  
*a, d* - 120 J/l atm; *b, e* - 190 J/l atm; *c, f* - 280 J/l atm;  
*a - c* -  $R_{\text{out}} = 65\%$ ; *d - f* -  $R_{\text{out}} = 7.5\%$ .

I, R arb. un.

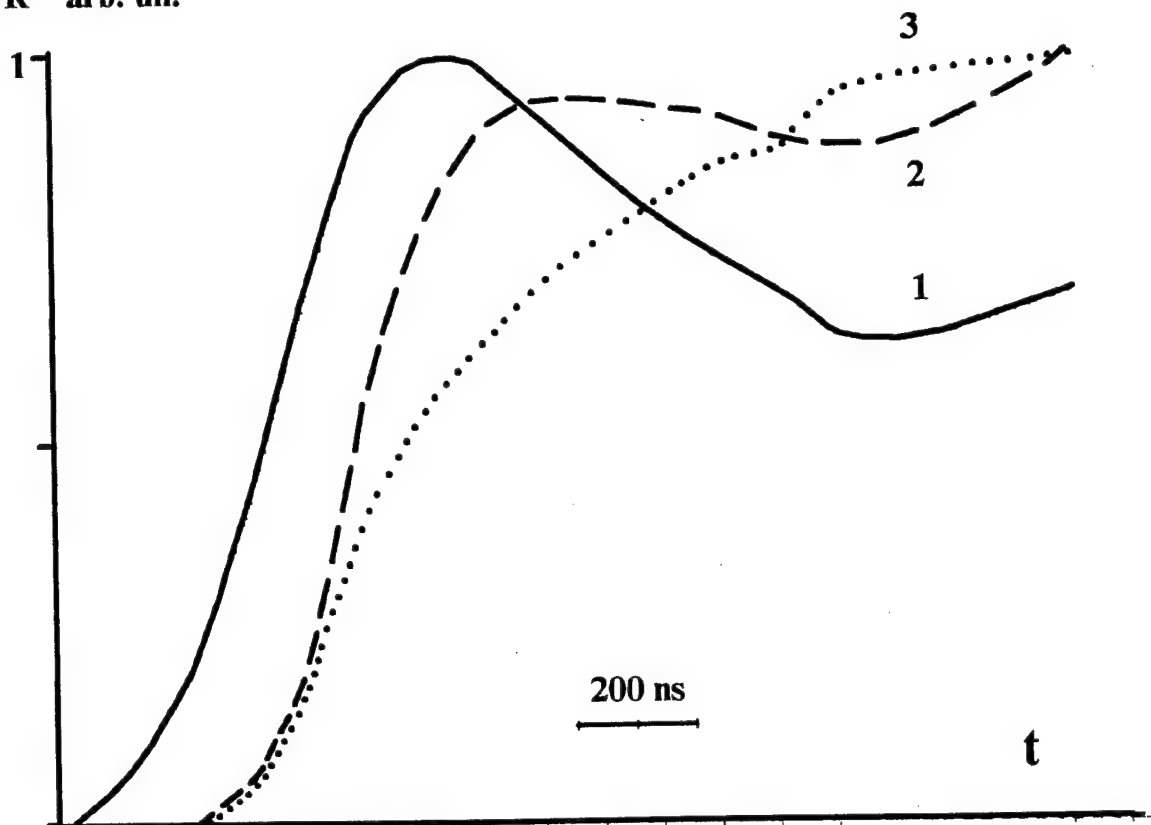


Fig. 3.25. The front parts of the probe (curve 1 - solid line), PC (curve 2 - dashed line) and PCR (curve 3 - dotted line) pulses for SIE 280 J/l atm,  $R_{out} = 65\%$ .

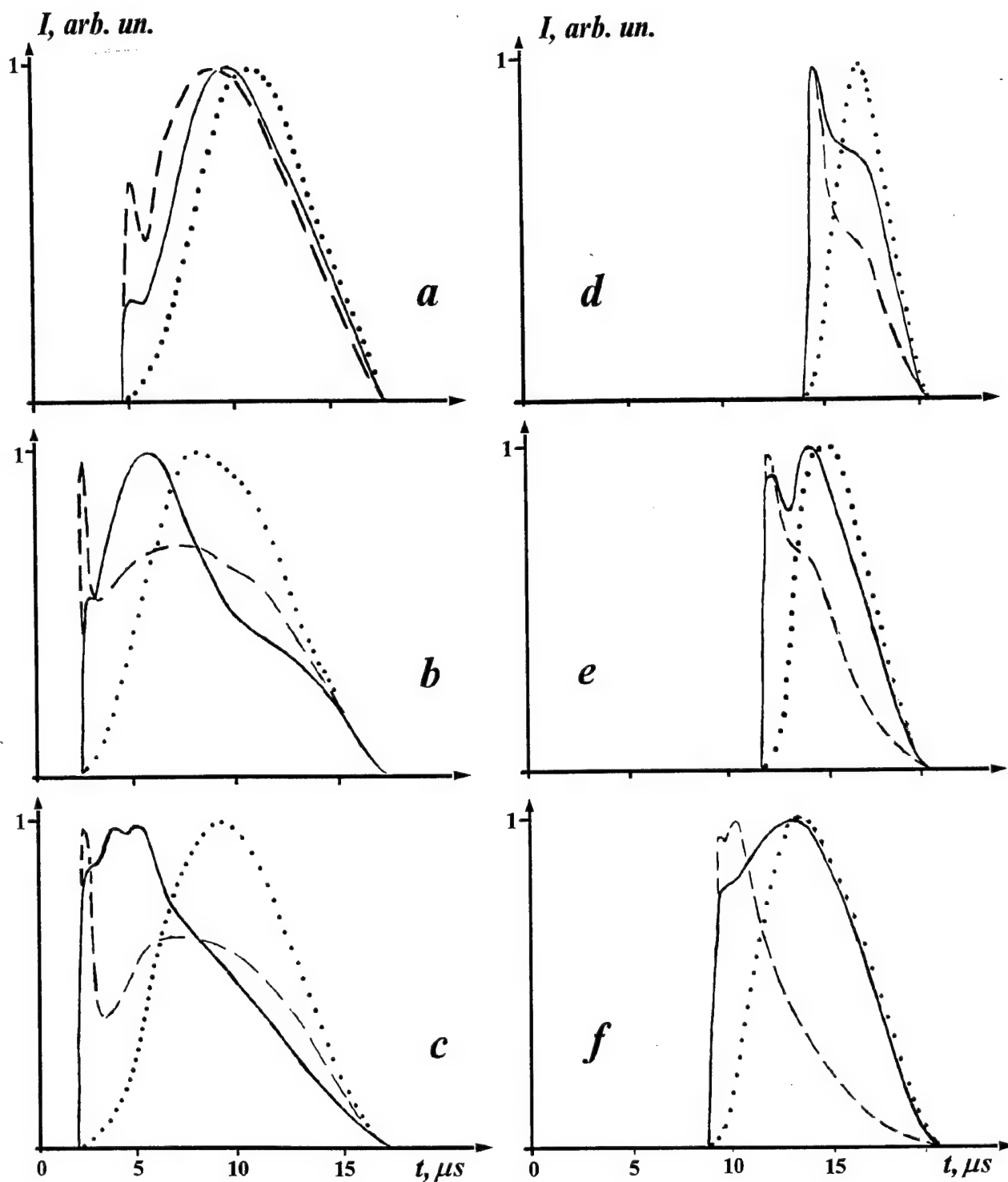


Fig. 3.26. Comparison of PC pulses (experiment -solid line, theory of resonance mechanism - dashed line, theory of thermal mechanism - dotted line) under different conditions:  
 a, d -  $120 \text{ J/l atm}$ ; b, e -  $190 \text{ J/l atm}$ ; c, f -  $280 \text{ J/l atm}$ ;  
 a - c -  $R_{out} = 65\%$ ; d - f -  $R_{out} = 7.5\%$ .

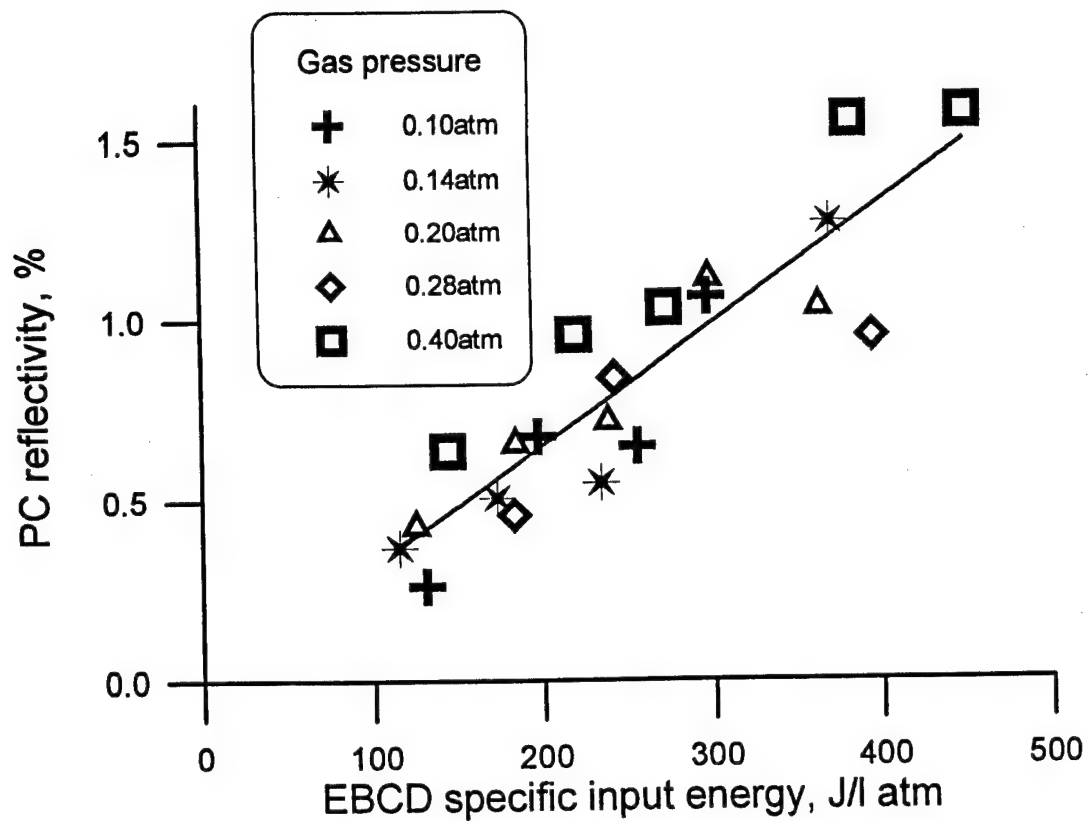


Fig. 3.27. PC reflectivity versus EB CD specific input energy for different laser gas pressures.

Table 3.9. PC reflectivity (R) versus EB CD specific input energy ( $Q_{in}^{sp}$ ) for different laser gas pressures (data for Fig. 3.27).

Gas mixture 1 : 2 : 4;

$R_{out} = 46\%$ ;

$I_1/I_3 = 1.4$ .

0.10atm		0.14atm		0.20atm		0.28atm		0.40atm	
$Q_{in}^{sp},$ J l atm	R, %	$Q_{in}^{sp},$ J l atm	R, %	$Q_{in}^{sp},$ J l atm	R, %	$Q_{in}^{sp},$ J l atm	R, %	$Q_{in}^{sp},$ J l atm	R, %
131	0.26	115	0.37	125	0.43	184	0.46	144	0.64
197	0.68	173	0.51	184	0.66	242	0.79	219	0.96
255	0.65	234	0.55	238	0.72	395	0.95	272	1.03
297	1.06	370	1.27	298	1.11	---	---	383	1.55
---	---	---	---	363	1.03	---	---	450	1.57

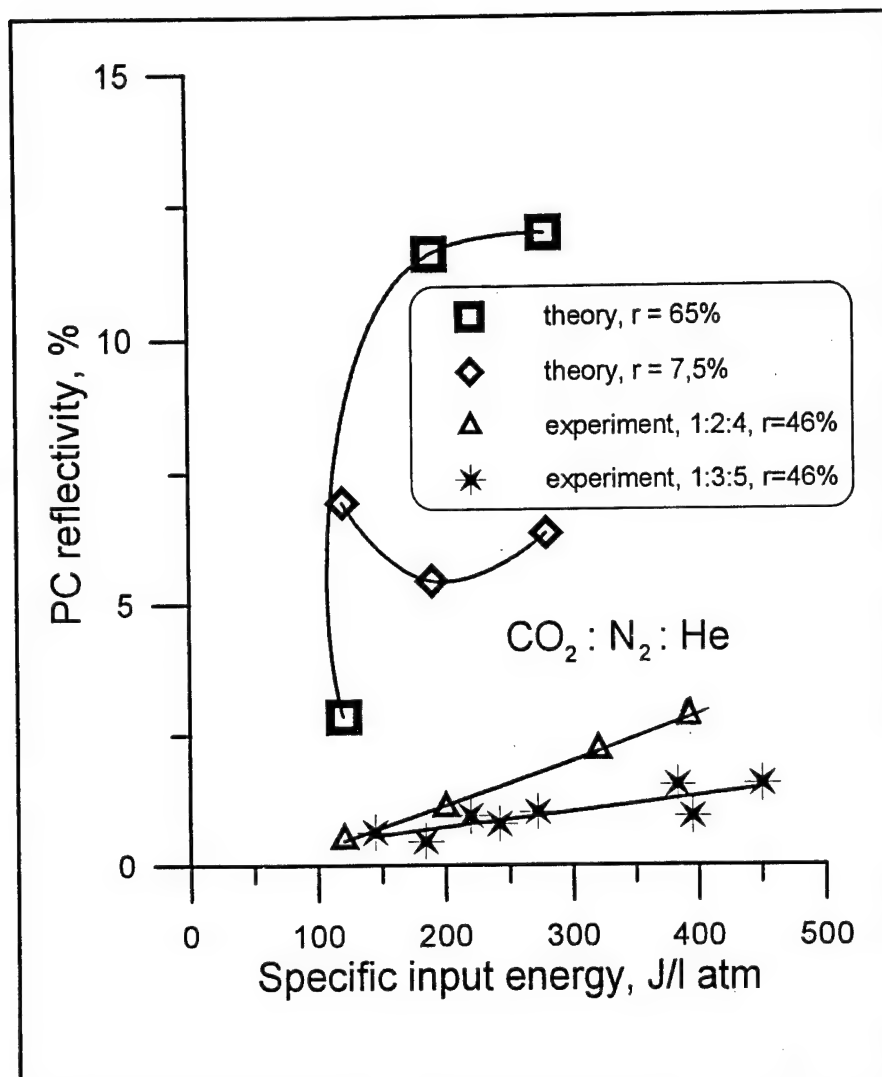
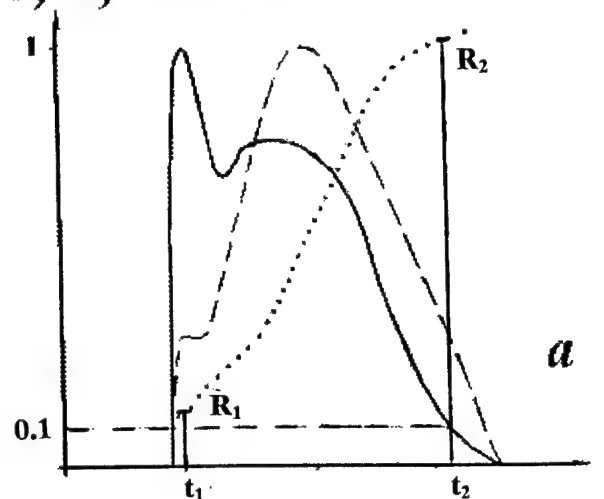


Fig. 3.28. PCR (on energy) versus SIE from experiment and from theory of Part 2.  
 $r$  - reflectivity of output coupler of laser resonator.

$I, R, \text{arb. un.}$



$I, R, \text{arb. un.}$

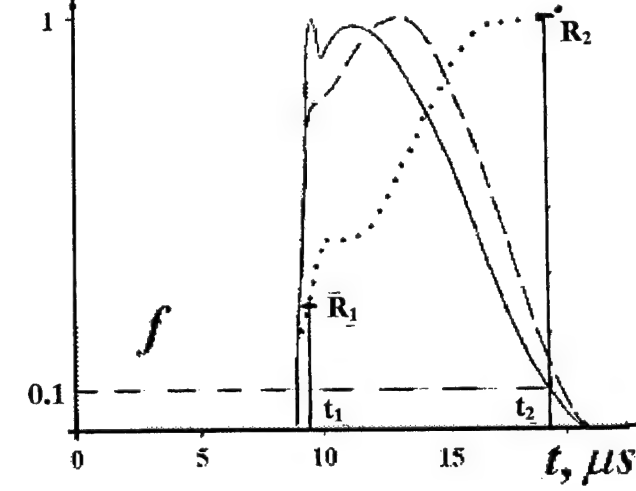
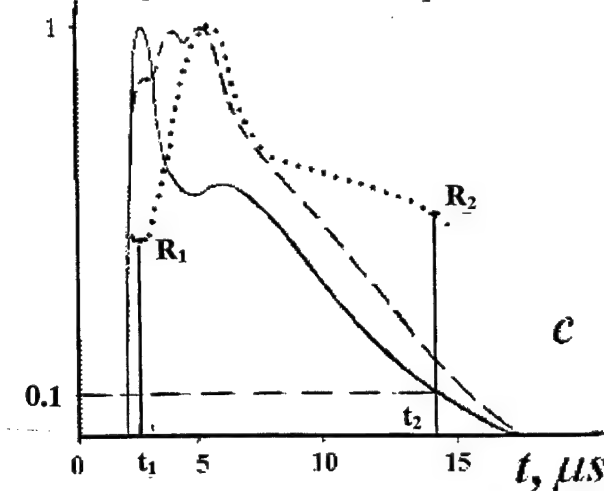
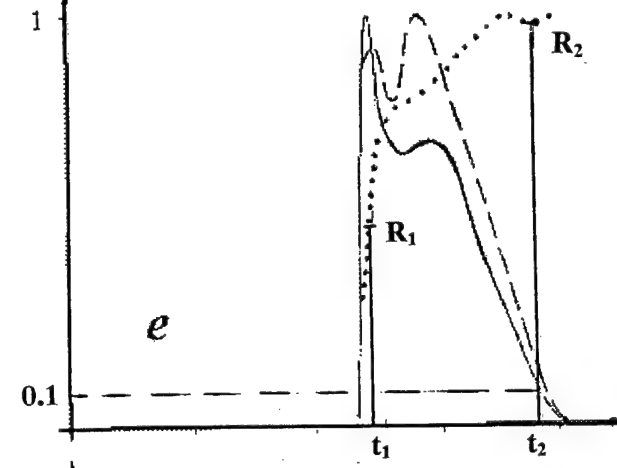
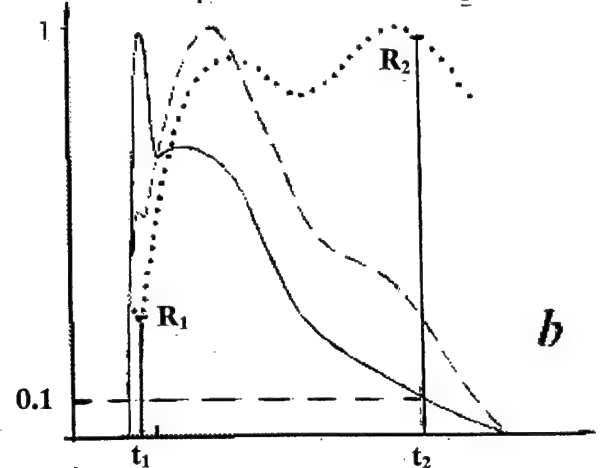
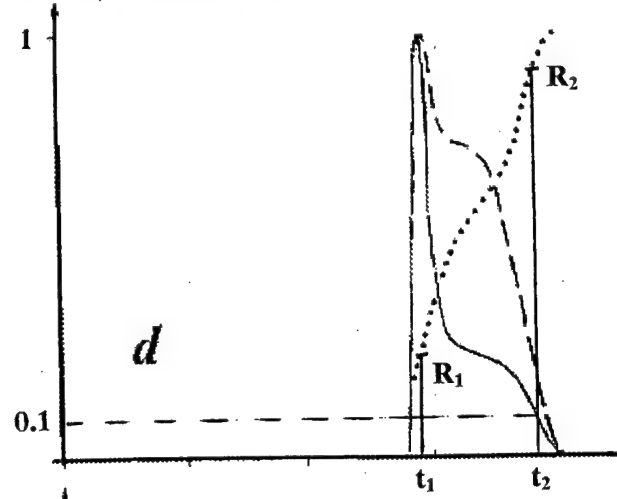
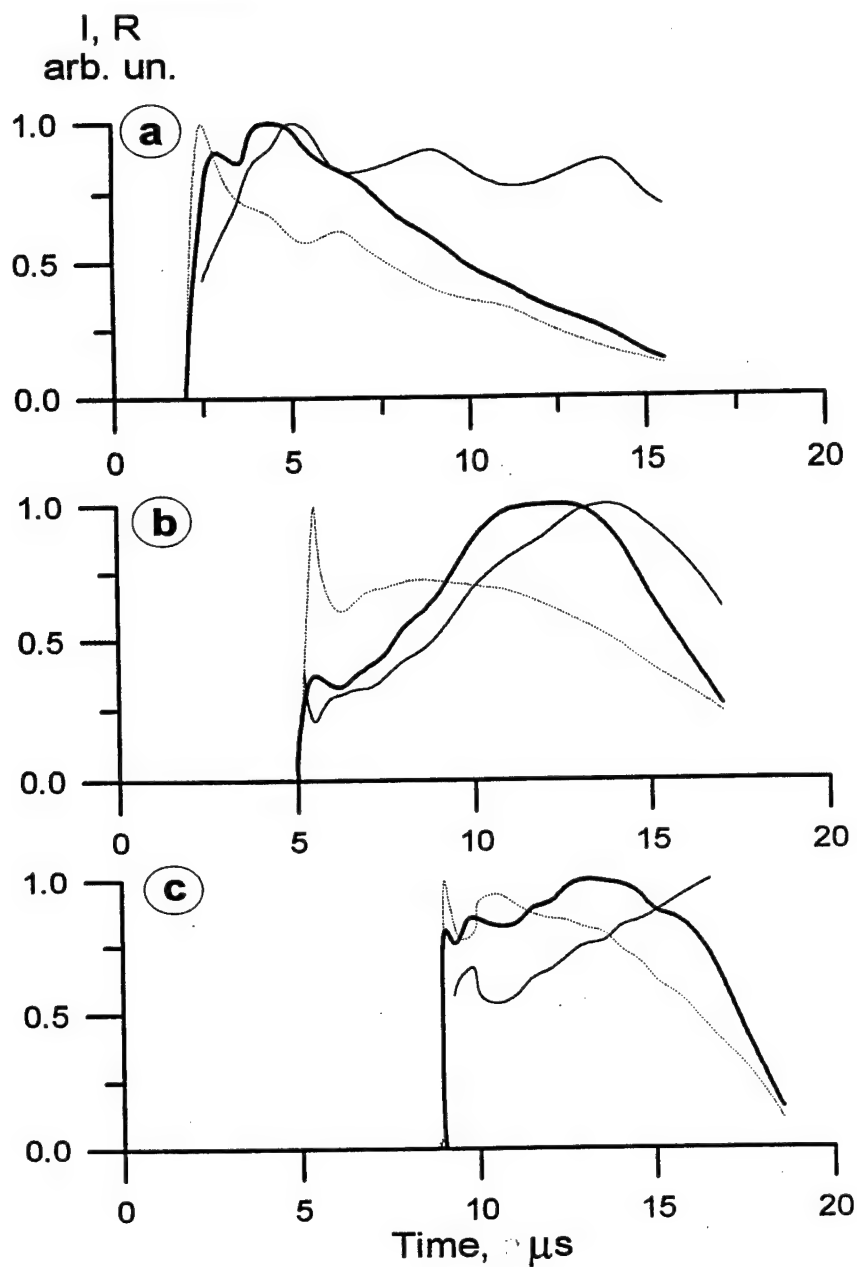


Fig. 3.29. Analysis of PCR pulse under different experimental conditions:  
a, d -  $120 \text{ J/l atm}$ ; b, e -  $190 \text{ J/l atm}$ ; c, f -  $280 \text{ J/l atm}$ ;  
a - c -  $R_{\text{out}} = 65\%$ ; d - f -  $R_{\text{out}} = 7.5\%$ .



..... probe signal  
 — PC signal  
 — PC reflectivity

Fig. 3.30. Time-history of the probe and PC signal and PC reflectivity for different Q-factor (reflectivity of the output mirror):

a 65%;  
 b 45%;  
 c 7.5%.

Gas mixture 1 : 2 : 4.  
 Gas pressure 0.28 atm.  
 EBCD specific input energy 280 J/l atm.



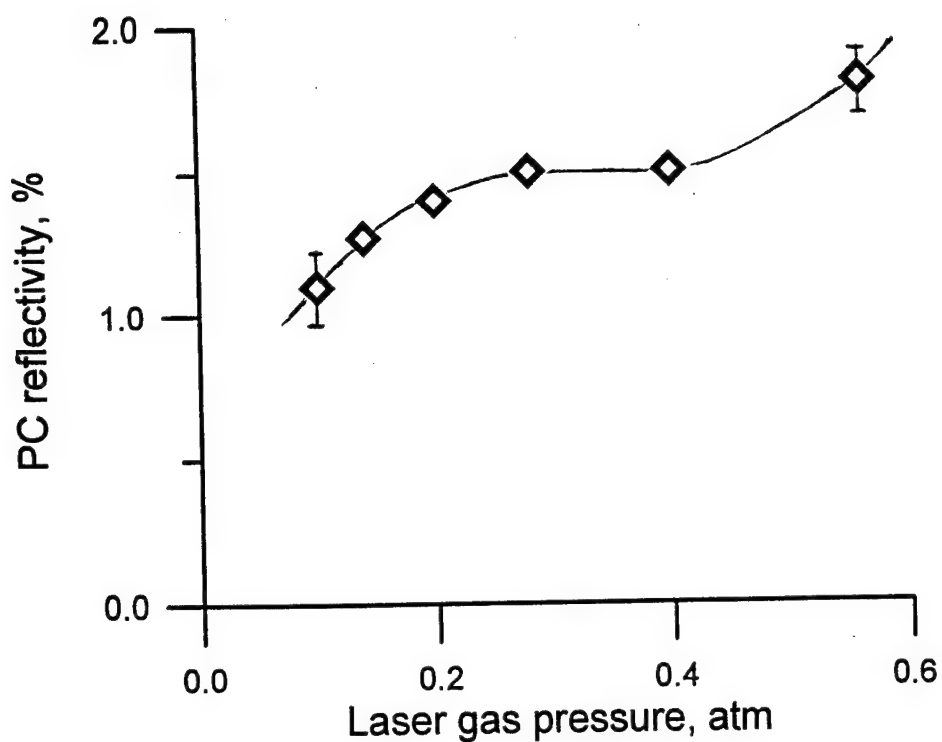


Fig. 3.31. PC reflectivity versus laser gas pressure for EBCD specific input energy 280 J/l atm.

Table 3.10. PC reflectivity (R) versus laser gas pressure (P). (data for Fig. 3.31).  
 EBCD specific input energy 280 J/l atm;  
 gas mixture 1 : 2 : 4;  
 $R_{out} = 46\%$ ;  
 $I_1/I_3 = 1.4$ .

P, atm	0.10	0.14	0.20	0.28	0.40	0.56
R, %	1.1	1.27	1.4	1.5	1.5	1.8

I, R, arb. un.

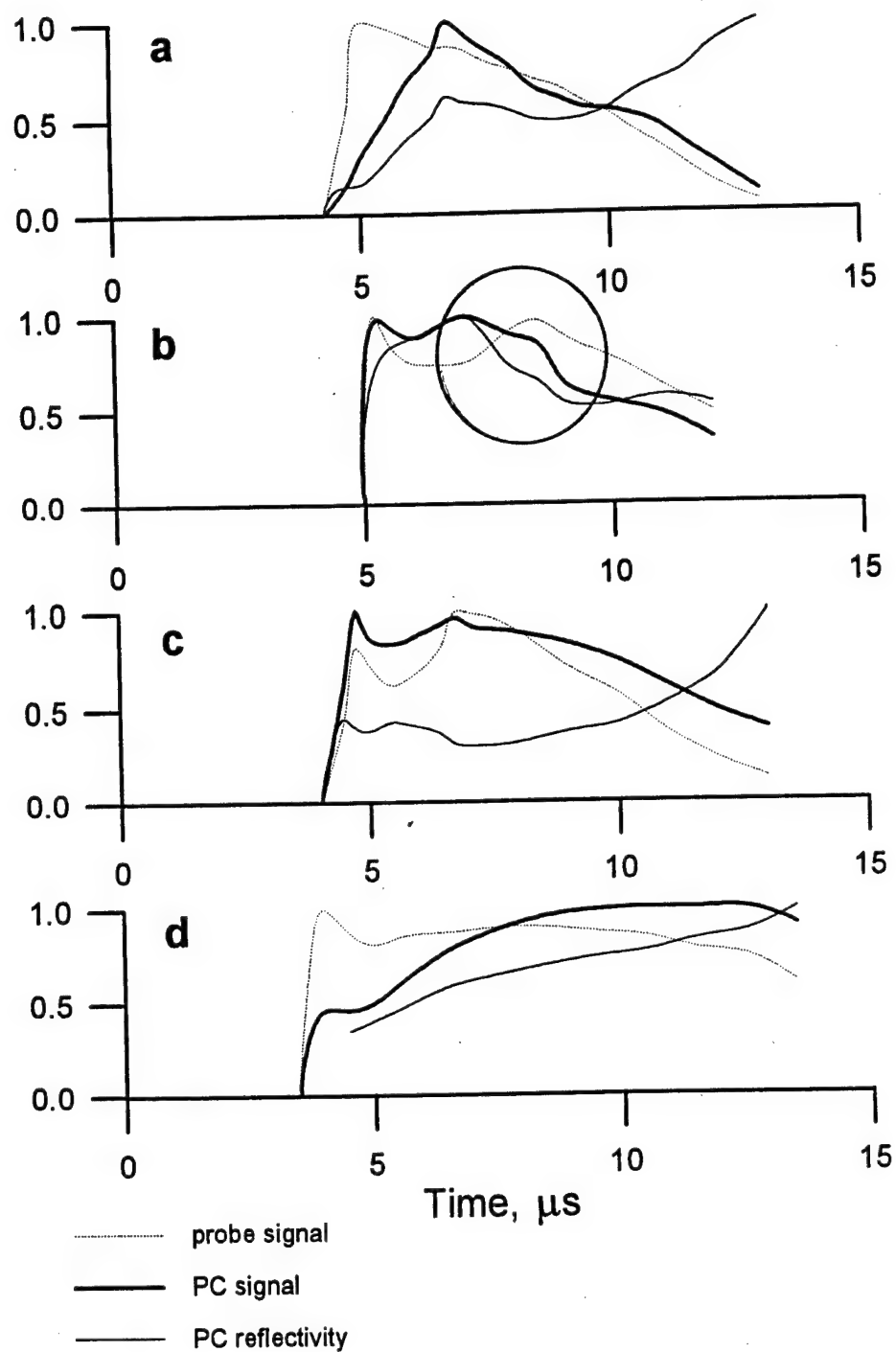


Fig. 3.32. Time-history of the probe and PC signal and PC reflectivity for laser output mirror reflectivity  $R_{\text{out}} = 65\%$  and different laser gas pressures:

a - 0.80 atm;

b - 0.56 atm;

c - 0.42 atm;

d - 0.28 atm.

Gas mixture

$\text{CO}_2 : \text{N}_2 : \text{He} = 1 : 2 : 4;$

$I_1 / I_3 = 5.$

I, R, arb. un.

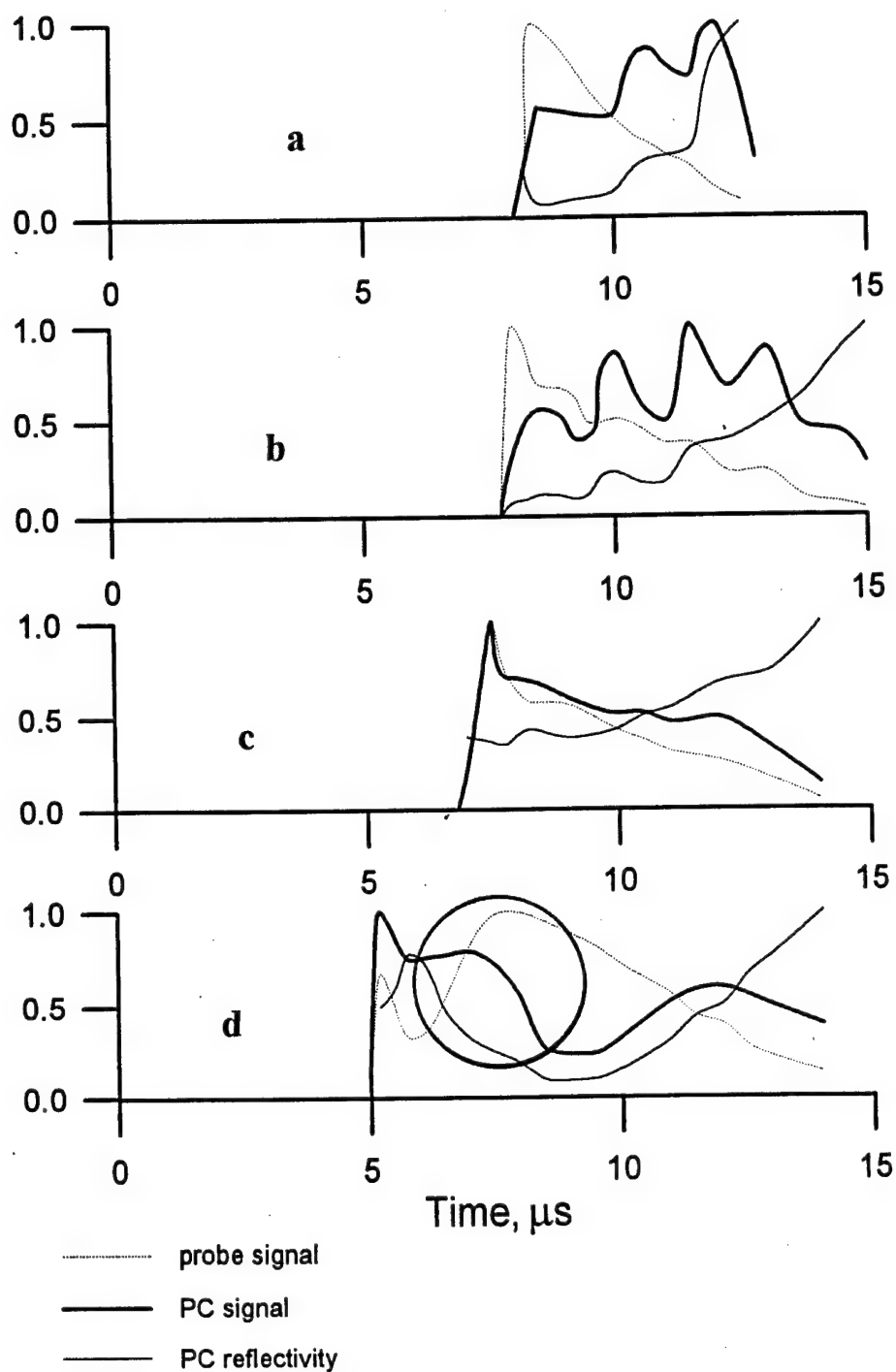


Fig. 3.33. Time-history of the probe and PC signal and PC reflectivity for laser output mirror reflectivity  $R_{\text{out}} = 8\%$  and different laser gas pressures:

a - 0.80 atm;

b - 0.56 atm;

c - 0.42 atm;

d - 0.28 atm.

Gas mixture

$\text{CO}_2 : \text{N}_2 : \text{He} = 1 : 2 : 4;$

$I_1 / I_3 = 0.5.$

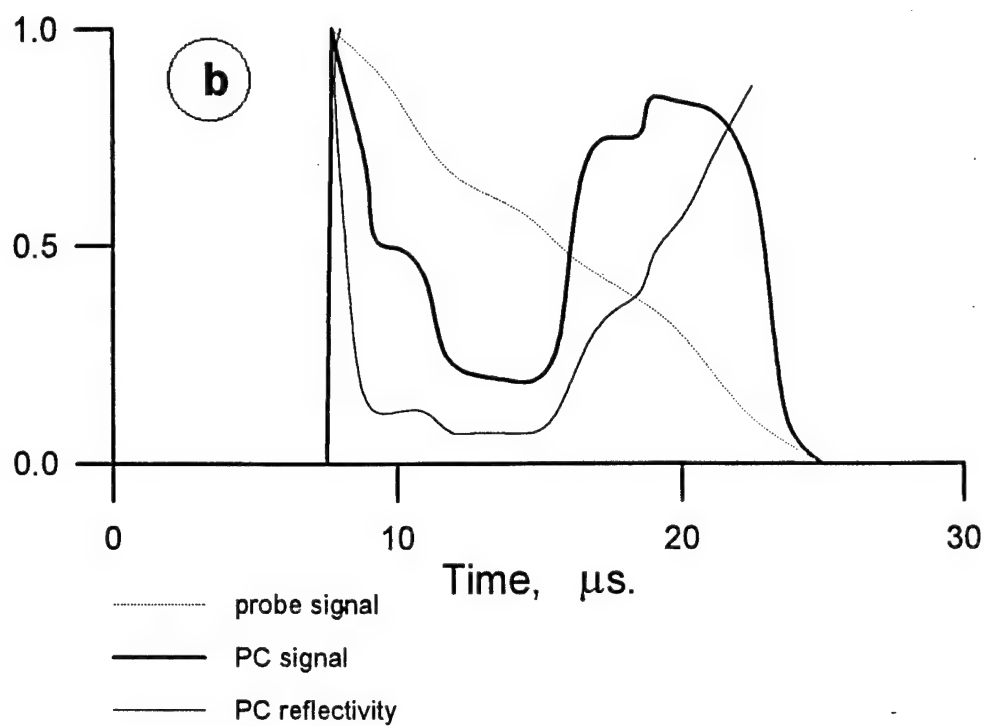


Fig. 3.34. Probe, PC and PCR pulses  
 for laser mixture  $\text{CO}_2\text{:N}_2\text{:He} = 1\text{:}5\text{:}3$ , 0.28 atm, SIE 280 J/l atm,  $R_{\text{out}} = 45\%$ .

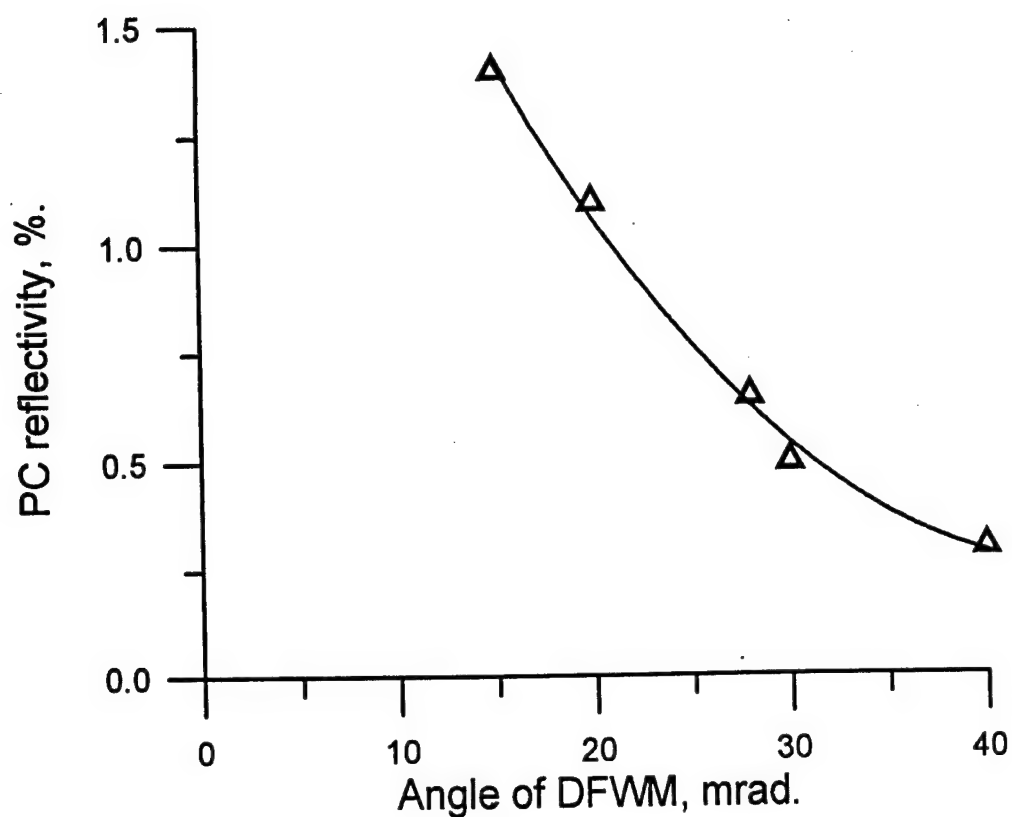


Fig. 3.35. PC reflectivity versus interaction angle of DFWM.

Table 3.11. PC reflectivity versus interaction angle of DFWM ( $\theta$ )  
(data for Fig. 3.35).

Gas mixture 1 : 2 : 7;  
gas pressure 0.25 atm;  
EBCD specific input energy 300 J/l atm;  
reflectivity of laser output mirror 46%.

$\theta$ , mrad.	15	20	28	30	40
PCR, %	1.4	1.1	0.65	0.5	0.3

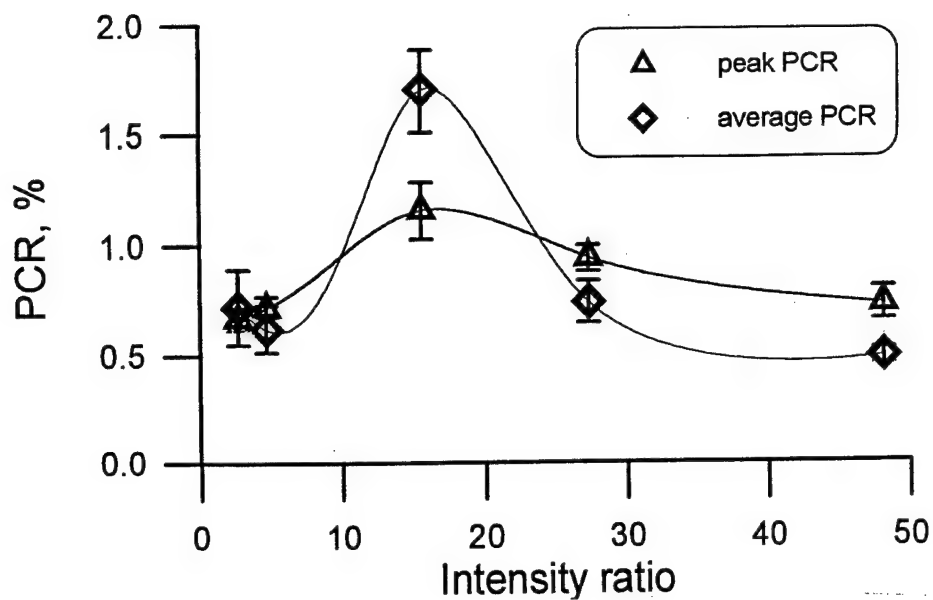


Fig. 3.36. PC reflectivity (peak and averaged) versus intensity ratio ( $I_1/I_3$ ).

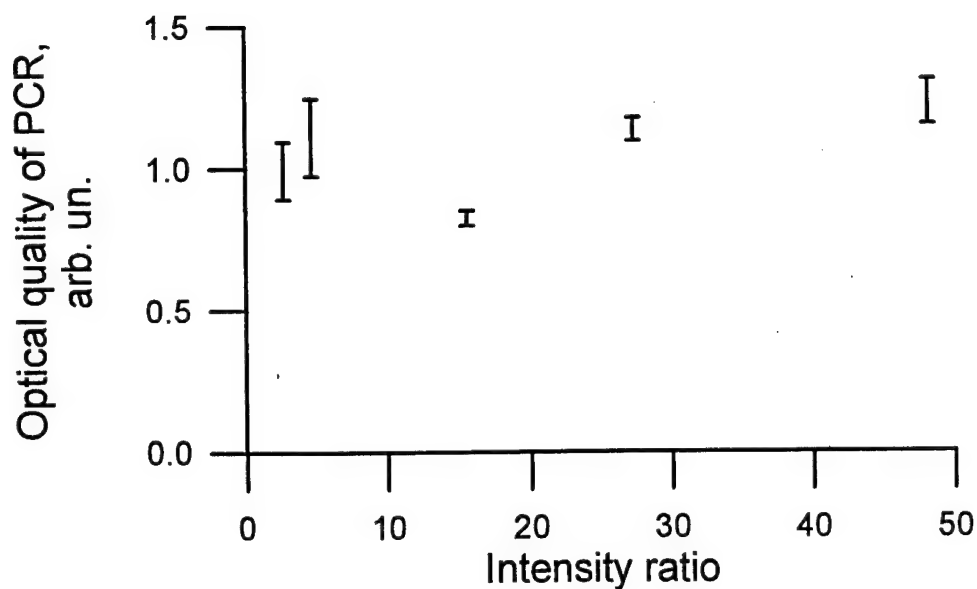


Fig. 3.37. Optical quality of PC reflectivity versus intensity ratio ( $I_1/I_3$ ).

Table 3.12. Optical quality and PC reflectivity (peak and averaged) versus intensity ratio ( $I_1/I_3$ ).

$I_1/I_3$	2.7	4.6	15.6	27.3	48.2
peak PCR, %	0.67	0.72	1.16	0.94	0.73
av. PCR, %	0.72	0.62	1.7	0.74	0.49
K	0.99	1.11	0.83	1.13	1.23

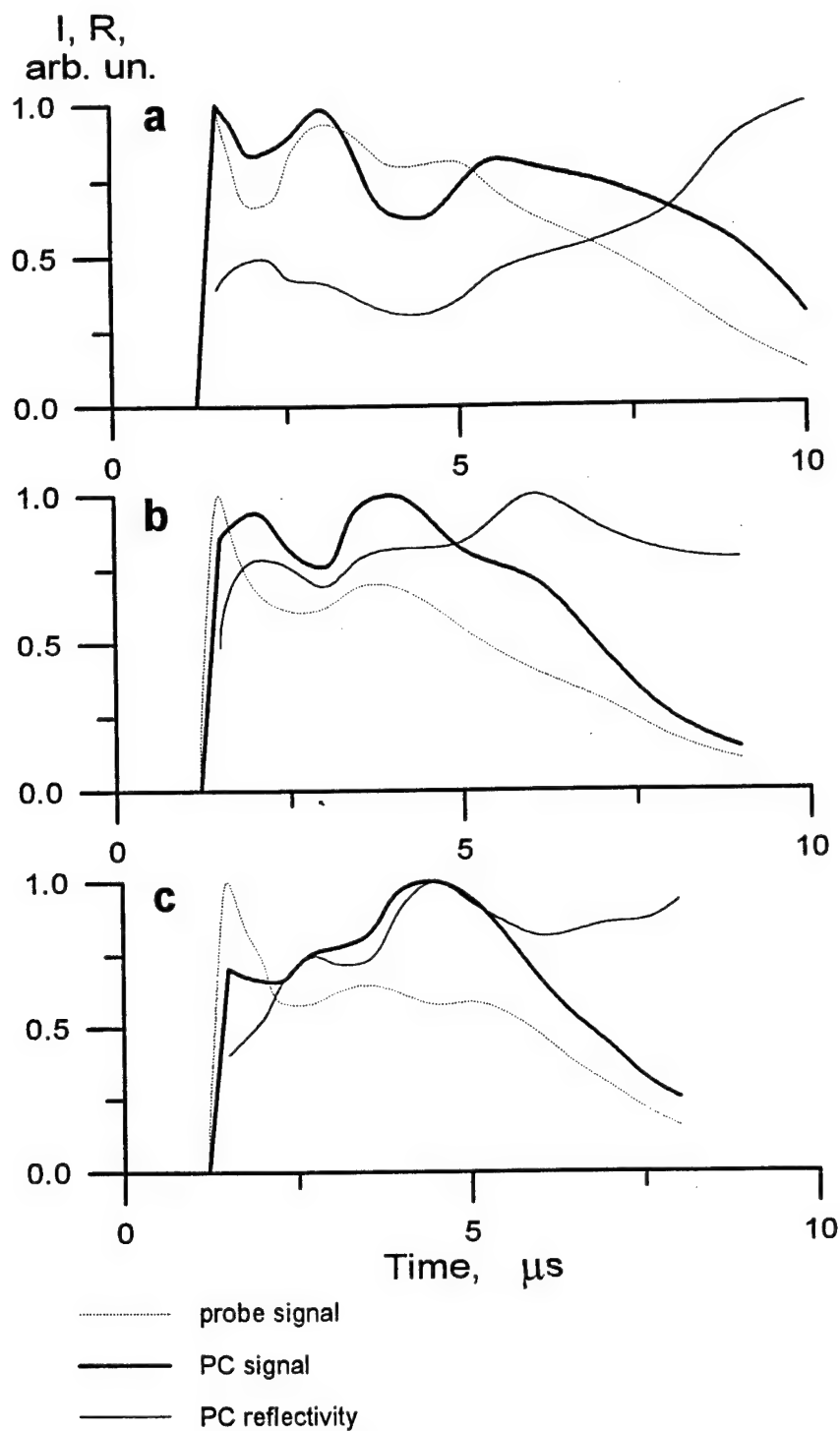


Fig. 3.38. Time-history of the probe and PC signal and PC reflectivity for different intensity ratio between pump and probe waves ( $I_1/I_3$ ).

a      0.2;  
b      0.6;  
c      2

Gas mixture  
Gas pressure  
EBCD specific input energy  
Reflectivity of output mirror

1 : 2 : 4.  
0.28 atm.  
280 J/l atm.  
8%

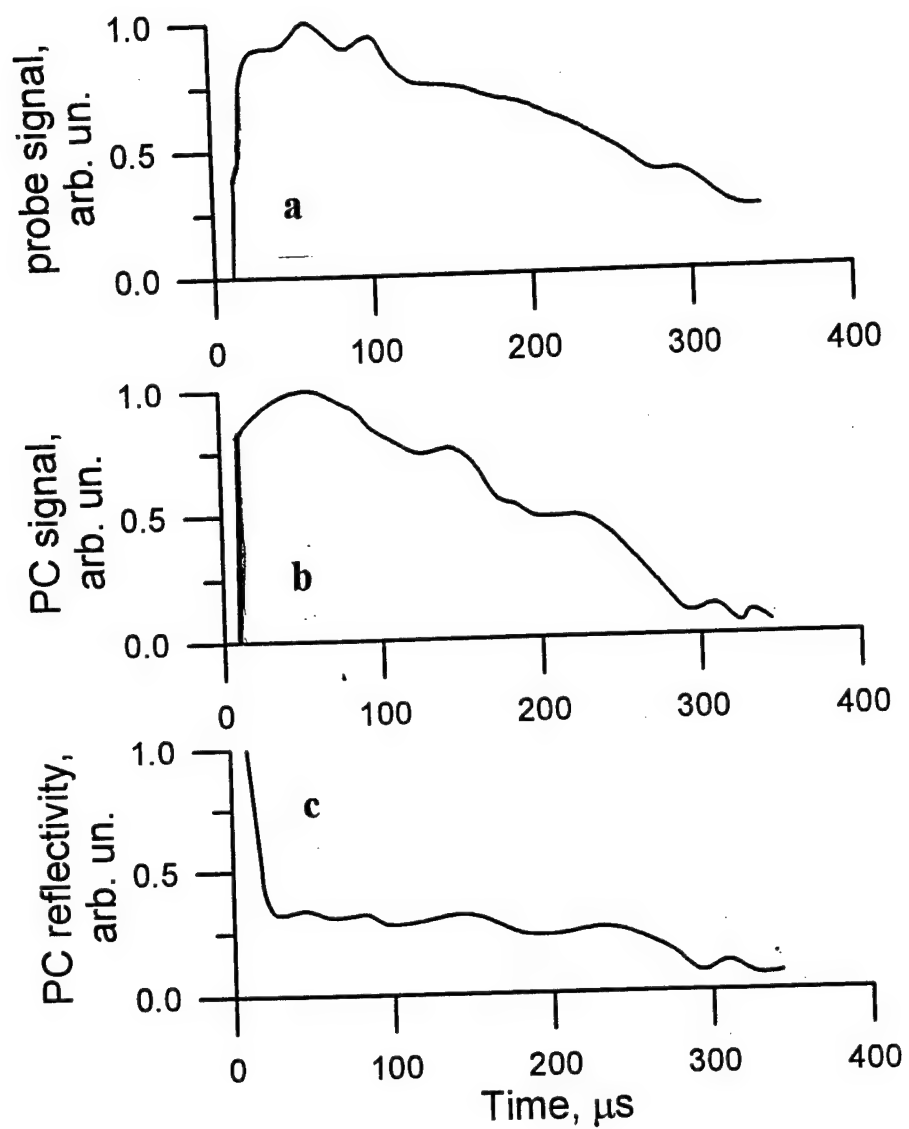


Fig. 3.39. Probe (a), PC (b) and PCR (c) profiles for DFWM of CO laser radiation:  
SIE 300 J/l Amagat, frequency selected resonator,  $5.39 \mu\text{m}$  spectral range



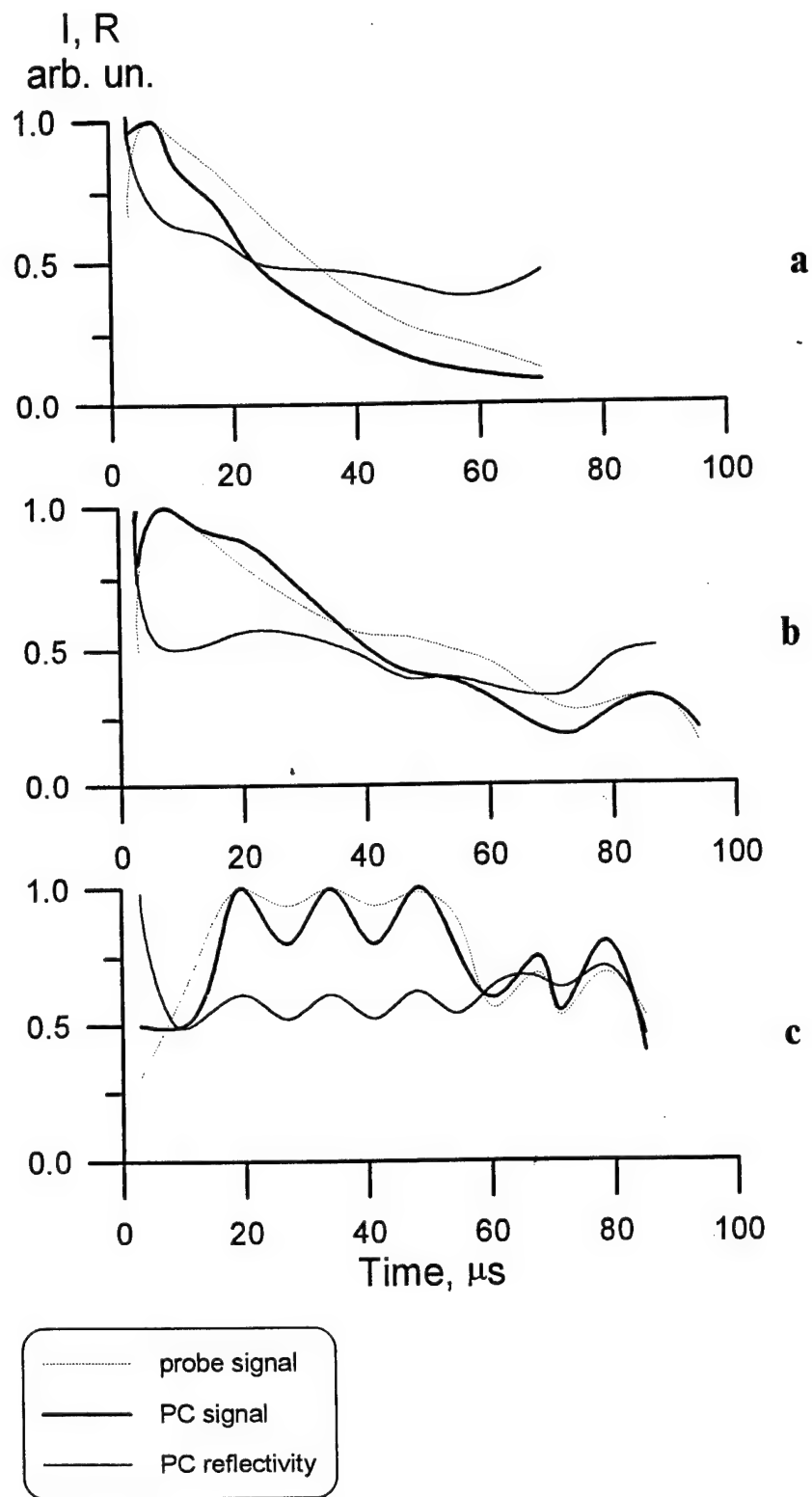


Fig. 3.40. Probe, PC and PCR signals for different spectral bands with center lines of 5.23  $\mu\text{m}$  (a), 5.39  $\mu\text{m}$  (b) and 5.52  $\mu\text{m}$  (c).

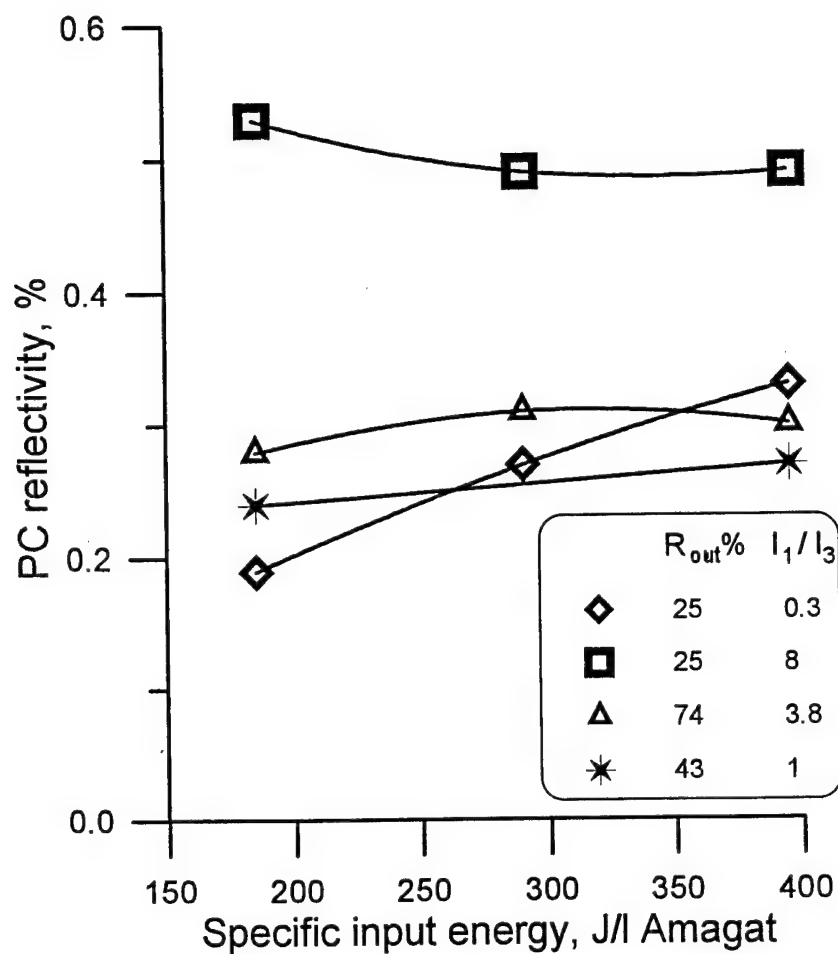


Fig. 3.41. PCR for various output couplers with reflectivities of 25%, 43% and 74%;  
threshold gain estimated is  $\alpha_{thr} = 0.6 \text{ m}^{-1}$ ,  $0.35 \text{ m}^{-1}$  and  $0.13 \text{ m}^{-1}$ ;  
5.40  $\mu\text{m}$  spectral band.

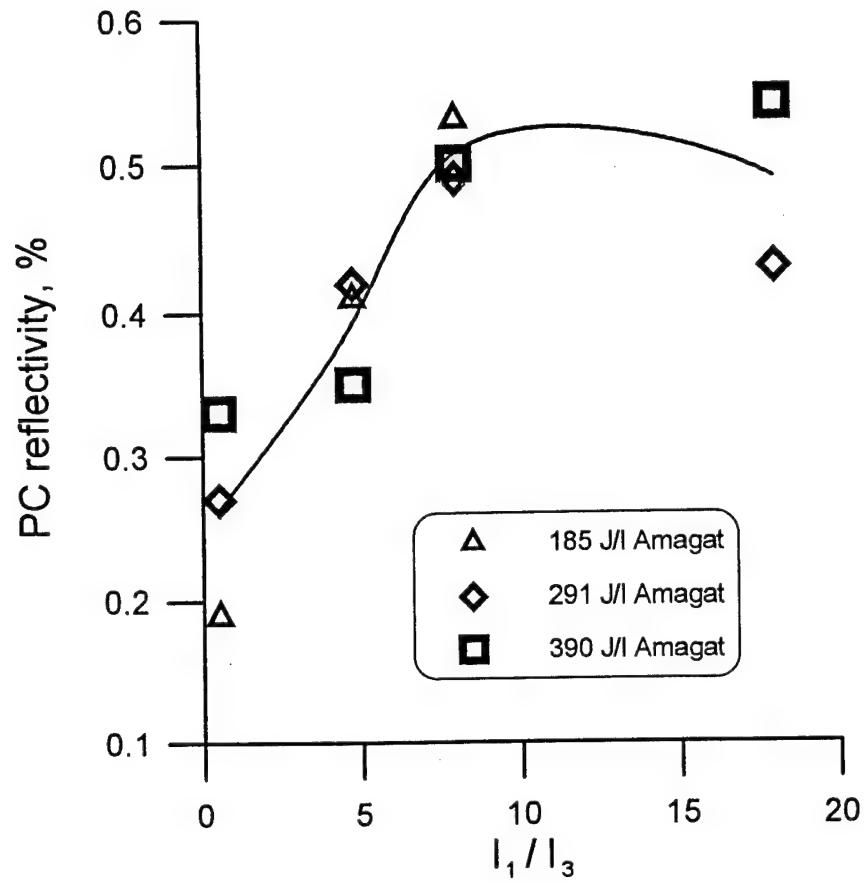


Fig. 3.42. PCR versus intensity ratio  $I_1/I_3$  for three values of SIE.

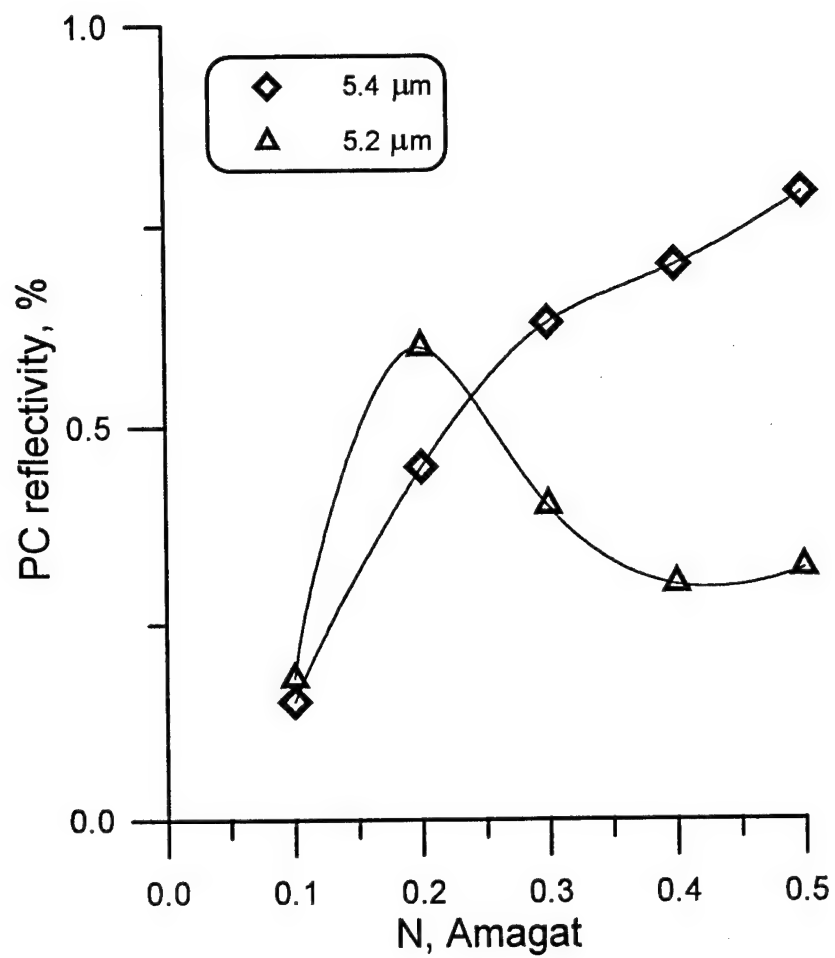


Fig. 3.43. PCR versus gas density for two spectral bands of 5.39  $\mu\text{m}$  and 5.23  $\mu\text{m}$ .

#### 4. High frequency temporal structure of laser and phase conjugated signals at intracavity DFWM of CO<sub>2</sub> and CO laser radiation in their inverted medium\*

The intracavity DFWM of pulsed CO and CO<sub>2</sub> laser radiation involves an appearance of PC signal backscattered relative to a probe wave. The PC signal is proved to have a complicated time behaviour Part 3 due to transient mechanisms of formation of diffraction gratings (saturated gain (or amplitude) grating and thermal (or phase) one) inside an active medium. The theory describing the PC process and the experiment itself Part 2 dealt with relative "smooth" CO<sub>2</sub> laser pulses not taking into consideration the high frequency (HF) temporal structure on the round-trip period (RTP) that can arise due to longitudinal mode beating and mode locking. As a matter of fact, the real CO<sub>2</sub> laser pulses, even "long" ones with pulse length  $\tau_{out} \geq \tau_{rel}$ , where  $\tau_{rel}$  is the relaxation time of upper laser level, do have such structure (chapter 3.2.2). The same situation seems to take place also for CO lasers, though up to now nobody attempted measurement of the structure, perhaps, on account of a very long pulse length ( $\sim 10^{-4}$  -  $10^{-3}$  sec). The objective of the paper is the experimental research of the temporal structure, including HF one on the RTP, for laser (probe) and PC signals at DFWM of long pulse CO and CO<sub>2</sub> lasers radiation with nanosecond resolution over the full pulse length.

##### 4.1. Experimental setup and optical scheme

The experiments were carried out on the e-beam controlled discharge (EBCD) CO<sub>2</sub> (CO) laser installation with active length of 120 cm. The pulse length for input power could vary and, normally, was 20  $\mu$ s, input energy being changed between 100 and 400 J/l Amagat. CO laser operated at gas temperature of  $\sim 100$  K. Laser mixture CO<sub>2</sub>:N<sub>2</sub>:He = 1:2:4 and CO:N<sub>2</sub>:He = 1:4:5 were used for CO<sub>2</sub> (CO) laser. Gas density amounted to 0.3 Amagat. The classical optical scheme for DFWM of CO<sub>2</sub> (CO) laser radiation was used in the experiment (Fig. 4.1). The laser resonator length was 18 m (RTP = 120 ns). A set of diaphragms was used for spatial selection of TEM<sub>00</sub> mode. The laser beam waist on the output coupler was 15 mm. The output energy was approximately about one Joule both for CO and CO<sub>2</sub> laser. The center of the active medium was situated at  $l = 7.5$  m from the output coupler (round-trip time is 50 ns). The reflectivity of the

---

\* This research work has been done together with C. Beairisto, R. Penny, S. Squires (Directorate of Applied Technology, USA) and R. Walter (WJSA, USA) in joint experiments at Lebedev Institute.

output coupler was 50% for CO<sub>2</sub> and 43% for CO laser. The diffraction grating (100 lines/mm, blazing angle 30°) was used in case of spectral selective resonator. Thus CO<sub>2</sub> and CO laser could operate both in single-line mode and nonselective one. It should be noted, that in case of CO<sub>2</sub> laser it operated on single line P(20) both with diffraction grating and without it. In selective mode CO laser operated on P<sub>10-9</sub>(15) line (5.40 μm). The probe beam  $I_3$  was directed to the active medium under the small angle of 10 mrad to the optical axis of the laser and after propagating through it was absorbed by an absorber. There was no time delay between the probe pulse  $I_3$  and intracavity co-propagating laser pulse  $I_1$  within the accuracy of  $\pm 0.3$  ns. The probe signal and PC signal  $I_4$  backscattered from the active medium were directed to photodetectors with controlled time delay of  $\sim 10$  ns which was reduced to zero when comparing oscilloscope traces for the probe and PC signals.

In measuring pulse profile and HF structure of the probe and PC signals HgCdTe photodetectors and photon drag detector with nanosecond response time and oscilloscope "TEKTRONIX" TDS680B were used.

## 4.2. Experimental results and discussion

### *Temporal behaviour of probe and PC signals for CO<sub>2</sub> laser.*

The time measurement fulfilled with much better nanosecond time resolution then in previous experiments Part 3 confirms the existence of very complicated structure on large temporal scale being dependent on a number of parameters such as specific input energy and power, intensity ratio for probe and co-propagating pumping wave etc. As it was emphasized in Part 3 these parameters strongly influence upon the relative role of two principal mechanisms of nonlinearity such as amplitude and phase ones. One can see from Fig. 4.2a bearing in mind the previous results the relative high amplitude of PC signal at the front of the pulse due to amplitude mechanism and strong PC reflectivity at the rear part due to thermal mechanism ( $q = 165$  J/l atm;  $I_1/I_3 = 4$ ). An increase of input power pulse length (Fig. 4.2b) leads to an increase of probe pulse length, a decrease of its average intensity (together with a decrease of small signal gain) and results in strong decrease of PC reflectivity on the front of pulse and rise of the PC signal on the pulse tail ( $q = 220$  J/l atm,  $I_1/I_3 = 11$ ). When increasing specific input energy together with intensity of probe beam ( $q = 300$  J/l atm,  $I_1/I_3 = 0.4$ ), the oscillation of the tail both of probe and PC signal with period of  $\sim 2$  μs is observed (Fig. 4.2c) being more distinctive for the PC signal. The absence of an accumulation of thermal nonlinearity, as one can see from all the diagrams of Fig. 4.2a-c

also confirms the conclusions of Part 3, that there are some effects preventing from such accumulation which are not taken in consideration by theoretical calculations.

One can see in Fig. 4.3 that both probe and PC pulses have a periodic structure with period of 120 ns corresponding to RTP and also have very deep, nearly 100% modulation. The first peak of the PC pulse, which can be seen in Fig. 4.3a, follows the probe pulse nearly noninertially, its front being more sharp. A spike with maximal amplitude of the first peak of the PC pulse does not always fit to that of the probe pulse (it depends on experimental conditions). And what it is more, the strong spike in PC signal correlates with weak one in probe signal very frequently on various temporal scales. Fig. 4.3b demonstrates the time behaviour of probe and PC signal for pulses of Fig. 4.2c at the seventh microsecond from the beginning of the laser pulse. The PC signal has an oscillation with the same period of 500 ns like for probe signal, however with opposite phase.

The typical first peak of the laser and PC pulses is presented in Fig. 4.4a,b with better resolution. The 100% modulation can be observed very clearly. The diagrams could explain the process of writing down and reading out the diffraction grating during first peak of the laser pulse, which, as was shown in Parts 2 and 3 was brought about by amplitude mechanism. One can easily see from Fig. 4.4a, that PC signal is observed of 50 ns later relatively the probe one. The reason of it that the grating begins to be written down in the active medium when a first spike goes out the laser resonator (wave  $I_3$ ) comes back to the active medium and interferes there with the same spike reflected from the output coupler back to the active medium (Fig. 4.1). The amplitude grating is read out by spike of intracavity wave  $I_2$  shifted on  $\tau_{\text{shift}} = 2l/c = 50$  ns relatively spikes of waves  $I_1$  and  $I_3$ . As a result of diffraction of the intracavity pulse  $I_2$  on the grating we observe PC signal  $I_4$ . Thus on the diagrams of Fig. 4.4a we have the signal reading out the diffraction grating (upper trace) and one being read by that signal, i.e. PC signal (bottom trace). Let's consider, for instance, the process of formation of spikes 2' and 4' belonging to PC signal (Fig. 4.4a). The spike 2' (4') is a result of diffraction of spike 2 (4) on grating written down by spike 1 (3) going from output mirror to the active medium by two equal ways  $OM_1 = M_1M_3O = l$ . This description explains the formation of large-scale grating with spatial period of  $\lambda/\theta$ .

Inasmuch as the CO<sub>2</sub> laser pulse (and CO laser pulse also) consists of spikes with length of  $\sim 10$  ns determined by pressure broadening, one should take into account the fact of existing of small scale grating with spatial period of  $\lambda/2$  which has never been considered for CO<sub>2</sub> and CO lasers, for they have believed that this grating is destroyed very quickly by heat conductivity. Like in case just described above there are three spikes being in the active medium simultaneously: spike 1 (3) from the wave  $I_1$ , spike 1 (3) from the wave  $I_3$  and spike 2(4) from the wave  $I_2$ . An interference of spike 1 (3) of wave  $I_3$  and spike 2(4) produces a grating which is read out by

spike 1 (3) of wave  $I_1$  bringing forth the PC signal spike 2' (4') (Fig. 4.4a). These two diffraction grating can work together resulting in complicated temporal structure on RTP.

The HF structure of PC signal is also complicated one because sometimes a spike (for instance, 1 or 2 in Fig. 4.4b) can not be brought forth by small scale grating, because there is too weak intensity on the tail of spike 4 and on the front of spike 3 to bring forth strong amplitude diffraction grating. The large scale grating seems to operate in this case and spike 1 is diffracted on grating obtained on the front of pulse 3 bringing forth the spike 1'. Spike 2' is a result of interaction of spike 2 with grating formed by spike 4 of wave  $I_1$  and  $I_3$ . Moreover, the amplitude of PC signal spike 2' for weaker spike 2 is higher than that of 1' for stronger probe pulse 1. The difference is that spike 2 is scattered on the grating, which still exists after the spike 4, and the spike 1 is scattered on diffraction grating corresponding to the front of the spike 3. From here it is possible roughly to estimate the life-time of the diffraction grating  $\sim 20$  ns, that is determined by gain recovering. The spike 5, which is scattered at the rear part of spike 3 designated like 6, when gain hole does still exist, bring forth the more intensive spike 5' in PC signal.

Of course, the process of formation of PC signal is much more complicated than qualitative illustration given above and the signal reflects the complex time behaviour of PC process, on which strongly influences also optical inhomogeneities arising in active medium during laser pulse. The inhomogeneities can bring forth the anomalies taking place on RTP during the laser pulse. One of the laser pulse and its PC signal (Fig. 4.2a) was analyzed with nanosecond resolution during its full length (Fig. 4.5). Though the laser probe signal is regular one (one of the spikes repeating itself with RTP is marked over the full pulse length), there is some destruction of PC signal (see Fig. 4.5b; 3.2  $\mu$ s after beginning of the laser pulse). Sometimes very weak probe signal brings forth strong PC signal (Fig. 4.5c; 6  $\mu$ s). In general, regular structure is kept till the end of laser pulse (Fig. 4.5d; 12.4  $\mu$ s), where thermal nonlinearity operates. It should be noted, that even for a very weak probe signal with intensity of one hundredth as much as that of the first peak of the laser pulse, we did observed yet PC signal (Fig. 4.5d) with PC reflectivity (on intensity) approximately twice as higher as for the first peak of the laser pulse. The results confirms the conclusions of Part 3, that the thermal grating is not accumulated in active medium as it follows from the theory.

As was already mentioned above the complicated HF structure of free-running  $\text{CO}_2$  laser pulse seems to be due to mode beating. The mode-locking leads to a higher intensity spike on the RTP. In our experiments the mode-locking regime of operation for EBCD  $\text{CO}_2$  laser was brought about by use of a plasma mirror [37]. The laser pulse consists of a set of pulses, some of them being mode-locked with a regular spike structure. Fig. 4.6a-c illustrates one of the pulses. Here the



PC signal does arise by diffraction of reading out wave on thermal grating produced by previous pulses, the last of which takes place  $\sim 6 \mu\text{s}$  before the mode-locked pulse presented on Fig. 4.6. Actually, the strong PC signal on amplitude grating could not arise because there was no strong spike writing down the grating at  $\sim 50 \text{ ns}$  before the reading out spike. The increase of pre-spike 2 and decrease of after-spike 3 (Fig. 4.6c) are connected with conditions of amplification and gain saturation inside active medium. The analysis of the results demonstrates, that the active medium should be situated near the output coupler (or near the rear mirror) to produce the same three spikes (probe one and two laser spikes for the two intracavity waves) in the same place simultaneously (in case the rear mirror, the reading out spike would be shifted at RTP with respect to writing down spikes). Though such disposition of laser resonator involves some experimental difficulties. It should be noted, that for mode-locking regime some anomalies also were observed like in case of free-running mode. See Fig. 4.6d where one can see disappearing of some spikes from PC signal and strong PC signal for the very weak spike.

*Time history of laser and PC signal at DFWM of CO laser radiation.*

As it is well known, free-running EBCD CO laser has of the order of magnitude longer pulse as compared to  $\text{CO}_2$  laser and irregular structure owing to kinetic processes taking place in multilevel active medium. This structure is normally measured with photodetectors with response time of  $\sim 1 \mu\text{s}$ . The measurement with nanosecond resolution demonstrates that CO laser also has periodic structure both for single line and multiline (non-selected) pulses with very deep (up to 100%) modulation (Fig. 4.7). The structure could arise as a result of longitudinal mode beating and/or mode locking due to a saturable absorber such as water vapors in long length laser cavity. The structure is kept during full pulse length, very regular structure being observed during RTP (see Fig. 4.7,c where the pattern corresponds to the third microsecond of pulse length). This structure has never been observed before. To say the truth, we expected to observe mode-beating as a ripple on the laser pulse envelope (in particular, for multiline CO laser pulse), and was really surprised in measuring very deep modulation. That modulation refers to a very low number of longitudinal modes taking part in lasing.

The interaction of probe beam with intracavity laser radiation (Fig. 4.8) disturbs slightly the regular structure on RTP though the strong modulation is kept during the full CO laser pulse. The PC signal differs from probe one, though also has regular structure with deep modulation both on large and small temporal scale (Fig. 4.9 and Fig. 4.10). It has sharper front (Fig. 4.9a-c). In case of strong probe signal (Fig. 4.9a) there are holes in PC signal intensity corresponding to

maximums of probe signal. At the front part of PC pulse maximum (on the temporal scale of  $\sim 1 \mu\text{s}$ ) also does not correspond to maximum of probe pulse. Like for  $\text{CO}_2$  laser, oscillations takes place both for probe and PC signal (see Fig. 4.2 and Fig. 4.9b,c.). The reason for these oscillations like in the case of  $\text{CO}_2$  laser could be acoustical disturbances taking place in the active medium of both lasers.

The HF structure for probe and PC signals of CO laser has rather more complicated behaviour than for  $\text{CO}_2$  laser. Part of the PC and probe signal are presented in Fig. 4.10a ( $\sim 600 \text{ ns}$  from the beginning of the pulse). The front of the laser pulse itself has a relative non-regular structure being noticeably changed from one RTP to another (Fig. 4.10a). This behaviour strongly differs from that of  $\text{CO}_2$  laser pulse which has strong periodic structure on its front (see Fig. 4.3, for example). The comparison between HF structures for the two signals is also complicated because of electromagnetic noise being just one third - one fourth as much as PC signal intensity at the front part of pulse. It should be noted that intensity of probe and PC signal approximately 100 times less than that of  $\text{CO}_2$  laser, particularly for its first peak. The regular periodic structure for both signal could be much easily seen far from the beginning of the pulse ( $\sim 10\text{-}25 \mu\text{s}$ ), where laser intensity much higher (Fig. 4.10b-d). As compared to that of  $\text{CO}_2$  laser, the structure of CO laser itself is changed slightly from one RTP to another (see Fig. 4.10b,c and d, obtained for  $\sim 10$  and  $24 \mu\text{s}$ , Fig. 4.10d corresponds to the other laser pulse).

The HF structure of PC signal for  $\text{CO}_2$  laser at long distance (Fig. 4.5a-d) nearly repeats that of probe pulse. The fact, as was mentioned above, refers to prevailing role of thermal PC mechanism at large temporal scale for  $\text{CO}_2$  laser. The situation seems to be quite different for CO laser. The HF structure of PC signal strongly differs from that of probe signal, reminding the HF structure behaviour for a first peak of  $\text{CO}_2$  laser pulse (Fig. 4.3 and 4.4), where amplitude mechanism is responsible for the PC process. In many cases the beginning of the probe spike (Fig. 4.10d) has much stronger PC reflectivity than following spikes. As a matter of fact, the amplitude mechanism, as was emphasized in theoretical paper [23-24] should be the main one for CO laser because of a slow V-T relaxation rate of CO molecule. The combination of mutual disposition of writing down and reading out spikes leads to the more complicated temporal behaviour of HF structure for CO laser. The rather more detailed analysis on the basis of comparison between experimental and theoretical data is needed for explanation of complicated temporal behaviour of HF structure for probe and PC signal of CO laser, that is more difficult as compared to  $\text{CO}_2$  laser on account of much more complicated kinetics of CO laser.

## Conclusions

The HF structure for PC signal of free-running and mode locked CO<sub>2</sub> laser, and for probe and for PC signal of free-running CO laser at DFWM in inverted medium was observed for the first time.

Together with large temporal scale behaviour the HF structure refers to two principal mechanisms of PC process (resonance and thermal ones) in CO<sub>2</sub> laser and resonance mechanism in CO laser. The existence of HF structure on nanosecond scale both for CO<sub>2</sub> and CO laser, which have never been taken into consideration both in experiment and theory makes reconsider the role of small scale diffraction grating in active medium, and also makes take into account the small temporal scale CO<sub>2</sub> and CO laser kinetics (for instance, hole burning in vibrational-rotational gain distribution etc.).

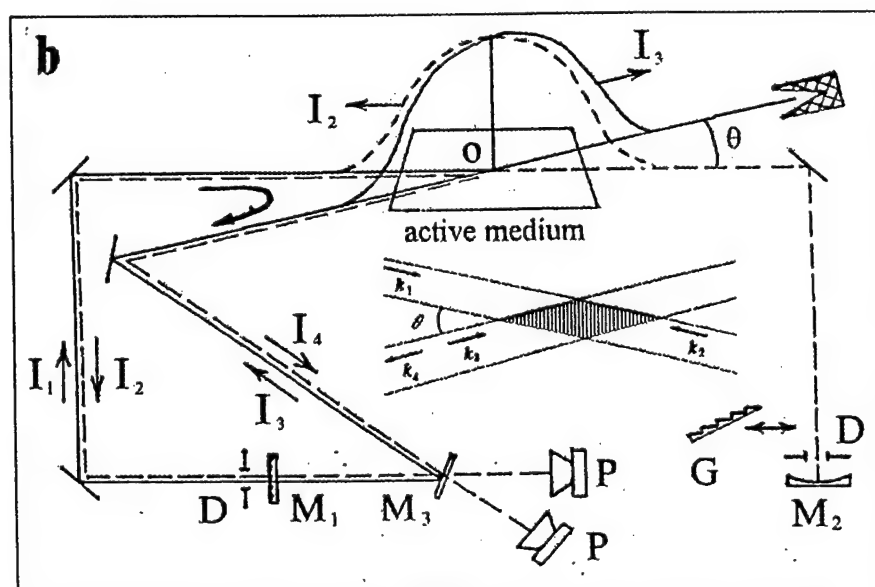
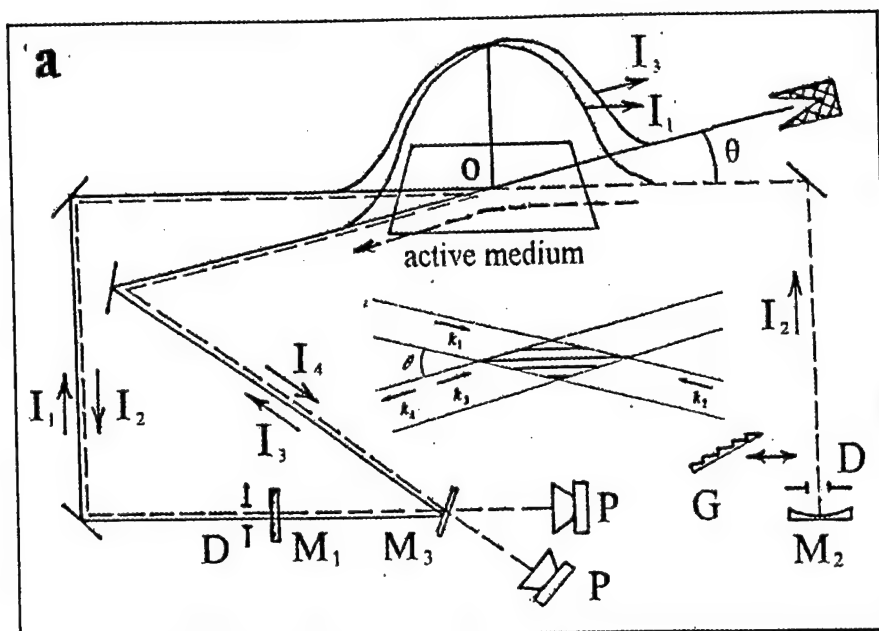


**Fig. 4.1.** Optical scheme for intracavity DFWM on large scale (a) and small scale (b) diffraction gratings in active medium.

$M_1$  - output coupler,  $M_2$  - rear concave mirror,  $G$  - diffraction grating,  $M_3$  - folded mirror,  $P$  - photodetector,  $D$  - diaphragm,  $O$  - active medium centre,  $OM_1 = M_1M_3O = l = 7.5$  m.

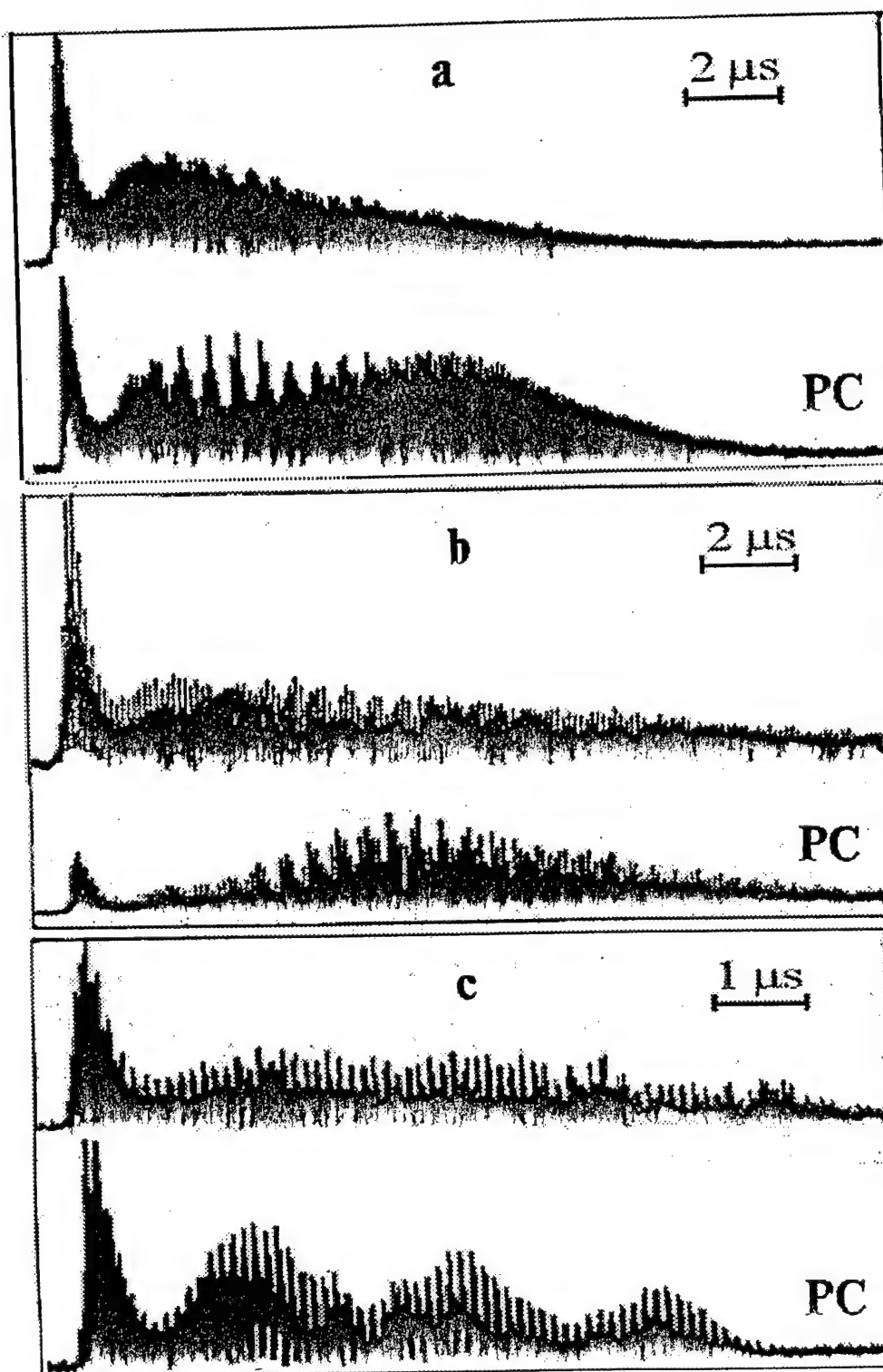
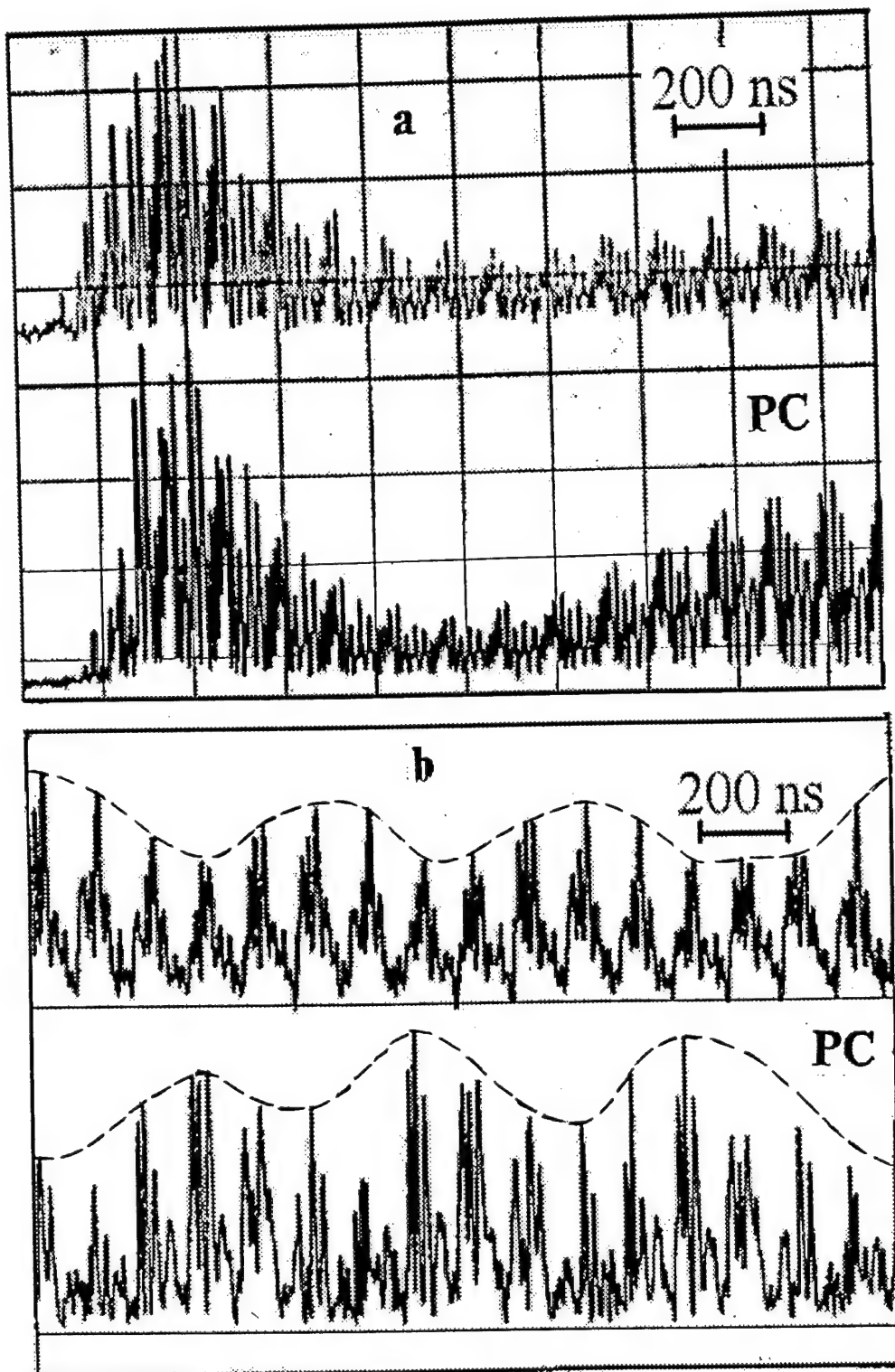


Fig. 4.2. Probe (upper trace) and PC (bottom trace) signals for free-running CO<sub>2</sub> laser  $q=165 \text{ J/l atm}$ ,  $I_1/I_3=4$  (a);  $q=220 \text{ J/l atm}$ ,  $I_1/I_3=11$  (b);  $q=300 \text{ J/l atm}$ ,  $I_1/I_3=0.4$  (c).



**Fig. 4.3.** First peak (a) of probe and PC pulses in Fig. 4.2c and the seventh microsecond (b) of pulses in Fig. 4.2b.  
Upper trace - probe pulse; bottom trace - PC pulse.

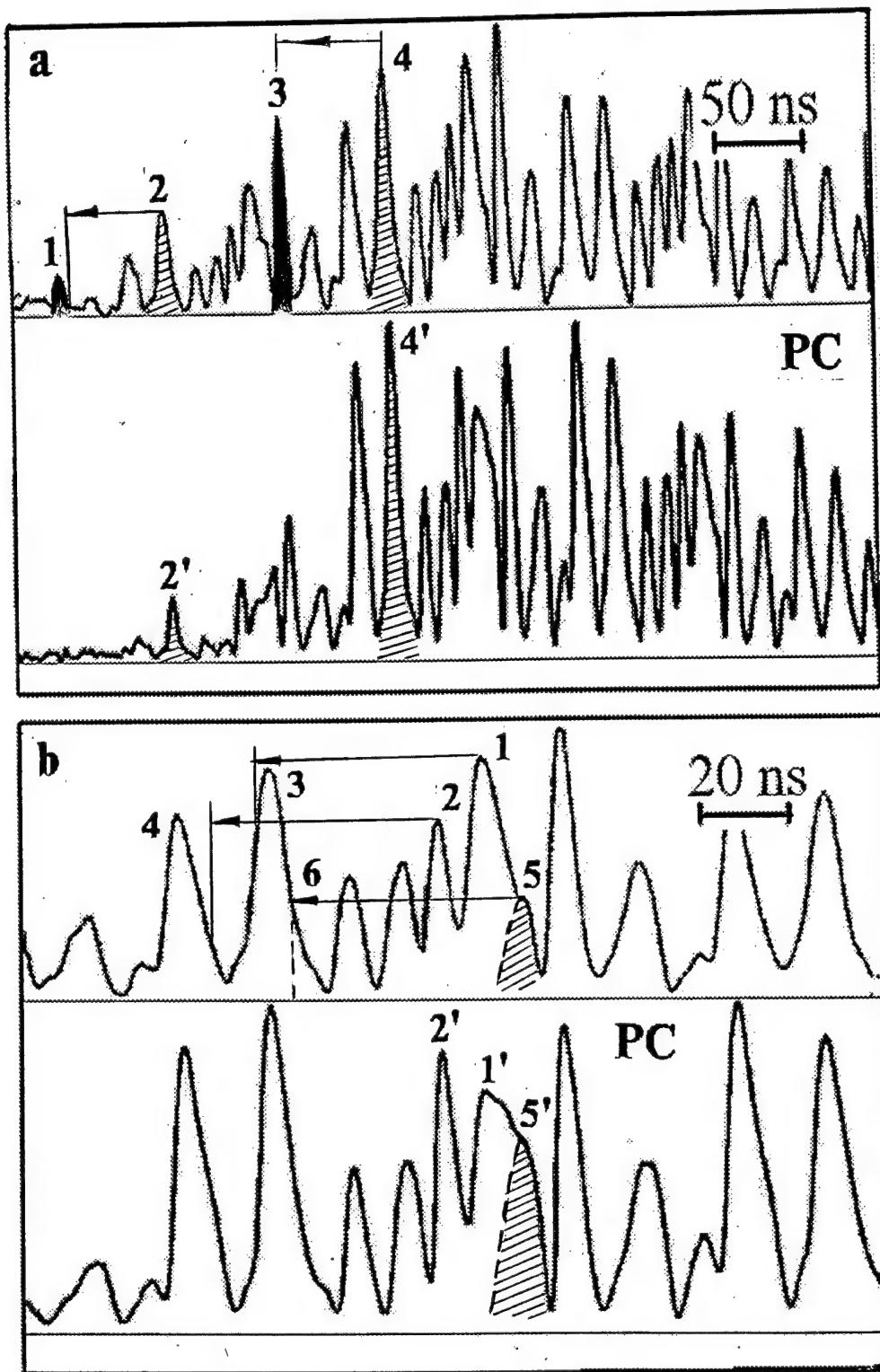


Fig. 4.4. First peak of CO<sub>2</sub> laser and PC pulses on different time scales.  
Upper trace - probe pulse; bottom trace - PC pulse.

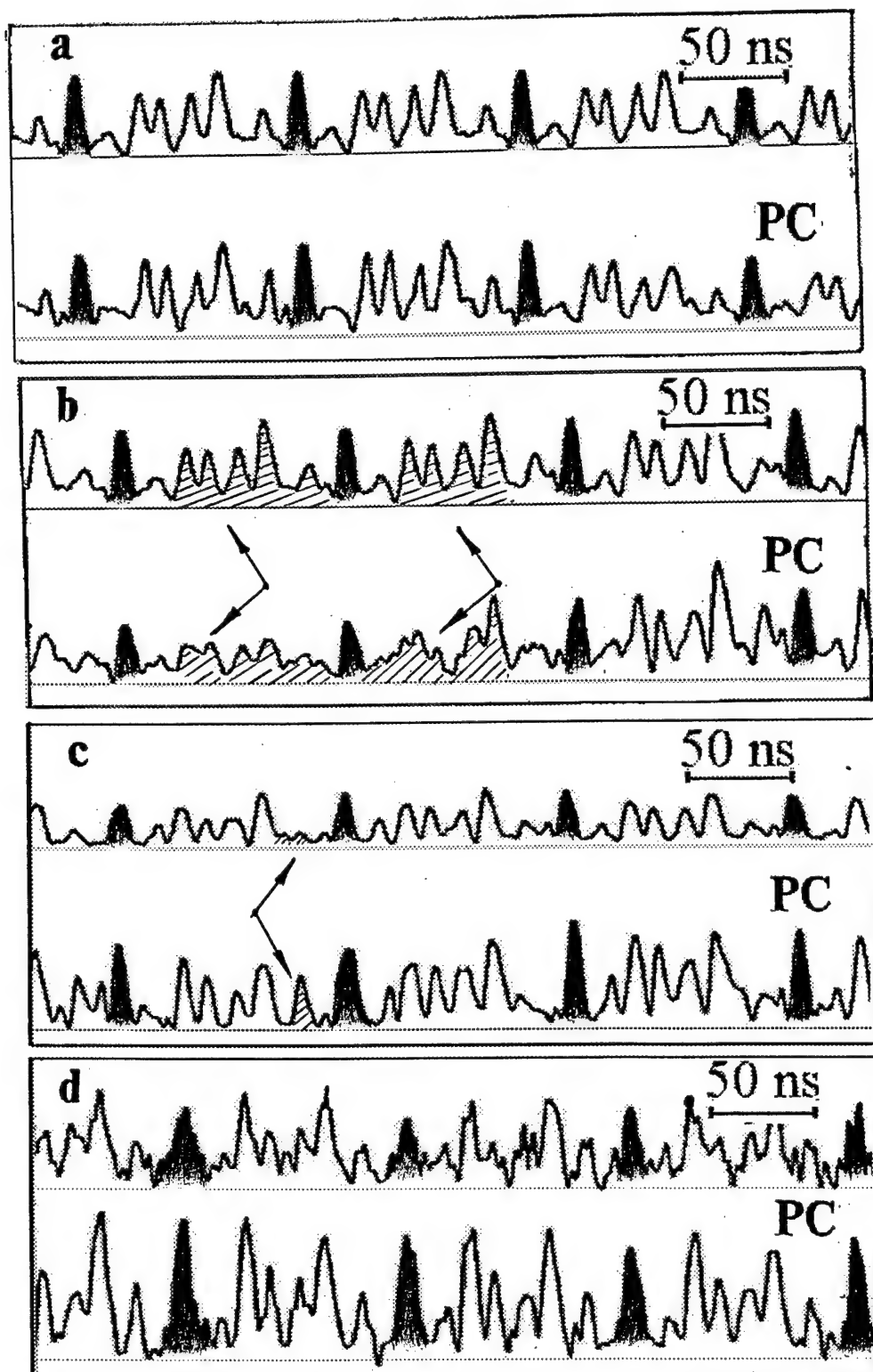


Fig. 4.5. CO<sub>2</sub> laser and PC pulses for different time intervals:

1.8  $\mu$ s (a), 3.2  $\mu$ s (b), 6.2  $\mu$ s (c), 12.4  $\mu$ s (d).

Upper trace - probe pulse; bottom trace - PC pulse. Arrows mark some anomalies.



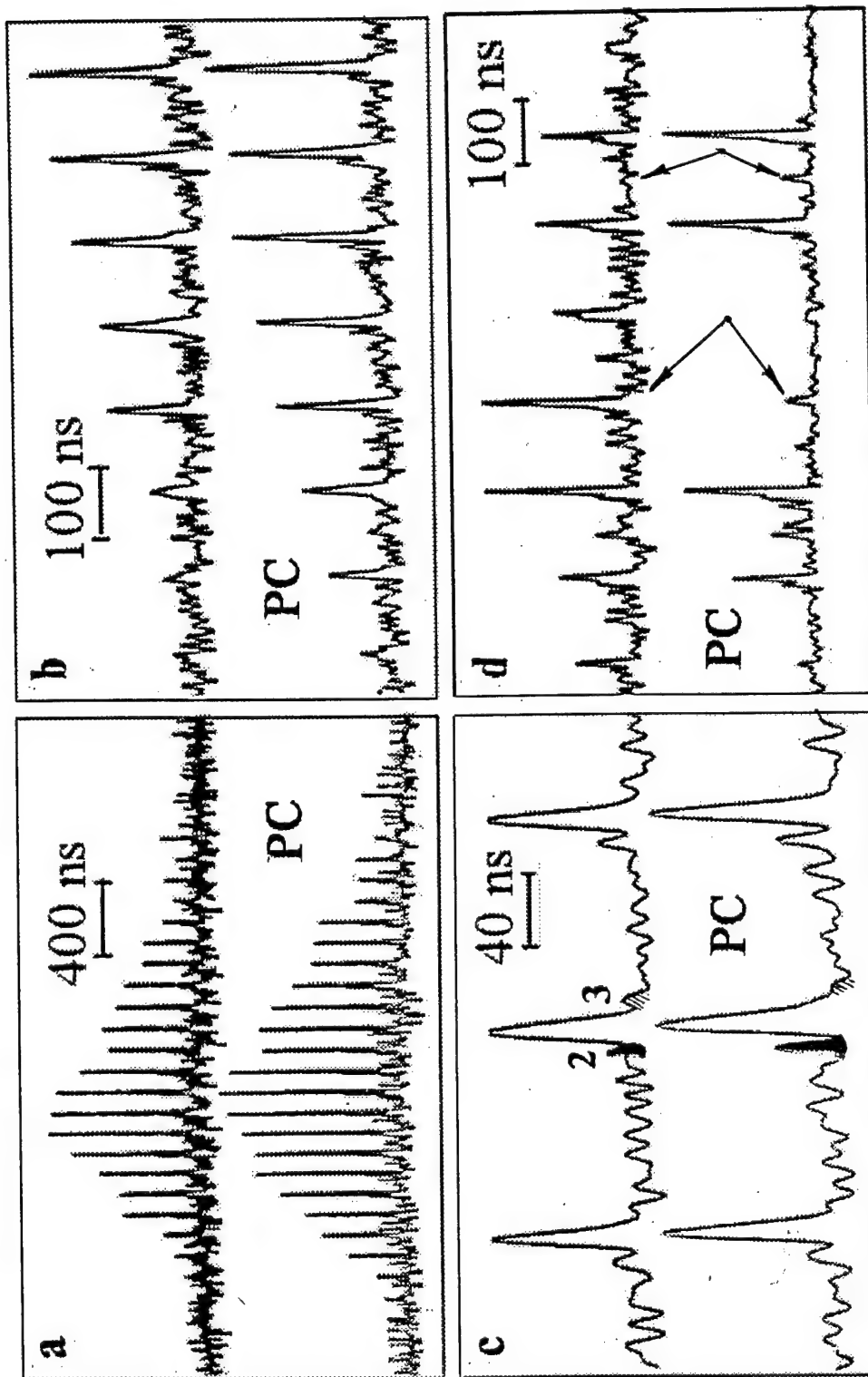


Fig. 4.6. Probe and PC signals for mode locked  $\text{CO}_2$  laser for the same (a-c) pulse and different (d) one. Upper trace - probe pulse; bottom trace - PC pulse.

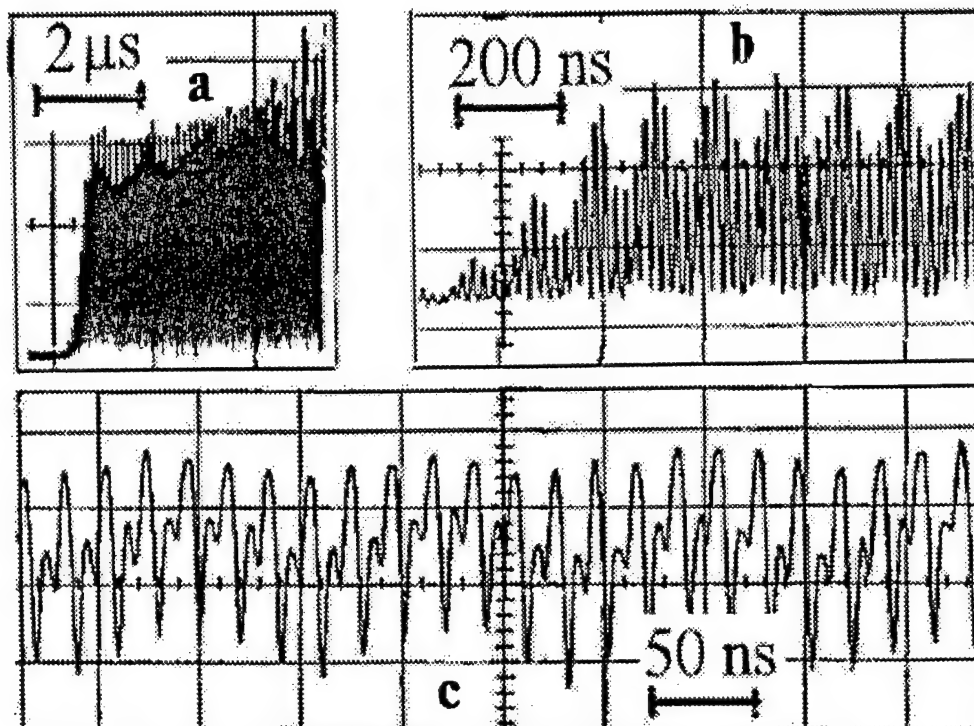


Fig. 4.7. Single line CO laser pulse without DFWM on different time scales.

The front of the pulse (a,b) and the third microsecond of the pulse (c).

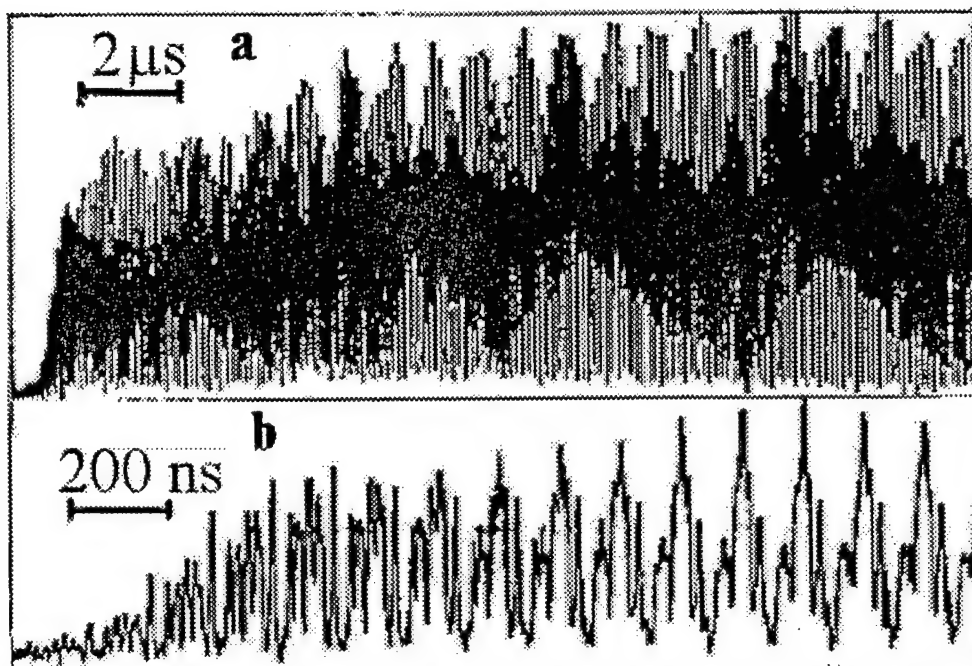


Fig. 4.8. Single line CO laser pulse with DFWM on different time scales.

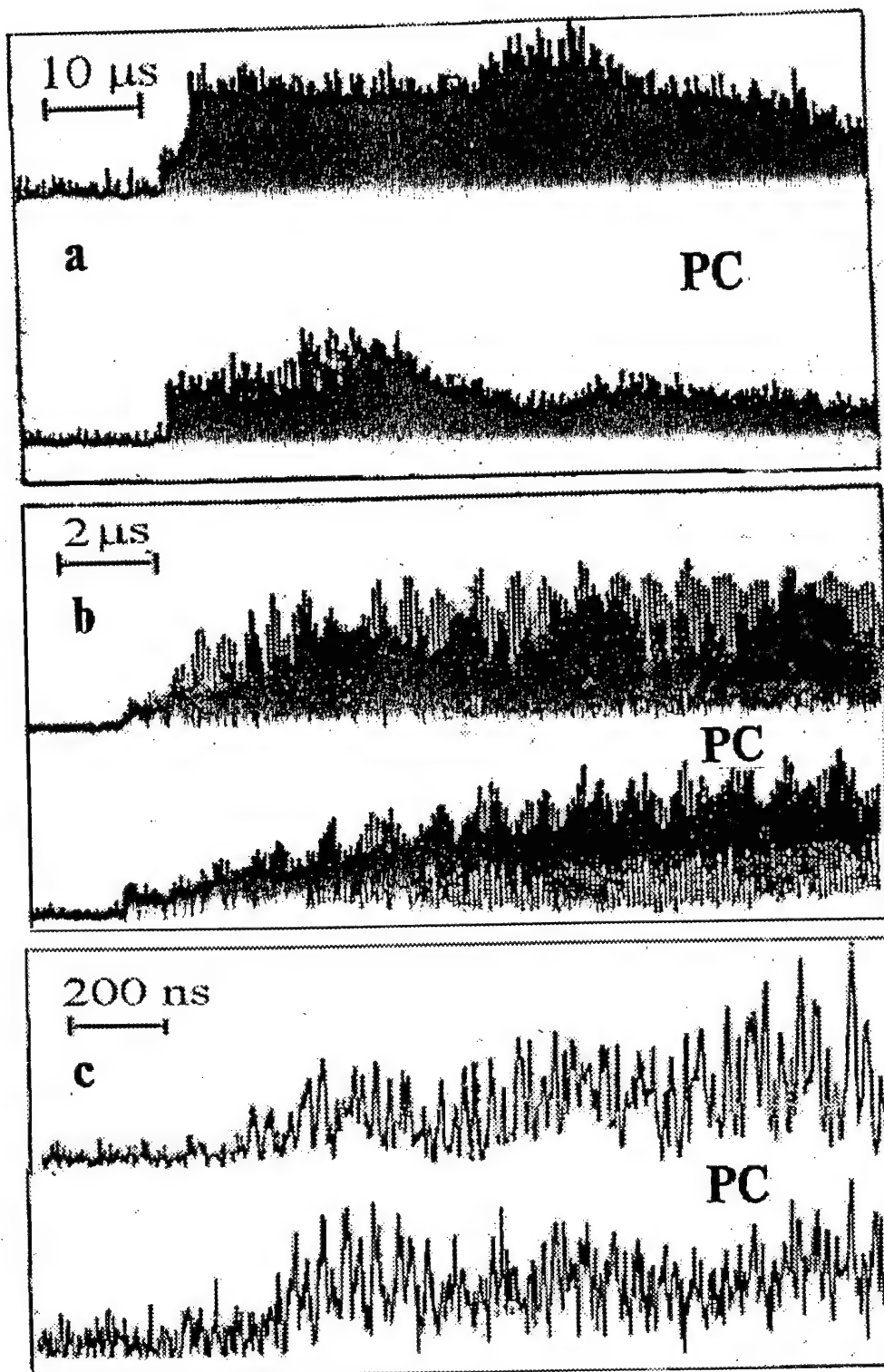
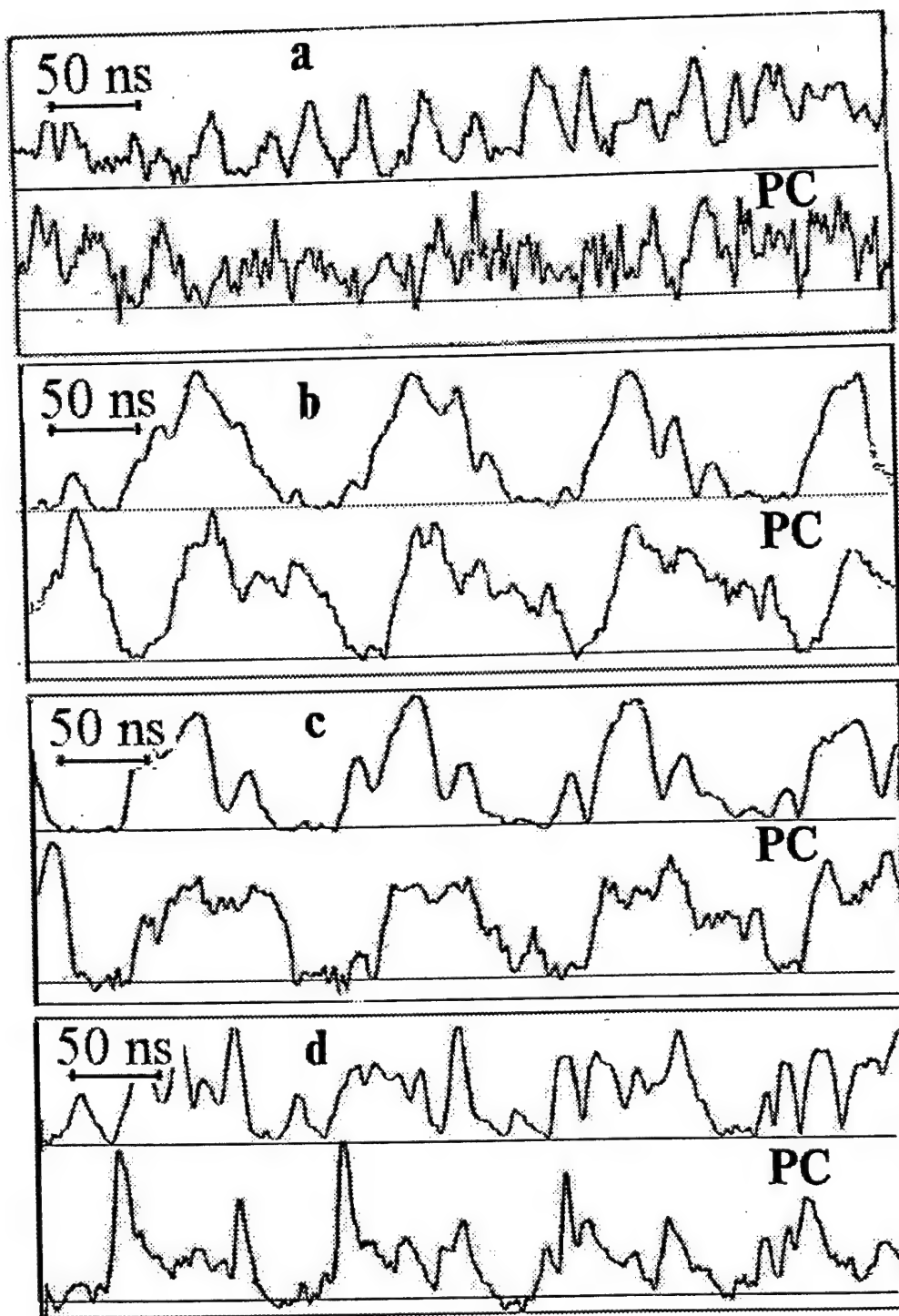


Fig. 4.9. Probe (upper trace) and PC (bottom trace) signals for free-running CO laser,  $q=220\ \text{J/l Amagat}$ ,  $I_1/I_3=1$ , multiline pulse (a);  $I_1/I_3=3.5$ , single line pulse (b,c) on different time scales.



**Fig. 4.10.** Probe (upper trace) and PC (bottom trace) signals for free-running CO laser,  $q=220 \text{ J/l Amagat}$ , single line,  $I_1/I_3=3.5$ ,  $640\text{ns}$  (a);  $10.0\mu\text{s}$  (b);  $23.5\mu\text{s}$  (c);  $I_1/I_3=1$ ,  $10\mu\text{s}$  (d).

## Conclusions

The PC process at DFWM inside CO<sub>2</sub> laser medium has been studied both experimentally and theoretically. The PC process inside CO laser medium has been studied experimentally. It has been shown, that the formation of the PC signal under the intracavity DFWM is characterized by a complicated time history that reflects the main relaxation processes taking place inside the inverted medium.

Theoretical research of DFWM inside EBCD CO<sub>2</sub> laser active medium has allowed to define temporal behaviour of PC wave intensity and PC reflectivity separately on transient gain (amplitude) and thermal (phase) gratings, that is very important for a study of properties of these complicated physical processes of light waves interaction. The time-history of the CO<sub>2</sub> laser and PC signal pulses, and PC reflectivity has been thoroughly investigated experimentally for different cavity Q factors and specific electrical energy inputs. The comparison of the theoretical and experimental data has confirmed the contribution of two different mechanisms of grating formation under DFWM inside the active medium of the CO<sub>2</sub> laser. At the beginning of the PC process the time-history of the PC signal agreed with results of theoretical calculation for resonant mechanism of nonlinearity. The rear part of the pulse may be described by thermal mechanism of nonlinearity.

The influence of different parameters such as gas pressure, specific input energy, laser mixture content, intensity ratio for probe and co-propagating pumping wave, coherency and geometry etc. upon characteristics of PC signal and PC reflectivity at intracavity DFWM of long pulse CO<sub>2</sub> and CO lasers radiation in their inverted medium has been studied experimentally, the PCR (on energy) being up to ~3% for CO<sub>2</sub> laser and 0.5% for CO laser. The parametric study of PCR at DFWM in active medium of EBCD CO laser has demonstrated that the functional dependencies of PCR and temporal behaviour of PC and PCR signals differ strongly from those obtained for EBCD CO<sub>2</sub> laser. The parametric study refers to the resonance mechanism to be responsible for PC process in CO laser active medium. A theory taking into account the real laser parameters should be developed for describing the PC process in active medium of CO laser.

The comparison of experimental and theoretical data for the PCR (on energy) inside CO<sub>2</sub> laser medium has demonstrated a disagreement between them. The disagreement between theoretical and experimental data might be due to processes taking place in active medium of CO<sub>2</sub> laser and being connected with self-influence of laser radiation. These processes were not taking into account in theory, but were observed when studying experimentally a temporal behaviour of PC and PCR signals. The theory should be developed taking into account laser induced medium perturbation, which seems to create not only phase diffraction grating at DFWM, but also destroy it via optical

disturbances. For the better understanding the phenomena the experiments should be carried out on smaller temporal scale with nanosecond resolution.

The HF structure for PC signal of free-running and mode-locked CO<sub>2</sub> laser, and for probe and for PC signal of free-running CO laser at DFWM in inverted medium was observed in our experiments for the first time. Together with large temporal scale behaviour the HF structure refers to two principal mechanisms of PC process (resonance and thermal ones) in CO<sub>2</sub> laser and resonance mechanism in CO laser. The existence of HF structure on nanosecond scale both for CO<sub>2</sub> and CO laser, which have never been taken into consideration both in experiment and theory makes reconsider the role of small scale diffraction grating in active medium, and also makes take into account the small temporal scale CO<sub>2</sub> and CO laser kinetics.

## References

1. Zel'dovich B.Y., Pilipetskii N.F., Shkunov V.V. "Wavefront Inversion", Nauka, Moscow, 1985 [in Russian].
2. Woerdman J.P. *Opt. Comm.*, **2**, 212 (1970).
3. Stepanov B.I., Shakin E.V., Rubanov A.S. *Doklady Akademii Nauk. SSSR.*, **196**, 567 (1971) [in Russian].
4. Bigio L.J., Feldman B.J., Fisher R.A. et al. *Proc. Int. Conf. Lasers '78, Orlando, Fla 1978*, McLean, Va. 531 (1979).
5. Bergman E.E., Bigio L.J., Feldman B.J. et al. *Optics Lett.*, **3**, 82 (1978)
6. Lind R.C., Steel D.G., Lam J.F. et al. *IEEE/OSA Conf. Laser Eng. and Appl., Washington, D. C., 1979. Dig. Techn. Pap., New York, N.Y.*, 70 (1979).
7. Lind R.C., Steel D.G., Klein M.B. et al. *Appl. Phys. Lett.*, **34**, 457 (1979).
8. Kovalev V.I. *Izvestiya Acad. Nauk SSSR. Ser. Phys.*, **54**, 1066 (1990) [in Russian].
9. Sherstobitov V.E., Kalinin V.P., Goryachkin D.A. et al. *Proc. SPIE*, **1415**, 79 (1991).
10. Betin A.A., Zinchenko V.I., Kalinin V.P. et al. *Proc. of National Conf. on Phase Conjugation '86*, Minsk, USSR, 22, (1987) [in Russian].
11. Likhanskii V.V., Matyutshenko I.D., Naumov V.G. et al. *Proc. of National Conf. on Phase Conjugation '89*, Minsk, USSR, 70, (1990) [in Russian].
12. Sherstobitov V.E., Ageichik A.A., Bulaev V.D. et al. *Proc. SPIE*, **1841**, 135 (1991).
13. R.L. Abrams, R.C. Lind. *Opt. Letts.*, **2**, 94 (1978); Erratum, *Opt. Lett.* **3**, 203 (1978).
14. Yariv A., Pepper D.M. *Opt. Letts.*, **1**, 16 (1977).
15. Lind R.C., Steel D.G. and Dunning G.J. *Opt. Eng.*, **21** 190 (1982).
16. Vasil'ev L.A., Galushkin M.G., Seryogin A.M., Cheburkin N.V. *Kvant. Electron*, **9**, 1571 (1982) [in Russian].
17. Dimakov S.A. and Robachevskaya M.A. *Proc. of National Conf. on Phase Conjugation '89*, Minsk, USSR, 75, (1990) [in Russian].
18. Ageichik A.A., Dimakov S.A., Resunkov Yu.A. et al. *Proc. SPIE*, **1840**, 166 (1991).
19. Gorton E.K. and Richmond A.M. *Opt. Comm.*, **86**, 341 (1991).
20. Afanas'ev L.A., Ionin A.A., Kiselev E.A. et al. *Quantum Electronics*, **24**(6), 513 (1994).
21. Afanas'ev L.A., Galushkin M.G., Ionin A.A. et al. *Proc. of Laser '95 Conf.*, STS Press, 1996, 556-563. *Izvestiya RAN, Ser. Phys.*, **60**, 41 (1996) [in Russian].
22. Belousov D.V., Gurashvili V.A. et al. *XIV Int. Conf. on Coherent and Nonlinear Optics, 1991. St. Peterburg, Russia Abstracts.*, **1**, 177, (1991).

23. Berdyshev A.V., Kurnosov A.K. and Napartovich A.P. *Kvant. Electron*, **20**, 529 (1993) [in Russian].
24. Berdyshev A.V., Napartovich A.P. et al. *Kvant. Electron.*, **21**, 91 (1994) [in Russian].
25. Vinetskiy. V.L., Kuhtarev N.V., Odulov S.G., Soskin M.S. *Uspehi Phys. Nauk.*, **129**, 113 (1979) [in Russian].
26. Beldugin I.M., Galushkin M.G., Zemskov E.M. *Kvant. Electron*, **11**, 887 (1984) [in Russian].
27. Betin A.A., Mitropolskiy O.V. *Kvant. Electron*, **14**, 1002 (1987) [in Russian].
28. Vasil'ev L.A., Galushkin M.G., Seryogin A.M., Cheburkin N.V. *Izvestiya Akad. Nauk SSSR. Ser. Phys.*, **45**, 1412 (1981) [in Russian].
29. Galushkin M.G., Seryogin A.M., Fyodorov A.B., Cheburkin N.V. *Kvant. Electron*, **10**, 2115 (1983) [in Russian].
30. Beldugin I.M., Galushkin M.G., Zemskov E.M. *Kvant. Electron*, **11**, 1794 (1984) [in Russian].
31. Kuznetsova T.N. *Kvant. Electron*, **7**, 1237 (1980) [in Russian].
32. Beldugin I.M., Galushkin M.G., Zemskov E.M. *Kvant. Electron*, **10**, 2066 (1983) [in Russian].
33. Bunkina M.V., Morozov V.V., Firsov K.N. *Kvant. Electron*, **7**, 2026 (1980) [in Russian].
34. Galushkin M.G., Dimakov S.A., Onoshko R.N. et al. *Izvestiya. Akad. Nauk SSSR. Ser. Phys.*, **54**, 1042 (1990) [in Russian].
35. Galushkin M.G., Mitin K.V., Seryogin A.M. *Izvestiya Akad. Nauk Ser. Phys.*, **58**, 60 (1994) [in Russian].
36. Vasil'ev L.A., Galushkin M.G., Seryogin A.M., Cheburkin N.V. *Kvant. Electron*, **9**, 1228 (1982) [in Russian].
37. N.G.Basov, I.A.Beregnoy et al, *Techn. Physics Letters*, **1**, 1105 (1975) [in Russian].



## Contents

<b>1. Introduction</b>	2
<b>2. Theoretical investigation of phase conjugation at DFWM of pulsed CO<sub>2</sub> laser radiation inside inverted medium</b>	5
<b>2.1. Transient theory of phase conjugation at degenerate four - wave mixing.</b>	6
2.1.1. Physical mechanisms of PC.	6
2.1.2. Medium nonlinearity.	6
<b>2.2 PC reflectivity calculation methods.</b>	6
2.2.1 DFWM on gain nonlinearity in active medium of EBCD CO <sub>2</sub> laser.	7
Wave mixing in a medium with a gain nonlinearity.	8
Equations for nonlinear medium	9
Definition of intensity variation	10
A coefficient of nonlinear coupling and equations for coupled waves.	11
Equations based on full kinetic model of a nonlinear medium.	12
A solution of equation set for coupled waves in approximation of constant pumping wave amplitude	13
A solution for the two-level model of a nonlinear medium	14
An amplification of mixing waves in nonlinear medium.	16
A nontransient solution for a coefficient of nonlinear coupling.	18
PC reflectivity at DFWM on gain nonlinearity.	19
2.2.2 DFWM on phase thermal gratings in the active medium of a EBCD CO <sub>2</sub> laser.	20
A specific power of heat liberation.	20
Two types of nonlinear heat liberation.	20
A thermal nonlinearity of CO <sub>2</sub> laser active medium.	21
A definition of medium density variation (a coefficient of nonlinear coupling).	23
Equations for coupled waves.	25
PC reflectivity at DFWM on thermal nonlinearity.	26
Equations based on a full kinetic model of a nonlinear medium.	27
<b>2.3. An influence of medium parameters on PC reflectivity at DFWM of CO<sub>2</sub> laser radiation.</b>	28
<b>2.4. Conclusions.</b>	30
Figers for Part 2	32
<b>3. Experimental investigation of PC at DFWM of pulsed CO<sub>2</sub> /CO laser radiation inside its inverted medium</b>	46
<b>3.1. Experimental laser setup</b>	46
EBCD laser chamber	46
Electron-beam gun	47
Test equipment and experimental techniques	47
<b>3.2. PC at DFWM inside inverted medium of EBCD CO<sub>2</sub> laser</b>	49
3.2.1. Characteristics of active medium of CO <sub>2</sub> laser	49
Input energy	50
Small signal gain	50
3.2.2. Characteristics of the EBCD CO <sub>2</sub> laser.	51
Laser output	52
Temporal behaviour of the laser output	53
Spatial and spectral characteristics	54
3.2.3. Experimental scheme of DFWM of CO <sub>2</sub> laser radiation inside its active medium	56
An influence of DFWM on the laser output	57
3.2.4. Experimental proofs for PC process.	58

Reconstruction of an optical image in near-field zone	58
Reconstruction of angular divergency in far-field zone	59
Coherent nature of backscattered signal	60
3.2.5. Two mechanisms of phase conjugation of CO <sub>2</sub> laser radiation at DFWM inside inverted medium	61
3.2.6. Parametric study of the PC process.	64
Specific input energy	64
Q factor of optical resonator	67
Gas pressure	69
Laser gas mixture	72
A degree of linear polarization of laser beam	73
Spectral range of CO <sub>2</sub> laser radiation	73
Interaction angle of DFWM	74
Optical delay between probe and co-propagating waves	75
Pumping and probe intensity ratio	75
3.3. PC at DFWM in active medium of CO laser.	77
An evidence of PC for CO laser	78
Temporal characteristics of PC process for CO laser	78
The influence of SIE on PC process.	80
Various output couplers.	80
Intensity ratio for intracavity co-propagating wave and probe signal.	81
Gas density influence upon PC process.	81
Gas temperature.	82
3.4 Conclusions	82
Figers for Part 3	84
4. High frequency temporal structure of laser and phase conjugated signals at intracavity DFWM of CO <sub>2</sub> and CO laser radiation in their inverted medium	124
4.1. Experimental setup and optical scheme	124
4.2. Experimental results and discussion	125
Temporal behaviour of probe and PC signals for CO <sub>2</sub> laser.	125
Time history of laser and PC signal at DFWM of CO laser radiation.	128
Conclusions	130
Figures for Part 4	131
Conclusions	140
References	142
Contents	144